Identification of novel targets for the treatment of endocrine-resistant breast cancer

Arany Soosainathan

A thesis submitted for the degree of Doctor of Philosophy

Breast Cancer Now Research Centre
The Institute of Cancer Research
237 Fulham Road
London

This thesis was completed under the supervision of Professor Clare M. Isacke, Dr Lesley-Ann Martin, and Professor Mitch Dowsett.

The work described here was carried out in the Breast Cancer Now Research Centre, The Institute of Cancer Research, 237 Fulham Road, London, SW3 6JB.

I, Arany Soosainathan, confirm that the work presented in this thesis is my own. Where information has been derived from other sources, I confirm that this has been indicated in the thesis.

Date: 26th November, 2021

……

Abstract

While endocrine therapy is an effective, well-tolerated treatment for oestrogen receptor positive (ER-positive) breast cancer, a large proportion of initial responders will develop hormone therapy resistance, and relapse. Two major challenges in determining the mechanisms underlying endocrine therapy resistance are our limited ability to recapitulate inter- and intra-tumour heterogeneity *in vitro*, and the lack of availability of tumour samples from women with disease progression or relapse, as most tissue banks are formed of diagnostic biopsies and primary tumours.

The overall aim of this PhD project was to investigate mechanisms contributing to endocrine resistance, and search for common vulnerabilities that could be targeted. Examination of the transcriptome of paired patient samples from before commencement of aromatase inhibitor therapy, and following progression or relapse on therapy, confirmed the heterogeneity that is observed under the umbrella term of ER-positive breast cancer. Few common transcriptional changes were observed among the post-aromatase inhibitor therapy samples, but a trend towards upregulation of pro-proliferative signalling pathways was noted. Pre-clinical 2D and 3D models of endocrine resistance and palbociclib resistance, with different molecular backgrounds, were subjected to high-throughput drug and siRNA screens. These confirmed the importance of proliferative pathways such as PI3K-AKT-mTOR, and highlighted cyclin dependent kinase (CDK) 7 and CDK9 and their roles in cell cycle regulation and transcription as common hits in multiple cell lines. Further investigation of these targets showed that drugs targeting CDK7 and CDK9 are able to inhibit cell proliferation in endocrine-resistant and palbociclib-resistant settings, in both 2D and 3D culture. Furthermore, some of the CDK7/9 inhibitors, which are currently in clinical trials, demonstrated synergy with palbociclib treatment in both palbociclib-sensitive and palbociclib-resistant contexts.

This thesis proposes that CDK7 and CDK9 are potential targets for therapy in advanced endocrine-resistant, palbociclib-resistant breast cancer settings, and that there is a potential for combination therapy of CDK7 or CDK9 inhibitors with palbociclib. Future studies are required to further elucidate the mechanism of action of these inhibitors in these resistant models, the mechanism of the synergy observed with palbociclib, and the potential for combination therapy *in vivo*.

Statement regarding impact of COVID-19 on PhD studies

I commenced my PhD at the ICR in October 2017. I had a period of maternity leave beginning in April 2019, and returned to work on 5th March 2020. When I returned this was to a different lab, with a different team and change of supervisor, as during the period of maternity leave, my initial supervisor Dr Lesley-Ann Martin left the post, and my previous lab was disbanded and shutdown.

Having commenced work on 5th March 2020, on 17th March my household had to go into isolation, as my husband and I were unwell with probable COVID-19 for approximately two weeks.

On 24th March 2020 the ICR went into lockdown, and I was placed on furlough as part of the ICR's response to COVID-19, utilising the Coronavirus Job Retention Scheme. While I tried to do some writing up and data analysis at home, this proved challenging due to the lack of childcare for my son, as his nursery was closed, and my husband had just started a new job.

When the nursery re-opened on 17th June 2020, I was able to do some writing up at home. I returned from furlough on 3rd August 2020, and commenced working at home on the data analysis and planning for my next set of experiments. My PhD timeline was extended by 2 months, to account for the 4+ months that I was on furlough and unable to work.

Following my return to the lab, the difficulties I faced were:

- Initially reduced time in tissue culture and in the lab, due to the limited number of staff allowed in at any one time and strictly enforced social distancing guidelines putting pressure on these shared resources. These restrictions were lifted in August 2021
- The closure of our collaborator's laboratory (Professor Chuck Perou) during the pandemic delayed by approximately 4 months the RNA-sequencing of the patient samples pre- and post-aromatase inhibitor therapy
- Lack of face-to-face interaction when needing help in how to analyse my results

- 4 periods of household isolation while waiting for COVID-19 swab results to come back due to COVID-19 symptoms
- 2 separate periods of 14 days household isolation (my son had COVID-19 and recovered, my grandmother developed COVID-19 and passed away) during which time I had no childcare to enable me to work from home.
- Due to COVID-19/Brexit, there were supply chain difficulties in obtaining the flasks I normally use for routine cell culture. In putting the cells into alternatives, they did not attach well, and died, so I could not run my experiments. It took approximately 6 weeks to discover that the flasks were contributing this problem.

Date: 26th November 2021

Arany Soosainathan Professor Clare M. Isacke

Acknowledgements

Firstly, I would like to thank God, through whom all things are possible.

I would like to thank my first supervisors, Professor Mitch Dowsett, Dr Lesley-Ann Martin, and Professor Stephen Johnston, for their guidance at the start of my studies. To Professor Clare Isacke, who graciously supervised me in her laboratory for the latter half of my PhD, my deepest thanks for her counsel, insights, time, and understanding.

I would like to thank all of the Isacke Lab members, current and past, for welcoming me to the team, for their instruction and valuable discussions, and for making the lab an enjoyable workplace during a testing time. My particular thanks to Marjan Iravani and Rebecca Orha for their patient teaching and willingness to help me problem solve. I would also like to thank the Martin and Dowsett Labs, and in particular Dr Eugene Schuster for his assistance in the bioinformatics analysis, and Dr Joanna Nikitorowicz-Buniak, and Dr Sunil Pancholi for their wisdom, guidance, and advice. I would like to thank Professor Perou's team at the University of North Carolina for their collaboration in carrying out the library preparation and RNA-sequencing of historic paired FFPE samples.

I am very grateful to the Wellcome Trust for funding my research fellowship, and Breast Cancer Now and the Institute of Cancer Research for funding the equipment and core facilities that have been invaluable during the course of my studies. Thank you to the Breast Cancer Research Bioinformatics Group, and in particular Dr John Alexander for his assistance in the analysis of the screening results.

Finally, thank you to my friends and family for all their love and encouragement. To Amma, Appa, and Dave, for all of the support, food, and unscheduled childcare, I owe a debt of thanks. To Samuel, and my dearly departed Ammammah, who have always trusted that I can do anything, thank you for believing.

Table of Contents

List of Figures

List of Tables

List of Abbreviations

ADCC	Antibody-dependent cellular cytotoxicity
AF	Activation function
AI	Aromatase inhibitor
AIB1	Amplified in breast cancer 1
AKT	Activated protein kinase B
AML	Acute myeloid leukaemia
AMPK	AMP-activated protein kinase
ATP	Adenosine triphosphate
BCL-2	B cell lymphoma 2
BH3	BCL-2 homology 3
BRD4	Bromodomain containing 4
CAK	CDK activating kinase
cAMP	Cyclic adenosine monophosphate
CBP	CREB-binding protein
CDK	Cyclin-dependent kinase
ctDNA	circulating cell-free tumour DNA
ctDNA	circulating tumour DNA
DBD	DNA binding domain
DCC-FBS	Dextran-charcoal stripped foetal bovine serum
DCIS	Ductal carcinoma in situ
ddPCR	Droplet digital PCR
DNA	Deoxyribonucleic acid
DSIF	DRB sensitivity-inducing factor
E2	Oestrogen
ECM	Extracellular matrix
EGF	Epidermal growth factor
EGFR	Epidermal growth factor receptor
ER	Oestrogen receptor
ERE	Oestrogen response element
ER^{MUT}	Mutant oestrogen receptor
ER^{WT}	Wild-type oestrogen receptor
FBS	Foetal bovine serum

FDR	False discovery ratio
FFPE	Formalin-fixed, paraffin-embedded
FSH	Follicle stimulating hormone
GPCR	G-protein-coupled receptor
GSEA	Gene set enrichment analysis
HAT	Histone acetylase
HDAC	Histone deacetylase
HER2	Receptor tyrosine-protein kinase erbB-2
Hes6	Hes family basic helix-loop-helix transcription factor 6
HEXIM	hexamethylene bisacetamide-inducible protein
HMT	Histone methyltransferase
HSP	Heat shock protein
HTS	High-throughput screens
IGF-1	Insulin-like growth factor 1
IHC	Immunohistochemical
IP6K3	Inositol hexakisphophate kinase 3
IRS	Insulin receptor substrate
LBD	Ligand binding domain
LH	Luteinising hormone
LTED	Long term oestrogen-deprived
MAPK	Mitogen-activated protein kinase
MCL-1	Myeloid cell leukaemia-1
MIND	Mouse mammary intraductal
MLL	Mixed lineage leukaemia
mTOR	mammalian target of rapamycin
NELF	Negative elongation factor
NGS	Next generation sequencing
NHS	National Health Service
NTC	Non-targeting control
OSNA	One-step nucleic acid amplification
p90RSK	Ribosomal S6 kinase
PARP	Poly-ADP ribose polymerase
PD-1	Programmed cell death 1

PD-L1	Programmed cell death ligand 1
PDK1	3-phosphoinositide-dependent protein kinase 1
PDO	Patient derived organoid
PDX	Patient derived xenograft
PI3K	Phosphatidylinositol 3-kinase
PIC	Pre-initiation complex
PIP_2	Phosphatidylinositol-4,5-bisphosphate
PIP_3	Phosphatidylinositol-3,4,4-trisphosphate
PKA	Protein kinase A
PR	Progesterone receptor
PROTAC	Proteolysis targeting chimeras
PTEF-b	Positive transcription elongation factor
Raptor	regulatory-associated protein of mTOR
Rb	Retinoblastoma
Rictor	Rapamycin-insensitive companion of mTOR
RNA Pol II	RNA polymerase II
RNA-seq	RNA sequencing
RT-qPCR	Real-time quantitative polymerase chain reaction
SERCA	Selective oestrogen receptor covalent antagonist
SERD	Selective oestrogen receptor downregulator
SERM	Selective oestrogen receptor modulator
SRC-1	Steroid receptor co-activator-1
TIF2	Transcriptional intermediary factor 2
TME	Tumour microenvironment
TNBC	Triple-negative breast cancer
TNF	Tumour necrosis factor
TRAIL	TNF-related apoptosis-inducing ligand
TSC1/2	Tuberous sclerosis complex 1/2
UK	United Kingdom
VEGFR	Vascular endothelial growth factor receptor
Wt	Wild-type
XPB	Xeroderma pigmentosum protein B
XPD	Xeroderma pigmentosum protein D

Chapter 1 Introduction

1.1 Breast Cancer

The simplest definition of cancer is a disease where an abnormal cell begins to divide in an uncontrolled fashion, and invade surrounding tissue. In reality, the term cancer encompasses a wide spectrum of diseases affecting a multitude of organs, each with their own classifications, treatment options, and prognosis. The common feature of all cancers is that it begins when cells develop genetic and epigenetic changes that allow these cells to circumvent the usual checks and balances on cellular proliferation. These common traits were originally described in a seminal paper by Hanahan and Weinberg (Hanahan and Weinberg, 2000), and termed the six "hallmarks of cancer". These characteristics were then updated in 2011 to recognise that the environment in which tumours develop also plays a role (Hanahan and Weinberg, 2011), and now include the following: self-sufficiency in growth-signalling, loss of growth suppressors, evasion of apoptosis, limitless replication, angiogenetic induction, genomic instability and mutation, avoiding immune detection, tumour-promoting inflammation, dysregulation of cellular energetics, and invasion and metastasis. Breast cancer therefore, is when cells in the breast tissue of a woman or man acquire some or all of these characteristics, and begin to divide uncontrollably.

1.1.1 Breast cancer epidemiology

Cancer of the breast accounts for 15% of all new cancer diagnoses in the UK each year, and is the most common cancer in the UK (Cancer Research UK, 2020) excluding non-melanomatous skin cancer. It is also a worldwide health problem, with over 2 million women being diagnosed with breast cancer across the globe in 2018 (World Cancer Research Fund, 2018). Furthermore, the incidence rates of breast cancer have been rising, with an increase of 3% in the last decade in the UK, and a projected increase of 2% between 2014 and 2035, to 210 cases per 100,000 women at the end of this period. The most recently reported lifetime risks of breast cancer in the UK are 1 in 7 for women, and 1 in 870 for men (Cancer Research UK, 2020). However, despite the increasing incidence, the survival rates have been improving. Over the last decade, the mortality

rates for female breast cancer have fallen by 21% in the UK, and almost three-quarters of women diagnosed in the UK have a ten year or greater survival period (Cancer Research UK, 2020). However, it remains the second most common cause of cancer death in women, with 11,400 deaths in 2017.

1.1.2 Breast cancer risk factors

Heritable risk factors for breast cancer include mutations in certain genes. Women with a *BRCA1* or *BRCA2* mutation have a 45-65% chance of developing breast cancer by age 70, but as these mutations are relatively rare, they account for between 1-5% of breast cancer cases overall (McClain et al., 2005, Newman et al., 1998). The risk of breast cancer is also twice as high in women who have one first-degree relative with the disease, in comparison to women with no family history. A significantly increased risk of breast cancer is also seen in several genetic syndromes, such as Li-Fraumeni syndrome, caused by mutations in *TP53*, or Cowden syndrome, most often caused by mutations in *PTEN*. Mutations in these genes result in a loss of their tumour suppressor function, and increase a person's chance of developing several types of cancer, as well as breast, over their lifetime. Other low to moderate penetrance gene mutations associated with breast cancer include mutations in *PALB2, BRIP1*, and *FGFR2*. Many of the proteins encoded by these genes are involved in DNA repair, as are *BRCA1* and *BRCA2*.

Environmental risk factors such as obesity, tobacco, alcohol consumption, and exposure to exogenous hormones (such as the oral contraceptive pill or hormone replacement therapy) are also associated with a higher risk of breast cancer. Finally, personal factors also have an influence on the risk of developing breast cancer. Women who have late menarche and early menopause, those who are multiparous, have their first child before the age of 30, and breastfeed their children, have a lower risk of developing breast cancer than those who do not.

1.1.3 Breast cancer diagnosis and staging

In the UK, breast cancer can be diagnosed via one of two routes: through routine breast screening by mammography, or through symptomatic presentation. The NHS breast screening programme invites women between the ages of 50 and 70 for an X-ray

examination of their breasts every 3 years, with the aim being to identify breast cancers at an early stage, to confer an improved chance of survival. Breast cancers can also present with a variety of symptoms, such as a palpable breast lump, nipple discharge, or skin changes or tethering.

Table 1.1: Classification of breast cancer, Cancer Research UK

Stage		Classification
Stage 0		Pre-invasive breast cancer/ductal carcinoma in situ (DCIS)
Stage 1	**A**	Tumour ≤2cm with no extramammary spread
	B	Micrometastases in axillary lymph nodes, and tumour ≤2cm
Stage 2	**A**	Tumour ≤2cm, with metastases in 1-3 axillary or internal mammary lymph nodes OR Tumour size 2-5cm, with no metastases to lymph nodes
	B	Tumour size 2-5cm, with metastases in 1-3 axillary or internal mammary lymph nodes OR 5cm < Tumour, with no metastases to lymph nodes
Stage 3	**A**	No tumour in breast, but metastases found in 4-9 axillary or internal mammary lymph nodes OR 5cm < Tumour, with metastases in 1-3 axillary or internal mammary lymph nodes
	B	Tumour of any size, involving skin or chest wall. Metastases in up to 9 axillary or internal mammary lymph nodes
	C	Tumour of any size, involving skin or chest wall, with metastases in 10 or more axillary, internal mammary, or supraclavicular lymph nodes
Stage 4		Tumour of any size, with or without lymph node involvement, that has metastasized to distant sites (e.g. liver, lung, brain)

Following diagnosis, the American Joint Committee on Cancer's TNM classification is typically used to stage breast cancer. T represents the tumour size and/or local invasion, N stands for ipsilateral axillary node involvement, and M indicates whether metastases

are present or not. The different classifications are presented in Table 1.1. The three factors taken together are used to determine the stage of the breast cancer, with stage 0 signifying *in situ* disease, up to stage 4 where the breast cancer has already metastasized and is advanced. The stage of the tumour is used to guide treatment options, and is an indication of prognosis (Figure 1.1).

Breast cancers diagnosed at the early stages of 1-2 tend to have a good prognosis with >95% 5-year survival rate, but unfortunately those diagnosed late have a lower survival rate with a poor prognosis.

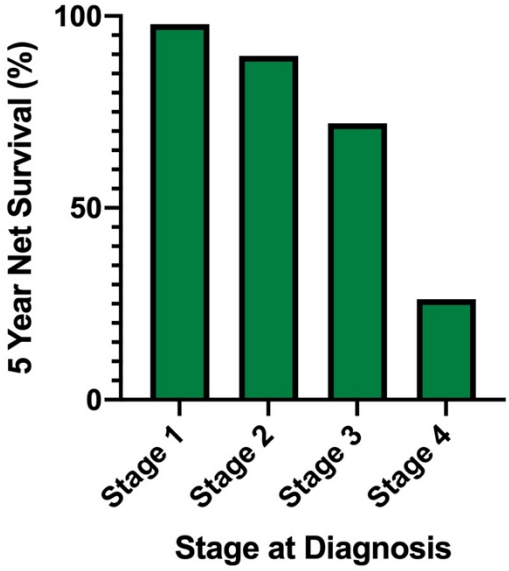

Figure 1.1: Bar graph showing 5-year survival of all women diagnosed with breast cancer from 2013-2017, grouped by TNM stage of when the cancer was first diagnosed. Adapted from Office of National Statistics, data published 2019.

1.1.4 Breast cancer subtypes

While the TNM classification and tumour stage are important in stratifying breast cancers, there are also defined subtypes of breast cancer characterised by their expression of three receptors. These three receptors are oestrogen receptor (ER), progesterone receptor (PR), and the signalling receptor ErbB2 (HER2). Most breast cancers (70-80%) express ER and/or PR, but not HER2, and are classified immunohistochemically as ER-positive cancers. Tumours that express high levels of

HER2 make up approximately 20% of all breast cancers, and may be further subdivided into those that are hormone receptor-negative or hormone receptor-positive. Finally, breast cancers that do not express any of the three receptors are termed triple-negative breast cancers (TNBC). These are the least common subtype, accounting for approximately 15% of cases. The different subtypes of breast cancer behave differently biologically, and the difference in receptor expression makes them susceptible to different treatments, and so this distinction is important.

Breast cancers may also be classified according to their gene expression profile, which is termed molecular or intrinsic subtyping. Global gene expression profiling by Perou and colleagues divided breast tumours into five subtypes: luminal A, luminal B, basal-like, HER2-enriched, and normal breast-like (Perou et al., 2000). Luminal A tumours are predominantly ER-positive, and tend to be of a low grade, and low proliferation rate. Luminal B tumours are also generally ER-positive, but may express lower levels of hormone receptors, and have a worse prognosis than luminal A tumours, tending to be of higher grade and more proliferative. The HER2-enriched subtype usually reflects amplification of the *ERBB2* gene, while the basal subtype mostly overlaps with TNBCs, has a cytokeratin expression pattern usually found in basal epithelium, and has a very aggressive phenotype. The normal breast-like subtype shows expression of genes typically expressed by non-epithelial cells and adipose tissue, and low expression of luminal epithelial genes, but questions have been raised as to whether this is a separate group, or represents poorly sampled breast tissue (Sorlie, 2007).

Overall, while there have been major advances in the molecular subtyping of breast cancers, treatment of tumours remains predominantly based on the immunohistochemical (IHC) receptor status, with confirmation of *ERBB2* amplification by *in situ* hybridization when required, and TNM classification of the cancer.

1.1.5 Breast cancer treatments

The treatment of breast cancer is usually multi-modal, including surgery, radiotherapy, and medical therapy, and is dependent on tumour characteristics, such as stage, hormone receptor status, and HER2 status, and on patient factors such as age at

diagnosis and menopausal status. Overall, early breast cancer is treated with curative intent, while treatments for metastatic breast cancer generally aim to prolong survival, but may involve any or all of the following modalities.

1.1.5.1 Surgery

Surgery forms the mainstay of treatment for most early breast cancers, and may achieve a "cure" if the cancer has not spread. The aim of surgery is to excise the tumour, with a specified margin of normal breast tissue surrounding it, to ensure that adequate margins have been achieved. This may be done through performing a wide local excision, also known as a "lumpectomy", where just the tumour is removed, or by performing a mastectomy, where the whole breast is removed. Factors influencing this decision include patient choice, the size and location of the tumour, the size of the breast, and the patient's general health. Breast reconstruction using the patient's own tissue, or prostheses, may be offered during the same procedure, or later in their course of treatment. At the same time as the tumour excision, a sentinel lymph node biopsy of the axillary lymph nodes is performed (unless there is clinical evidence of disease in the axilla prior to surgery). By removing the first lymph node that drains the breast (identified using either a dye or a radioactive tracer, or both) and examining it histologically or via the PCR-based one-step nucleic acid amplification (OSNA) assay, spread beyond the primary tumour can be determined. If this sentinel lymph node is found to contain cancerous cells, a second surgical procedure to remove all of the axillary lymph nodes, known as an axillary clearance, is usually scheduled.

Surgery is often the first step in a patient's breast cancer journey, but some patients are offered neoadjuvant treatments – that is, treatment prior to removal of the primary tumour. This may be in the form of chemotherapy or endocrine therapy, with the aim often being to reduce the size of the primary tumour, to improve the surgical outcome. Furthermore, a patient's response to neoadjuvant chemotherapy can provide prognostic information, with pathologic complete response to neoadjuvant chemotherapy correlating with disease-free survival (Spring et al., 2020).

Surgery plays a much smaller role in the management of metastatic breast cancer, where it is usually not recommended. This is because surgery to remove metastatic

disease such as spread to the liver or the bone can be risky procedures with a prolonged recovery, and generally only confer a survival benefit in selected cases (Friedel et al., 2002). Similarly, removing the primary tumour in the presence of metastatic disease has not been shown to improve outcome (Khan et al., 2020). The exception to this is where surgery may offer symptomatic relief from the primary tumour, for example where there is skin involvement from a fungating tumour, or significant pain and arm immobility from axillary disease.

Following surgery, adjuvant treatments, such as radiotherapy, endocrine therapy, chemotherapy, or immuno-modulatory drugs, are usually offered. The aims of these treatments are to reduce the risk of local recurrence, and eradicate any hitherto undetected metastatic disease.

1.1.5.2 Radiotherapy

Radiotherapy uses the ionizing properties of X-ray waves to treat cancer. The X-rays either directly or indirectly ionize the atoms making up the DNA chain, which results in single-strand, or double-strand DNA breaks. Cancer cells have a reduced ability to repair this damage, and it is this differential in repair ability that allows radiotherapy to be used in cancer treatment.

The most common form of radiotherapy is external beam radiotherapy, where radiation is delivered from an external source. The beam is targeted to the breast, to minimise exposure to the rest of the body, and often a “boost” is given to the tumour bed, from where the primary tumour was excised. Breast brachytherapy is another form of radiotherapy, where radioactive pellets are placed within hollow applicators in the breast, and emit radiation directly to the tumour bed. Finally, intrabeam radiotherapy involves giving radiotherapy during the operation to remove the primary tumour, with a recent randomised trial demonstrating non-inferiority to whole breast radiotherapy in selected patients (Vaidya et al., 2020).

Complications of radiotherapy include acute redness, peeling, and blistering of the skin over the area that was being targeted, as well as late-occurring normal tissue fibrosis. Furthermore, despite attempts to focus the beam at the tumour bed, lymph nodes and

ducts may be damaged resulting in lymphoedema of the arm, and the lung and heart may also be damaged, resulting in lung or cardiac fibrosis.

1.1.5.3 Chemotherapy

Chemotherapy, in the original sense of the word, are chemicals that can bind to and specifically kill microbial cells. In the modern day, it refers to drugs that can stop the growth of cancerous cells, either by stopping proliferation, or by causing cell death. There are multiple different chemotherapeutic agents currently licensed, with different mechanisms of action. The most common use of chemotherapy in breast cancer treatment is in the adjuvant setting, to reduce the systemic risk of recurrence. It may also be used in the neoadjuvant setting, to reduce the size of a primary tumour to achieve a better surgical outcome. For patients suffering with triple negative breast cancer (TNBC), chemotherapy is the primary form of adjuvant treatment, and a significant proportion of patients suffering with other forms of breast cancer will also receive chemotherapy.

There are multiple different mechanisms of action that may be employed by chemotherapeutic agents, and many of them are used in combination in breast cancer treatment. For example, 5-fluorouracil inhibits DNA synthesis by mimicking the nucleotide uridine. Through this, it is able to irreversibly inhibit the enzyme thymidylate synthase, which synthesises thymine, thus preventing DNA synthesis. Doxorubicin (also known as adriamycin) and epirubicin are members of the anthracycline drug family, and work through intercalating between base pairs in DNA, and by inhibiting topoisomerase II, resulting in DNA double strand breaks. Cyclophosphamide is an alkylating agent, and functions by cross-linking guanine bases in the DNA double helix, thus preventing the strands from uncoiling, which is necessary for DNA replication. Taxane-based drugs, such as docetaxel and paclitaxel, disrupt microtubule function by stabilising GDP-bound tubulin, thus preventing depolymerisation and spindle formation, which is needed for mitosis.

These drugs are given systemically, and as such, non-malignant cells are also subjected to these toxic agents. Therefore, they are often administered as combination

treatments, for example as FAC/T (5-fluorouracil, doxorubicin, cyclophosphamide, and taxol). In this way, lower doses of the drugs can be given while achieving the same effect, as they all have different mechanisms of action, and reduce the probability of resistance developing. Meta-analyses have shown that combinations of anthracyclines and taxanes are more effective than either treatment alone (Piccart-Gebhart et al., 2008). Combining the treatments also minimises the side-effects of the chemotherapy, as does administering it in cycles, which gives the non-malignant cells time to recover.

The classical theory underlying the effectiveness of chemotherapy is that as cancerous cells proliferate at a faster rate than normal cells, they are more vulnerable to chemotherapeutic agents, accumulating errors in their DNA replication and synthesis pathways that activate mitotic checkpoints. However, it is becoming increasingly clear that proliferation rate alone cannot explain the differential sensitivity of malignant cells to chemotherapy, and that factors such as mitochondrial priming (Certo et al., 2006), or genetic streamlining leading to deficiencies in DNA repair pathways (Kaelin, 2009), make malignant cells more susceptible.

Unfortunately, despite the measures taken to reduce the impact on normal cells, the fact remains that chemotherapy is a systemic treatment, and so non-malignant cells are affected. Common side effects of chemotherapy are often as a result of other cells that have a rapid turnover in the human body, causing hair loss, skin rashes and hypersensitivity, and gastro-intestinal disturbances, as well as temporary immune suppression. There are also longer-term consequences, such as peripheral neuropathy, reduced fertility, and cardiotoxicity. Therefore, chemotherapy places a significant burden on the body, which may be poorly tolerated by patients already in frail health.

1.1.5.4 Targeted agents

The need to selectively target cancerous cells and reduce the impact of systemic therapy on patients is one of the driving forces behind the development of drugs known as targeted agents. These are drugs that inhibit specific cellular targets upon which the cancerous cells are dependent for survival (Higgins and Baselga, 2011).

Trastuzumab (trade name Herceptin) is arguably the most famous of this class of drugs, and is a humanized monoclonal antibody that targets the receptor tyrosine kinase HER2. Expression of this receptor is upregulated in HER2-positive breast cancers. HER2 is a member of the epidermal growth factor family and promotes mitotic signalling pathways. Trastuzumab binds to the extracellular portion of HER2, thus stopping the formation of a homodimer with another HER2 receptor. This prevents the activation of the downstream signalling pathways promoting cell proliferation. Trastuzumab also acts to mediate antibody-dependent cellular cytotoxicity (ADCC), engaging the immune system in targeting the HER2-expressing cells (Gennari et al., 2004). The discovery of this drug opened another avenue of treatment for patients with HER2-positive disease, which had previously been much more difficult to tackle. It has now been demonstrated that the combination of trastuzumab with traditional chemotherapy is more effective in metastatic HER2-positive disease than standard chemotherapy alone (Slamon et al., 2001), and that combination with aromatase inhibitors (AIs) is beneficial for those patients who have HER2-positive/ER-positive disease (Kaufman et al., 2009). Attempts to further utilise the targeting properties of trastuzumab have also proved fruitful, such as the antibody-drug conjugate trastuzumab emtansine (trade name Kadcyla or T-DM1). Emtansine is a cytotoxic microtubule inhibitor, and can be targeted for intracellular delivery to HER2-overexpressing cells by its conjugation to trastuzumab (Lewis Phillips et al., 2008). The KATHERINE trial demonstrated that patients with HER2-positive early breast cancer who still had residual disease following neoadjuvant therapy had a reduced risk of recurrence or death when they were given adjuvant trastuzumab emtansine versus trastuzumab alone (von Minckwitz et al., 2019).

As well as targeting cell surface receptors, drugs acting on intracellular signalling machinery have also been developed. An example of this is everolimus, which acts to inhibit mammalian target of rapamycin (mTOR). mTOR is a significant component in the phosphatidylinositol 3-kinase/activated protein kinase B (PI3K/AKT) signalling pathway, which when activated, promotes mitosis and proliferation (further discussed in Section 1.3.3). This pathway is often aberrantly active in cancerous cell populations, and so by inhibiting mTOR, the proliferation of malignant cells relying on PI3K-AKT-mTOR signalling can be targeted. The combination of everolimus with an AI has been shown to improve progression-free survival of patients who had shown recurrence or progression

while treated with AI therapy alone (Baselga et al., 2012), and further work to target the upstream signalling components such as PI3K and AKT is ongoing.

Another area of the cell signalling machinery that has been successfully targeted is that which controls progression through the cell cycle. The interplay between cyclins and cyclin-dependent kinases (CDKs) ensure an ordered progression through the cell cycle, and deregulation of the cell cycle is a hallmark of cancer. The exit from the quiescent phase of G_0 in response to mitogenic signals is achieved through the formation of the cyclin D-CDK4/6 complex, which phosphorylates retinoblastoma (Rb) and releases E2F transcription factors. These activate the transcription of S-phase promoting genes. Palbociclib, ribociclib, and abemaciclib are drugs that inhibit CDK4/6, and thus induce cell cycle arrest, blocking progression of the cancer. The PALOMA trials (Finn et al., 2015, Cristofanilli et al., 2016) compared the progression-free survival when patients with advanced ER-positive/HER2-negative breast cancer were treated with palbociclib and the AI letrozole, versus letrozole alone, and the MONALEESA-2 trial performed a similar comparison using ribociclib (Hortobagyi et al., 2016), and both demonstrated superiority over the previous standard therapy. As a result, in 2017 these therapies were approved for the first-line treatment of advanced ER-positive/HER2-negative breast cancer. Following this, in 2019 after the MONARCH trials (Sledge et al., 2019), the third CDK4/6 inhibitor abemaciclib was approved for the treatment of advanced ER-positive/HER2-negative breast cancer in the UK. It was noted in the NICE committee discussion that the three CDK4/6 inhibitors could be considered as a class, with similar effectiveness, but slight differences in side-effect profile and dosing regimens, thus offering patients a choice in their treatment ((NICE), 2019).

A separate mechanism employed by targeted agents is that of synthetic lethality, illustrated by the development of poly-ADP ribose polymerase (PARP) inhibitors. The enzyme PARP is part of the DNA repair machinery in a cell, as are the proteins encoded by the genes *BRCA1* and *BRCA2*. BRCA1/2 proteins are necessary for the homologous recombination pathway, which is a DNA repair process that utilises the undamaged sister chromatid to perform high-fidelity repairs of double-stranded DNA breaks that often occur during DNA synthesis. As discussed previously, *BRCA1/2* mutations are the

highest heritable risk locus for breast cancer (Section 1.1.2). PARP-inhibitors, such as olaparib, target cells with *BRCA1/2* mutations by using synthetic lethality – where the mutated cells are already deficient in one element of their DNA-damage response, by blocking another mechanism by using PARP inhibitors, the cells cannot continue proliferating and die (Farmer et al., 2005). PARP inhibitors cause PARP-1 to be trapped on DNA repair intermediates. This then obstructs replication forks, which require BRCA-dependent homologous recombination for resolution (Pommier et al., 2016). Trials have shown that olaparib improved progression-free survival in comparison to single-agent standard chemotherapy in patients with metastatic HER2-negative breast cancer and a germline *BRCA* mutation (Robson et al., 2017). As such, olaparib was approved by the European Medicines Agency for patients with advanced breast cancer who have inherited *BRCA* gene mutations.

A promising developing class of targeted agents for use in breast cancer is that of immunotherapy. This is a class of agents that aids the immune system to recognise and target cancer cells as foreign. Under normal conditions, there is an interplay between stimulatory and inhibitory receptors and ligands in the immune system, known as immune checkpoints, that allow the body to recognise what is self, and what is foreign. There is growing evidence demonstrating that tumours can utilise these mechanisms to evade the immune system to progress and metastasize (Keir et al., 2008). One example of this is the programmed cell death 1 and programmed cell death ligand 1 (PD-1/PD-L1) axis. PD-1 is a cell surface membrane protein expressed by immune cells including T-cells. Upon activation by its ligands PDL-1 and PDL-2, PD-1 promotes T-regulatory cell function, and moderates lymphocyte activation. In normal homeostasis, PDL-1 and PDL-2 are expressed on antigen-presenting cells, but recent works have shown that cancers are able to express PD-L1 and thus attenuate immune response (Iwai et al., 2002, Dong et al., 2002). Following the reporting of the KEYNOTE-522 and -355 trials (Schmid et al., 2020, Cortes et al., 2020), FDA approval was granted for the PD-L1 inhibitor pembrolizumab, in combination with chemotherapy for the treatment of patients with advanced TNBC whose tumours are PD-L1 positive, and for high-risk early stage TNBC as neoadjuvant treatment, with continued use as single agent adjuvant treatment following surgery.

1.1.5.5 Endocrine therapy

The first step to discovering the link between oestrogen and breast cancer was in 1896, where Beatson described that by removing the ovaries of premenopausal patients, regression of metastatic breast cancer and improved prognosis was seen in some patients (Beatson, 1896). Thus, some factor produced by the ovaries was thought to promote the growth of breast cancers. As the side effects of oophorectomy were too significant for this to be considered a practical treatment for breast cancer, pharmacological suppression of this factor was then explored, and testosterone was used for this purpose between the 1930s and 1960s. However, it was not until 1962 and the discovery of the oestrogen receptor (ER) by Jensen and Jacobsen (Jensen, 1962) that a target upon which anti-oestrogens could be developed that true endocrine therapy became a viable option.

Oestrogen and progesterone are reproductive hormones. In premenopausal women, oestrogen is secreted predominantly by the ovaries, in response to follicle stimulating hormone (FSH) and luteinising hormone (LH), which are produced by the pituitary gland. Oestrogen then reduces the secretion of FSH and LH via negative feedback loops, and it is this cyclical nature of production that regulates the menstrual cycles. Oestrogen and progesterone also regulate the development of mammary tissue during puberty, pregnancy, and lactation, through acting on receptors expressed on breast epithelial cells (ER and PR). ER-positive cancers continue to express these receptors, and utilise the transcription pathways activated by ER to proliferate. In postmenopausal women, the ovaries no longer secrete oestrogen, and so the oestrogen that remains is produced by the conversion of androgens to oestrogen through the action of the enzyme aromatase. This enzyme is found in many peripheral tissues such as the liver, muscle, and in the adipose tissue in the breast.

Endocrine therapies therefore, are drugs that target oestrogen signalling to prevent the proliferation of cancer cells dependent on these pathways for survival, and are recommended as part of adjuvant therapy for all luminal-like breast cancers (Cardoso et al., 2019). Endocrine treatment can be broadly divided into three categories (Figure 1.2):

selective ER modulators (SERMs), which antagonise oestrogen binding to ER through competitive inhibition; selective ER downregulators (SERDs), which promote the degradation of ER; and AIs, which prevent the production of oestrogen in the peripheral tissues.

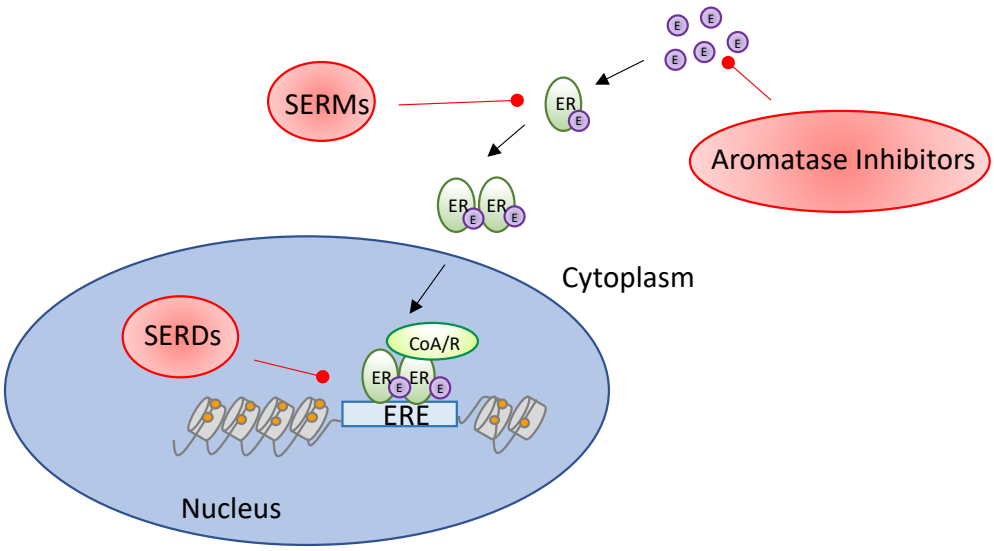

Figure 1.2: Sites of anti-oestrogen action. Oestrogen binding to ER results in phosphorylation, dimerization, and translocation to the nucleus where ER associates with co-activators (CoA) or co-repressors (CoR) and binds to oestrogen response elements (EREs) on target genes. Endocrine agents target this pathway: aromatase inhibitors (AIs) block the conversion of androgens to oestrogens; Selective ER modulators (SERMs) compete with oestrogen for binding to the ligand binding domain (LBD); selective ER downregulators (SERDs) inhibit ER dimerization and ERE binding, as well as promoting ER degradation. (Figure adapted from (Johnston and Dowsett, 2003)

Tamoxifen was the first clinically useful anti-oestrogen and the best known example of a SERM. Tamoxifen competes with oestrogen for binding to the ligand-binding domain (LBD) of ER, and induces a conformational change that inhibits gene transcription (see Section 1.2 for further detail on ER function). One feature of a SERM such as tamoxifen is that its effect on ER signalling is tissue-specific: in breast cells, tamoxifen is an ER-antagonist, but in other cell types such as the endometrium and bone, it is a partial agonist. As a result, the side-effects of the drug are tissue-specific: stimulation in the bone avoids the osteoporosis seen with other anti-oestrogens, but its effect in the endometrium results in an increased risk of endometrial cancer. Therefore, the search is ongoing for the ideal SERM, which would be an antagonist in the breast, an agonist in the bone, and neutral elsewhere (Shang, 2006). Currently in premenopausal women,

tamoxifen is the standard of care, and may also be given to postmenopausal women who show disease progression on other forms of endocrine therapy.

Fulvestrant is currently the only clinically licensed SERD, and in contrast to tamoxifen, is a pure anti-oestrogen, and so does not have the partial agonist side-effects of SERMs (Wakeling et al., 1991). Fulvestrant competes with oestrogen for ER binding, and inhibits dimerization and activation of ER, and its subsequent binding to DNA. Furthermore, it also downregulates ER by targeting it for proteolytic degradation. In clinical trials, fulvestrant has been shown to be as effective as an AI in patients who have progressed following tamoxifen (Howell et al., 2002), and the combination of an AI with fulvestrant was superior to the AI alone or in sequence for treating ER-positive advanced breast cancer (Mehta et al., 2012). Furthermore, fulvestrant has also been shown to improve the survival of patients with metastatic cancer where mutations in the *ESR1* gene have been detected (Fribbens et al., 2016).

AIs are the third category of endocrine therapy, and are the first line treatment for postmenopausal patients with ER-positive breast cancer. They deprive the cancer from proliferative oestrogen signalling by blocking the conversion of androgens to oestrogen, which is the main route of oestrogen production in the postmenopausal patient. The most commonly used AIs are the reversible, non-steroidal AIs, anastrozole and letrozole, and the irreversible, steroidal AI, exemestane. Clinical trials have demonstrated the superiority of AIs over SERMs in advanced breast cancer (Milla-Santos et al., 2003), and the large scale ATAC trial (anastrozole, tamoxifen, alone or in combination) showed an improvement in disease-free survival in ER-positive early breast cancer patients in the AI treatment arm (Cuzick et al., 2010).

Endocrine therapies tend to be safe and well-tolerated by patients (Ohno, 2016), but some ER-positive breast cancers show *de novo* insensitivity to them, and unfortunately as many as half of those patients initially responsive to endocrine therapies will develop resistance to these drugs (Anderson et al., 2007). Acquired resistance may develop through activating mutations in *ESR1*, altered cross-talk in pro-proliferative signalling pathways, or epigenetic changes, and these will be discussed in Section 1.3 in more

detail. The challenge of addressing endocrine resistance is a complex one, and can be illustrated by further examination of the roles oestrogen and ER play in breast cancer.

1.2 The oestrogen receptor

The ER is a nuclear transcription factor. There are two main isoforms of ER, ERα and ERβ, encoded by the genes *ESR1* and *ESR2*, respectively. This study has focused on ERα, which will be referred to as ER throughout. ER contains a DNA-binding domain (DBD) which determines the activation of target genes, by recognising oestrogen response elements (EREs) with two cysteine-rich zinc fingers (Kumar et al., 1987, Ruff et al., 2000). ER also contains two transcriptional activation function (AF) domains (Figure 1.3), AF-1, in the N-terminal region, and AF-2 in the C-terminal region. AF-2 is integral to the ligand-binding domain (LBD), and is activated by oestrogen (Kumar et al., 1987), while AF-1 activity is regulated by phosphorylation (Kato et al., 1995), and can be independent of ligand binding. Full agonist activity of ER requires synergism between AF-1 and AF-2 (Tora et al., 1989), and there is evidence that they have cell population-specific functions in breast cells (Cagnet et al., 2018). AF-1 is connected to the DBD and LBD by a hinge region, which is able to bind chaperone proteins.

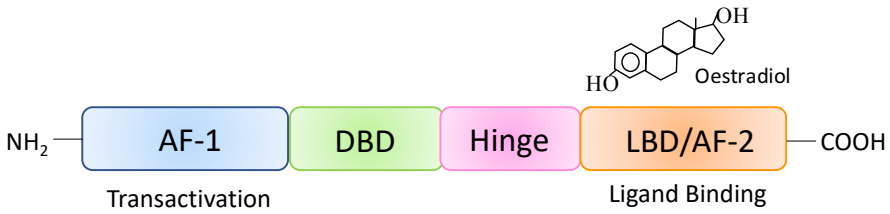

Figure 1.3: Schematic of ER structure. ER has two distinct activation function (AF) domains, the transactivation AF-1 domain, and the ligand binding domain (LBD) AF-2, connected by a hinge region and a DNA-binding domain (DBD). (Figure adapted from (Saha et al., 2021)

1.2.1 Mechanisms of ER activation

The classical mechanism of ER signalling is through direct genomic effects via a ligand-dependent mechanism of activation. Oestrogen binding to ER in the LBD induces a major conformational change that generates surfaces for the formation of the functionally

active ER dimer (Bai and Giguere, 2003) and for co-regulatory proteins (Mak et al., 1999) to interact with the dimer. The dimer then translocates to the nucleus, where it binds to chromatin at EREs – which are cis-acting enhancers – of target genes. The DNA-bound dimer then associates with cellular transcription machinery either directly or indirectly via cofactor proteins (McKenna et al., 1999) (Figure 1.4A), and depending on the context of the cell and the promoter, ER either promotes or represses the expression of the target gene.

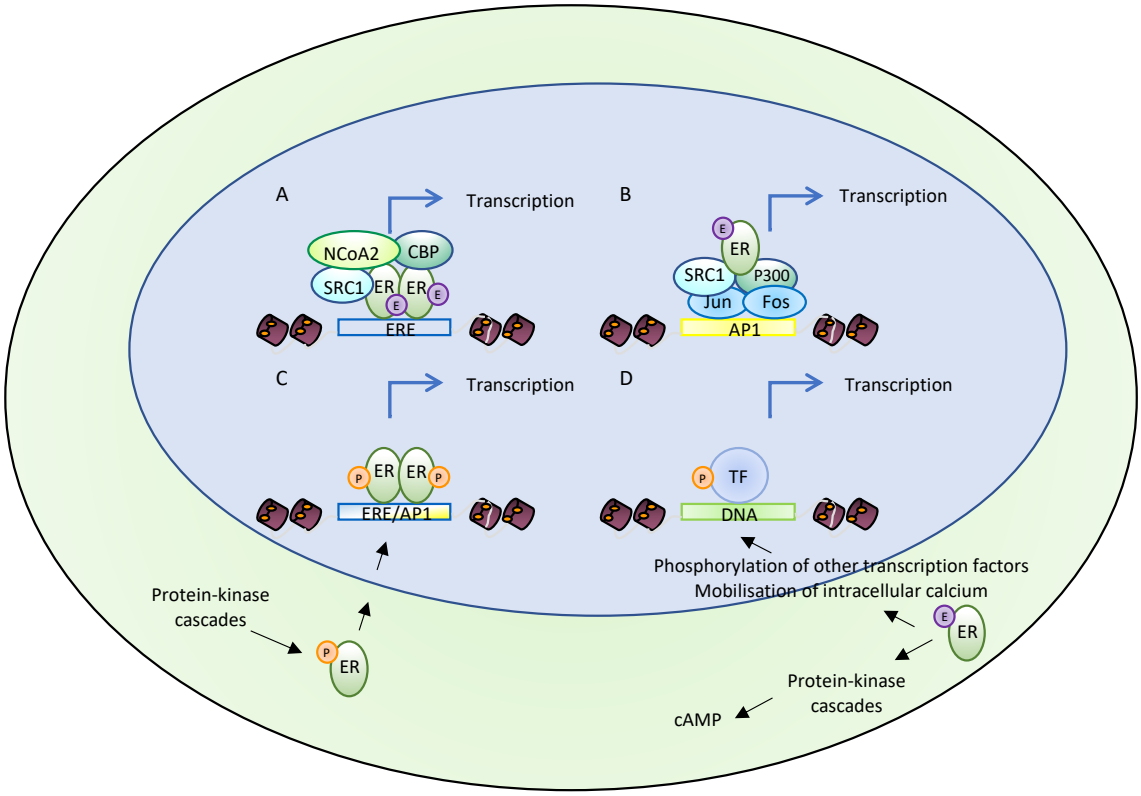

Figure 1.4: Mechanisms of ER activation and signalling. A. Classical ER signalling: Dimers of ER, activated through the binding of the ligand oestrogen, bind directly to EREs in the promoters of target genes, recruit cofactor proteins and transcription machinery, and alters the transcription of the gene. **B. Non-classical ER signalling:** Ligand-bound ER acts as a co-factor, tethered through protein-protein interactions to promote the transcription of genes without an ERE sequence in the promoter. **C. Ligand-independent signalling:** ER is activated through phosphorylation of sites in the AF-1 domain, altering the transcription of genes with EREs, in the absence of oestrogens. **D. Nongenomic actions of ER:** Membrane-bound ER, activated by oestrogens, activate protein-kinase cascades, resulting in altered signalling, e.g. through production of cAMP, or changes of gene expression through phosphorylation and activation of other transcription factors. (Figure adapted from (Bjornstrom and Sjoberg, 2005)

ER may also modulate gene expression through non-classical methods, without direct binding of the receptor to DNA at an ERE (Figure 1.4B). This may be termed indirect genomic signalling, or transcriptional cross talk (Gottlicher et al., 1998). This is where an ER dimer activated by oestrogen interacts with another DNA-bound transcription factor, and either stabilises this factor, or recruits further additional cofactors to the transcription initiation complex. For example, the transcription of genes such as those for cyclin D1 (Sabbah et al., 1999) and insulin-like growth factor (IGF-1) (Umayahara et al., 1994) is activated through the interaction of ER with Fos and Jun proteins at AP-1 binding sites. Similarly, ER recruits additional cofactors to promote transcription when it interacts with the cofactor Sp1 (Scholz et al., 1998, Porter et al., 1997), which then activates the transcription of genes such as c-*fos*, and *CCND1*. This mechanism explains how oestrogen may regulate target genes that do not contain an ERE in its regulatory sequence, as approximately one third of the human genes regulated by ER do not contain EREs (O'Lone et al., 2004).

Whether by the classical method or the indirect route, ER-mediated activation of transcription in response to oestrogen is complex, as the ability of ER to regulate gene transcription is influenced by the activity of multiple cofactor proteins. The most well-characterised of these are coactivators and corepressors from the p160 families. These include steroid receptor coactivator-1 (SRC1/NCoA1), transcriptional intermediary factor-2 (TIF2/NCoA2), amplified in breast cancer 1 (AIB1/NCoA3), and nuclear hormone receptor-corepressor (NCoR) (Onate et al., 1995, Hong et al., 1996, Anzick et al., 1997, Chen and Evans, 1995). In the absence of oestrogen, corepressors such as NCoR bind to ER, and recruit histone deacetylases (HDACs) (Jones and Shi, 2003) which by creating a tighter chromatin conformation, represses transcription. When oestrogen binds to ER, a docking site within the AF-2 domain of ER interacts with the LxxLL motif of these co-regulatory proteins. The p160 coactivators are able to recruit histone acetylases (HATs) and histone methyltransferases (HMTs) to the ER transcriptional complex (Chen et al., 2000a), which then increase the accessibility of chromatin for transcription. Other cofactors such as CREB-binding protein (CBP) and p300 which also have intrinsic HAT activity (Chen et al., 1997) also play a role in initiating transcription in this way, and have been shown to interact with ER via the p160 proteins in a hormone-dependent manner (Hanstein et al., 1996). The binding position of the ER transcriptional complex is

determined by further cofactors that interact with ER, such as the forkhead protein FOXA1 (Cirillo and Zaret, 2004, Carroll et al., 2005). These pioneer factors can directly bind condensed chromatin, bookmarking the promoter, which then allows ER to bind. The actions of the ER transcription complex then allow RNA polymerase II and transcription machinery to bind and initiate transcription.

ER may also be activated in a ligand-independent manner to act on the genome (Figures 1.4C and 1.5). ER has been shown to be activated through growth factor signalling pathways, such as by epidermal growth factor (EGF) (Ignar-Trowbridge et al., 1992) and insulin-like growth factor (IGF-1) (Ma et al., 1994). This is mediated through the phosphorylation of ER at different sites within AF-1. For example, serine-118 may be phosphorylated by mitogen-activated protein kinase (MAPK) and induce transcriptional activity (Kato et al., 1995). Similarly, the ribosomal S6 kinase (p90RSK), when activated by growth factor signalling, is able to phosphorylate ER at serine-167 and promote transcription (Joel et al., 1998), and thus ER may be activated as part of the Ras-MAPK cascade of growth factor signalling pathways. The PI3K-AKT-mTOR pathway, another important route of growth factor signalling, can also activate ER through phosphorylation at the serine-167 residue, resulting in increased ER-genomic activity (Campbell et al., 2001). The ligands of G-protein-coupled receptors (GPCR) that activate adenylyl cyclase can lead to an ER phosphorylation event at serine-236 that causes its dimerization through protein kinase A (PKA). This same kinase can phosphorylate the serine-305 residue in the hinge region, which has been suggested to promote ER binding to an alternate set of binding sites to those mediated by oestradiol activation (de Leeuw et al., 2013). ER can also be phosphorylated via CDK2-Cyclin A and this interaction has been shown to enhance ER-dependent transcription (Rogatsky et al., 1999). The interplay between growth factor signalling pathways and ER is implicated in the mechanisms of endocrine resistance, and will be discussed in more detail in Section 1.3.3

Finally, there is evidence that oestrogen has non-genomic actions, such as stimulating cyclic adenosine monophosphate (cAMP) production (Aronica et al., 1994), and mobilising intracellular calcium (Improta-Brears et al., 1999) (Figure 1.4D). These actions are too rapid to be accounted for by the process of gene transcription, and it has been

suggested that they are mediated through a subgroup of ERs localised to the plasma membrane (Razandi et al., 1999), although controversy exists about this. It is likely that ERs at the plasma membrane, in association with multiple other signalling molecules also present in this location, mediate the nongenomic actions of oestrogen (Kousteni et al., 2001). However, the clinical role that membrane-associated ER signalling plays in breast cancer remains elusive.

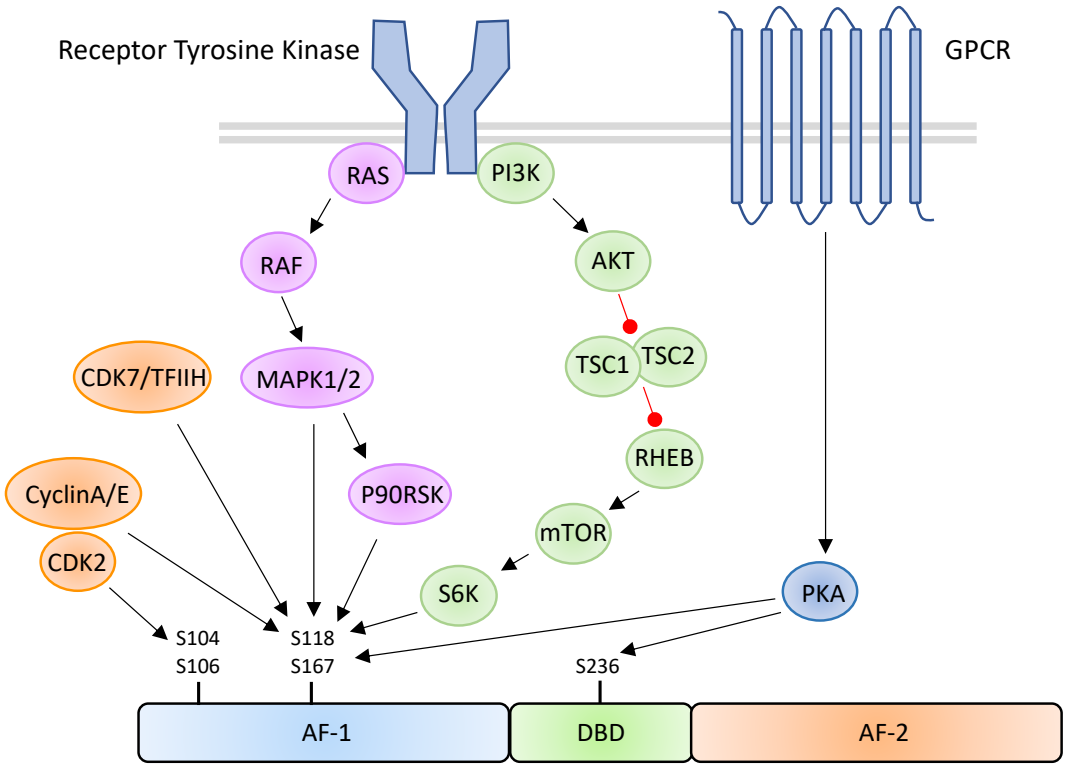

Figure 1.5: Post-translational modifications affecting ER activity. Several receptor tyrosine kinases are implicated in the activation of ER. Their downstream signalling pathways such as Ras-Raf-MAPK can phosphorylate ER at Ser118, leading to ligand-independent activity. Similarly, stimulation of the PI3K-AKT-mTOR pathway downstream of receptor tyrosine kinases can activate ER in a ligand-independent manner via phosphorylation at Ser167. ER may also be activated through pathways downstream of G-protein coupled receptors (GPCR) activating PKA, which has also been shown to phosphorylate ER. ER may also be phosphorylated and activated via cyclin-dependent kinases (CDKs), such as the CDK2-Cyclin A complex, or the CDK7-TFIIH complex, although this latter one is oestrogen-dependent (Figure adapted from (Ribas et al., 2018)

1.2.2 Role of ER and oestrogens in breast carcinogenesis

The molecular mechanisms of how oestrogen and oestrogen-mediated ER signalling contribute to the development of breast cancer continue to be investigated to this day. One widely accepted model of carcinogenesis is that stimuli that drive increased proliferation result in the accumulation of multiple genetic errors induced through the process of cell division, and this promotes the transformation from normal to malignant cells (Preston-Martin et al., 1990). Furthermore, factors that result in altered cell cycle control, and inhibition of apoptosis will also contribute to carcinogenesis, as these are some of the hallmarks of cancer.

Oestrogen and oestrogen-mediated ER signalling have been shown to play a role in each of these pathways that contribute to breast carcinogenesis. There are several transcriptional targets of ER that promote proliferation in response to oestrogen stimulation, such as Hes family basic helix-loop-helix transcription factor 6 (Hes-6) (Hartman et al., 2009), or the *LRP16* gene (Zhao et al., 2005). Oestrogen-activated ER also plays a role in non-transcriptional signal transduction pathways that lead to proliferation, such as activation of the PI3K-AKT-mTOR axis that can promote cell growth of breast cancer cells (Lee et al., 2005). Oestrogen-mediated ER signalling is a key contributor to the loss of cell cycle control seen in breast cancer. Exit from the quiescent phase of G_0 is achieved through the formation of cyclin D-CDK4/6 complexes, which phosphorylate Rb and release E2F transcription factors. These activate the expression of S-phase promoting genes, such as *CCNE1*. The expression of cyclin D1 is upregulated in response to oestrogen-mediated ER signalling (Sabbah et al., 1999), representing a key pathway by which oestrogens are able to stimulate progression through the cell cycle, and thus promote proliferation.

ER signalling is also able to promote cell survival by inhibiting apoptosis. Studies have demonstrated that in the presence of oestrogen, ER can block the induction of pro-apoptotic target genes, which are usually induced in response to p53 signalling (Bailey et al., 2012). Oestrogens have also been shown to increase the expression levels of the antiapoptotic protein Bcl-2 in breast cancer cells (Gompel et al., 2000). As such it can be seen that oestrogen and ER can play a myriad of roles that can promote breast carcinogenesis.

1.3 Endocrine resistance

As discussed in Section 1.1.5.5, the pivotal role that oestrogens and ER play in the development of breast cancer has been utilised clinically by developing agents that target oestrogen and ER to treat ER-positive breast cancer. Unfortunately, resistance to endocrine therapy remains a significant problem. This may be in the adjuvant setting, where resistance is seen as relapse or recurrence during or after completion of adjuvant endocrine setting. Alternatively, resistance to endocrine treatment can be seen in the neoadjuvant setting, manifesting either as a lack of response early in treatment, suggesting *de novo* resistance, or after a period of initial response, suggesting acquired resistance. It has been suggested that as many as 40-50% of all patients with ER-positive breast cancer will relapse following adjuvant endocrine therapy (Ma et al., 2009), and this poses a significant clinical problem. As discussed earlier, in general endocrine therapies are better tolerated by patients than other therapies with respect to their side-effect and safety profiles. As a result, in the often older, frailer patient encountered in the relapse setting, their treatment options may be significantly limited if they no longer respond to endocrine treatment, and are not fit enough to tolerate chemotherapies or targeted treatments. As such, the mechanisms by which ER-positive tumours develop endocrine resistance are subject to intense study, as if these mechanisms can be targeted, this would provide another avenue of treatment for patients suffering from relapse. Some of these mechanisms are outlined below, focusing predominantly on those seen in acquired resistance, as the ones relevant to the topic of this project.

1.3.1 *ESR1* mutations

Mutations within the *ESR1* gene have been described for many years, but as their prevalence in primary disease is rare, their clinical significance was not initially considered. However, more recently sequencing of metastatic ER-positive tumours has identified point mutations that may play a role in the development of acquired resistance following endocrine therapy, with prevalence rates of 15-20% (Jeselsohn et al., 2015). The majority of the mutations are located in the LBD (Y537N/C/S, and D538G) (Merenbakh-Lamin et al., 2013, Robinson et al., 2013). Functional studies of these mutants using ectopic overexpression demonstrate that the mutations confer constitutive ligand-independent activity to ER, by increasing the stability of the agonist

conformation of ER (Toy et al., 2013). This same study by Toy et al additionally showed that this constitutive activity was maintained even in the presence of tamoxifen or fulvestrant. More recently BC cell lines have been developed that have been adapted to long-term oestrogen deprived (LTED) conditions, and these LTED cells have been found to harbour mutations in ER (Martin et al., 2017). This work demonstrated that the mutant ER acts on a comparable set of EREs as the ligand-dependent wild-type (wt) ER. Furthermore, the mutant ER was found to interact with a similar portfolio of proteins, but with increased association with certain proteins such as FOXA1, which could contribute to the cells' ability to proliferate independently of oestrogen. Furthermore, multiple studies have demonstrated enrichment for *ESR1* mutations following endocrine therapy, particularly after AI treatment. One large whole-exome sequencing study of ER-positive/HER2-negative breast cancers found *ESR1* mutations as one of 32 genes significantly enriched in metastases (Razavi et al., 2018). In one study of patients treated with AIs in the metastatic setting, *ESR1* mutations were detected in 38% of samples (Schiavon et al., 2015), while in another patients with a detectable *ESR1* mutations showed reduced progression-free survival with AI treatment, as well as *ESR1* mutations being enriched in the metastatic cohort (Zundelevich et al., 2020). These data suggest that AI treatment may promote *ESR1* mutation acquisition, and that patients with an *ESR1* mutation have poorer outcomes with AI therapy.

While mutations in *ESR1* may contribute to some of the acquired resistance to AIs seen in advanced breast cancer (Jeselsohn et al., 2014), the low prevalence in primary breast cancer (Cancer Genome Atlas, 2012) suggests that this is not a significant mechanism of *de novo* resistance. Furthermore, although *ESR1* mutations are enriched for in advanced disease as described above, the majority of patients do not harbour an *ESR1* mutation, and therefore there must be alternate mechanisms of acquired resistance also in place.

1.3.2 Loss of ER expression

A proportion of patients will develop acquired resistance due to loss of ER expression, demonstrating a greater reliance on other proliferative pathways for growth. However, this is only seen in a proportion (10-20%) of ER-positive endocrine-resistant disease (Ellis et al., 2008, Hoefnagel et al., 2012). Furthermore, most ER-positive breast cancers that later recur remain ER-positive on biopsy, and continue to show response to second and

third line endocrine therapies, implying that tumour heterogeneity with loss of ER-positive cells, or selective growth of the ER-negative cell population, are not major contributors to acquired resistance.

1.3.3 Altered cross-talk between ER and growth factor pathways

As discussed in Section 1.3.3 and illustrated in Figure 1.5, there is considerable bi-directional cross-talk between ER and many growth factor pathways, and these have been implicated in contributing to resistance to endocrine therapy. The most commonly implied mechanism of action is the ability of growth factor receptors to activate ER in the absence of oestrogen (Clarke et al., 1989). Furthermore, many of the signal transduction pathways activated by growth factor receptors make use of kinase pathways such as Ras-Raf-MAPK, or PI3K-AKT-mTOR, which can activate ER by phosphorylation of the AF-1 domain (Figure 1.5). This may account for some of the resistance seen to AIs and SERMs, but may not be sufficient to explain resistance to SERDs, which degrade ER reducing ER-signalling, whether activated or not. The most studied pathways linked with endocrine resistance are epidermal growth factor receptor (EGFR) and HER2 signalling, and the PI3K-AKT-mTOR pathway.

ER-positive breast cancers that overexpress HER2 often demonstrate a reduced, although still clinically significant response to endocrine therapy (De Laurentiis et al., 2005). Further studies have demonstrated that EGF signalling can induce an ER-transcriptional programme that is distinct from the typical ER cistrome, that could provide a mechanism to evade endocrine therapy by facilitating proliferation independent of oestrogen signalling (Lupien et al., 2010). This is further supported by evidence of increased expression levels of EGFR and HER2 in breast cancer models of tamoxifen or AI resistance (Knowlden et al., 2003, Brodie et al., 2007). However, there has been little success in targeting tyrosine kinase signalling in clinical studies of endocrine-resistant disease (Burstein et al., 2014, Smith et al., 2007), the exception being HER2, where it has been shown that a combination of endocrine treatment and HER2-targeted therapy does provide benefit in ER-positive/HER2-positive patients (Koeberle et al., 2011, Marcom et al., 2007).

The PI3K-AKT-mTOR pathway is involved in the regulation of cell proliferation and survival, and in energy metabolism. It is the most frequently altered pathway in breast cancer (Miller et al., 2011, Tokunaga et al., 2008) whether this is through mutation/amplification of genes such as *PIK3CA* or *AKT1*, overexpression of receptors that signal through this pathway, such as EGFR or HER2, overexpression or activation of the downstream signalling components of the pathway such as *AKT*, or loss of the regulators of the pathway, such as phosphatase and tensin homolog (*PTEN*). PI3K is activated by many growth factor receptors and G-protein-coupled receptors (GPCRs), and Figure 1.6 illustrates the cascade initiated upon activation, resulting in the promotion of proliferation, angiogenesis, and transcription. Aside from these roles, there is significant crosstalk between the PI3K pathway and ER. As discussed previously, activation of the PI3K pathway can lead directly to activation of ER (through phosphorylation at Ser-167 by AKT or S6K) to promote ER-mediated, ligand-independent transcription. PI3K also promotes phosphorylation and activation of the transcription factor c-Jun (Logan et al., 1997), which then can complex with c-Fos to form the AP-1 complex, which can aid ER-mediated transcription (Petz et al., 2002). Many of the genes that are under ER-transcriptional control are components of signalling pathways that in turn activate PI3K, resulting in a positive feedback loop. Studies investigating this pathway have demonstrated causality between PI3K activation and resistance to endocrine therapy. Overexpression of oncogenes that activate PI3K signalling such as *HER2* or *AKT* (Shou et al., 2004, Campbell et al., 2001), or knockdown of *PTEN* that relieves PI3K pathway inhibition (Miller et al., 2009) have shown that this activation of PI3K can confer resistance to endocrine therapy, and oestrogen deprivation. Furthermore, ER-positive cell lines cultured under oestrogen deprived conditions have shown amplification of PI3K signalling (Miller et al., 2010). This same study demonstrated that treatment with inhibitors of the PI3K pathway of these ER-positive cell lines in LTED culture would then inhibit growth.

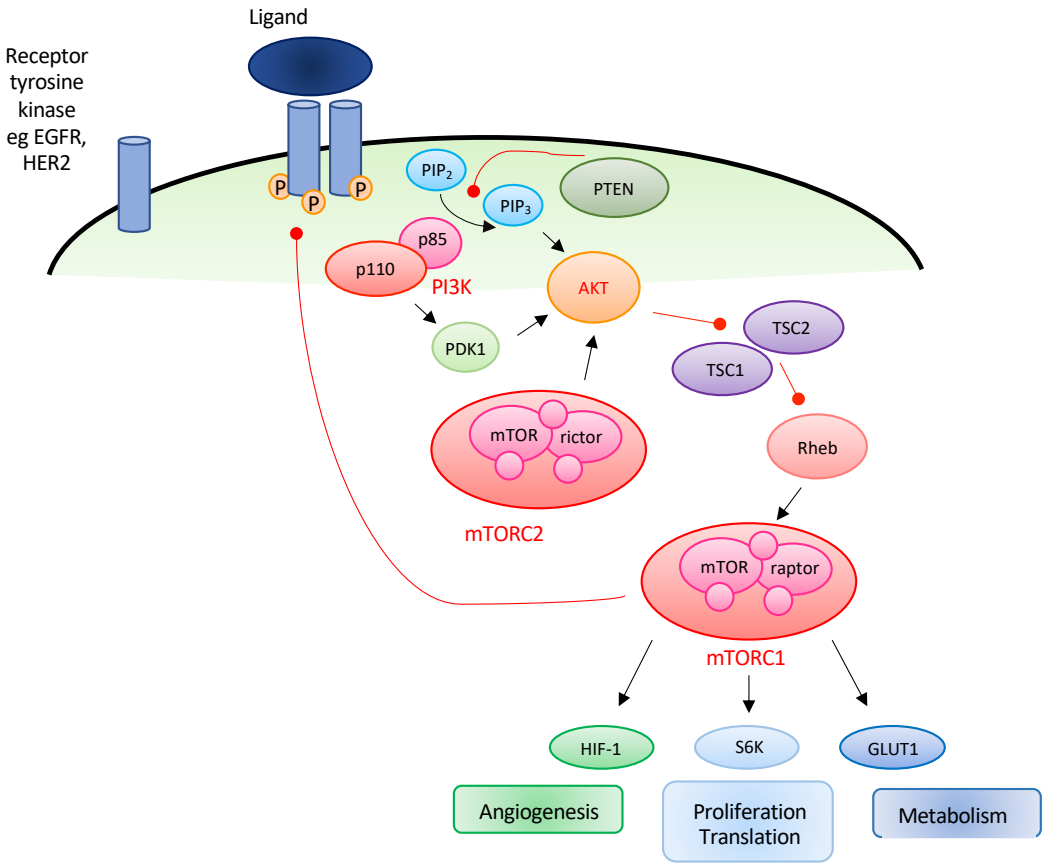

Figure 1.6: Schematic of PI3K-AKT-mTOR pathway. Activation of the pathway is initiated through various ligands binding to receptor tyrosine kinases. The receptor dimerizes, is autophosphorylated, and recruits adaptor proteins (not shown here) such as insulin receptor substrate 1 (IRS1) and IRS2. These recruit the PI3K heterodimer, formed of the p110 catalytic subunit, and the p85 regulatory subunit. PI3K then phosphorylates the signalling messenger phosphatidylinositol-4,5-bisphosphate (PIP_2) to phosphatidylinositol-3,4,4-trisphosphate (PIP_3), which then leads to the phosphorylation of AKT, the next significant kinase in this pathway. The activation of AKT inhibits tuberous sclerosis complex 1/2 (TSC1/2). mTOR is a serine/threonine protein kinase, and refers to two different complexes, mTORC1 and mTORC2, depending on which cofactors mTOR associates with (regulatory-associated protein of mTOR (raptor) and rapamycin-insensitive companion of mTOR (rictor) respectively). The inhibition of TSC1/2 by AKT results in the release of Rheb from TSC1/2 inhibition, allowing it to activate mTORC1. mTORC1 can then act to promote protein synthesis, proliferation, angiogenesis, and metabolic pathways. mTORC1 also acts to inhibit IRS1/2, thus providing negative feedback on the pathway.
PI3K may also lead to AKT activation through activating 3-phosphoinositide-dependent protein kinase 1 (PDK1), which then activates AKT. mTORC2 can also act upstream of mTORC1, by activating AKT. The tumour suppressor PTEN acts in direct opposition to PI3K, by dephosphorylating PIP_3 to PIP_2, thus counteracting the whole pathway. (Figure adapted from (McAuliffe et al., 2010)

However, the clinical outcome of the crosstalk between ER and the PI3K pathway is clearly complex. For example, despite the fact that genetic mutations that activate the PI3K pathway are seen in ~70% of all breast cancers (Lee et al., 2015), and in ~40% of the ER-positive subset (Vasan et al., 2019b), which would be expected to lead to increased pro-tumourigenic signalling, *PIK3CA* mutations have been shown to be associated with a good long-term outcome in primary ER-positive disease (Loi et al., 2010). Conversely, in the setting of advanced breast cancer, *PIK3CA* mutations are an adverse prognostic factor (Xu et al., 2014, Mollon et al., 2020). While the BOLERO-2 trial, which evaluated the addition of everolimus (an mTOR-targeted therapy) to a steroidal AI in women who had relapsed or progressive advanced ER-positive breast cancer, showed an improvement in progression free survival (Baselga et al., 2012), the HORIZON trial which evaluated another mTOR inhibitor, temsirolimus, did not (Wolff et al., 2013). The BELLE2 study sought to target the cross-talk between ER and PI3K by utilising combination therapy of buparlisib (a pan-PI3K inhibitor) and fulvestrant (Baselga et al., 2017, Campone et al., 2018). While a small but significant increase in progression-free survival was seen, there was no significant increase in overall survival, and the combination treatment was not well tolerated. Interestingly, a prospective analysis was performed of the patients' *PIK3CA* activation status using circulating tumour DNA (ctDNA) prior to treatment, and in the subset with PI3K activating mutations, the patients received a greater benefit from combination therapy. Trials of AKT inhibitors have also not been definitive. A phase 2 trial of the AKT inhibitor MK2206 showed limited clinical activity (Xing et al., 2019), but combination therapy of the AKT inhibitor capivasertib with fulvestrant has been shown to improve progression-free survival (Jones et al., 2020). This variance in results may in part be due to feedback loops within the pathway. Inhibiting mTORC1 will relieve the inhibition on PI3K and AKT, which may then signal through alternative routes such as the MAPK pathway (Carracedo et al., 2008). Inhibition of PI3K or AKT can act to upregulate pro-survival growth factor receptors (Chakrabarty et al., 2012, Chandarlapaty et al., 2011). It may be that more specific inhibitors of the PI3K-AKT-mTOR pathway are required, and promising results were seen in the SOLAR-1 (Andre et al., 2019) and SANDPIPER trials (Baselga et al., 2018), both investigating combination therapy of endocrine treatment and a PI3Kα inhibitor (alpelisib and taselisib, respectively, discussed further in Section 1.6.1). The inconsistency in the ability to translate pre-clinical data to clinically meaningful advances

may reflect the inability of the laboratory models to replicate the heterogeneity or the microenvironment of breast cancers *in vivo.*

1.3.4 Cell cycle dysregulation

Endocrine therapy has been shown to have both cytostatic and cytotoxic effects, with reduced proliferation, reduced rate of growth, and increased induction of apoptosis, by causing cell cycle arrest in the G_1 phase (Dowsett et al., 2006). As such, aberrant expression of molecules that promote the G_1 to S phase transition have been associated with endocrine therapy resistance. Overexpression of *MYC* (Venditti et al., 2002), *CCND1* (Hui et al., 2002), and *CCNE1* (Dhillon and Mudryj, 2002) have all been shown to confer endocrine resistance *in vitro*. Clinically, there is also evidence that overexpression of these factors is associated with tamoxifen resistance in patients (Butt et al., 2005). As well as overexpression of molecules that promote progression through the cell cycle, decreased expression of factors that place checks on cell cycle progression is also associated with endocrine resistance. Inactivation of Rb (Bosco et al., 2007), and decreased expression of p21 or p27, which inhibit CDKs, confer endocrine resistance *in vitro* (Cariou et al., 2000).

As discussed in Section 1.1.5.4, the targeting of cell cycle machinery has been successful through the development of CDK4/6 inhibitors, which have nullified one route that cancer cells may utilise to overcome endocrine therapy-induced cell cycle arrest. However, the development of resistance to these agents is considered near inevitable (McCartney et al., 2019), with pre-clinical work suggesting that tumour cell re-wiring occurs on the development of palbociclib resistance, and highlighting CDK7, ErbB signalling, and G_2/M checkpoint proteins as potential areas of dependence that could be targeted (Pancholi et al., 2020).

1.4 Tumour heterogeneity

One of the challenges in tackling endocrine resistance is the heterogeneity displayed in breast cancers. The very nature of cancer evolution from a non-malignant cell to a malignant one through the acquisition of alterations conferring the hallmarks of cancer is dynamic, and fosters the development of a tumour made of cells that display a variety

of molecular changes, and could therefore have different levels of sensitivity to antitumour agents.

Tumour heterogeneity may be divided into intertumoural heterogeneity – the differences between patients who have tumours of the same histological classification – and intratumoural heterogeneity, which refers to the variety seen between tumour cells in the same patient. Intratumoural heterogeneity may be further subdivided into spatial heterogeneity, where diverse molecular alterations are seen in different tumour sites, or even within the same site, and temporal heterogeneity, which describes how a tumour may change and evolve over time.

The observation that tumours can display spatial and temporal heterogeneity lends credence to the view of cancer as a dynamic disease, and that it is partly through this heterogeneous evolution that drug resistance, including endocrine resistance, may be developed.

1.4.1 Mechanisms conferring intratumoural heterogeneity

One potential cause of heterogeneity is that cancers are inherently genomically unstable, whether this is through endogenous defects in DNA repair pathways, or through exposure to carcinogenic substances such as cigarette smoke, asbestos, or even chemotherapeutic agents. As such cancer cells have a high mutation rate, although the hypothesis that cancer transformation relies on an increased mutation rate has not been proven. Nevertheless, the fact remains that many cancers display changes to increase the overall burden of mutation. For example, the enzyme APOBEC3B, which normally plays a role in deaminating cytosine to uracil to hyperedit cDNA intermediates and thus restrict retroviruses, has been shown to be co-opted by cancers for its mutagenic properties (Kuong and Loeb, 2013). The expression of *APOBEC3B* is elevated in many forms of cancer in comparison to lower levels seen in normal tissues (Burns et al., 2013), and a whole-exome sequencing study of approximately 1500 ER-positive breast cancer samples demonstrated a link between poorer disease-free survival and overall survival and high levels of APOBEC3B (Sieuwerts et al., 2017). This tendency of malignant cells to seek out mechanisms to increase their overall variability is therefore one mechanism that contributes to intratumoural heterogeneity.

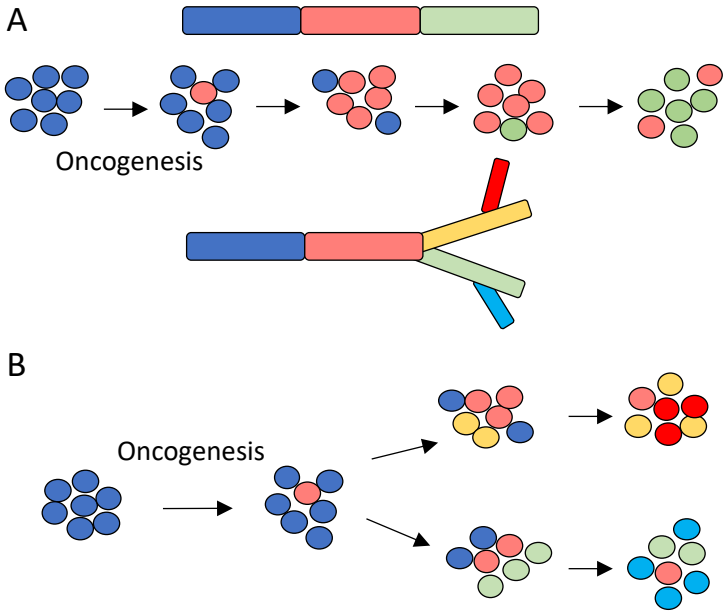

Figure 1.7: Comparison of selective vs branched evolution models. Oncogenesis causes transformation of a non-malignant cell **(a)** In the linear selection model, genetic instability results in the new clones. When a clone develops a survival advantage as a result of this, it outcompetes the previous generations, leading to sequential evolution. **(b)** In the branched evolution model, the genetic instability allows for the development of multiple subclonal populations, which can diverge from the evolution timeline at different times, conferring heterogeneity. (Figure adapted from (Dagogo-Jack and Shaw, 2018)

Another theory for the development of intratumoural heterogeneity, which utilises genomic instability as a contributing factor, is that of branching evolution of the tumour. The classical clonal evolution and/or selection model postulates that an acquired alteration in a normal cell confers a survival or growth advantage, and that these changes continue in a stochastic manner until the cell is transformed into a malignant cell and proliferates (Nowell, 1976). As the cancer cells are genomically unstable, they continue to mutate and diverse subpopulations emerge, of which one subclone will outcompete and replace the original malignant cells, until this population is itself taken over by sequential subclones harbouring advantageous mutations. An alternative theory to this is that of branching evolution, where genomic instability results in the proliferation of multiple, genetically diverse, subclonal populations, arising from a common ancestral clone, which may diverge from the evolutionary tree at different time points, and in different sites. As the schematic in Figure 1.7 demonstrates, this mechanism of evolution is more likely to result in a heterogeneous tumour, and is seen

more commonly in solid malignancies than in certain haematological cancers that demonstrate a more linear pattern (Hiley et al., 2014).

Hence, the inherent genomic instability of tumours, together with the dynamic nature of the cancer disease process, are the main contributors to the development of intratumoural heterogeneity.

1.4.2 Spatial heterogeneity

Spatial heterogeneity may be seen between metastatic deposits at different sites, different areas within one organ as in multi-focal disease, or even between different cells within the same tumour. It has been demonstrated through multiregional sampling, that is, biopsy sampling of many regions within a single tumour, in a variety of cancer types (Jamal-Hanjani et al., 2017, Gerlinger et al., 2014, Yates et al., 2015). Intratumour variation has also been shown in a landmark study utilising single-nucleus sequencing of cells from TNBC specimens that revealed three distinct clonal subpopulations (Navin et al., 2011). Spatial heterogeneity may be displayed as different key oncogenic drivers in different regions of the tumour, or as uniform distribution of vital drivers with an unequal display of additional molecular changes (Harbst et al., 2016). Spatial heterogeneity has also been demonstrated in multifocal tumours, for example where multiregional sampling of separate foci of multifocal breast cancers confirmed that they were clonally related, but had also developed subclonal private mutations (Yates et al., 2015). Spatial heterogeneity between sites adds in further factors that may enhance diversity; firstly that the time at which the metastasis occurred may influence genetic variance, as early spread would be hypothesised to display more heterogeneity; and secondly that the interaction of the malignant cells with the tumour microenvironment at distinct sites could promote genetic diversity.

The role that spatial heterogeneity plays in resistance is key, as multiregional sampling studies have shown that the uneven distribution of driver or passenger mutations across the tumour can lead to the misrepresentation of subclonal mutations as clonal (Jamal-Hanjani et al., 2017) if fewer samples are taken. Therefore, this heterogeneous gene expression pattern may affect both the use of gene expression signatures for prognostication (as the calculations may vary depending on which section of the tumour

is sampled) and the treatment decisions for therapy targeting key drivers. Unfortunately, it is not feasible to perform multiregional sampling for all tumours, as surgical specimen sizes may not be large enough for this in early disease, and in advanced disease surgical resection may not be indicated, and carrying out multiple biopsies carries its own risk.

1.4.3 Temporal heterogeneity

Temporal heterogeneity, the changing genetic make-up of a tumour over time, has been demonstrated on studies utilising serial biopsies. In particular, temporal changes often occur in response to a selection pressure, such as chemotherapy (Murugaesu et al., 2015), or targeted therapies (Gainor et al., 2016). Many of the insights into temporal heterogeneity have been observed as a result of monitoring response to targeted treatments, as these agents aim to exploit a key driver vulnerability. Often there is a significant response to initial treatment, followed by relapse a few years later, with resistance being mediated through the acquisition of mutations and cross-talk in signalling pathways. While these resistance mechanisms are considered as acquired rather than *de novo*, studies have revealed that certain mutations may be in place at low variant allele frequencies (Yu et al., 2014), or specific pathway activity may be upregulated in response to the targeted therapy.

Temporal heterogeneity is a feature of endocrine resistance because, as discussed in Section 1.3, exposure to endocrine agents can induce the adaptations seen in such as *ESR1* mutations and cross-talk between signalling pathways. Furthermore, endocrine agents have been shown to induce significant growth inhibition and cell cycle arrest (Otto et al., 1996). Following 5-10 years of endocrine treatment, these agents may drive cells into a growth arrest that becomes epigenetically imprinted, resulting in tumour dormancy, only to relapse many years later (Clarke et al., 2015). Consequently, there is a need to monitor patients over time to enable early detection of resistance, using a method both acceptable to the patient and capable of detecting genetic variations, and this need may be met by the use of sampling circulating cell-free tumour DNA (ctDNA) from blood samples. This has shown promising results in a study examining plasma samples from the PALOMA III trial (O'Leary et al., 2021). While no predictive genomic alterations were identified using the ctDNA in the plasma, a high ctDNA fraction, *TP53*

mutations, and *FGFR1* amplification were found to be independently associated with a risk of early relapse in both the fulvestrant only, and fulvestrant plus palbociclib groups. This may therefore be a promising technique for the ongoing monitoring of tumours to detect temporal heterogeneity that may predispose to resistance.

1.5 Different models of cancer

Given the wide range of spatial and temporal heterogeneity displayed in cancer, and the difficulties seen in attempts to translate *in vitro* work on endocrine resistance into the clinic, it is clear that better models are needed at the bench that more accurately reflect the complexities displayed by tumours. The ideal model of breast cancer for the discovery of new therapeutic targets should recapitulate intratumoural heterogeneity, demonstrate the gradients of hypoxia and nutrients seen in three-dimensional tumours, be reproducible, and display the interactions seen between the tumour, and the tumour microenvironment (TME).

Many of the experiments investigating breast cancer, and endocrine resistance, thus far have been performed using cell lines cultured *in vitro* in two dimensions. While these have provided important insights, and have the benefit of being scalable to high-throughput assays, reproducible, and relatively user-friendly to both set up and to analyse, 2D models are not able to accurately display the complexity of signalling within a 3D tumour, or its dynamic interactions with the TME. In 2D culture, the cells grow as a flat monolayer, and so natural cell shape is altered, and may lose polarity (Mabry et al., 2016). As a result of the unnatural growth pattern, gene expression, especially those involved in cell adhesion, proliferation, and survival, may be altered (Melissaridou et al., 2019). The ability to model tumour heterogeneity is limited, as all cells have equal access to nutrient medium (Costa et al., 2016). Finally, without growing in a 3D environment, 2D models cannot accurately react and respond to mechanical or biochemical stimuli which may come from any direction, as *in vivo* (Riedl et al., 2017). As such, various methods have been developed to enable 3D culture systems, to study cells in a spatially relevant model that preserves cell-cell and cell-matrix interactions.

1.5.1 Tumour tissue explants

Tumour tissue explants are one of the first 3D models of cancer (Freeman and Hoffman, 1986), and involves utilising tumour biopsy tissue, removal of fat and necrotic tissue, and placing it on a tissue culture plate coated with matrix (Figure 1.8A). The tumour adheres or becomes embedded in the matrix, and grows within media, enabling the architecture of the tumour to be preserved and studied. However, this technique is limited due to the difficulty of maintaining the tumour in culture for prolonged periods without tissue degeneration and necrosis. Furthermore, there is a natural lack of reproducibility due to the heterogeneity of the donor tissue samples, and this technique does not lend itself to high-throughput drug discovery methods.

1.5.2 Xenografts

Xenografts offer the opportunity to study cancers in a living model. The definition of a xenograft is a tissue graft or an organ transplant derived from a species that is different to the recipient. When immortalised cell lines are engrafted, usually into an immunodeficient mouse model, they are able to organise into a solid tumour, co-opting the stromal tissue of the mouse to form the TME. However, it has been observed that the process of generating immortalised lines can result in the gain or loss of genetic information, variations in the ability to proliferate and invade, and loss of certain cell populations (Gillet et al., 2011). The development of patient derived xenograft (PDX) models is an attempt to circumvent this, and hopefully maintain the complex heterogeneity of tumours seen in the clinic. There are many different methodologies for generating PDX models, varying according to tumour type and implantation type. Overall, tumour samples, either from a primary tumour, or from fluid such as malignant ascites or pleural effusions, are implanted into an immunodeficient mouse, either as pieces, single-cell suspension, or in co-culture with fibroblasts and other cells necessary for the formation of the TME (Hidalgo et al., 2014). The tumour cells may be implanted heterotopically in the dorsal fat pad as shown in Figure 1.8B, or using the mouse mammary intraductal (MIND) model where breast cancer cells are injected directly into mouse mammary ducts (Behbod et al., 2009).

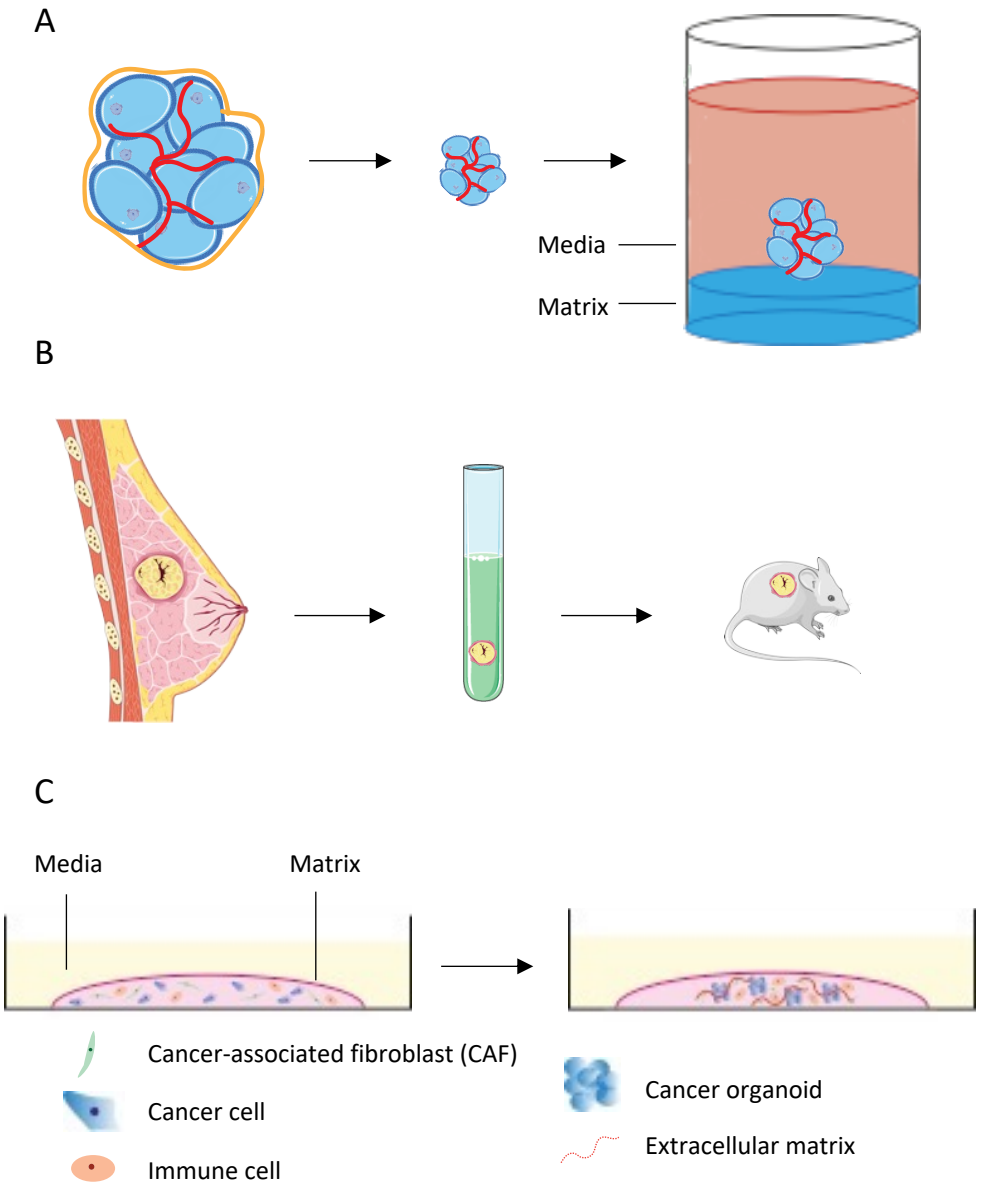

Figure 1.8. Cancer models (a) tumour explants. The tumour tissue is excised. The biopsy is processed to remove fat tissue, and the tumour is cut into small pieces. The pieces are then placed on or embedded in a matrix in a tissue culture plate. Media is added and the tumour is cultured. **(b) Patient-derived xenografts (PDXs)**. Tumour tissue from the patient is excised, processed, and cultured in media, before then being implanted into the animal model. **(c) Organoids.** Cancer cells are cultured within a matrix, with added media and associated cells such as cancer-associated fibroblasts and immune cells. The cells proliferate and self-organise to produce organoids of cancer cells surrounded by stromal cells and produce natural extracellular matrix. (Figure adapted from (Rodrigues et al., 2021)

The hypothesis underlying the development of PDX models is that these will be more representative of human cancer biology, as well as offering the potential for personalised precision oncology treatment based on the individual patient tumour. Work on establishing PDX models of breast cancer has demonstrated high fidelity between the PDX and the original patient tumour (Reyal et al., 2012). However, developing ER-positive PDX models has been challenging, with take rates as low as 2.5% seen for luminal tumours (Cottu et al., 2012). Furthermore, traditional engraftment of ER-positive tumours into mouse fat pads has been shown to induce basal differentiation, and the need of non-physiological hormone supplementation to grow (Sflomos et al., 2016). It has been possible to circumvent this through the use of a MIND approach, which also achieved a higher engraftment rate, but this is necessarily more labour-intensive, and takes several weeks or months for the tumours to establish. While PDX engraftment rates for ER-positive breast cancers have improved in more recent studies (9% for primary ER-positive tumours and 16% for metastatic cancers) (Guillen et al., 2021), and PDX models with features of endocrine resistance have been established in this study, the fact remains that PDX models pose significant ethical and cost challenges to be used in high-throughput drug discovery platforms.

1.5.3 Organoids

Classically organoids are defined as 3D tissue cultures generated by the proliferation and self-organisation of a progenitor stem cell (Drost and Clevers, 2018) predominantly grown within a scaffold or matrix structure to provide an environment for cell adhesion, proliferation, and differentiation, as demonstrated in Figure 1.8C. A scaffold can provide support for 3D organisation of tumour cells, and provide an opportunity to study cell-cell and cell-matrix interactions. An example is Matrigel, a common commercial biological scaffold derived from secreted basement membrane extracts of mouse sarcoma cells, which is rich in extracellular matrix (ECM) components, and several soluble factors. However, these factors do increase the variation in culture conditions between batches, and can therefore reduce the reproducibility of drug-discovery assays.

Tumour organoids are usually derived from multiple cells and can therefore recapitulate intratumoural heterogeneity due to their response and interaction with different environmental cues. As a result, patient-derived organoids (PDOs) can offer a bridging

gap in preclinical models of cancer between PDX models and 2D culture. Indeed, a landmark study succeeded in generating a biobank of PDOs from metastatic gastrointestinal tumours (Vlachogiannis et al., 2018). These organoids revealed high fidelity to the parent tumours, and were able to recapitulate spatial and temporal heterogeneity. Most strikingly, the PDOs were able demonstrate very high positive and negative predictive values in forecasting response to chemotherapy or targeted agents in the clinic. A similar biobank has been successfully set up from multiple subtypes of breast cancer (Sachs et al., 2018) which has the potential to bring personalised precision medicine to the treatment of breast cancer. However, the timeline of culture of organoids remains on the spectrum of weeks to months, and these organoids require several non-physiological supplementations to their growth media, which could feasibly confound the analysis of the signalling pathways and resistance mechanisms that are the subject of study.

1.5.4 Spheroids

Spheroids are another form of 3D cell culture, but rather than 3D shape developing over time according to genetic programming (as in organoids), an aggregation of tumour cells (usually of immortalised tumour cell lines), are encouraged to form into the 3D construct (Figure 1.9). While this method sacrifices some of the natural heterogeneity displayed in organoid production, it allows for the relatively rapid formation of 3D models that still display the characteristics of growth kinetics, signal pathway activity, and gene expression (Friedrich et al., 2009). Large spheroids (over 500 μm) also display gradients of oxygen, nutrients, and metabolic waste (Groebe and Mueller-Klieser, 1991, Swietach et al., 2008), and thus allow for the study of the effects of hypoxia (Meehan et al., 2017) and nutrient deprivation (Schroll et al., 2016) on gene expression and signalling pathway modulation.

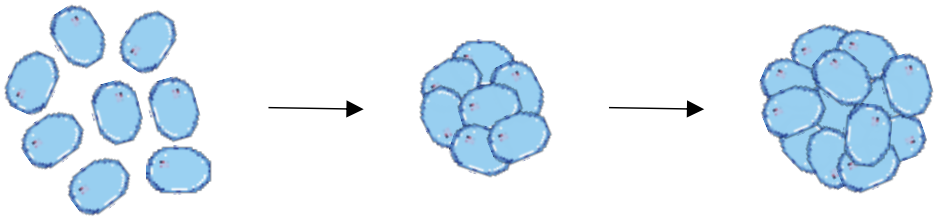

Figure 1.9. Schematic of spheroid development. Cancer cells in culture are subjected to forced aggregation, or may have aggregation enhancers added to form small spheroids. Following proliferation, dense larger spheroids, which exhibit oxygen and nutrient gradients, are formed to model tumour conditions in vivo. (Figure adapted from (Nath and Devi, 2016)

Furthermore, signalling pathways and gene expression have been shown to vary between cells grown in spheroids in comparison to 2D monolayers, with more accurate reflection of the signatures observed *in vivo* (Cesarz et al., 2016). Spheroids may be generated within a scaffold, or in a scaffold-free manner, and their complexity may be influenced by cell seeding density, coculture with stromal cells, duration of culture, and mechanism of generation. The fact that spheroids may be generated rapidly, over the course of days, in a uniform manner, and still recapitulate the heterogeneous features discussed have led to their common and widespread use in the study of tumour biology and high-throughput screening (Rodrigues et al., 2021), and some of the methods used to generate spheroids are outlined below and in Figure 1.10.

1.5.4.1 Matrix-on-top and matrix-embedded

This is a scaffold-based method where cells are either seeded on top of a solidified layer of matrix, with spontaneous aggregation of the cells to form spheroids (matrix-on-top) or the cells are seeded with liquid matrix, with embedding occurring upon matrix gelation (Figure 1.10A). While this method does allow for recovery of cells post culture, and offers the ability to study cell-matrix interactions, it often yields heterogeneous spheroids, and imaging and staining of the embedded spheroids can be challenging.

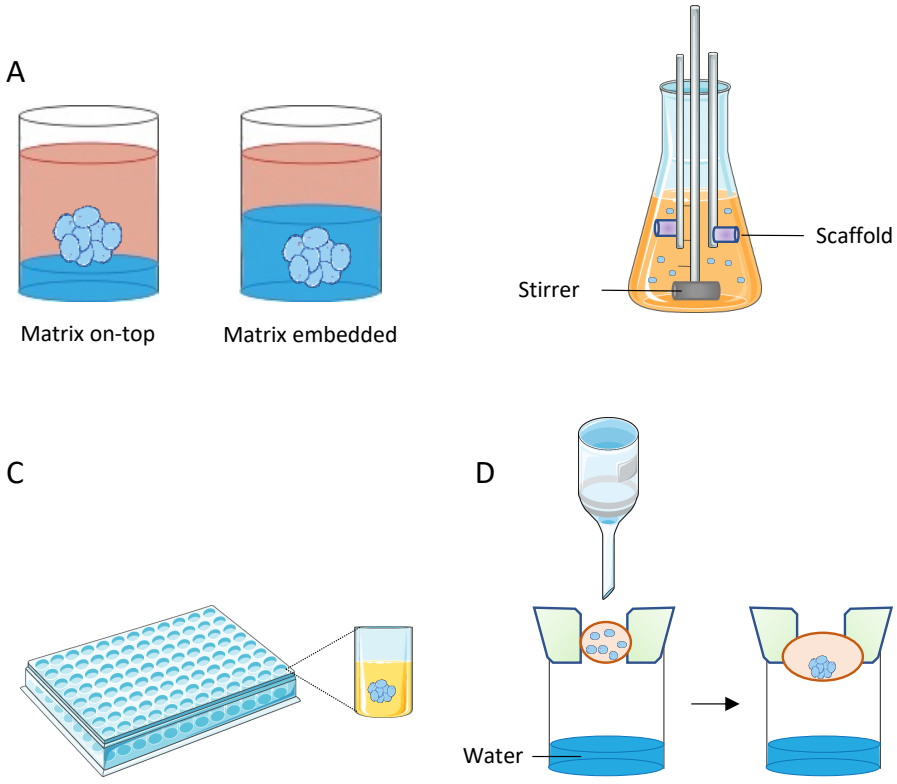

Figure 1.10. Methods of spheroid generation. (a) Matrix-on top or matrix embedded. Cancer cells are seeded on top of or within matrix, with spontaneous aggregation of the cells to form spheroids. **(b) Spinner flasks**. Stationary scaffolds within the flask form a base for the circulating tumour cells in the media to attach and form aggregates. **(c) Ultra-low attachment plates**. Each well of the plate is coated with an inert substrate. Cancer cells are seeded into the well, and then forced to aggregate through low speed centrifugation. **(d) Hanging drop method**. Droplets of cell suspension hang above the culture array plates, such that the cells aggregate into spheroids under the influence of gravity. (Figure adapted from (Finn et al., 2015)

1.5.4.2 Spinner flasks

The spinner flask method is often used for large-scale production of tumour spheroids. In this method the scaffold is stationary within a flask containing the cell suspension, and a magnetic stirrer ensure an ongoing flow of oxygen and nutrients through the culture medium (Figure 1.10B). The tumour cells flow across the scaffold to form spherical aggregates (Kunz-Schughart et al., 1998). However, the centrifugal force experienced due to the motion of the stirrer can have adverse effects on the physiology of the models (Lin and Chang, 2008).

1.5.4.3 Ultra-low attachment plates

This is a scaffold-free method that is able to generate a large number of spheroids in a relatively user-friendly manner in a limited space. The wells in ultra-low attachment plates are coated with an inert substrate that prevents cell attachment (Figure 1.10C). The cell suspension is added to the plates which are then centrifuged at a low speed to force them to aggregate into a 3D structure (Vinci et al., 2012). With this method, it is possible to perform endpoint analysis such as cell viability assays, in the same plate. However, this can generate heterogeneous spheroids, particularly if cells do attach in some wells but not in others.

1.5.4.4 Hanging drop method

This alternative scaffold-free technique involves suspending droplets of cell suspension from spheroid culture array plates, such that the droplets hang due to surface tension (Figure 1.10D). Under the effect of gravity, the cells in the suspension aggregate spontaneously to form spheroids (Torisawa et al., 2007). While this technique tends to give spheroids of uniform size, the method is labour intensive, and can be hampered by evaporation of the media from the droplet, resulting in loss in viability of the model.

1.5.5 Future developments in 3D models

Each of these methods of preclinical cancer modelling has benefits and drawbacks. When considering novel target discovery employing a high-throughput approach, it is likely that organoids and spheroids possess the most suitable characteristics. Their ability to model the tumour environment may be further enhanced by incorporating microfluidics or 3D bioprinting into the experimental design. The study of microfluidics has enabled the development of platforms known as ‘organ-on-chip’ devices. These consist of microwells, connected by microfluidic channels that mimic organ vasculature. The tumour cells, spheroids, or organoids are cultured above a layer of matrix-coated porous membranes, while nutrient medium and immune cells can navigate through the microchannels. Their design can be specifically controlled to alter the orientation of tissue interfaces, the nutrient gradients, and the mechanical forces applied (Bhatia and Ingber, 2014) to enable the study of specific interactions. For example, a microfluidic colorectal tumour-on-chip device has been designed to investigate the real-time

interactions between endothelial cells and cancer cells as the stromal cells migrated into the VEGF-infused tumour core (Carvalho et al., 2019).

In a similar fashion, 3D bioprinting is a technique that can allow for the formation of increasingly complex 3D models. Models can be formed using bioinks of cancer cells, immune cells, and cancer-associated fibroblasts, with or without a scaffold. The use of computer-aided design and the printing method means that the model can be very precisely designed to answer a specific question, and reproducible (Langer et al., 2019). There remain challenges in that printing speeds can be slow, the bioink must be non-toxic, the process of printing should not damage the cells, but this could potentially be an exciting avenue of development to design models that can precisely control the placement of cells, and the spatiotemporal variation of molecular gradients.

1.6 Future developments in treating advanced ER-positive breast cancer

1.6.1 Targeting PI3Kα

Given the frequency of alteration of the PI3K-AKT-mTOR pathway in breast cancer (Miller et al., 2011, Tokunaga et al., 2008) and its contribution to the development of endocrine resistance, there have been a plethora of efforts to target this pathway, with mixed clinical results (Section 1.3.3). The development of more selective inhibitors acting on the PI3Kα subunit is a step towards success in this area. In the SOLAR-1 trial (Andre et al., 2019) the combination of the PI3Kα inhibitor alpelisib with fulvestrant was administered to patients with advanced ER-positive/HER2-negative breast cancer who had previously received endocrine therapy, and the outcome compared with fulvestrant alone. In patients with *PIK3CA*-mutated cancer, progression-free survival was prolonged with the combination therapy. The SANDPIPER trial (Baselga et al., 2018, Dent et al., 2021) evaluated the combination of the PI3Kα inhibitor taselisib with fulvestrant in patients with ER-positive/HER2-negative breast cancer that had progressed following AI therapy. In this study, the primary endpoint was improved progression-free survival in the combination arm in patients with *PIK3CA*-mutated tumours. This was met, but the improvement was only two months, and the trial concluded that there was no clinical utility of combining taselisib with fulvestrant, due to the observed safety profile and only

modest clinical benefit. However, the BYLieve study (Rugo et al., 2021) has shown significant promise in targeting PI3Kα in endocrine-resistant and CDK4/6 inhibitor-resistant disease. Patients with ER-positive/HER2-negative breast cancer that harboured a *PIK3CA* mutation, and had progressed on AIs and CDK4/6 inhibitors, were treated with a combination of alpelisib and fulvestrant, and showed a significant improvement in progression-free survival. As such, PI3Kα inhibitors continue to be an area of intensive research, particularly as patients harbouring an activating *PIK3CA* mutation derive significant benefit.

1.6.2 Targeting AKT

In addition to aberrant PI3K-AKT-mTOR signalling mediated by PI3K, dysregulated AKT activity has also been implicated in cancer pathways (Shariati and Meric-Bernstam, 2019). Activating somatic mutations in *AKT1* have been identified in eight percent of breast cancers (Carpten et al., 2007), and *AKT* amplification has also been observed. Consequently, inhibitors of AKT have been under development, one example being capivasertib. While the BEECH study (Turner et al., 2019) evaluating the combination of capivasertib with paclitaxel in patients with metastatic breast cancer did not prolong progression-free survival, when combined with endocrine therapy, capivasertib has shown positive results. The FAKTION trial (Jones et al., 2020) examined the effect of adding capivasertib to fulvestrant in patients with ER-positive/HER2-negative locally advanced or metastatic breast cancer who had progressed on AI therapy. The results showed a significant improvement in progression-free survival, and that the benefit was observed regardless of the mutation status of *PIK3CA*. The TAKTIC trial (NCT03959891) is currently recruiting to evaluate the efficacy of another AKT inhibitor, ipatasertib, in combination with endocrine therapy and/or palbociclib in advanced ER-positive/HER2-negative breast cancer. Thus, targeting AKT provides an alternative route to perturb the aberrant PI3K-AKT-mTOR signalling observed in ER-positive breast cancer.

1.6.3 Targeting ER

1.6.3.1 SERDs

At present, fulvestrant is the only clinically licensed SERD, but novel SERDS are being developed, with particular interest in oral bioavailability, given that fulvestrant is

administered as an intramuscular injection. Elacestrant/RAD1901 is one such orally bioavailable SERD that has shown anti-tumour growth in ER-positive PDX models (Bihani et al., 2017), including models of different *ESR1* mutations and of CDK4/6 inhibitor resistance (Patel et al., 2019). Following promising results in a phase 1 trial in patients previously exposed to multiple lines of therapy (Bardia et al., 2021), elacestrant/RAD1901 is being evaluated in the EMERALD study (Bardia et al., 2019) to compare its safety and efficacy in advanced ER-positive/HER2-negative breast cancer to standard of care endocrine therapy.

Another orally bioavailable SERD in development is AZD9496. In PDX models harbouring a D538G *ESR1* mutation, AZD9496 demonstrated greater anti-tumour activity than fulvestrant (Weir et al., 2016). The same study showed that combination therapy of AZD9496 with PI3K-inhibitors or CDK4/6 inhibitors caused tumour regression in mouse models of endocrine-resistant disease. A phase 1 study examining the efficacy of AZD9496 in patients who had progressed following at least six months of endocrine therapy demonstrated an acceptable safety profile, and treatment achieved stable disease in 20% percent of patients at six months (Hamilton et al., 2018). Further work is being carried out on another SERD brilanestrant/GDC-810 (Joseph et al., 2016). It is to be expected that this class of drugs targeting ER will be expanded further in the future.

1.6.3.2 Selective oestrogen receptor covalent antagonists

Selective oestrogen receptor covalent antagonists (SERCAs) are a novel class of drug designed against ER. One such example is H3B-5942, which targets a cysteine residue (Cys530) in the ligand binding pocket of ER that is not conserved in other hormone receptors, and enforces an irreversible antagonist conformation (Puyang et al., 2018). This antagonism was seen regardless of the mutation status of ER, and synergism with CDK4/6 inhibitors and mTOR was also observed. The SERCA H3B-6545 is currently undergoing a phase 1 trial in combination with palbociclib in heavily pre-treated metastatic ER-positive/HER2-negative breast cancer, and thus far has demonstrated an acceptable safety profile (Johnston et al., 2021).

1.6.3.3 Proteolysis targeting chimeras

Proteolysis targeting chimeras (PROTACs) are small molecules designed of a ligand that binds a protein to be degraded, and a ligand for an E3 ubiquitin ligase. The PROTAC thereby mediates a bridging that facilitates the ubiquitination of the protein, labelling it for degradation in the proteasome (Ocana and Pandiella, 2020). The PROTAC ARV-741 which facilitates the interaction between ER and an intracellular E3 ligase has been shown to achieve effective degradation of ERs, regardless of mutation status, and combination with a CDK4/6 inhibitor was shown to confer a more pronounced anti-tumour effect than monotherapy (Flanagan et al., 2019). A phase 1 trial of ARV-741 alone and in combination with palbociclib for the treatment of metastatic and locally advanced breast cancer is currently underway (NCT04072952).

1.6.4 Targeting BCL-2

As apoptosis inhibition is a hallmark of cancer, studies have examined the balance of pro- and anti-apoptotic signalling in cancer, with the aim of modulating this signalling to direct cancerous cells towards apoptosis. There have been two main apoptotic pathways characterised: the extrinsic pathway, activated by ligands binding to death receptors at the cell surface such as tumour necrosis factor (TNF) receptors, and TNF-related apoptosis-inducing ligand (TRAIL) receptors; and the intrinsic pathway, which is triggered by the collapse of the mitochondrial membrane potential (Voutsadakis, 2000). The mitochondrial membrane potential is maintained by anti-apoptotic members of the B cell lymphoma 2 (BCL-2) family, including BCL-2 and MCL-1. Pro-apoptotic BCL-2 proteins such as BAD and BIM have a BCL-2 Homology 3 (BH3) domain by which they interact with and inhibit the anti-apoptotic proteins to activate apoptosis. The BCL-2 inhibitor venetoclax, currently approved for haematological malignancies, has been shown to inhibit tumour growth in PDX models of breast cancer (Vaillant et al., 2013). In the first clinical study to evaluate venetoclax in a solid tumour, the combination of venetoclax and tamoxifen showed a confirmed radiological response, and tolerable safety profile in ER-positive, BCL-2-positive metastatic breast cancer (Lok et al., 2019). As over half of these patients had received previous endocrine therapy or chemotherapy, this combination of treatments is promising for the endocrine-resistant setting.

1.7 Project aims

Endocrine-resistant breast cancer is a significant, and common, problem in the treatment of breast cancer, which is itself a leading cause of mortality. If the mechanisms by which endocrine-resistance is achieved could be better characterised, they could be targeted such that endocrine therapy regained its effectiveness. The challenge lies in the considerable heterogeneity of mechanisms utilised by cancers to circumvent endocrine therapy, with no "one size fits all" approach. The initial goal of this project was to investigate the processes contributing to endocrine resistance. Over the course of this thesis, this was expanded to include palbociclib resistance, as the clinical challenge of CDK4/6 inhibitor resistance became more apparent. The aims were:

1. To use RNA-sequencing of paired clinical samples collected before starting AI therapy, and after progression or relapse on AI therapy to examine for transcriptomic changes that may contribute to AI resistance
2. To develop multiple 3D models of endocrine therapy resistance and palbociclib resistance
3. To use the 3D models, and 2D culture, in high-throughput drug and siRNA screens to identify pathways key to survival and proliferation
4. Identify and validate hits that are common to several cell lines of different molecular backgrounds displaying endocrine-resistance and palbociclib-resistance that promote tumour cell proliferation/survival.

Chapter 2 Materials and Methods

2.1 Materials

All solutions purchased from the Central Sterile Stores Department (CSSD) of the Institute of Cancer Research unless otherwise stated. Recipes and preparation protocols are listed on their Intranet page:

https://nexus.icr.ac.uk/Lists/ICR%20Tasks/DispForm.aspx?ID=495

All reagents were stored at room temperature unless stated otherwise.

2.1.1 General reagents

β-mercaptoethanol: (Sigma Aldrich, M7154)

Charcoal: activated Pure: (Merck, 1.02183.1000)

Dextran: from Leuconostoc Spp: (Sigma, 31390)

DMSO: (Sigma Aldrich, D8779)

EDTA 0.5 M: 186.1 g di-sodium salt of ethylenediaminetetraacetate dissolved in 1 L H_2O and pH adjusted to 8.0 with NaOH

Ethanol: (VWR, 101077Y)

Methanol: (VWR, 20847-30)

Nuclease-free water: (Ambion, AM9937)

PBS: (137 mM NaCl, 2 mM KCl, 8 mM Na_2HPO_4, 1.5 mM KH_2PO_4 in H_2O. pH adjusted to 7.4 with HCl (CSSD). Stored at 4°C.

SDS: sodium dodecyl sulphate 10% stock in H_2O

Ultra-filtered (UF) water: 17 Mega Ohms filtered water (CSSD)

2.1.2 Reagents for cell culture and cell-based assays

17β-oestradiol: (SigmaAldrich, E2758) dissolved in 100% ethanol, 10 mM stock solution stored at -20°C

Adhesive foil seal for 384-well plates: (Corning 6569)

Adhesive foil seal for 96-well plates: (Corning 6570)

Cell scraper: (Sarstedt, 83.3951)

CellTiter-Glo Luminescent Cell Viability Assay: (Promega, G7570) stored at -20°C

Countess automated cell-counter slides: (Invitrogen, by Thermo-Fisher, C10283)

CryoTube 1.8 mL vials: (Thermo Scientific, 170106)

DMEM/F12 media: (Gibco by ThermoFisher, 11330-032) stored at 4°C

Flat-bottom 384-well plates for 2D culture: (Grenier Bio-One, 781098)

Flat-bottom 96-well plates for 2D culture: (Grenier Bio-One, 655098)

Foetal bovine serum (FBS): (Gibco by ThermoFisher, 10106-169) stored at -20°C

Modified IMEM media: (Gibco by ThermoFisher, A1048-01) stored at 4°C

RPMI media 1640: (Gibco by ThermoFisher, 11835-063) stored at 4°C

Screw-cap 1.5 mL vials: (Sarstedt, 72.692.005)

T75 tissue culture flasks, Nunc delta-surface (ThermoFisher, 156499)

Trypsin: phenol red-free trypsin 0.05% in versene 0.02% (CSSD)

U-bottom ultra-low attachment 384-well plates for 3D culture: (Corning, CLS-3830)

U-bottom ultra-low attachment 96-well plates for 3D culture: (Corning, CoStar 7007)

2.1.3 Reagents for protein manipulation

Blocking buffer: 5% Marvel milk powder diluted in TBS-T

ECL substrate: Equal volumes of Clarity Western Peroxide solution and Clarity Western Luminol/enhancer solution (BioRad, 10026385A and 10026384A)

Electrophoresis buffer: 1x solution of Tris/Glycine/SDS, diluted in H_2O (BioRad, 161-0772)

Electrophoresis gels: 10-well or 12-well combs Mini PROTEAN TGX 4-15% precast polyacrylamide gels (BioRad, 4561083, 4561085). Stored at 4°C

Laemmli sample buffer: 4x (BioRad, 1610747)

Nunclon Delta 6 cm plate: (ThermoFisher Scientific, 150288)

Nunclon Delta 10 cm plate: (ThermoFisher Scientific, 150350)

Protein ladder: 250 kDa dual colour ladder (BioRad, 161-0374). Stored at -20°C

PVDF membranes: TransBlot-Turbo Mini PVDF membranes (BioRad, L002047A)

RIPA lysis buffer: 1x complete tablets mini EASYpack (Roche, 04693124001), 1xPhosSTOP EASYpack (Roche, 04906837001), both dissolved in 10 mL RIPA buffer (Sigma, R0278). Stored at -20°C

NP250 lysis buffer: 20 mM Tris pH 7.6, 1 mM EDTA, 0.5% NP40, 250 mM NaCl

TBS-T: 10% 10X TBS (CSSD), 0.25% Tween 20 (Sigma Aldrich, P1379), diluted in H_2O.

Transfer buffer: 60% H_2O (LSS), 20% TransBlot-Turbo 5x transfer buffer (BioRad, 10026938), 20% ethanol. Stored at 4°C

Transfer stacks: TransBlot-Turbo Mini Transfer stacks (BioRad, L002043A)

2.1.4 Antibodies for Western blotting (WB)

Table 2.1: Antibodies and their applications

Antibody	Source	Code	Species	Applications and dilutions
α-tubulin	Cell Signalling Technology	2125	Rabbit	WB 1:1000
CDK4	Cell Signalling Technology	12790	Rabbit	WB 1:1000
CDK6	Cell Signalling Technology	13331	Rabbit	WB 1:1000
CDK7	Cell Signalling Technology	2916	Mouse	WB 1:2000
CDK7-T170	Abcam	Ab155976	Rabbit	WB 1:1000
CDK9	Cell Signalling Technology	2316	Rabbit	WB 1:1000
Cyclin E	Cell Signalling Technology	4129	Mouse	WB 1:1000
Histone H3	Cell Signalling Technology	9715	Rabbit	WB 1:1000
MYB	Cell Signalling Technology	12319	Rabbit	WB 1:1000
RNA Pol II-S2	Abcam	Ab5131	Rabbit	WB 1:1000
RNA Pol II-S5	Abcam	Ab5095	Rabbit	WB 1:1000
RNA Poll II	Abcam	Ab26721	Rabbit	WB 1:1000
Vinculin	Abcam	Ab219649	Rabbit	WB 1:1000
Anti-rabbit IgG (HRP)	Abcam	Ab205718	Goat	WB 1:10000
Anti-mouse IgG (HRP)	Abcam	Ab205719	Goat	WB 1:2000
All antibodies stored at -20°C				

2.1.5 Reagents for DNA and RNA extraction

AllPrep DNA/RNA FFPE kit: (Qiagen, 80234)

DNA LoBind tubes, 1.5 mL, PCR clean: (SigmaAldrich, Z666548)

DNeasy blood and tissue kit: (Qiagen, 69504)

QiaShredder columns: (Qiagen, 79656)

Qubit dsDNA broad range (BR) assay kit: (ThermoFisher, Q32850)

RNase-free water: (Qiagen, 129112)

RNeasy Mini kit: (Qiagen, 74104)

2.1.6 Reagents for real-time quantitative PCR (RTqPCR)

0.2 mL PCR 8-strip tubes, clear: (Thistle Scientific, AX-PCR-0208)

2xqPCR Precision Plus mastermix: (Primer design JN150101-46188)

Microamp optical 384-well reaction plate: (Applied Biosystems, 4343814)

Microamp optical adhesive film: (Applied Biosystems, 4311971)

Quantitect reverse transcription kit: (Qiagen, 205313)

TaqMan gene expression assays: (ThermoFisher Scientific, 4331182) stored at -20°C, listed in Table 2.2.

Table 2.2: Taqman gene expression assays, ThermoFisher Scientific

Probe ID	Gene Symbol	Species	Gene Name	Reporter
Hs00187842_m1	*B2M*	Human	Beta-2-microglobulin	FAM
Hs00361486_m1	*CDK7*	Human	Cyclin dependent kinase 7	FAM
Hs00977896_g1	*CDK9*	Human	Cyclin dependent kinase 9	FAM
Hs01046818_m1	*ESR1*	Human	Oestrogen receptor	FAM
Hs00914057_m1	*IPO8*	Human	Importin 8	FAM

2.1.7 Reagents for droplet digital PCR (ddPCR)

0.2 mL PCR 8-strip tubes, clear: (Thistle Scientific, AX-PCR-0208)

ddPCR assays: (BioRad) listed in Table 2.3

ddPCR supermix for probes: (BioRad, 180-3010) stored at -20°C

Droplet generator cartridges and gaskets: (BioRad, 186-3006)

Droplet generator oil for probes: (BioRad, 186-3005)

PCR 96-well microplate: (ThermoFisher, MPA-670-010R)

Table 2.3 BioRad multiplex ddPCR assays

Multiplex	Mutations	Catalogue Number
ESR1 multiplex 1	L536R, c.1607T>G; Y537C, c.1610A>G; D538G, c.1613A>G; E380Q, c.1138G>C	12004118
ESR1 multiplex 2	Y537S, c.1610A>C; Y537N, c.1609T>A; S463P, c.1387T>C	12003910
PIK3CA multiplex	E542K, c.1624G>A; E545K, c.1633G>A, H1047L, c.3140A>T; H1047R, c.3140A>G	12003121

2.1.8 Reagents for siRNA transfection

5x siRNA buffer: (Horizon, B-002000-UB-100) stored at 4°C

Kinome library: (Dharmacon, G-103505-01) ON-TARGETplus siRNA Library-Human Protein Kinases, stored at -80°C

Lipofectamine RNAiMAX: (ThermoFisher Scientific, 13778150) stored at 4°C

Lyophilised siRNA SMARTpools: (Dharmacon) stored at -20°C, listed in Table 2.4

OptiMEM: (Gibco by ThermoFisher, 31985062), stored at 4°C

Table 2.4: ON-TARGETplus siRNA SMARTpools, Dharmacon

Gene Symbol	Gene Name	Catalogue Number
ESR1	Oestrogen receptor	L-003401-00-0005
PLK1	Polo-like kinase 1	L-003290-00-0005
CDK9	Cyclin dependent kinase 9	L-003243-00-0005
CDK7	Cyclin dependent kinase 7	L-003241-00-0005
Control pool	Non-targeting control	D-001810-10-20

2.1.9 Reagents for RNA-seq library preparation

TruSeq RNA Unique Dual Index adaptor sequences: (Illumina, 20022371)

TruSeq Stranded Total RNA Library Prep Gold: (Illumina, 20020598)

2.1.10 Drugs

Kinase inhibitor drug library: (SelleckChem, L1200) containing 378 compounds.

Additional drugs are listed below in Table 2.5

Table 2.5: Drugs and storage conditions

Drug Name	Source and catalogue code	Concentration and solvent
A485	SelleckChem, S8740	10 mM, DMSO
A674563	SelleckChem, S2670	10 mM, DMSO
Abemaciclib	Molecular Endocrinology lab stocks	1 mM, DMSO
ABT 19-9	SelleckChem, S8048	10 mM, DMSO
AD80	SelleckChem, S8518	10 mM, DMSO
Alisertib	SelleckChem, S1133	10 mM, DMSO
Alpelisib	SelleckChem, S2814	10 mM, DMSO
Aurora A inhibitor 1:	SelleckChem, S1451	10 mM, DMSO
AZD4573	SelleckChem, S8719	10 mM, DMSO
AZD5363	SelleckChem, S8019	10 mM, DMSO
AZD9496	SelleckChem, S8372	10 mM, DMSO
BBT-594	MedChemExpress, HY-18840	10 mM, DMSO
BGJ398	SelleckChem, S2183	10 mM, DMSO
BGT226	SelleckChem, S2749	10 mM, DMSO
BI2536	SelleckChem, S1109	10 mM, DMSO
Continued overleaf		

Binimetinib	SelleckChem, S7007	10 mM, DMSO
BMS-754807	SelleckChem, S1124	10 mM, DMSO
BS-181	SelleckChem, S1572	10 mM, DMSO
CCT245747	Molecular endocrinology lab stocks	10 mM, DMSO
CCT346	Molecular endocrinology lab stocks	10 mM, DMSO
CH5132799	SelleckChem, S2699	10 mM, DMSO
CHIR-124	SelleckChem, S2683	10 mM, DMSO
Crizotinib	SelleckChem, S1068	10 mM, DMSO
CT7001	Molecular endocrinology lab stocks	1 mM, DMSO
CUDC-101	SelleckChem, S1194	10 mM, DMSO
CUDC-907	SelleckChem, S2759	10 mM, DMSO
Dinaciclib	SelleckChem, S2768	10 mM, DMSO
Dovitinib	SelleckChem, S1018	10 mM, DMSO
Enobosarm	SelleckChem, S1174	10 mM, DMSO
Enzalutamide	SelleckChem, S1250	10 mM, DMSO
Everolimus	Molecular endocrinology lab stocks	1 mM, DMSO
Flavopiridol	SelleckChem, S2679	10 mM, DMSO
Foretinib	SelleckChem, S1111	10 mM, DMSO
Fulvestrant	Tocris, 1047	10 mM, DMSO
GDC-0879	SelleckChem, S1104	10 mM, DMSO
GDC-810	MedChemExpress, HY-12864	10 mM, DMSO
Gefitinib	SelleckChem, S8740	10 mM, DMSO
GSK461364	SelleckChem, S2193	10 mM, DMSO
GSK690693	SelleckChem, S1113	10 mM, DMSO
H365	Molecular endocrinology lab stocks	1 mM, DMSO
ICEC0942	SelleckChem, S8722	10 mM, DMSO
Iressa	Molecular endocrinology lab stocks	1 mM, DMSO
Lapatinib	SelleckChem, S5241	10 mM, DMSO
LDC000667	SelleckChem, S7461	10 mM, DMSO
Linsitinib	SelleckChem, S1091	10 mM, DMSO
MK-2206	SelleckChem, S1078	10 mM, DMSO
MK1775	SelleckChem, S1525	10 mM, DMSO
Neratinib	Molecular endocrinology lab stocks	1 mM, DMSO
Nilotinib	SelleckChem, S4895	10 mM, DMSO
Nintedanib	SelleckChem, S1010	10 mM, DMSO
NMS-P937	SelleckChem, S7255	10 mM, DMSO
NMSP715	Molecular endocrinology lab stocks	10 mM, DMSO
NVP-2	SelleckChem, S8981	10 mM, DMSO
NVP-BVU972	SelleckChem, S2761	10 mM, DMSO
Olaparib	SelleckChem, S1060	10 mM, DMSO
Omipalisib	SelleckChem, S2658	10 mM, DMSO
P-276-00	SelleckChem, S8059	10 mM, DMSO
Palbociclib	Molecular endocrinology lab stocks	1 mM, DMSO
PD168393	SelleckChem, S7039	10 mM, DMSO
PF-04691502	SelleckChem, S2904	10 mM, DMSO
PIK-75	SelleckChem, S1205	10 mM, DMSO
Pimasertib	SelleckChem, S1475	10 mM, DMSO
Ponatinib	SelleckChem, S1490	10 mM, DMSO
PP-121	SelleckChem, S2622	10 mM, DMSO
RAD1901	Molecular endocrinology lab stocks	1 mM, DMSO
Ribociclib	Molecular endocrinology lab stocks	1 mM, DMSO
Continued overleaf		

Ridaforolimus	SelleckChem, S1022	10 mM, DMSO
Sapinisertib	SelleckChem, S2192	10 mM, DMSO
SB203580	SelleckChem, S1076	10 mM, DMSO
Selumetinib	SelleckChem, S1008	10 mM, DMSO
SNS-032	SelleckChem, S1145	10 mM, DMSO
Sorafenib	SelleckChem, S1040	10 mM, DMSO
Staurosporin	SelleckChem, S1421	10 mM, DMSO
Sunitinib	SelleckChem, S1042	10 mM, DMSO
Tamoxifen	Molecular endocrinology lab stocks	1 mM, DMSO
Temsirolimus	SelleckChem, S1044	10 mM, DMSO
THZ1	MedChemExpress, HY-80013	10 mM, DMSO
Tyrphostin-9	SelleckChem, S2895	10 mM, DMSO
U0126	SelleckChem, S1102	10 mM, DMSO
Volarsertib	Molecular endocrinology lab stocks	1 mM, DMSO
WYE-125132	SelleckChem, S2661	10 mM, DMSO
Stocks of 1 mM stored at -20°C. Stocks of 10 mM stored at -80°C.		

2.1.11 Equipment

BioAnalyser: (Agilent)

BioRad imager: (BioRad)

BioRad QX-200 droplet reader: (BioRad)

Countess II cell counter: (Invitrogen)

DirectDetect Spectrophotometer: (Milipore)

ECHO550 acoustic liquid handler: (Labcyte)

EVOS FL Cell Imaging System: (Life Technologies)

Hamilton liquid handler: (Hamilton, Microlab Star)

Illumina HiSeq 2500: (Illumina)

Incucyte S3 Live Cell Analysis System: (Sartorius)

Multidrop Combi: (ThermoFisher)

Nanodrop 8000 Spectrophotometer: (ThermoFisher, ND-8000-GL)

QuantStudio 6: (Applied-Biosystems)

Qubit fluorometer: (Invitrogen)

TurboBlot transfer machine: (BioRad)

Victor X5 plate-reader: (PerkinElmer)

2.1.12 Cells

Cell lines and their media requirements are listed below in Table 2.6.

Table 2.6 Cell lines, model type, and media requirements

Cell Line	Model	Source	Media	Media supplement
MCF7	ER-positive endocrine sensitive breast cancer	American Type Culture Collection	Phenol red-free RPMI 1640	10% FBS 1 nM estradiol
MCF7 LTED^{WT}	ER-positive endocrine-resistant breast cancer, wild-type *ESR1*	Molecular Endocrinology laboratory stocks, Institute of Cancer Research	Phenol red-free RPMI 1640	10% DCC-FBS
MCF7 LTED^{Y537C}	ER-positive endocrine-resistant breast cancer, mutant *ESR1*	Molecular Endocrinology laboratory stocks, Institute of Cancer Research	Phenol red-free RPMI 1640	10% DCC-FBS
MCF7 LTED^{PalboR}	ER-positive, endocrine-resistant, palbociclib-resistant breast cancer, mutant *ESR1*	Molecular Endocrinology laboratory stocks, Institute of Cancer Research	Phenol red-free RPMI 1640	10% DCC-FBS 1 μM palbociclib
HCC1428	ER-positive endocrine sensitive breast cancer	American Type Culture Collection	Phenol red-free RPMI 1640	10% FBS 1 nM estradiol
HCC1428 LTED	ER-positive endocrine-resistant breast cancer	Molecular Endocrinology laboratory stocks, Institute of Cancer Research	Phenol red-free RPMI 1640	10% DCC-FBS
HCC1428 LTED^{PalboR}	ER-positive, endocrine-resistant, palbociclib-resistant breast cancer	Molecular Endocrinology laboratory stocks, Institute of Cancer Research	Phenol red-free RPMI 1640	10% DCC-FBS 1 μM palbociclib
SUM44	ER-positive endocrine sensitive breast cancer	American Type Culture Collection	Phenol red-free RPMI 1640	10% FBS 1 nM estradiol
SUM44 LTED^{WT}	ER-positive endocrine-resistant breast cancer, wild-type *ESR1*	Provided by Dr Oesterreich, University of Pittsburgh (Sikora et al., 2016)	Modified IMEM	2% DCC-FBS
SUM44 LTED^{Y537S}	ER-positive endocrine-resistant breast cancer, mutant *ESR1*	Molecular Endocrinology laboratory stocks, Institute of Cancer Research	Phenol red-free RPMI 1640	10% DCC-FBS
T47D	ER-positive endocrine sensitive breast cancer	American Type Culture Collection	Phenol red-free RPMI 1640	10% FBS 1 nM estradiol
T47D-LTED	ER-positive endocrine-resistant breast cancer	Molecular Endocrinology laboratory stocks, Institute of Cancer Research	Phenol red-free RPMI 1640	10% DCC-FBS
ZR75.1	ER-positive endocrine sensitive breast cancer	American Type Culture Collection	Phenol red-free RPMI 1640	10% FBS 1 nM estradiol
ZR75.1 LTED	ER-positive endocrine-resistant breast cancer	Molecular Endocrinology laboratory stocks, Institute of Cancer Research	Phenol red-free RPMI 1640	10% DCC-FBS
MCF10A	Non-tumourigenic breast tissue	Provided by Dr Poulogiannis, Institute of Cancer Research (Koundouros et al., 2020)	DMEM/F12	5% Horse serum 20 ng/mL Epidermal growth factor 0.5 mg/mL hydrocortisone 100 ng/mL cholera toxin 10 μg/mL insulin 50 U/mL penicillin/streptomycin

2.2 Methods

2.2.1 Tissue culture

All adherent tissue culture cell lines were cultured in T75 flasks in humidified incubators at 37°C and 5% CO_2. Cells were grown to 80-90% confluency and passaged at the desired fraction every 2-4 days. Foetal bovine serum (FBS) was used as a media supplement for the parental cell lines. FBS was stripped of steroids using dextran and charcoal (Darbre et al., 1984), termed DCC-FBS, for use as a media supplement for the long-term oestrogen-deprived (LTED) derivatives. Estradiol was removed from the media of the parental cells 48 hours prior to each experiment unless otherwise stated. Similarly, palbociclib was removed from the media of the palbociclib-resistant cells 48 hours prior to each experiment. All cell lines were authenticated by short tandem repeats (STR) profiling, and routinely screened for mycoplasma contamination. Cells were kept to low passage numbers, with only 10-15 passages of each cell line prior to discarding.

2.2.1.1 Passaging of cells

Adherent cells were grown in tissue culture flasks until they were 80-90% confluent. Culture medium was aspirated, and cells were washed with PBS at 37°C such that the flask was covered. Cells were detached using a covering volume of phenol red-free trypsin/versene, with a 2-10 minute incubation at 37°C (cell line dependent). Once cells were detached, the trypsin was neutralised by addition of fresh culture medium. The cell suspension was then diluted at the desired fraction in fresh medium and re-plated into a fresh culture flask. Cells were counted using a stain of 0.4% Trypan Blue and a Countess automated cell counter system.

2.2.1.2 Freezing cells for long-term storage

Adherent cells were detached as described. Following resuspension in fresh medium, the cell suspension was centrifuged at 260 x *g* for 5 minutes. The cell pellet was resuspended in cell freezing medium (culture medium plus 10% DMSO) and 1 mL transferred to CryoTube vials. Vials were frozen slowly in Corning CoolCell LX cell freezing vial containers at -80°C for 2 - 5 days, before being transferred to liquid nitrogen for long term storage.

2.2.1.3 Spheroid formation

Cell lines were seeded as a single cell suspension in their respective media into ultra-low attachment U-bottom 96-well or 384-well plates, at a density of 2500 cells per well. Plates were then centrifuged at 200 x *g* for 10 minutes, and placed in an incubator without disturbance for 72 hours.

2.2.2 Cell imaging

2.2.2.1 Incucyte time course assays

1.5 x 10^4 cells were seeded in 2 mL onto 24-well plates. Cell proliferation was monitored using the Incucyte S3 Live-Cell Analysis System. Images were acquired every 6 hours over 5 days. The instrument's software was used to create an image mask for each cell line to calculate the percentage change in confluence in each well over time.

2.2.2.2 Static imaging

Snapshot brightfield images of spheroids were taken using the EVOS microscope.

2.2.3 2D drug screen

2.2.3.1 Formation of 2D drug screen

The 2D drug screen was comprised of the SelleckChem 378 kinase inhibitor library, and the additional 18 drugs listed in Table 2.7. Staurosporin was used as the positive control, and DMSO-vehicle as the negative control. The drugs were diluted in DMSO from the 100 μM stock into four doses (dispensing 0 nL, 5 nL, 50 nL, and 500 nL to create wells of final concentration 0 nM, 10 nM, 100 nM, 1000 nM when 50 μl cell suspension was added) in 384-well 2D culture plates using the ECHO550 acoustic liquid handler to form a high-throughput screen. Each independent biological replicate of the screen was comprised of five 384-well plates. The plates were then sealed using aluminium adhesive foil seals and stored at -80°C until required. Prior to cell seeding, plates were defrosted at room temperature for 30 minutes on the orbital shaker, and centrifuged at 1000 x *g* for 5 minutes.

Table 2.7: Drugs added to kinase inhibitor library 2D screen		
RAD1901/elacestrant	Abemaciclib	CT7001
AD80	LDC000667	MK1775
THZ1	NMS-P715	CCT245747
ABT19-9	AZD9496	Ribociclib
Neratinib	GDC-810	Iressa
Tamoxifen	Fulvestrant	CCT346

2.2.3.2 2D drug screen protocol

1200-2400 cells/well were seeded into the 2D 384-well drug screen plates described above in 50 μL of their respective media. Cell seeding number was adjusted to allow for ~80% confluence in the control wells at the end of the experiment. After five days, cell viability was determined using CellTiter-Glo, according to manufacturer's protocol. The plates were incubated on an orbital shaker at room temperature for 15 minutes, before measuring the luminescence signal using the Victor X5 microplate reader for 0.1 second per well. Assay was performed with three independent biological replicates for each cell line.

2.2.4 3D drug screen

2.2.4.1 Formation of 3D drug screen

The 3D drug screen was comprised of the 72 drugs listed in Table 2.8. Staurosporin was used as the positive control, and DMSO-vehicle as the negative control. Drugs were dispensed from 1 μM stock onto ultra-low attachment 96-well 3D culture plates using the Hamilton liquid handler such that a final concentration of 250 nM would be achieved once 100 μL cell suspension was added. Each independent biological replicate was formed of one 96-well plate. The plates were then sealed using aluminium adhesive foil seals and stored at -80°C until required. Prior to cell seeding, plates were defrosted at room temperature for 30 minutes on the orbital shaker, and centrifuged at 1000 x *g* for 5 minutes.

Table 2.8: Drugs used in 3D drug screen			
A674563	Enobosarm	THZ1	BGJ398
AZD5363/capivasertib	Enzalutamide	NVP-2	Dovitinib
GSK690693	H365 (SERCA)	LDC00067	Neratinib
MK2206	Tamoxifen	CHIR-124	BMS-754807
WYE-125132	Fulvestrant	PF-477736	Linsitinib
Everolimus	RAD1901	Olaparib	Selumetinib
Sapinisertib	GDC-910	BI2536	Pimasertib
Temsirolimus	AZD9496	NMS-P937	Binimetinib
Ridaforolimus	Alisertib	GSK461364	U0126
PF-04691502	Aurora A Inhibitor 1	Volarsertib	NVP-BVU972
BGT226	Flavopiridol	MK1775	Foretinib
Omipalisib	P-276-00/Riviciclib	GDC0879	SB203580
Alpelisib	Dinaciclib	Nilotinib	Tyrphostin-9
CH5132799	Abemaciclib	A485	PP-121
PIK-75	Palbociclib	Gefitinib	Sorafenib
CUDC-907	SNS-032	Lapatinib	BBT-594
PD168393	BS-181	CUDC-101	Crizotinib
Nintedanib	Ponatinib	Sunitinib	

2.2.4.2 3D drug screen protocol

2500 cells/well were seeded in 100 μL of their respective media into the 96-well 3D drug screen plates as described above, and spheroids formed as described in Section 2.2.1.3. Palbociclib-resistant cell lines were seeded without palbociclib. After 7 days, cell viability was quantified by adding 100 μL undiluted CellTiter-Glo reagent and plates were incubated on an orbital shaker at room temperature for 45 minutes. The luminescence signal was measured using the Victor X5 microplate reader for 1 second per well. Three independent biological replicates were performed for each cell line.

2.2.5 2D siRNA screen

This work was performed by Dr Nikitorowicz-Buniak prior to the start of this PhD project.

2.2.5.1 Formation of 2D siRNA screen

The screen was created using the ON-TARGETplus siRNA Human Protein Kinase Library consisting of SMARTpools of siRNA targeting 709 protein kinases. The library was supplemented with non-targeting siRNA (NTC) and siRNA against *PLK1* as negative and positive controls, respectively. siRNA SMARTpools were dispensed from the library stock into 96-well 2D culture plates using the Hamilton liquid handler to achieve a final concentration of 25 nM siRNA once cell suspension was added. Each independent

biological replicate was formed of ten 96-well plates. The plates were sealed using aluminium adhesive foil seals and stored at -80°C until required. Prior to cell seeding, plates were defrosted at room temperature for 30 minutes on the orbital shaker, and centrifuged at 1000 x *g* for 5 minutes.

2.2.5.2 2D siRNA screen protocol

A reverse transfection protocol was used. 10 μL of Lipofectamine RNAiMAX transfection agent (diluted 1:10 with OptiMEM) was added to each well of the 96-well plates and incubated for 30 minutes at room temperature. 1200-2400 cells/well were seeded per well in a volume of 35 μL of their respective media using the Multidrop Combi (cell seeding density adjusted to allow for ~80% confluence in negative control wells at the end of the experiment). After 6 days cell viability was assessed using CellTiter-Glo according to manufacturer's protocol. The plates were incubated on an orbital shaker at room temperature for 15 minutes, before measuring the luminescence signal using the Victor X5 microplate reader for 1 second per well. Each screen was performed using three independent biological replicates per cell line.

2.2.6 3D siRNA screen

2.2.6.1 Formation of 3D siRNA screens

The 3D siRNA screens were formed in the same manner as the 2D siRNA screens (Section 2.2.5.1), except that the library was dispensed into ultra-low attachment 96-well 3D culture plates. Each independent biological replicate was formed of ten 96-well plates.

2.2.6.2 3D siRNA screen protocol

Once the 3D siRNA plates had defrosted, 10 μL of Lipofectamine RNAiMAX transfection agent (diluted 1:10 with OptiMEM) was dispensed into each well of the 96-well plates, and incubated at room temperature for 30 minutes. 2500 cells/well were then seeded in a volume of 100 μL using the Multidrop Combi. The spheroids were formed as described in Section 2.2.1.3. After 7 days cell viability was assessed by adding 100 μL undiluted CellTiter-Glo reagent, and plates were incubated on an orbital shaker at room temperature for 45 minutes. The luminescence signal was measured using the Victor X5

microplate reader for 1 second per well. Each screen was performed using three independent biological replicates per cell line.

2.2.7 siRNA transfection

A reverse transfection protocol using SMARTpools of siRNA was performed for all siRNA transfection experiments. Lyophilised oligonucleotides were reconstituted in siRNA buffer to 20 μM and aliquots were stored at -20°C. ON-TARGETplus SMARTpools consist of four different siRNAs targeting the same gene, and the non-targeting control pool was made up of four non-targeting siRNAs. A final concentration of 25 nM siRNA was used for all experiments unless otherwise stated. siRNA was incubated with the lipid transfection Lipofectamine RNAiMAX for 15 minutes. Cell suspension was then added at the required density and incubated for 24 hours. For real-time quantitative polymerase chain reaction (RTqPCR), cells were then washed with ice-cold PBS and stored at -80°C until RNA was extracted. For Western blotting, exchange of fresh culture media was performed at 24 hours, with protein extraction occurring on day 5.

2.2.8 RNA extraction and RTqPCR

Cells for RNA extraction were seeded in 6 cm plates. Growth medium was aspirated from the plates, and cells were washed with ice-cold PBS. 350 μL of ice-cold RLT lysis buffer containing 1:100 β-mercaptoethanol was added to each plate. Cells were detached by scraping. mRNA was extracted from these cell lysates using the Qiagen RNeasy kit, performed according to the manufacturer's protocol. RNA was eluted in 40 μL nuclease-free water, and concentration determined by measuring a 2 μL sample on the Nanodrop-8000 spectrophotometer. cDNA was produced by reverse transcribing 500 ng of RNA using the Qiagen Quantitect kit, according to the manufacturer's protocol. Quantitative PCR reactions were performed using 11.25 ng cDNA, 5 μL 2x qPCR mastermix, and 0.5 μL Taqman Gene Expression Assay probe (Table 2.2) in a 10 μL reaction. The QuantStudio6-Flex sequence detection system was used to perform relative quantification, with all reactions performed in triplicate. Data analysis was performed using the Applied Biosystems QuantStudio 6 software. The endogenous controls *B2M* and *IPO8* were used to perform normalisation, and all expression data was normalised to the non-targeting control or DMSO-vehicle samples for each experiment.

2.2.9 DNA extraction

Cells for DNA extraction were seeded in T75 flasks. Growth medium was aspirated from the plates, and cells were washed with PBS. Cells were detached as described in Section 2.2.1.1, fresh media used to neutralise the trypsin, and the cell suspension centrifuged at 260 x *g* for 5 minutes. The media was aspirated, and the cell pellet resuspended in 200 μL PBS. DNA was extracted using the Qiagen DNeasy blood and tissue kit, according to manufacturer's protocol. DNA was quantified using Qubit.

2.2.10 Droplet digital PCR (ddPCR)

This work was performed by Kate Tourna in the Turner laboratory at the Institute of Cancer Research.

Droplet digital PCR (ddPCR) was performed on a QX-200 ddPCR system using TaqMan chemistry with assays developed for *ESR1* and *PIK3CA* hotspot mutations (Table 2.3). FAM-labelled probes were designed for the mutant allele while HEX-labelled probes were designed for the corresponding wild-type allele. Primers and probes were used at a final concentration of 900 nM and 250 nM respectively. PCR reactions were prepared as shown in Table 2.9 with 10 ng of cell line DNA (approximately 1,500 diploid genomes equivalents) and partitioned into a median of 20,000 droplets per sample in a manual droplet generator according to manufacturer's instructions. Emulsified PCR reactions were run on 96-well plates on a G-Storm GS4 thermal cycler with conditions as shown in Table 2.10. Plates were read on a BioRad QX-200 droplet reader using QuantaSoft v1.7.4 software from BioRad to assess the number of droplets positive for mutant DNA, wild-type DNA, both, or neither. A non-targeting control well with no DNA was included for each assay in each run. A minimum of 10,000 droplets total and 2 FAM positive droplets were required for an assay to be considered successful.

Cell lines that showed a mutant population by a multiplex ddPCR assay were validated with the identified mutation as a singleplex ddPCR as described above.

Table 2.9: ddPCR reaction mix	
Component	**Volume (µL)**
DNA (10 ng)	2
BioRad multiplex or singleplex	1
Supermix for probes	10
Water	8

Table 2.10: ddPCR protocol		
Step	**Temperature (°C)**	**Time**
Heated lid	105	-
Step 1	95	10 minutes
Step 2, 40x	95	15 seconds
	52 (*ESR1*), 54 (*PIK3CA*)	1 minute
Step 3	98	10 minutes
Holding	10	Indefinite
Temperature ramp increment of 2.5°C/second for all steps		

2.2.11 Western blotting

2.2.11.1 Protein extraction from 2D culture

Cells for protein extraction were seeded in 6 cm or 10 cm plates. Growth medium was aspirated from the plates, and cells were washed with ice-cold PBS. 100 µL ice-cold RIPA buffer was added to each plate, and cells were detached by scraping. The lysates were sonicated for 30 seconds in 1.5 mL screw-top vials, centrifuged at 8000 x *g*, and the supernatant stored at -20°C in fresh vials.

Of note, a different cell lysis protocol was used to probe for retinoblastoma and CDK6. Cells for protein extraction were seeded in 6 cm or 10 cm plates. Growth medium was aspirated from the plates, and cells were detached using a covering volume of phenol red-free trypsin/versene, with a 2-10 minute incubation at 37°C (cell line dependent). Once cells were detached, the trypsin was neutralised by addition of fresh culture medium. The cell suspension was centrifuged at 260 x *g*. The resulting cell pellet was washed with ice-cold PBS twice. The PBS was aspirated, and the cell pellet frozen at -80°C. The pellet was then resuspended in 500 µL of NP-250 lysis buffer containing PhosSTOP protease inhibitor cocktail, and incubated for 30 minutes on a carousel

rotating shaker at 4°C. The samples were then vortexed and subsequently centrifuged at 9000 x *g* for 10 minutes. The supernatant containing the extracted protein was transferred to fresh vials and stored at -20°C.

2.2.11.2 Protein extraction from 3D culture

Spheroids for protein extraction were seeded as described above in ultra-low attachment 96-well 3D culture plates. The spheroids were harvested from each well using a 1 mL pipette into a 15 mL Falcon tube. Growth medium was aspirated, and the cells were washed with ice-cold PBS. 1 mL RIPA buffer was added to the tube, and the spheroids were sonicated for 1 minute. The lysates were then centrifuged at 8000 x *g*, and the supernatant stored at -20°C in fresh screw-cap vials.

2.2.11.3 Protein electrophoresis and detection

Protein concentrations were determined using a Direct Detect spectrometer (Milipore) or a Bradford assay. 15 μg of lysates were diluted in either RIPA or NP-250 lysis buffer (according to the buffer used to lyse the cells) and Laemmli sample buffer. 18 μL of each sample was loaded onto the gel and run at 100 V for 1 hour in electrophoresis buffer.

Protein from the polyacrylamide gels was transferred onto PVDF membranes pre-hydrated in methanol using transfer stacks pre-soaked in transfer buffer and the mixed molecular weight settings on the TransBlot-Turbo transfer system. After transfer, the membranes were incubated in blocking buffer for 1 hour at room temperature on the orbital shaker. The membranes were then washed 3x for 5 minutes in TBS-T before incubation in the relevant primary antibody (diluted according to manufacturer's instructions, Table 2.1) at 4°C overnight on an orbital shaker.

Membranes were washed 3x for 5 minutes in TBS-T before incubation in secondary antibody diluted in blocking buffer for 1 hour at room temperature on an orbital shaker. Membranes were then washed 3x for 5 minutes in TBS-T and developed in ECL substrate prior to imaging on the BioRad imager.

2.2.12 Drug assays

Parental cells were incubated in culture media supplemented with DCC-FBS with no supplemental estradiol for 48 hours prior to seeding for drug assays. Drug treatments for parental cells were made up in culture media supplemented DCC-FBS with supplemental estradiol to achieve a final concentration of 0.01 nM estradiol in the well. Palbociclib-resistant cells were incubated in culture media supplemented with DCC-FBS with no supplemental palbociclib for 48 hours prior to seeding for drug assays.

2.2.12.1 2D drug treatments

4000-8000 cells/well were seeded in 2D 96-well plates in 100 μL, with seeding number adjusted per line to allow ~80% confluence in the control wells at the end of the experiment. Stock drugs were diluted into culture media supplemented with DCC-FBS such that treatments of 100 μL/well would achieve the final desired concentration in the well, with first treatment dispensed at 24 hours. After 72 hours, growth media was aspirated, and the second drug treatment was applied (stock drugs diluted into culture media supplemented with DCC-FBS such that treatments of 200 μL/well would achieve the final desired concentration in the well). Cell viability was assessed using CellTiter-Glo after 7 days.

2.2.12.2 3D drug treatments

2500 cells/well were seeded in 96-well ultra-low attachment 3D culture plates in 100 μL, and spheroids formed as described in Section 2.2.1.3. Stock drugs were diluted into culture media supplemented with DCC-FBS such that treatments of 100 μL/well would achieve the final desired concentration in the well, with first treatment dispensed at 3 days. After 6 days, the second drug treatment was applied (stock drugs diluted into culture media supplemented with DCC-FBS such that treatments of 100 μL/well would achieve the final desired concentration in the well). After 10 days, 75 μL growth media was aspirated from each well, and cell viability was assessed using CellTiter-Glo using an equivalent volume of undiluted CellTiter-Glo to the volume of media remaining in the well.

2.2.12.3 2D combination drug treatments

800-5000 cells/well were seeded in 2D 96-well plates in 50 μL, with seeding number adjusted per line to allow ~80% confluence in the control wells at the end of the experiment. The two stock drugs were diluted into each cell line's growth media such that treatments of 50 μL/well of each drug would achieve the final desired concentration in the well, with first treatment dispensed at 24 hours. After 72 hours, growth media was aspirated, and the second drug treatment was applied (the two stock drugs diluted into growth media such that that treatments of 100 μL/well of each drug would achieve the final desired concentration in the well). Cell viability was assessed using CellTiter-Glo after 7 days.

2.2.12.4 3D combination drug treatments

2500 cells/well were seeded in 96-well ultra-low attachment 3D culture plates in 100 μL, and spheroids formed as described in Section 2.2.1.3. The two stock drugs were diluted into culture medium supplemented with DCC-FBS such that treatments of 50 μL/well of each drug would achieve the final desired concentration in the well, with first treatment dispensed at 3 days. After 6 days, the second treatment was applied. After 10 days, 75 μL growth media was aspirated from each well, and cell viability was assessed using CellTiter-Glo, using an equivalent volume of undiluted CellTiter-Glo to the volume of media remaining in the well.

2.2.13 Characterisation of paired patient samples

2.2.13.1 Previous studies using this cohort of samples

A UK cohort of paired tumour biopsies prior to AI therapy, and following progression or recurrence on AI treatment has previously been reported on (Lopez-Knowles et al., 2019). In this study, formalin-fixed paraffin-embedded (FFPE) tissue marked for the tumour rich region was manually microdissected and DNA and RNA were co-extracted using the AllPrep DNA/RNA FFPE kit according to manufacturer's instruction. The RNA was then stored at -80°C. This study was approved under the National Research Ethics Service (approval number: 08/H0801/111) and the Royal Marsden Committee for Clinical Research (number 3002).

2.2.13.2 Ethical approval for characterisation performed in this thesis

As part of this thesis project, a new ethical approval submission was made to the London-Brighton and Sussex Research Ethics Committee, and to the Royal Marsden Committee for Clinical Research, to allow for the samples to be sequenced, and for the sample set to be expanded. This was granted by the Health Research Authority (REC number 20/LO/0269), and by the Committee for Clinical Research (number 5117). Further FFPE blocks were then identified to increase the number of pairs, and RNA was extracted from these using the same protocol as described above.

2.2.13.3 RNA quality assessment, library preparation, and sequencing

This work was performed by Professor Perou's group at the University of North Carolina, Chapel Hill, USA. RNA quality was assessed using a BioAnalyzer, with a threshold of DV_{200} greater than 30% required to proceed to library construction. Libraries were constructed using the Illumina TruSeq Stranded Total RNA Library Prep Gold kits and Illumina TruSeq RNA Unique Dual Index adaptor sequences according to manufacturer's instructions. This included the Ribo-ZERO method to remove ribosomal RNA. Libraries were sequenced using an Illumina HiSeq 2500. The FastQ files were then transferred to the Institute of Cancer Research.

2.2.13.4 Processing of FastQ data

This work was performed by Dr Gene Schuster, senior bioinformatician at the Ralph Lauren Centre for Breast Cancer Research, Royal Marsden and Breast Cancer Now Research Centre, Institute of Cancer Research. Illumina adaptors were trimmed from the raw FastQ files using Trim Galore (Krueger, 2019), and aligned to coding and non-coding transcripts using the human reference genome Gencode v22 GTF (Frankish et al., 2019) with Salmon (Patro et al., 2017). Genes were filtered to those expressed in at least 70% of patients in one subtype category, with counts greater than 10. Nanostring subtype calling had been used in the previous studies (Lopez-Knowles et al., 2019), but had been unable to define molecular subtypes for 12 of the samples. Therefore, PAM50 subtype calling was performed by using a modified subgroup-specific gene-centreing method (Zhao et al., 2015) and compared to the previous Nanostring subtype calling for validation. 7 samples using this method were assigned a different molecular subtype

from their Nanostring PAM50 subtype, but for consistency across the samples, the subgroup-specific gene-centred method was used throughout.

2.2.13.5 Analysis of RNA-seq data

This work was performed by Arany Soosainathan as part of this thesis, aided by Dr Gene Schuster. Differential expression of individual genes between different pre- and post-AI samples, and between different molecular subtypes, was calculated using the R package DESeq2 (Love et al., 2014), which tests for differential expression through using negative binomial linear models. Gene set enrichment analysis was performed using the R package clusterProfiler (Yu et al., 2012), with the function GSEA, and the hallmark gene sets from the Molecular Signatures Database (Liberzon et al., 2015). R version 1.3.1093 was used for the analysis. Significant differences between groups were tested by Mann-Whitney tests, performed in R.

2.2.14 Statistics

All statistical tests were performed in GraphPad Prism 9 except those performed on RNA-seq data and high-throughput screen data. Error bars indicate ± standard error of the mean (SEM). Significant differences were calculated by one-way analysis of variance (ANOVA), with Tukey's correction for multiple comparisons, and confidence intervals of 95%. For analyses of two or more variables, a two-way ANOVA was used, with Sidak's correction for multiple comparisons, with confidence intervals of 95%. Dose-response curves and IC_{50} values were calculated using a 4-parameter non-linear regression. *p*-values are noted where significant, or indicated as not significant with ns.

Venn diagrams were formed using an interactive web tool Venny (Oliveros, 2017-2015). Synergy plots for combination drug treatments were formed using SynergyFinder (Ianevski et al., 2020). Protein-protein interaction networks were formed using String-DB (Szklarczyk et al., 2015).

2.2.14.1 Analysis of 2D and 3D siRNA high-throughput screens

Assay quality was assessed using calculation of Z-prime (Zhang et al., 1999). Assay quality was assessed per plate, and only plates with Z-prime of ≥0.5 were taken for

further analysis. Three independent biological replicates (each replicate formed of ten plates) were performed with to reduce the risk of false hit identification. The R package cellHTS2 was used to calculate the robust Z-score (Malo et al., 2006) for each siRNA, in collaboration with Dr John Alexander, Institute of Cancer Research. A robust Z-score of ≤-2 was used as a threshold to classify the hits.

2.2.14.2 Analysis of 2D drug high-throughput screens

Assay quality was assessed and robust Z-scores were calculated as described above (each replicate formed of five plates). However, it was noted that the range of robust Z-scores varied considerably between the cell lines, and thus setting a threshold of robust Z-score ≤-2 to classify and compare hits was not considered to be appropriate. Therefore, the raw luminescence value for each well was normalised by dividing this value by the median value of the negative controls on the plate to generate a percentage of control (POC) score. The mean of the POC scores of the three independent biological replicates was then used to generate a mean response score for each drug, at each concentration tested. A threshold of 50% growth inhibition was selected as the cut-off to classify hits.

2.2.14.3 Analysis of 3D drug high-throughput screens

This was performed according to the same protocol as the siRNA screens, described in Section 2.2.14.1, but the threshold for the robust Z-score was set at ≤-1.65 to classify and compare hits.

Chapter 3 Characterising paired patient samples by RNA-sequencing

3.1 Introduction

ER-positive breast cancer is categorised into distinct subtypes (Section 1.1.4). These subtypes contribute to the heterogeneity observed in ER-positive disease, and have different patterns of behaviour with cancer progression (Castaneda et al., 2012). Changes contributing to the evolution of tumours are still poorly understood, partly because of the paucity of patient samples of progressive disease (discussed further in Section 3.1.3). As part of this project's aim to examine the mechanisms contributing to endocrine resistance, RNA-sequencing (RNA-seq) of paired patient samples from before and after the development of resistance to aromatase inhibitors was undertaken to evaluate transcriptomic changes that could underpin the development of resistance mechanisms.

3.1.1 Cancer genomics

The study of cancer genomics has been transformational in contributing to our understanding of cancer biology and tumour progression. From the discovery of the Philadelphia chromosome in chronic myeloid leukaemia (Rowley, 1973), to the completion of the Human Genome Project in 2004, which aided the discovery of mutations in EGFR that could predict response to tyrosine kinase inhibitors in lung cancer (Lynch et al., 2004), the information that can be gleaned from a better understanding of the molecular footprint of cancer is significant for both scientific advances and clinical application. Whole genome sequencing can identify point mutations, structural changes such as copy number aberrations, translocations, and inversions, insertion/deletion mutations, and aneuploidy analyses. RNA-seq (sequencing of the whole transcriptome) adds an element of quantitative analysis by yielding information on differential gene expression. Furthermore, while the gene expression changes captured by microarray technology was limited by pre-defined definitions of genes, RNA-seq methods are not limited by prior knowledge, and as such may be used to discover novel gene structures and gene fusion events. RNA-seq has also broadened the understanding of the regulation of gene expression by enhancer RNAs (Li et al., 2016) and non-coding RNAs (Morris and Mattick, 2014). Further developments

in next generation sequencing (NGS) include methyl-seq, looking for aberrations in the DNA methylation process that could lead to genetic instability or transcriptional silencing, and ATAC-seq (Assay for Transposase Accessible Chromatin), which assesses genome-wide chromatin accessibility. Therefore, it can be seen that NGS technologies and bioinformatic processing to interpret that data has considerably furthered our understanding of cancer as a disorder of the genome/epigenome.

3.1.2 Clinical applications of cancer genomics in breast cancer

The information derived from cancer genomics and NGS has already advanced the diagnostic and treatment decisions made by clinicians. The discovery of the *BRCA1* gene, sequenced in 1994 (Goldgar et al., 1994, Miki et al., 1994), has transformed the management of patients with this hereditary condition. Similarly, the discovery of the *ERBB2* gene amplification as a cancer driver has led to the development of trastuzumab targeting the HER2 receptor. Furthermore, the information from RNA expression profiling has been critical in developing technologies such as Oncotype-Dx, a 21-gene expression assay that has been validated to predict benefit from chemotherapy in early ER-positive/HER2-negative breast cancer. Indeed, the results from the use of Oncotype-Dx in the TAILORx study (Sparano et al., 2018) has allowed a significant proportion of women to avoid undergoing adjuvant chemotherapy with little benefit to their risk of recurrence.

3.1.3 Limitations to NGS

As illustrated above, NGS is a powerful tool, but cancer samples do pose obstacles to clean data acquisition from these sequencing methods. Solid tumours are made up from not only tumour cells, but also stromal tissue, immune cells, and blood vessels, and the genetic material from these components will dilute down the genomic DNA or RNA in the extraction. Furthermore, the methods for preserving tumour samples present challenges to sequencing. Formalin fixation can cause cross-linking of the phosphodiester skeleton of DNA and RNA, leading to fragmentation, and paraffin tissue embedding can also lead to degradation. An additional limitation conferred by fragmentation is that if the origin of the read is in a highly repetitive region, or if there are multiple genes within the genome with similar sequences, this can prove challenging

to align and pinpoint the genomic location. Finally, the availability of samples to answer the clinical question at hand can be challenging. Most tumour banks are formed of primary tumours excised by surgery. However, to address the issues of what genomic changes underly dormancy, resistance to targeted therapy, and disease progression, samples of recurrence and metastasis are required, but these are not often obtained through a patient's clinical course. One mechanism around this is the use of liquid biopsy, to obtain ctDNA (Murtaza et al., 2013), but unfortunately it remains the case that our understanding of the genomic changes underlying resistance to therapy, and metastasis, is limited.

3.1.4 Paired patient sequencing to understand tumour evolution

Current guidelines for locally recurrent or metastatic ER-positive/HER2-negative breast cancer recommend the use of aromatase inhibitors (AIs) as first-line therapy in the post-menopausal setting (Cardoso et al., 2012). Given the significant issues that acquired resistance to endocrine therapy can pose, it is critical to gain a greater understanding of the key molecular drivers, especially those changes that occur while on therapy, that can mediate escape mechanisms. The ability to longitudinally sample specimens from the same patient, about whom the clinical demographics and treatment are known, is a powerful tool. However, cohorts of such paired samples are rare, as illustrated by the sequencing study of a large cohort of breast cancer patients (Razavi et al., 2018). Within their group of 1918 tumours sequenced, only 74 pre- and post-progression matched samples from patients who had received hormonal therapy were identified. The importance of characterising paired samples has been recognised in the design of the AURORA study (Aftimos et al., 2021), which aims to profile 1000 matched primary and metastatic breast cancer samples using a multi-omics approach.

Previous work has been done on a UK set of paired tumour biopsies prior to AI therapy, and following progression or recurrence on AI treatment, by Professor Dowsett's group. The first study on 55 of these pairs involved immunohistochemical assessment of ER, PGR, HER2, insulin receptor substrate -1 (IRS-1), stathmin, PTEN and Ki67, and showed that the AI-resistant phenotype is highly variable (Arnedos et al., 2014). Further work on these samples using targeted DNA and RNA sequencing demonstrated that three genes were exclusively mutated in the post-treatment sample (*ERBB2, MAP2K4,* and *ESR1*) but

that otherwise there was a high degree of heterogeneity between the resistant specimens, with few apparent common gene expression patterns that could mediate the development of resistance (Lopez-Knowles et al., 2019). The main mechanism of AI resistance suggested by this study was the development of *ESR1* mutations, allowing for higher expression of oestrogen-regulated genes, despite treatment with AIs. This is corroborated by the pre-clinical finding that long-term culture of cells under oestrogen-deprived conditions enriches for *ESR1* mutations (Martin et al., 2017). Furthermore, clinical data have also found that *ESR1* mutations are associated with AI resistance in metastatic breast cancer. One study has shown that 30% of patients with metastatic breast cancer treated with an AI had an *ESR1* mutation at the time of progression (Clatot et al., 2016), with another showing that patients with an *ESR1* mutation demonstrated reduced progression-free survival with AI treatment (Zundelevich et al., 2020). Finally, *ESR1* mutations in the ctDNA of patients with metastatic disease were almost exclusively found in those demonstrating resistance to AI therapy (Fribbens et al., 2016). However, the study by Lopez-Knowles et al was limited to looking at RNA expression of 209 genes, as the Nanostring technology relies on probe hybridization to selected genes. New advances in RNA-sequencing have allowed the use of smaller quantities of RNA, extracted from formalin-fixed, paraffin-embedded (FFPE) material, and thus permitted these samples to be submitted for RNA-sequencing.

3.1.5 Aims and hypothesis

The hypothesis underpinning the work in this chapter is that a comprehensive NGS technique, RNA-sequencing, which significantly increases the number of genes counted, may shed additional light on the molecular changes occurring in these specimens as a result of AI treatment, and contributing to AI resistance. The aim therefore, would be to identify these alterations in the patterns of gene expression, examine whether these changes could logically contribute to mechanisms of AI resistance, and determine whether they could be targeted to tackle the obstacle of endocrine therapy resistance.

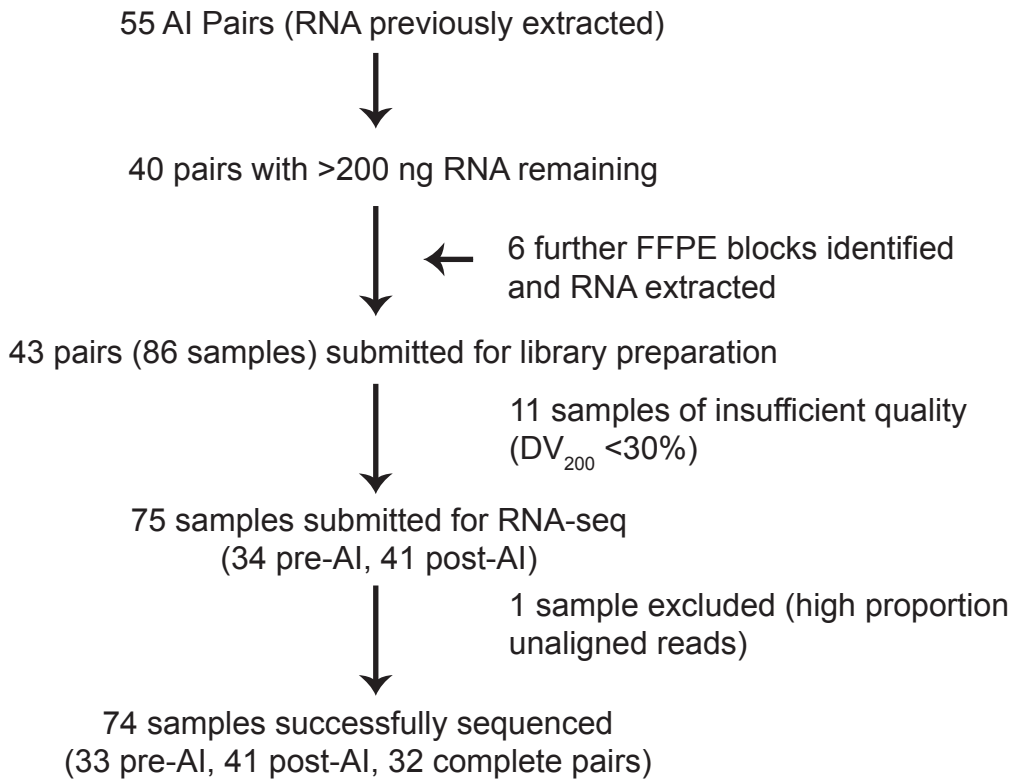

Figure 3.1: Consort diagram of the 55 AI paired samples considered for RNA-sequencing

3.2 Results

3.2.1 Patient demographics

Figure 3.1 illustrates which of the samples detailed in the previous work on this cohort (Lopez-Knowles et al., 2019) had sufficient remaining RNA to be utilised in this work, and Table 3.1 outlines the clinical characteristics of this group. In summary, the first biopsy (pre-AI) was most commonly obtained from the primary tumour (65%) in the setting of either early or locally advanced breast cancer. The second, post-AI biopsy was most frequently taken from a local recurrence (60%), in the setting of metastatic or locally advanced cancer. The median time to treatment failure on the first AI was 12 months, with a median overall survival of 7.5 years.

Table 3.1: Patient demographics. The clinical characteristics of 42 patients with RNA-seq data				
Clinical Characteristics			***n***	**(%)**
Diagnosis	Age (years)	Median	56	
		Range	33-86	
	Disease status	Early BC	31	(72)
		Locally advanced	7	(16)
		Metastatic	5	(12)
Age at start of AI treatment (years)		Median	65	
		Range	37-88	
Pre-AI biopsy	Site	Primary	28	(65)
		Local recurrence	14	(33)
		Distant recurrence	1	(2)
	Disease status	Early BC	21	(49)
		Locally advanced	19	(44)
		Metastatic	3	(7)
AI therapy	Type	Anastrozole	19	(44)
		Letrozole	23	(53)
		Exemestane	1	(2)
	Treatment setting	Neoadjuvant	6	(14)
		Local recurrence	23	(53)
		Metastatic	14	(33)
Post-AI biopsy	Site	Primary	4	(9)
		Local recurrence	26	(60)
		Distant recurrence	13	(30)
	Disease status	Early BC	1	(2)
		Locally advanced	17	(40)
		Metastatic	25	(58)
Endocrine therapy prior to AI		None	9	(21)
		Tamoxifen	31	(72)
		Tamoxifen + AI	2	(5)
		Goserelin	1	(2)
Endocrine therapy after progression on AI		None	14	(33)
		Exemestane	27	(63)
		Tamoxifen	1	(2)
		Fulvestrant	1	(2)
HER2 status		HER2 positive[a]	6	
Overall survival[b]		Median (years)	7.5	
		Range (years)	1-33	
Time to Treatment Failure on 1st AI		Median (months)	12	
		Range (months)	0-65	

BC: breast cancer, AI: aromatase inhibitor

[a] Either pre-AI or post-AI biopsy

[b] Defined as time from primary diagnosis of breast cancer to death (patients alive at time of last follow-up excluded)

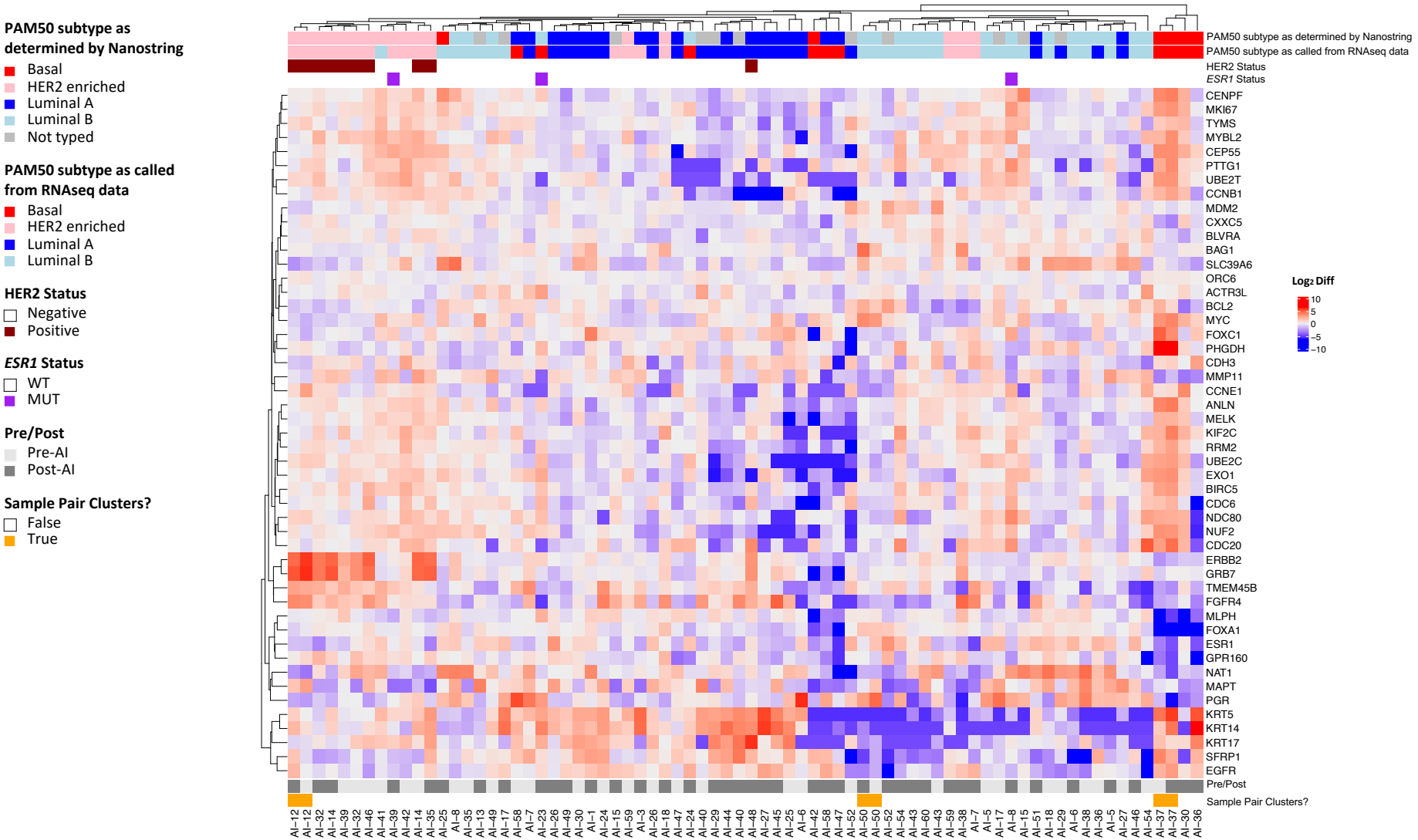

Figure 3.2: Heatmap of unsupervised hierarchical clustering of RNA-seq data based on PAM50 geneset

Figure 3.2 Heatmap of unsupervised hierarchical clustering of RNA-seq data based on PAM50 geneset. Subtypes were classified to luminal A, luminal B, HER2-enriched and basal according to previous Nanostring analysis (top row), and from subgroup-specific gene-centred subtype calling of PAM50 genes from the RNA-seq data (second row). Heatmap colours from blue to red represent low to high expression of the PAM50 genes. Samples with *ERBB2* amplification (third row), and those that acquired an *ESR1* mutation (fourth row) are highlighted, as are the pre-AI and post-AI pairs that clustered together (bottom rows).

3.2.2 Characterisation of molecular subtyping

Initial exploration of the data was done through the use of unsupervised hierarchical clustering from the PAM50 geneset, illustrated in Figure 3.2, to see if there were broad patterns of behaviour common to each subtype. As discussed in Section 1.1.4, breast cancer may be divided into molecular subtypes, each of which demonstrate typical patterns of behaviour. The PAM50 gene set is a list of 50 genes that classify breast cancers into these subtypes (Perou et al., 2000), and were refined from a larger list of genes found through microarray studies that were subjected to statistical analyses to identify those which showed high correlation to each intrinsic subtype.

Subtyping was characterised by a subgroup-specific gene-centering method which was validated through comparison with the Nanostring subtyping performed in the previous study (Lopez-Knowles et al., 2019). This initial analysis shows that samples tended to cluster according to their molecular subtype, rather than within their pairs. Furthermore, the post-AI samples tend to cluster together more than the pre-AI samples when characterised by the PAM50 geneset, suggesting that that while the pre-AI samples may commence from a variety of molecular backgrounds, the changes they undergo tend towards similarity. It can also be seen that the HER2-enriched samples, particularly those with *ERBB2* amplification, retained upregulation of *ERBB2* expression, whether pre-AI or post-AI. Of note, of the seven HER2-positive patients in this cohort, two received trastuzumab prior to the pre-AI sample, one received it between the pre-AI and post-AI biopsy, three were treated with it following the post-AI biopsy, and one patient did not receive trastuzumab. The luminal A samples tended to maintain ER-signalling and show lower expression of proliferation related genes, while the opposite was true of the luminal B and basal subtypes. While the majority of samples that have been called as basal are post-AI samples – that is, following AI-therapy their molecular

behaviour is more characteristic of a basal subtype – there is one pair for which the pre-AI and post-AI samples are characterised as basal, by both Nanostring and from the RNA-seq data itself. The IHC of this sample has been checked and found to be ER-positive, but given that the pre-AI sample for this pair is of a very different molecular background to the rest of the pre-AI cohort, this pair has been excluded from differential expression and gene set enrichment analyses.

Given this difference in behaviour between the molecular subtypes, principal component analysis (PCA) of all the samples was performed (Pearson, 1901) using the prcomp function in R, and is illustrated in Figure 3.3. Of note, 16 of the 32 pairs changed molecular subtype over the course of the study, as illustrated in Table 3.2. As such, the classification for comparison is based on the subtype of the pre-AI sample, with the aim of capturing the changes that occur on AI treatment. Given that there were 10 samples with no corresponding pair, these have been coloured black. As can be seen in Figure 3.3A and 3.3B, while the pre-AI and post-AI samples of the luminal B and HER2-enriched subtypes seem to cluster together, there is separation of luminal A subtypes from the non-luminal A subtypes. Furthermore, the pre-luminal A subtypes appear to undergo the greatest change on AI treatment, as illustrated in Figure 3.3B and 3.3D, with a significant difference in the change in Euclidean distance between pairs between luminal A and luminal B subtypes (p=0.03) and a non-significant distance between luminal A and HER2-enriched subtypes (p=0.07). This PCA analysis suggests that the cancers that start with a luminal A phenotype undergo the greatest change on AI treatment.

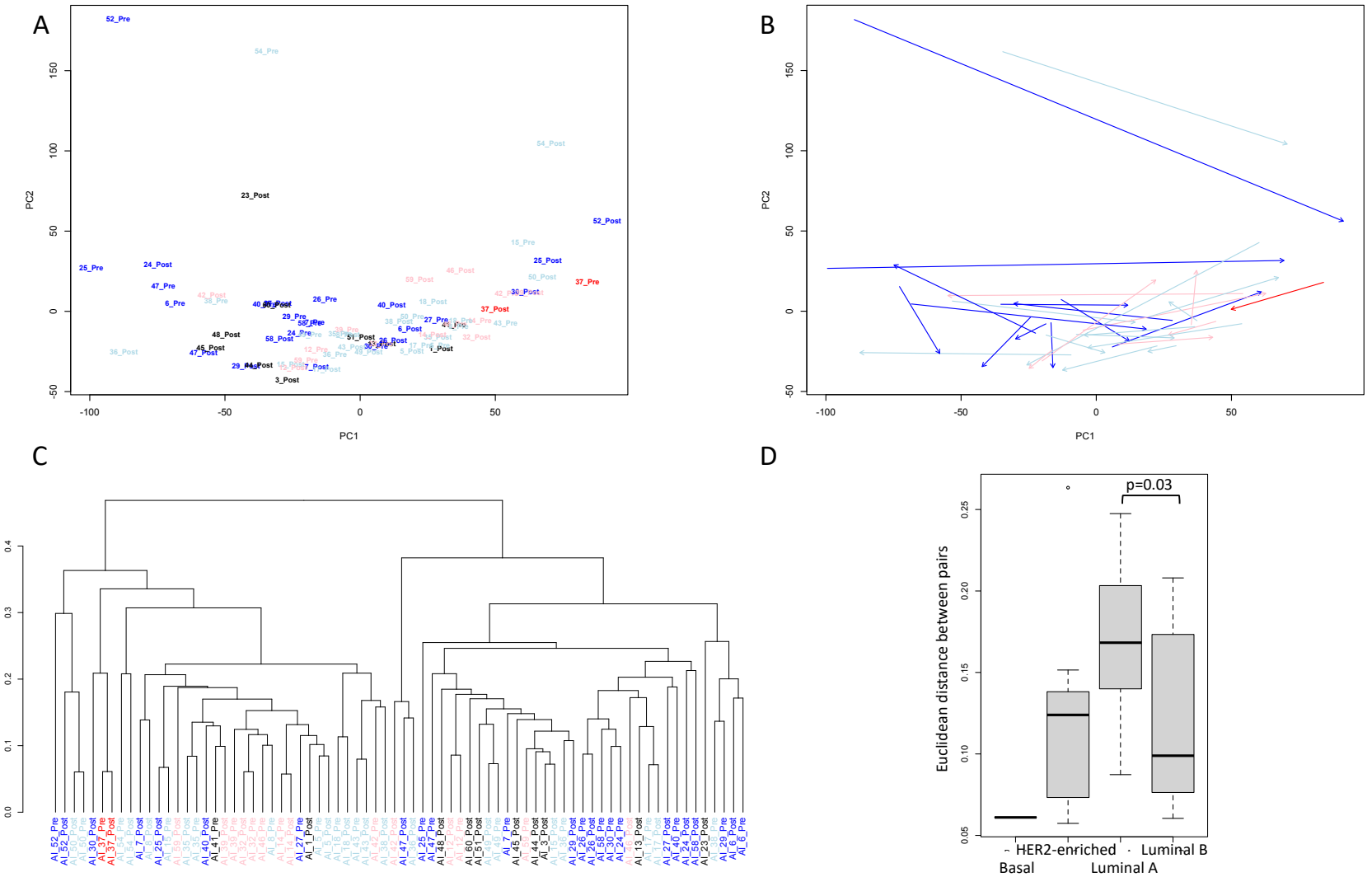

Figure 3.3: Characterisation of sample set

Figure 3.3 Characterisation of sample set. (A) Principal component analysis (PCA) of samples in cohort. Plot of the 1st and 2nd principal components of PCA analysis using prcomp function from 'stats' package in R. PCA based on log_2 normalized counts of expressed genes. Samples are named according to their pair number, and whether they are pre-AI or post-AI. Samples are coloured according to the molecular subtype of the pre-AI sample (dark blue - luminal A, light blue – luminal B, pink – HER2-enriched, red – basal, black – sample has no corresponding pair). **(B) PCA of samples demonstrating links between pre-AI and post-AI samples** Plots of the 1st and 2nd principal components of the PCA analysis with arrow linking pre- and matched post-AI sample. Arrow colours based on the pre-AI samples (dark blue – luminal A, light blue – luminal B, pink – HER2 enriched, red – basal) **(C) Unsupervised clustering of samples utilising all expressed genes from RNA-seq data**. Dendrogram based on hierarchical cluster analysis using Spearman's correlation of log_2 normalized counts of expressed genes, Euclidean distance, and ward.d2 minimum variance method to cluster patients. Sample naming and colouring as per panel A. **(D) Boxplots of Euclidean distance between the pairs of samples, categorised by subtype**. Mann-Whitney test to determine differences between groups. Euclidean distance based on method used for calculation of dendrogram as per panel (C).

Table 3.2: Number of molecular subtypes pre- and post-AI therapy

		Post-AI Subtype			
Pre-AI Subtype		Luminal A	Luminal B	HER2-enriched	Basal
	Luminal A	5	3	1	5
	Luminal B	1	6	5	0
	HER2-enriched	0	1	5	0

n=32 complete pre- and post AI pairs

3.2.3 Comparison of all pre-AI *vs* all post-AI samples

Following preprocessing of the raw count data, 21242 genes were used in the analysis of all pre-AI and all post-AI samples. Differential expression of individual genes between the pre-AI and post-AI samples was detected using the package DESeq2. Comparisons were drawn between all pre-AI and post-AI samples, and also within subtypes, namely, luminal A, luminal B, and those that were HER2-positive. There were small numbers of HER2-enriched and basal subtypes and so subgroup analyses were not performed on these samples. Tables 3.3 and 3.4 outline the significantly upregulated and down-regulated genes in all post-AI samples compared to all pre-AI samples, with the false discovery ratio (FDR) being set at ≤0.1. Genes are ranked by FDR and by the log_2 fold change.

Table 3.3: Significantly upregulated genes in response to aromatase inhibitor therapy			
Gene ID	**Description**	**FDR**	**log_2 fold change**
ACSBG1	Long chain fatty acid CoA ligase	0.02	2.73
CLEC11A	C-type lectin domain family 11 member A	0.02	1.42
KRT10	Keratin, type I cytoskeletal 10	0.02	1.81
CYP26B1	Cytochrome P450 26B1	0.02	1.60
DPF3	Zinc finger protein DPF3	0.02	2.17
KLF5	Krueppel-like factor 5	0.03	1.56
HBB	Haemoglobin subunit beta	0.03	2.19
HBA1	Haemoglobin subunit alpha 2	0.03	2.56
MASP1	Mannan-binding lectin serine protease 1	0.03	2.19
KCNJ15	ATP-sensitive inward rectifier potassium channel 15	0.06	1.43
SCML2	Sex comb on midleg-like protein 2	0.06	1.37
MMP9	Matrix metalloproteinase-9	0.07	2.04
TYRO3	Tyrosine-protein kinase receptor 3	0.07	1.11
ST3GAL2	CMP-N-acetylneuraminate-beta-galactosamide-alpha-2,3-sialyltransferase 2	0.07	0.85
ANGPTL1	Angiopoietin-related protein 1	0.07	1.65
SLC39A14	Metal cation symporter ZIP14	0.07	0.64
RORB	Nuclear receptor ROR-beta	0.07	1.90
ATP1A2	Sodium/potassium-transporting ATPase subunit alpha-2	0.07	1.63
CUBN	Cubilin	0.07	1.32
EGFR	Epidermal growth factor receptor	0.07	1.19
PALM2AKAP2	PALM2 and AKAP2 fusion	0.07	0.54
HBA2	Haemoglobin subunit alpha 2	0.08	2.20
RSPO3	R-spondin-3	0.08	1.66
CACHD1	VWFA and cache domain-containing protein 1	0.08	0.77
PGAP4	Post-GPI attachment to proteins factor 4	0.08	1.80
PDE8A	High affinity cAMP-specific and IBMX-insensitive 3',5'-cyclic phosphodiesterase 8A	0.08	0.53
FCN1	Ficolin-1	0.09	1.37
RAVER1	Ribonucleoprotein PTB-binding 1	0.09	0.78
NLGN1	Neuroligin-1	0.09	2.15
TRPC6	Short transient receptor potential channel 6	0.09	1.12
ADGRF1	Adhesion G-protein coupled receptor 1	0.10	1.46
TTC33	Tetratricopeptide repeat protein 33	0.10	0.70
HSD17B2	17-beta-hydroxysteroid dehydrogenase type 2	0.10	2.26
Comparison of all pre-AI samples (n=33) and post-AI samples (n=41), FDR≤0.1			

Table 3.4: Significantly downregulated genes in response to aromatase inhibitor therapy			
Gene ID	**Description**	**FDR**	**log_2 fold change**
TPH1	Tryptophan-5 hydroxylase-1	0.00	-2.22
C5AR2	C5a anaphylatoxin chemotactic receptor 2	0.00	-1.00
PGR	Progesterone receptor	0.00	-2.23
RMST	Rhabdomyosarcoma 2 associated transcript	0.02	-2.93
ERICH3		*0.02*	*-3.09*
NRAV	Negative regulator of antiviral response	0.02	-0.62
AC013652.1		*0.02*	*-1.68*
GABRG3	Gamma-aminobutyric acid type A receptor subunit gamma-3	0.03	-2.06
DCDC1	Doublecortin Domain Containing 1	0.03	-2.11
ADCY1	Adenylate cyclase 1	0.03	-1.53
AL591845.1		*0.03*	*-1.41*
AL138889.1		*0.04*	*-0.68*
C6orf141	Chromosome 6 open reading frame 141	0.04	-1.94
AC091181.1		*0.05*	*-0.64*
KDM4B	Lysine demethylase 4B	0.06	-0.79
PTGES	Prostaglandin E synthase	0.06	-1.40
SLC6A4	Solute carrier family 6 member 4	0.06	-1.92
GREB1	Growth regulating estrogen receptor binding 1	0.06	-1.65
AC092969.1		*0.06*	*-1.90*
AC004494.1		*0.07*	*-1.24*
Z83745.1		*0.07*	*-0.57*
ZNF552	Zinc finger protein 552	0.07	-1.06
FAR2P1		*0.07*	*-1.92*
MC2R	Melanocortin 2 receptor	0.08	-1.02
GP2	Glycoprotein 2	0.08	-1.77
TPBG	Trophoblast glycoprotein	0.08	-0.74
CCDC30	Coiled-coil domain containing 30	0.08	-0.54
ZNF587	Zinc finger protein 587	0.08	-0.61
CEP85	Centrosomal protein 85	0.08	-0.77
EVL	Enah/vasp-like	0.08	-0.87
PUS10	Pseudouridine synthase 10	0.09	-0.64
ZNF8	Zinc finger protein 8	0.09	-0.31
GRB14	Growth factor receptor bound protein 14	0.09	-2.46
LSM2	LSM2 homolog U6 small nuclear RNA and mRNA degradation associated	0.10	-0.64
DPPA4	Developmental pluripotency associated 4	0.10	-0.95
Comparison of all pre-AI samples (n=33) and all post-AI samples (n=41), FDR≤0.1 Non-coding RNAs and pseudogenes are denoted in blue font			

The first conclusion to be drawn from the comparison of significantly differentially expressed genes in all post-AI samples against all pre-AI samples is that the numbers of genes are low (33 upregulated genes and 35 downregulated genes). These genes were inputted into functional enrichment analysis software such as g:Profiler (Raudvere et al.,

2019), and databases assessing protein-protein interactions such as STRING-db (Szklarczyk et al., 2015) with no relevant results. However, literature review of the genes did provide support for the validity for the results of this study. The upregulation of genes such as *MMP9*, a matrix metalloproteinase with a role in establishing the metastatic niche in breast cancer (Owyong et al., 2019), *ST3GAL2*, a predictive biomarker of breast cancers resistant to chemotherapy (Aloia et al., 2015), *KLF5*, a transcription factor that can promote cell proliferation and survival, as well as being associated with shorter breast cancer survival (Zheng et al., 2009), and *RSPO3,* a secreted protein that plays a role in cell proliferation regulation, high expression of which has been significantly correlated with PI3K/AKT pathway activity and epithelial-mesenchymal transition (Gu et al., 2020), has biological validity for this group of patients who have progressed on AI therapy. Similarly, both *PGR* and *GREB1*, genes under the transcriptional control of ER, are downregulated in the post-AI samples, as is *PTGES*, a prostaglandin E-synthesising enzyme, which is usually upregulated in breast cancer cells in response to oestrogen (Frasor et al., 2008). These results suggest that while there are not enough significantly differentially expressed genes to suggest a common pathway by which breast cancers may develop resistance to AI therapy, exposure to AIs may have had an effect on the transcriptome of these samples.

3.2.4 Individual changes in gene expression by subtype

When looking at the genes differentially expressed according to subtype, it can be seen that there is a high degree of mutual exclusivity as to the expression of which genes are altered, as demonstrated in Figure 3.4A, and the greatest changes in individual gene expression were seen in the luminal A subtype. This finding is also represented in Figure 3.4B, which illustrates the difference in the changes in gene expression between the various subtypes. These results show that of the changes that do occur following AI therapy, the alterations in expression are governed by the subtype of breast cancer, and that it is the luminal A subtype that demonstrates the greatest change in gene expression.

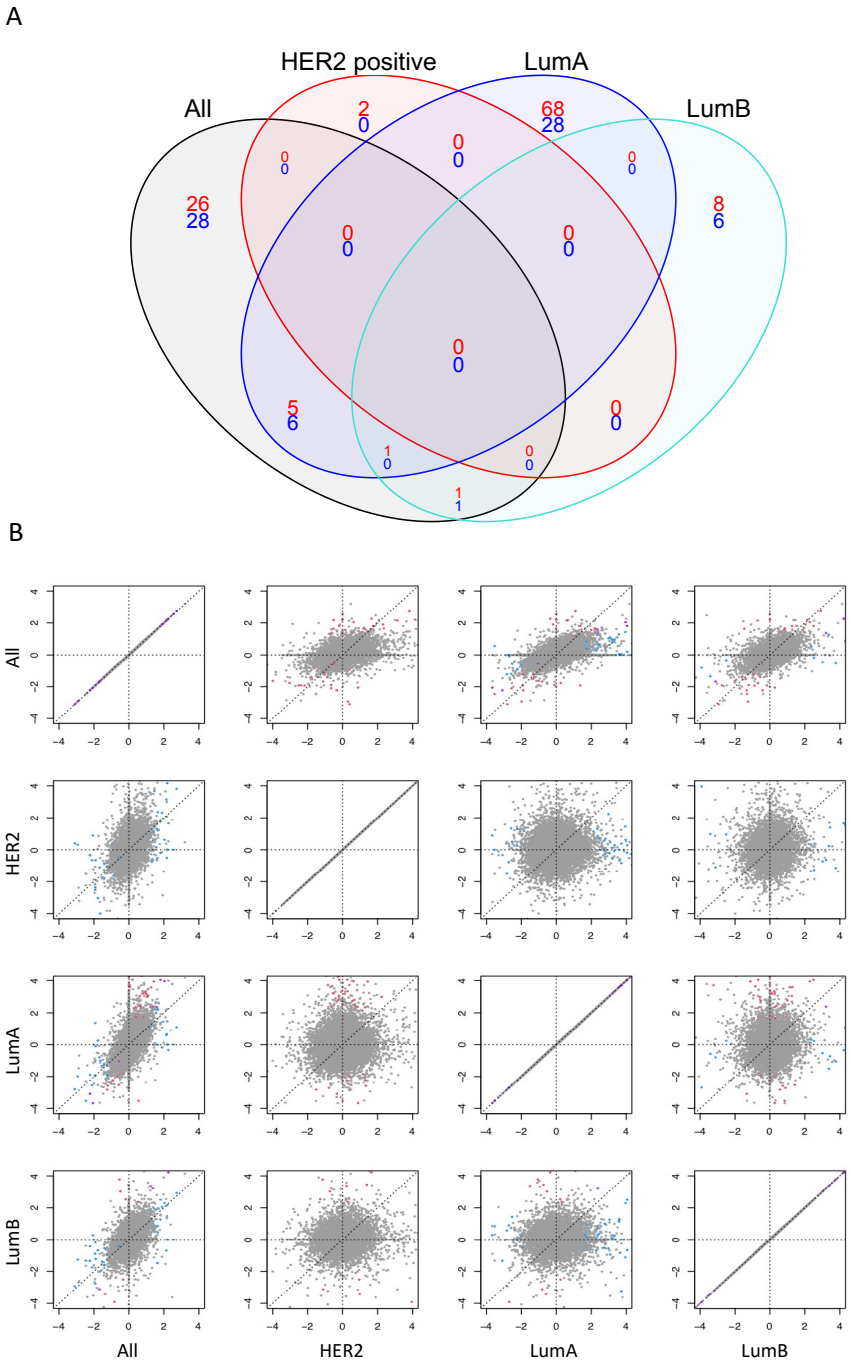

Figure 3.4 Significant differentially expressed genes in post-AI samples compared to pre-AI samples, classified by subtype. (A) Venn diagram of numbers of significantly upregulated and downregulated genes according to subtype. LumA samples are paired samples where the pre-AI biopsy was subtyped as luminal A. LumB samples are paired samples where the pre-AI biopsy was subtyped as luminal B. HER2 samples are samples where either the pre-AI or post-AI sample was HER2-positive. The category 'All' encompasses all samples, whether or not they had a corresponding pair. The category 'All' also includes those samples subtyped as HER2-enriched without demonstrating *ERBB2* amplification, or subtyped as basal. Number of significantly upregulated genes are noted in red, and significantly downregulated noted in blue, with threshold of significant set at FDR ≤0.1). **(B) Scatterplots of $\log_2$ fold change of post-AI *vs.* pre-AI gene expression, compared by subtype.** Scatterplots show the log2 fold change of each

gene's expression following AI-therapy in the x-axis subtype, *vs.* y-axis subtype. Red indicates a significant change in expression pre-AI *vs*. post-AI in the x-axis subtype, blue indicates a significant change in expression pre-AI *vs.* post-AI in the y-axis subtype, and purple indicates significant change in both subtypes (threshold of significance set at FDR ≤0.1).

The lists of differentially upregulated and downregulated genes following AI therapy by subtype were inputted into the same functional enrichment software and protein databases, but did not reveal any potential pathways of resistance (data not shown). These genes were also inputted into the COSMIC database (Tate et al., 2019), but no known somatic mutations in breast cancer associated with these genes were found (data not shown). However, literature review of some of the individual genes did reveal potential areas of interest.

Expression of *MMP9* and *CD68*, a macrophage marker, were both significantly upregulated in the samples categorised pre-AI therapy as luminal A subtype. High co-expression of these markers has been associated with poorer overall survival in ER-positive cancers (Pelekanou et al., 2018). Other biomarkers of poorer prognosis, cell migration, and resistance to chemotherapy, such as *HMGA2, SMARCA5,* and *CTSL* (Wu et al., 2016, Jin et al., 2015, Zhao et al., 2019) were also upregulated in the luminal A post-AI samples in comparison with the pre-AI biopsy. Downregulated genes included *STAG2*, a tumour suppressor gene which is part of the cohesion complex that tethers chromatids and mediates DNA repair (Benedetti et al., 2017), and *DRG1*, which has been identified as a metastasis suppressor gene (Baig et al., 2012, Bandyopadhyay et al., 2004), again suggesting a change in molecular drivers toward more aggressive, metastatic behaviour. Mechanisms for epigenetic mediation of resistance to endocrine therapy may also play a role in these samples, as the long non-coding RNA H19 was also found to be upregulated. Increased expression of H19 has been observed when endocrine-therapy resistant cell lines were treated with tamoxifen or fulvestrant, and inhibiting expression of H19 can reverse resistance to these agents (Basak et al., 2018, Wang et al., 2019). The study by Basak et al. also suggested that H19 can regulate expression of ER, and suggested that targeting H19 provides an indirect way of reducing ER-signalling upon which many ER-positive breast cancers are reliant. Therefore, the findings from this RNA-seq dataset suggest that the luminal A subtypes have upregulated markers of more aggressive, invasive, and proliferative disease, and suggest

a potential mechanism for development of endocrine-therapy resistance through epigenetic modification by the long non-coding RNA H19.

In the luminal B subtype, while literature review of the downregulated genes did not reveal any relevant findings, the genes encoding the transcription factor *E2F2*, and the cytoskeletal protein *ANK1*, were significantly upregulated. The E2F family of transcription factors, as well as playing a well-characterised role in cell cycle control in the activation of the transcription of S-phase promoting genes, as described in Section 1.1.5.4, have also been shown to control the expression of genes necessary for angiogenesis and ECM remodelling, necessary for metastasis (Hollern et al., 2014). The induction of transcription of *ANK1* has been related to the actions of p53 following DNA damage, and the correlation of high *ANK1* expression with decreased breast cancer disease-free survival has led to the hypothesis that elevated ankyrin-1 levels may enhance the spread of cells that are resistant to chemotherapy (Hall et al., 2016). Interestingly, another long non-coding RNA, Linc00514, was found to be overexpressed in the luminal B subtypes. Linc00514 has been shown to be highly expressed in breast cancer cell lines and breast cancer tissue, and overexpression has been shown to promote proliferation and invasion in breast cancer cell lines, and development of metastatic lung deposits in mouse models via Notch signalling (Tao et al., 2020). Therefore, there is evidence from this RNA-seq dataset that the post-AI samples of the luminal B subtype have developed more invasive and metastatic behaviour, although the individual significant differentially expressed genes do not point to a specific pathway by which AI therapy resistance is mediated.

In looking at the HER2-positive group, there were very few genes significantly differentially expressed between the pre-AI and post-AI samples. This is likely due to the limited numbers of HER2-positive samples. Of the genes identified, literature review did not reveal any findings of note.

There were small numbers of significantly differentially expressed genes, in all comparisons, and consequently few clear pathways identified that could be mediating AI therapy resistance. Furthermore, given the small number of genes identified, and the FDR threshold set at ≤0.1, reservations must be borne regarding the strength of

conclusions drawn from this data. Therefore, gene set enrichment analysis was carried out to identify if global gene expression changes had resulted in an alteration to whole signalling pathways which could contribute to endocrine resistance.

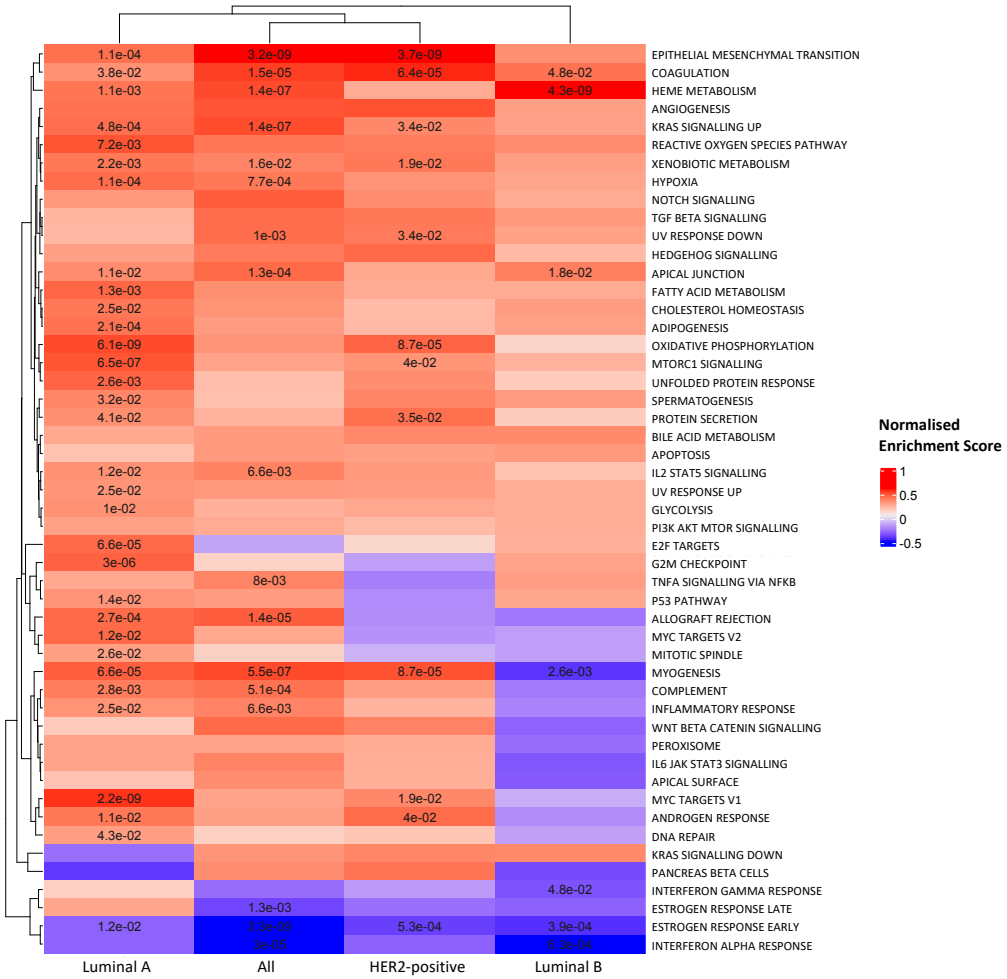

Figure 3.5. Gene set enrichment analysis (GSEA) of hallmark gene sets of the change from pre- to post-treatment by molecular subtype. The $\log_2$ fold change of all genes from pre- to post-AI for each subtype was calculated using the DESeq2 programme in R. This was used to perform GSEA using the hallmark gene sets. Heatmap shows the normalised enrichment scores for each hallmark pathway, with heatmap colours from blue to red representing low to high enrichment. Where FDR ≤0.1, adjusted *p*-value is included within the heatmap. Luminal A samples are paired samples where the pre-AI biopsy was subtyped as luminal A. Luminal B samples are paired samples where the pre-AI biopsy was subtyped as luminal B. HER2-positive samples are samples where either the pre-AI or post-AI sample was HER2-positive. 'All' samples encompasses all samples, whether or not they had a corresponding pair, and includes those subtyped as HER2-enriched without demonstrating *ERBB2* amplification, and basal samples.

3.2.5 Gene set enrichment analysis

Gene set enrichment analysis (GSEA) is a statistical method that can look for overall changes to signalling pathways. Interventions, such as AI therapy, may alter the expression levels of individual genes by a large margin, or they may alter the expression levels of several genes involved in a pathway in a such a way that overall no individual gene is more significantly upregulated or downregulated, but that small changes in each gene causes up- or downregulation of entire pathway. The statistical method employed is a version of a rank sum test, where GSEA can look at a group of genes in a pathway and determine how biased is the rank sum against what would be expected by chance.
The scoring from GSEA of the change from pre-AI to post-AI treatment according to the hallmark gene sets is illustrated in Figure 3.5. This figure again illustrates that the luminal A pre-AI subtypes undergo the greatest change in pathway signalling following AI therapy, with 32 out of 50 hallmark gene sets showing significantly altered expression between pre-AI and post-AI samples, compared to 7 out of 50 in luminal B pre-AI subtypes, and 12 out of 50 in the HER2-positive samples (FDR set at $\leq$0.1 for significance). From this heatmap, it can be seen that early oestrogen response signalling is significantly downregulated in all subgroups, which is to be expected following AI therapy, and demonstrates that the post-AI tumour is less reliant on oestrogen-regulated signalling for growth. Conversely, the epithelial mesenchymal transition pathway is significantly enriched post-AI therapy in all groups except luminal B, which suggests transition to more invasive, metastatic disease.

To examine the significant hallmark pathways in more detail, the average $\log_2$ expression of each gene involved in the pathway in each patient was plotted according to the pre-AI subtype category, as shown in Figure 3.6. There was a clear downregulation of oestrogen response genes across all the pre-AI subtypes, suggesting a loss of oestrogen regulation, even in those where the primary tumours may be less reliant on oestrogen signalling – for example in the HER2-positive patients. The greatest differences between the subtypes were in MYC targets, and MTORC1 signalling, as well as in E2F targets, and G_2M checkpoint genes. In these pathways, there was a drive to higher expression in the luminal A post-AI samples, whereas expression of these pathways were already high in the pre-AI samples of luminal B and HER2-positive groups.

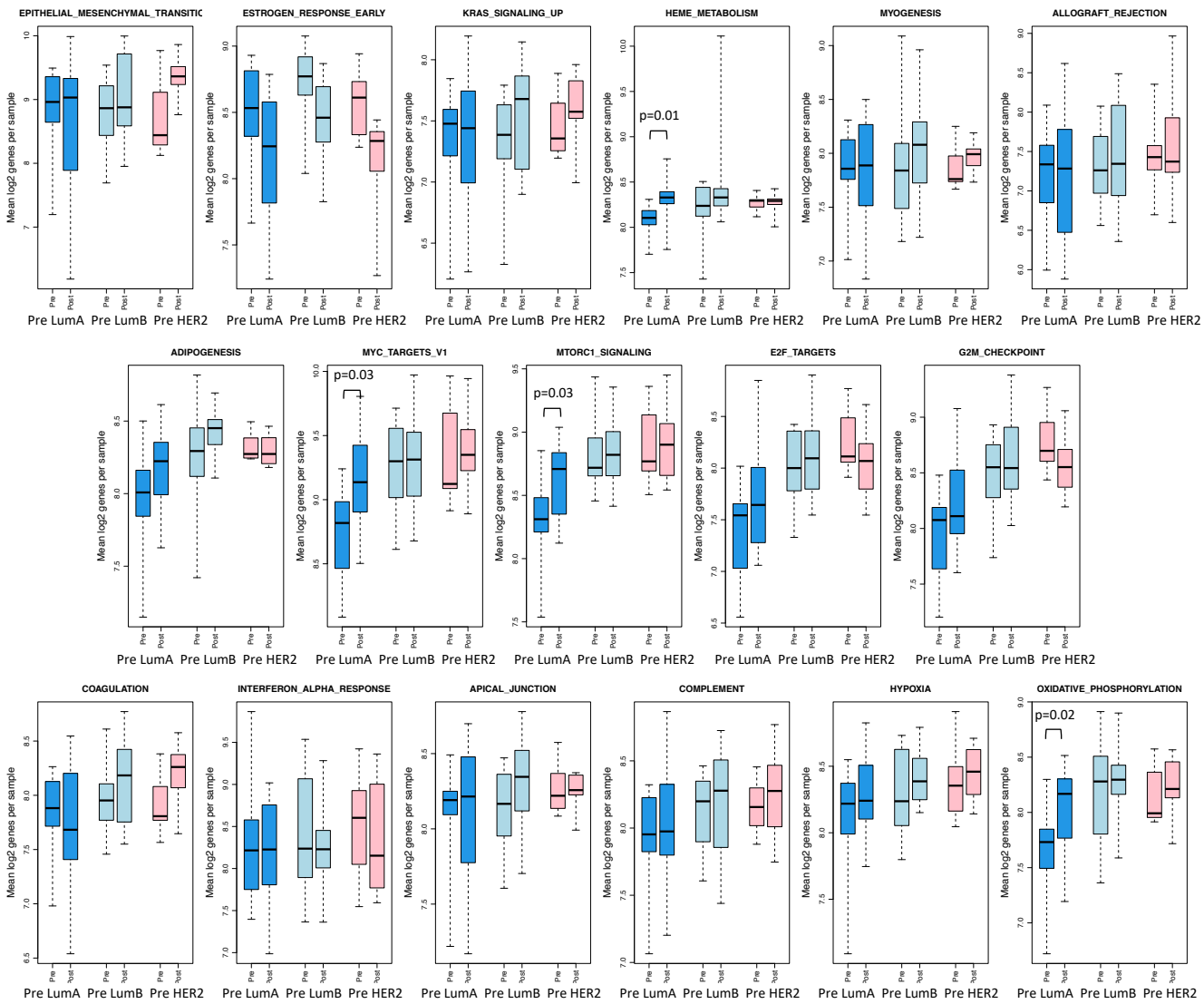

Figure 3.6: Boxplots illustrating average $\log_2$ expression of genes in significant GSEA hallmark pathways according to molecular subtype

Figure 3.6. Boxplots illustrating average log_2 expression of genes in significant GSEA hallmark pathways according to molecular subtype. GSEA data from Figure 3.5 were used to identify the significant hallmark pathways, with threshold of significance set at adjusted *p*-value<0.0001 in at least one subtype. Boxplots of the mean log_2 expression of the genes in each pathway per sample were formed to compare between pre- and post-AI samples.
Samples are allocated according to the pre-AI molecular subtype, with post-AI samples being defined by their pre-AI status. Central mark indicates median, edges of the box are 25^{th} and 75^{th} percentiles, with whiskers extending to the most extreme data points not considered outliers. Difference in log_2 expression of genes between pre-AI and post-AI samples assessed by Mann-Whitney test, with significant *p*-values listed.

The most striking observation from these figures is that while there is little change between pre-luminal B and post-luminal B, pre-HER2-enriched and post-HER2-enriched, and pre-basal and post-basal, there is a clear difference between the pre-luminal A and post-luminal A samples, even at the individual gene level as shown for the genes in the MYC targets and MTORC1 signalling pathways as shown in Figures 3.7A and 3.7B. Furthermore, it can be seen that the post-luminal A samples have changed such that they approximate the patterns seen in the luminal B and HER2-enriched samples. This suggests that exposure to AI therapy may precipitate the pre-luminal A samples to adopt proliferative and invasive behaviours that are associated with the other more aggressive subtypes.

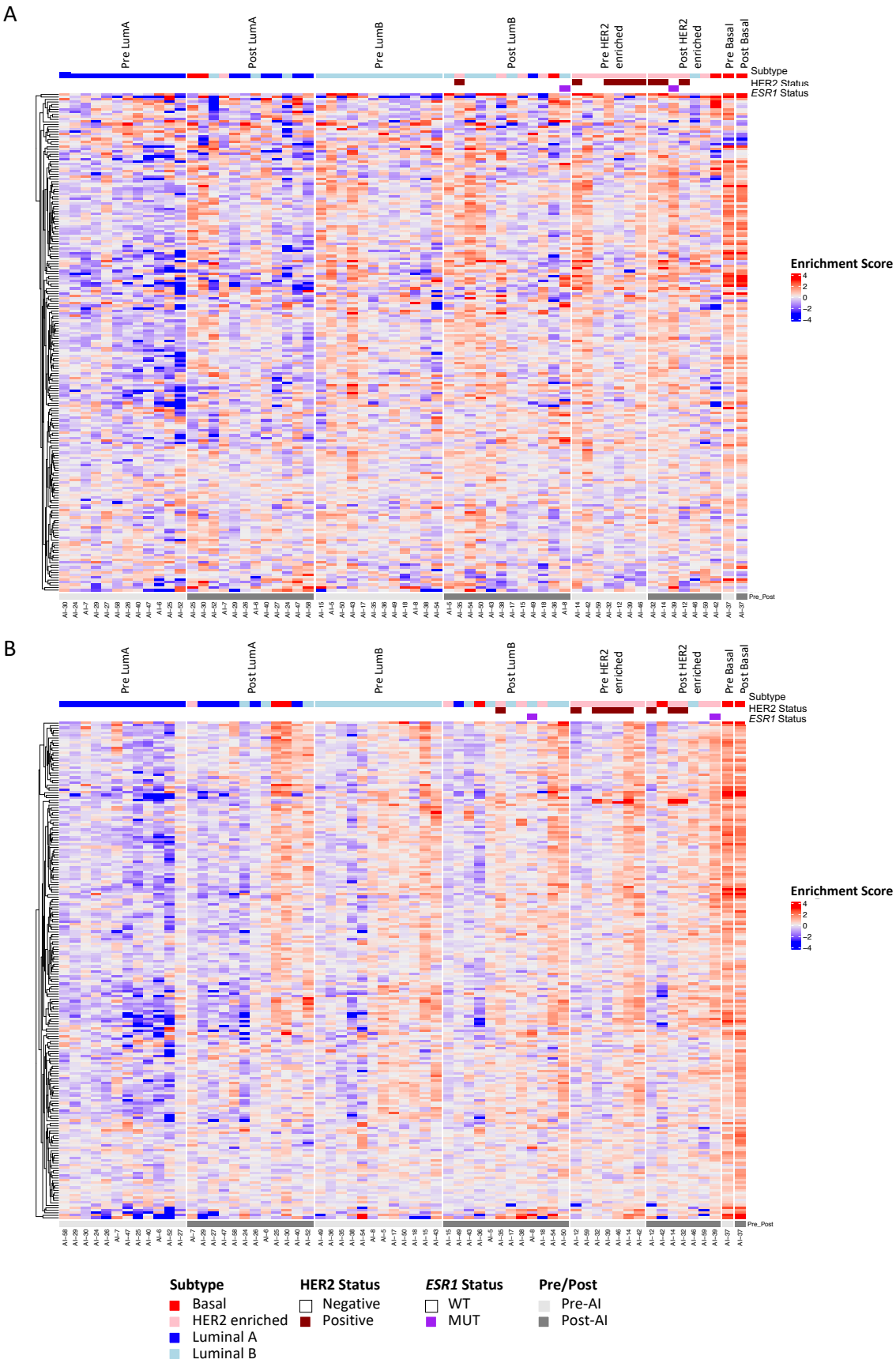

Figure 3.7: Median centred individual gene expression for genes in GSEA hallmark pathways

Figure 3.7. Median centred individual gene expression for genes in GSEA hallmark pathways. (A) MTORC1_SIGNALLING Hallmark pathway. **(B)** MYC_TARGETS V1 Hallmark pathway. Heatmaps of median centered log_2 expression values of expressed genes within the (A) MTORC1_SIGNALLING and (B) MYC_TARGETS V1. Samples are allocated according to the pre-AI PAM50 molecular subtype classification, with post-AI samples being defined by their pre-AI status. The subtype classification based on subtype calling of the post-treatment samples is illustrated in the top row of the figure. Heatmap colours from blue to red represent low to high enrichment. Only paired samples are included in this analysis. Row clustering-based defaults parameters of Heatmap function in 'ComplexHeatmap' package in R (Euclidean distance based on Pearson correlation with the 'complete' clustering method). The pre-AI samples were sorted by dendrogram order produced by default parameters of dendsort function in R

To examine any differences between the pre-AI subtypes, the differential expression of individual genes between the pre-luminal A, pre-luminal B, and pre-HER2-positive samples was examined. This revealed that the REACTOME cell cycle and G_1/S transition pathways were significantly downregulated in the pre-AI luminal A samples compared to the other pre-AI samples (adjusted *p*-value $2.67x10^{-22}$, and $1.66x10^{-10}$ respectively – data not shown). Examination of the genes undergoing the greatest change in expression within these pathways between pre-AI and post-AI luminal samples identified *HSP90AA1*, *CCNA2*, *DBF4*, and *PCNA*, as illustrated in Figure 3.8. These are all markers of proliferation. HSP90AA1 is a molecular chaperone protein that has been shown to activate oncogenic proteins, promote cell proliferation and metastasis (Liu et al., 2021), and overexpression has been linked to a poor breast cancer prognosis (Klimczak et al., 2019). Cyclin A2 is necessary to activate CDK2 and complete the G_1/S transition, as well as triggering the G_2/M transition. DBF4 is a zinc finger protein that forms a complex with cell division cycle 7-related kinase which is essential for the initiation of DNA replication (Jiang et al., 1999). PCNA (proliferating cell nuclear antigen) plays a myriad of roles in initiating DNA replication and replication-associated DNA repair (Boehm et al., 2016). As shown in Figure 3.8, that while comparatively lowly expressed in the pre-luminal A samples, these genes are upregulated in post-luminal A samples such that they approach the levels seen in the luminal B and HER2-positive subtypes. Furthermore, as the levels of these genes do not vary significantly between the pre-AI and post-AI samples of the luminal B and HER2-positive subtypes, this again suggests that the proliferative and invasive behaviours are present in these tumours from the outset, whereas they develop in the luminal A subtypes later in the disease process, perhaps in response to AI therapy.

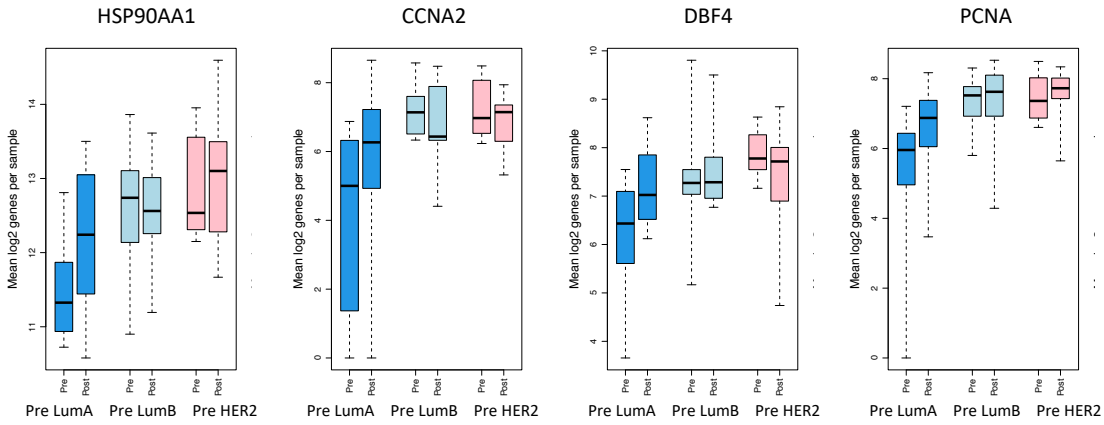

Figure 3.8 Boxplots of genes involved in REACTOME cell cycle and G1/S transition pathways. Boxplots of mean $\log_2$ gene expression per sample of the top four genes in the Cell Cycle and G_1/S transition REACTOME pathways undergoing the greatest change in expression between pre-luminal A and post-luminal A samples, plotted by molecular subtype. Samples are allocated according to the pre-AI molecular subtype. Central mark indicates median, edges of the box are 25th and 75th percentiles, with whiskers extending to the most extreme data points not considered outliers.

Finally, the list of genes upregulated in the post-AI samples of the luminal A subtype, and the list of genes with higher expression in the pre-AI luminal B and HER2-positive subtypes *vs* the pre-AI luminal A samples was compared. This was to examine for individual genes whose expression in the pre-AI luminal A samples were upregulated after therapy to match the levels seen in the pre-AI samples of other subtypes. This revealed 24 genes (data not shown) which were predominantly genes involved in nucleosome assembly and histone subunits. However, this analysis did reveal 2 genes, *ENO1*, a glycolytic enzyme, and *HNRNPAB*, a heterogeneous ribonucleoprotein, that have both been highlighted as potential biomarkers of more aggressive disease in breast cancer (Cancemi et al., 2019, Cao et al., 2020).

The overall trend in pattern of behaviour towards a more aggressive phenotype is demonstrated in Figure 3.9. These boxplots illustrate that the post-AI samples show a reduction in the correlation coefficient with their defined pre-AI molecular subtype (Haibe-Kains et al., 2012) following AI treatment. Concurrently, there is an increase in the post-AI samples' correlation with more proliferative subtypes: for example, the

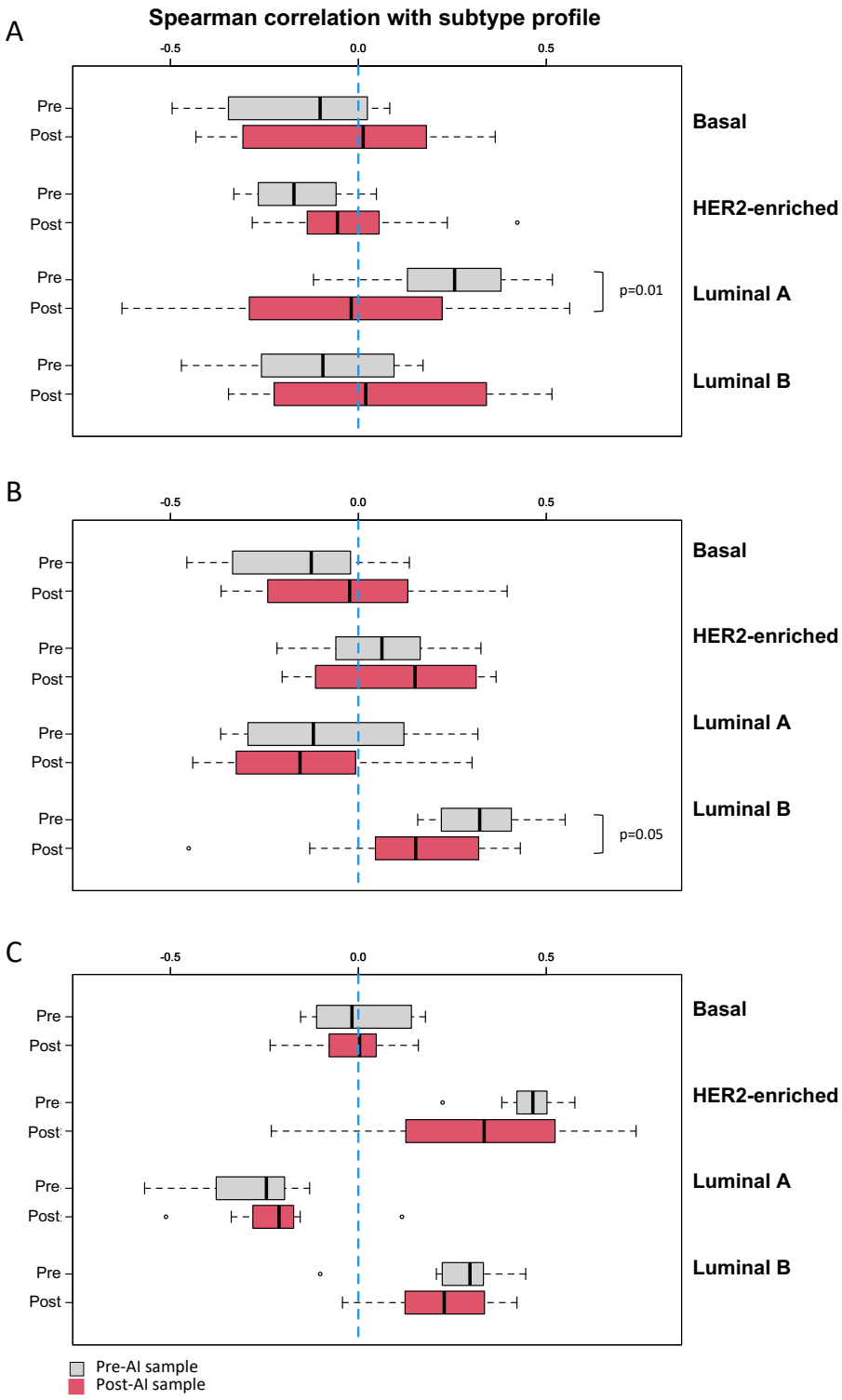

Figure 3.9: Changes in sample correlation with PAM50 molecular subtype profile pre- and post-AI therapy. (A) Samples defined as luminal A in pre-AI biopsy (B) Samples defined as luminal B in pre-AI biopsy luminal B samples (C) Samples that are HER2-positive in pre-AI biopsy. Samples were divided into molecular subtypes according to their pre-AI status, and then correlated with the defined PAM50 molecular subtype. Boxplots illustrate the Spearman's rank correlation coefficients for the samples in each group when compared to the PAM50 molecular subtype on the right. Grey boxes are

pre-AI samples, red boxes are post-AI samples. Central mark indicates mean, edges of the box are 25th and 75th percentiles, with whiskers extending to the most extreme data points not considered outliers. Difference between pre-AI and post-AI samples in subtype profile correlation tested by Mann-Whitney test, with significant *p*-values listed.

luminal A post-AI samples show an increased correlation with the luminal B and basal subtypes, and similarly, the luminal B post-AI samples show an increased correlation with HER2-enriched and basal subtypes. These plots therefore suggest that following AI treatment, the samples trend away from luminal A-type, ER-driven behaviour towards the more proliferative, ER-independent behaviour seen in other molecular subtypes of breast cancer. These results are supported by the first reports from the AURORA study (Aftimos et al., 2021), where the intrinsic subtype of 36% of cases was found to change following disease progression, usually to a more aggressive form.

3.3 Discussion

Cancer is a dynamic disease process, and the key driver changes that allow breast cancers to become resistant to AIs, a well-tolerated therapy, continue to elude us. This cohort of paired samples offered the opportunity to look for patterns of change to shed light on this clinical hurdle. The initial study characterising the biomarkers on these paired samples concluded that in the post-AI samples there was a loss of ER expression (perhaps contributing to AI resistance), reduced PGR expression, consistent with reduced ER-signalling, and higher Ki67 levels, indicative of a more aggressive disease phenotype (Arnedos et al., 2014). The second study confirmed the heterogeneity seen between the samples in the first study, reiterated the downregulation of ER-mediated signalling, and identified mutations in *PIK3CA*, *CDH1, MAP2K4*, and *ESR1*, that could contribute to resistance mechanisms (Lopez-Knowles et al., 2019). The findings from this project support the findings of the previous studies, and while profiling the whole transcriptome has not illuminated any new avenues regarding mechanisms of resistance development, the results obtained suggest a potential role for epigenetic modification by long non-coding RNAs in promoting resistance and a more aggressive phenotype. Finally, pathway analysis indicates that the cancers that are luminal A prior to commencing AI therapy can change such that they become more proliferative and invasive, thus taking on characteristics of the other, more aggressive, subtypes.

3.3.1 Limitations of RNA-seq in this cohort

3.3.1.1 Sample heterogeneity

While there is one clear unifying characteristic of these samples in that each pair represents a patient pre-AI and post-AI therapy, there is significant heterogeneity within the population. The primary cancer diagnosis ranges from 0-20 years prior to the pre-AI biopsy being taken. As a result, the pre-AI biopsy may be the diagnostic biopsy, or represent a recurrence after many years of dormancy. Similarly, the post-AI biopsy is any biopsy taken after progression on AI therapy, and is not necessarily the first sample diagnosing relapse. The heterogeneity between samples is best illustrated by the following three cases.

Patient number 6 (AI-7 and AI-8) was diagnosed with breast cancer in 1977. The pre-AI punch biopsy sample was taken in 2003 in the context of metastatic disease, and the post-AI core biopsy in 2008. Patient number 42 (AI-55 and AI-56) was diagnosed in 1999, with the pre-AI surgical specimen sample taken in 2007 due to local recurrence, and the post-AI surgical specimen sample obtained in 2008 following relapse. Patient number 49 (AI-69 and AI-70) was diagnosed in 2005, with the pre-AI sample being the diagnostic core biopsy. The post-AI sample was the surgical specimen, obtained a few months later, with the AI being used in a neoadjuvant context. This variation in disease and biopsy pattern will naturally increase the variability of the molecular changes identified with RNA-seq.

An additional area of variability is that many of the patients received tamoxifen and/or chemotherapy and/or radiotherapy in the intervening period between the two samples, or prior to the pre-AI biopsy. These treatment modalities may also have had an impact on gene expression that may have been wrongly attributed to AI therapy.

3.3.1.2 Methodological limitations

One of the most significant difficulties in this cohort is that the RNA samples were all extracted from FFPE tissue. As discussed in Section 3.1.3, this RNA is therefore more prone to being modified or cross-linked than RNA from fresh frozen tissue, and so the RNA may be more fragmented. Furthermore, the samples had been in storage for 10-22 years, and so may have degraded over time. More degraded samples have less

amplifiable RNA, lower library yields, and consequently fewer mappable reads. One of the quality control measures employed in assessing RNA quality was the DV_{200} metric, which is the percentage of RNA fragments with over 200 nucleotides. Given the age and nature of the samples, it was not surprising that the majority of the DV_{200} measurements were between 30-50%, which is categorised as 'low-quality' but in context of RNA-sequencing of historic FFPE samples, this is a reasonable result.

A second potential limitation of the methods is that total RNA-seq was used as the sequencing method. While this method does yield the most comprehensive transcriptome analysis, and the RIBO-Zero method removes the ribosomal RNA to allow sequencing to be focused on the desired transcripts, non-coding RNA is still included, and this reduces the read-depth on coding sections of the genome. Furthermore, due to the fragmentation levels of the input RNA, it was not possible to examine for splice variants, which is one of the advantages of total RNA-seq. Another consequence of the level of fragmentation of these samples is that sequencing techniques such as whole-exome sequencing, or methyl-seq, which may have been better able to identify drivers of resistance mechanisms and somatic mutations, was not possible.

Finally, as many of the samples were exhausted following the sequencing process, and due to the time constraints of the project, it was not possible to undertake any validation experiments of the above findings.

3.3.2 Concluding remarks

The challenge of treating relapsed or progressive disease is the key issue faced by patients in the clinic, and the aim of the work presented here was to characterise a rare set of longitudinally matched patient samples. However, even with this extended study of the transcriptome of this cohort, few key targets beyond the acquisition of *ESR1* mutations in the post-AI samples have been identified. The RNA-seq data show a high degree of inter-patient heterogeneity, with a drive towards proliferation and MTORC signalling in the post-AI samples (Figure 3.7). The luminal A subtypes show the greatest change in transcription from pre-AI to post-AI (Figure 3.4A), with an overall trend away from ER-driven signalling to more proliferative behaviour in all samples such that there is a decrease in correlation with their pre-AI subtype (Figure 3.9). Consequently, in

designing experimental work to examine the mechanisms of endocrine resistance, it is necessary to consider how to model the degree of heterogeneity displayed by endocrine-resistant ER-positive breast cancers. This was addressed by using cell lines of different molecular backgrounds (discussed further in Section 4.1) and by using 2D and 3D models of breast cancer.

Chapter 4 Characterisation of resistant models

4.1 Introduction

As discussed in Section 3.3, there is considerable heterogeneity displayed within the class of ER-positive breast cancer. Consequently, investigation of cancer pathways and mechanisms of endocrine resistance necessitates the use of multiple models of breast cancer that can reflect this variation. The cell lines used (Section 2.1.11) were chosen to encompass a range of molecular contexts, as described in Table 4.1. The parental cell lines all express ER, and are classified as luminal A (Dai et al., 2017).

Each of the parental cell lines had been cultured long term in the absence of exogenous oestrogen (E2) to generate models that could proliferate in an E2-independent manner, thus modelling breast cancer that has become resistant to aromatase inhibitor (AI) therapy (Chan et al., 2002, Martin et al., 2003, Martin et al., 2011). Subsequent characterisation of these long-term oestrogen-deprived lines (LTED) by sequencing showed that the SUM44 LTED cells harbour an *ESR1*^{Y537S} activating point mutation (Martin et al., 2017). This cell line is designated SUM LTED^{Y537S}. Validation by ddPCR showed that this mutation was detectable from twelve weeks of transfer to an E2-deprived medium, and thereafter the variant allele frequency increased up to 50%, indicating temporal enrichment of *ESR1* mutations through oestrogen deprivation. As part of the same study, independently derived MCF7 LTED lines were characterised in a similar fashion, showing that one harboured an *ESR1*^{Y537C} activating mutation (termed MCF7 LTED^{Y537C}) while the other was wild-type for *ESR1* (termed MCF7 LTED^{WT}). A further LTED model of SUM44 cells that were wild-type for *ESR1* (termed SUM44 LTED^{WT}) was kindly provided by Dr Oesterreich's group (University of Pittsburgh) (Sikora et al., 2016).

In addition to endocrine-resistance, during the course of this project the challenge of endocrine-resistant, palbociclib-resistant disease became more evident, following the licensing of CDK4/6 inhibitors for advanced breast cancer treatment in 2017. To ensure this study remained relevant to the clinical scenarios patients face, it was decided to include models of endocrine-resistant, palbociclib-resistant disease.

Table 4.1: Characteristics of cell lines used				
Cell line	**ER protein expression**	***ESR1* mutational status**	**Tumour type**	**Reference**
MCF7	Yes	WT	Invasive ductal carcinoma	(Riaz et al., 2013, Neve et al., 2006)
MCF7 LTED^{WT}	Yes	WT	Invasive ductal carcinoma	(Chan et al., 2002, Martin et al., 2003, Martin et al., 2017)
MCF7 LTED^{Y537C}	Yes	MUT	Invasive ductal carcinoma	(Martin et al., 2017)
MCF7 LTED^{PalboR}	Yes	MUT	Invasive ductal carcinoma	(Pancholi et al., 2020)
SUM44	Yes	WT	Invasive lobular carcinoma	(Riaz et al., 2013, Hollestelle et al., 2010)
SUM44 LTED^{WT}	Yes	WT	Invasive lobular carcinoma	(Sikora et al., 2016)
SUM44 LTED^{Y537S}	Yes	MUT	Invasive lobular carcinoma	(Martin et al., 2017)
HCC1428	Yes	WT	Adenocarcinoma	(Neve et al., 2006, Lehmann et al., 2011)
HCC1428 LTED	Yes	WT	Adenocarcinoma	(Ribas et al., 2015)
HCC1428 LTED^{PalboR}	Yes	WT	Adenocarcinoma	(Pancholi et al., 2020)
T47D	Yes	WT	Invasive ductal carcinoma	(Riaz et al., 2013, Hollestelle et al., 2010)
T47D LTED	No	WT	Invasive ductal carcinoma	(Ribas et al., 2015)
ZR75.1	Yes	WT	Invasive ductal carcinoma	(Riaz et al., 2013, Neve et al., 2006)
ZR75.1 LTED	No	WT	Invasive ductal carcinoma	(Ribas et al., 2015)

These models were generated by long-term culture of LTED cell lines in the continuous presence of 1 μM palbociclib until resistance developed (approximately six months) (Pancholi et al., 2020). The palbociclib-resistant MCF7 LTED models (termed MCF7 LTED^{PalboR}) were generated from the MCF7 LTED^{Y537C} cell line (i.e. harbouring the activating *ESR1* point mutation Y537C). The palbociclib-resistant HCC1428 LTED models (termed HCC1428 LTED^{PalboR}) were generated from the HCC1428 LTED cell line.

This chapter describes the characterisation of the cell lines that was performed to demonstrate that the models used were appropriate for this project.

4.2 Results

4.2.1 Investigation of oestrogen-independence

To confirm the E2-independent phenotype of LTED cell lines, proliferation assays were performed under E2-deprived conditions (Figure 4.1). These showed that while the parental MCF7, HCC1428, SUM44, T47D, and ZR75.1 cell lines require E2-supplementation to proliferate, the LTED cells grow in an E2-independent manner. Consequently, this project uses the model where parental cells cultured in the presence of 1 nM E2 models a breast cancer at primary diagnosis; parental cells that are cultured in media supplemented with foetal bovine serum (FBS) that has been stripped with dextran and charcoal to removed steroids (DCC-FBS) (Darbre et al., 1984) models tumours on treatment with an AI; and LTED-cells proliferating in media supplemented with DCC-FBS model tumours that have developed AI-resistance.

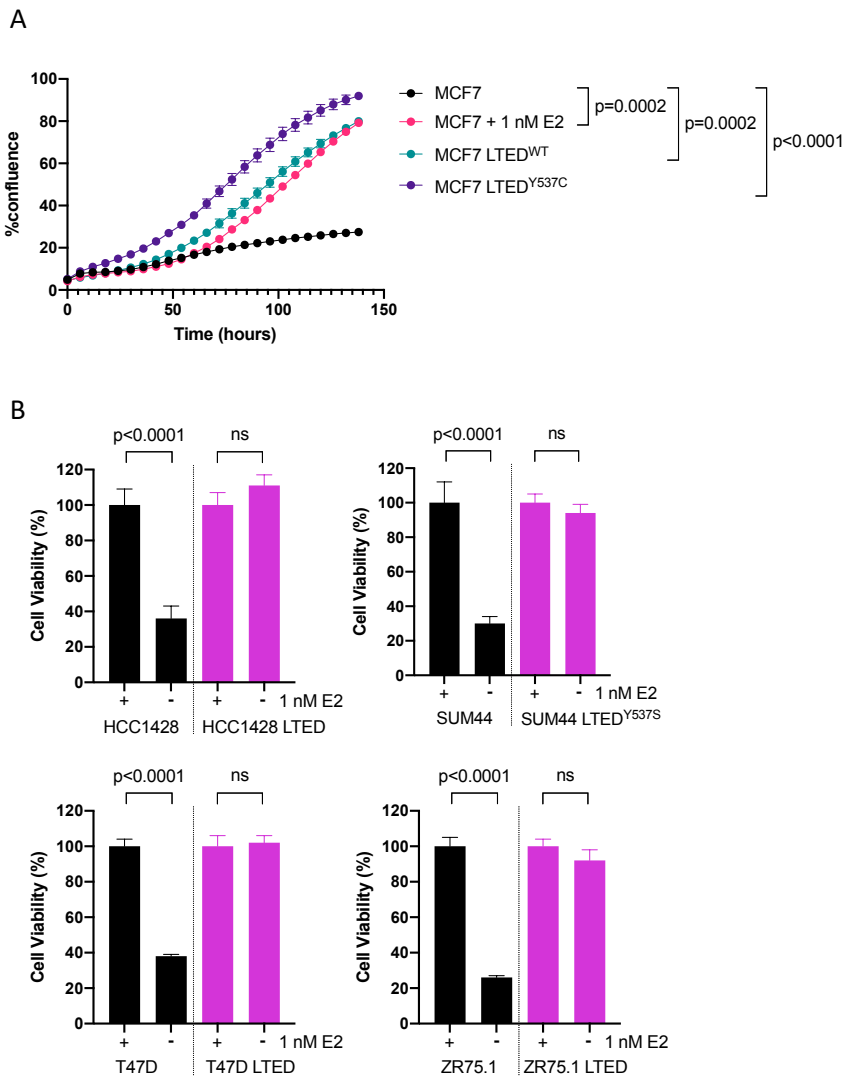

Figure 4.1 Effect of E2 on parental and LTED cell lines (A) Proliferation of parental and LTED MCF7 lines in E2-deprived conditions. 1.5 x 10^4 cells/well of MCF7, MCF7 LTED^{WT} and MCF7 LTED^{Y537C} cell lines were seeded onto 24-well plates in RPMI 1640 media supplemented with 10% DCC-FBS +/- E2 (as indicated). Cell proliferation was monitored over 138 hours using Incucyte, with images taken every 6 hours. Graph shows mean changes in confluence relative to time zero ±SEM. n=2 biological replicates, n=6 technical replicates. Differences in growth curves tested by 2-way ANOVA **(B) Proliferation assays of parental and LTED cells with and without supplemental E2**. 2000-4000 cells/well of HCC1428, SUM44, T47D, and ZR75.1, and their LTED derivatives, were seeded into 96-well 2D culture plates in RPMI 1640 media supplemented with 10% DCC-FBS +/- E2 (as indicated). After 5 days, cell viability was assessed using CellTiter-Glo. Graphs show mean percentage change in viability relative to E2-treated parental cell line. n=2 biological replicates, n=8 technical replicates, error bars represent ±SEM. Difference in viability tested by one-way ANOVA.

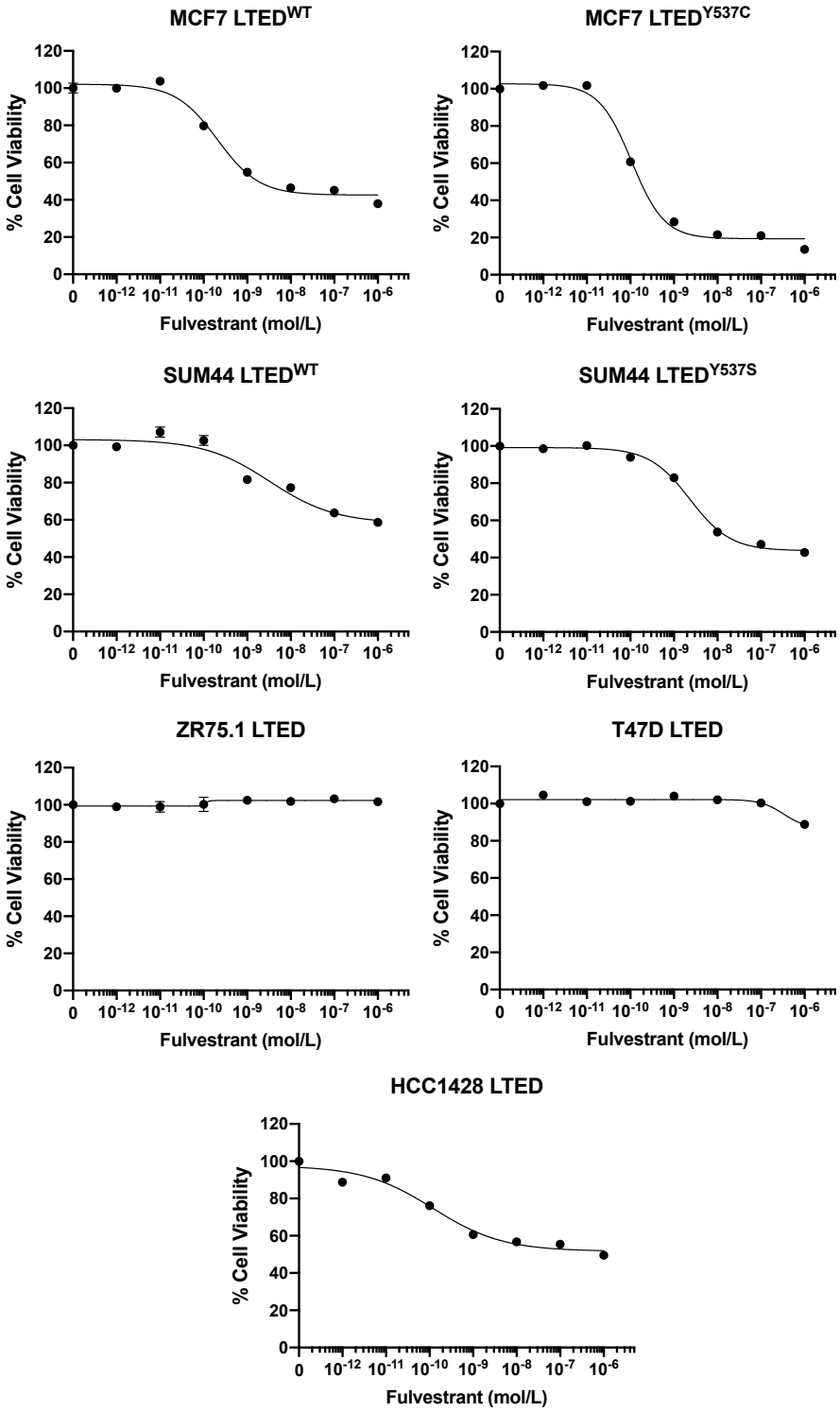

Figure 4.2 Fulvestrant dose-response assays in LTED models. 2000-4000 cells/well of the LTED cell lines were seeded onto 96-well 2D culture plates. After 24 hours, the cells were treated with fulvestrant. Cell viability was assessed using CellTiter-Glo after 6 days. Dose-response graphs show effect of escalating concentrations of fulvestrant on the viability of LTED breast cancer cell lines. Data represent percentage of viable cells compared with vehicle control. n=2 biological replicates, n=8 technical replicates, error bars represent means ±SEM.

4.2.2 Investigation of ER-independence

Given that the results of the proliferation assays indicate that E2 is no longer required for LTED cell proliferation, this raised the query of whether ER itself had become redundant for cell proliferation. Consequently, dose-response assays with fulvestrant – a SERD that targets ER for degradation – were performed (Figure 4.2). These results show a drop in proliferation in the MCF7, SUM44 and HCC1428 LTED cell lines with escalating doses of fulvestrant, indicating that ER is necessary for cell proliferation, but through an E2-independent mechanism. The results corroborate the findings of Martin et al where these LTED cell lines were exposed to fulvestrant along with their parental cell lines, where both the parental and LTED derivative cell lines show a reduction in proliferation following treatment, with an eventual plateau at 20-50% cell viability (Martin et al., 2017). There was no change in proliferation in the T47D LTED and ZR75.1 LTED lines, but this is to be expected as both of these cell lines lose ER expression in their adaptation to E2-deprived conditions (Ribas et al., 2015), and therefore would not be affected by an agent that degrades ER.

4.2.3 Characterisation of palbociclib resistance

The palbociclib-sensitive cell lines, and their palbociclib-resistant derivatives, were subjected to 2D dose-response assays to palbociclib (Figure 4.3A). The results show that the MCF7, MCF7 LTED^{WT}, and MCF7 LTED^{Y537C} lines are sensitive to palbociclib, while the MCF7 LTED^{PalboR} line has an IC_{50} almost five-fold higher than the mean plasma concentration achieved clinically of 259 nM (FDA, 2014) (Figure 4.3B,C). As expected, the HCC1428 line is sensitive to palbociclib and the HCC1428 LTED^{PalboR} line resistant. Surprisingly, the HCC1428 LTED line showed an intermediate phenotype. Given there remains a significant difference in sensitivity between the HCC1428 LTED and HCC1428 LTED^{PalboR} lines (p<0.0001 for difference due to cell line by 2-way ANOVA), these cell lines continue to be used as models of palbociclib-sensitive and resistant disease in this study.

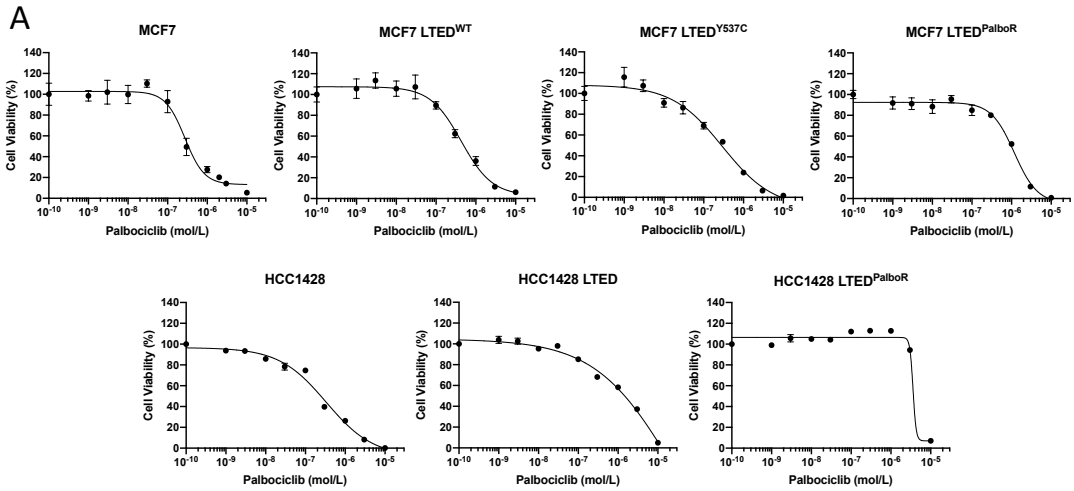

B

Cell Line	Palbociclib IC50 2D (nM)
MCF7	273
MCF7 LTED^{WT}	430
MCF7 LTED^{Y537C}	296
MCF7 LTED^{PalboR}	1179
HCC1428	332
HCC1428 LTED	1000
HCC1428 LTED^{PalboR}	30000

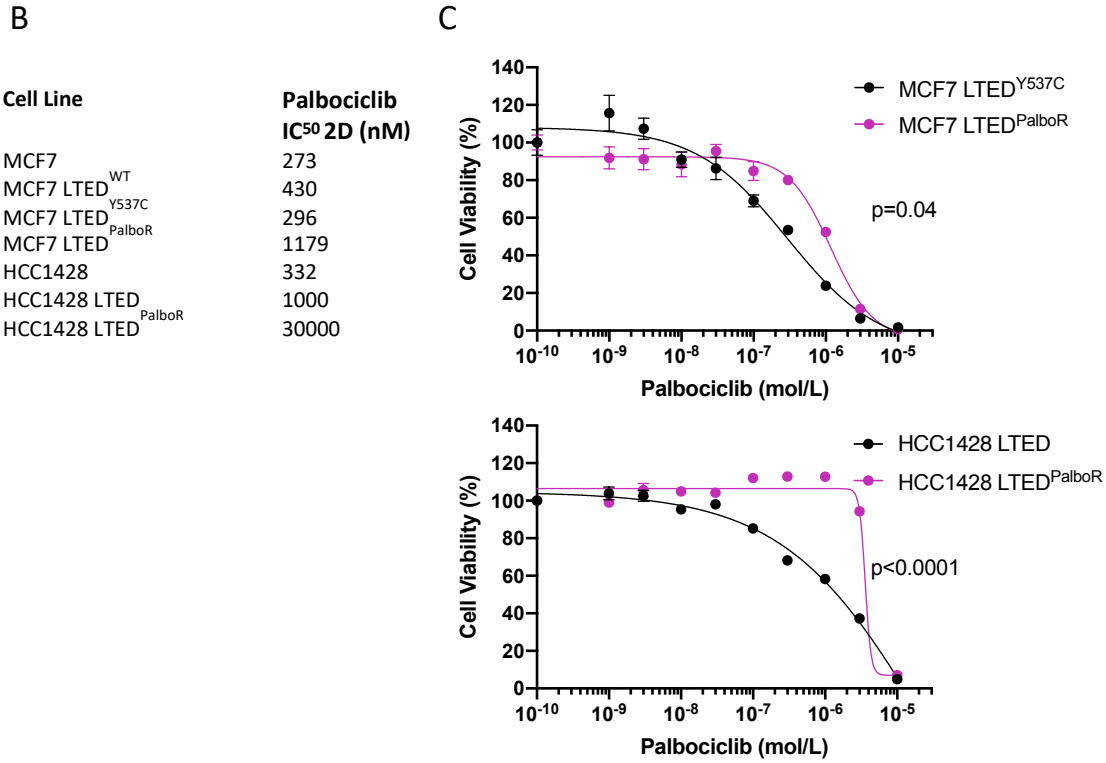

Figure 4.3 Effect of palbociclib on cell proliferation. **(A)** 4000-8000 cells/well were seeded into 2D 96-well plates (seeding number adjusted per line to allow ~80% confluence in the control wells at the end of the experiment). Cells were treated with palbociclib at 24 hours, with a second treatment at 72 hours. Cell viability was assessed using CellTiter-Glo after 7 days. Dose-response graphs show effect of escalating concentrations of palbociclib on viability of breast cancer cell lines. Data represent percentage of viable cells compared with vehicle control. n=2 biological replicates, n=4 technical replicates, error bars represent means ±SEM. **(B)** IC_{50} values for palbociclib calculated from these experiments using 4-parameter non-linear regression. **(C)** Comparison of the effect of palbociclib on the palbociclib-sensitive MCF7 LTED^{Y537C} and HCC1428 LTED cell lines, and their respective palbociclib-resistant derivatives (data from panel A). Difference in dose-response curves tested by two-way ANOVA.

4.2.4 Confirmation of *ESR1* and *PIK3CA* mutational status

The parental MCF7 and HCC1428 cell lines and their LTED derivatives have previously been characterised as to their *ESR1* and their *PIK3CA* mutational status (Martin et al., 2017, Ribas et al., 2015). To confirm the cell lines used in this study had not undergone phenotypic drift, and to characterise the status of the palbociclib-resistant lines, droplet digital PCR (ddPCR) was used. DNA from each of the cell lines was extracted, with the ddPCR assays being kindly performed by Kate Tourna in the Turner laboratory at the ICR. A multiplex ddPCR assay was performed in the first instance looking for the common hotspot mutations (as detailed in Table 2.3), with subsequent singleplex ddPCR of the identified mutation to validate the result. The results (Table 4.2) show that the MCF7 LTED^{Y537C} line continues to express an ER with the Y537C point mutation (mutant allele fraction of 0.24), and that this is also the case in its palbociclib-resistant derivative (mutant allele fraction of 0.21). The MCF7 lines harbour an activating *PIK3CA* hotspot mutation as previously reported (Ribas et al., 2015). Surprisingly, Ribas et al. reported the parental HCC1428 to be wild-type for *PIK3CA*, but in this ddPCR analysis the E545K activating hotspot mutation was detected. However, the results are concordant with Ribas et al. in showing that none of the common activating *PIK3CA* mutations are present in the HCC1428 LTED line, nor in the HCC1428 LTED^{PalboR} cell line.

Table 4.2: ddPCR results of MCF7 and HCC1428 lines and their derivatives

Cell line	*ESR1* mutation	Mutant allele fraction	*PIK3CA* mutation	Mutant allele fraction
MCF7	No	-	E545K	0.704
MCF7 LTED^{WT}	No	-	E545K	0.416
MCF7 LTED^{Y537C}	Y537C	0.235	E545K	0.743
MCF7 LTED^{PalboR}	Y537C	0.207	E545K	0.653
HCC1428	No	-	E545K	0.557
HCC1428 LTED	No	-	No	-
HCC1428 LTED^{PalboR}	No	-	No	-

4.3 Discussion

The LTED cell line models developed by the Martin group have previously been shown to proliferate in an E2-independent manner (Martin et al., 2011, Martin et al., 2017). The characterisation performed as part of this study confirms that they remain E2-independent for growth, but that many of the cell lines still require ER for proliferation, indicating E2-independent ER-signalling may play a role. The cell lines developed to model palbociclib-resistance (Pancholi et al., 2020) were confirmed to retain palbociclib-resistance in dose-response assays. Finally, the ddPCR confirms that the mutant allele frequency of the MCF7 LTED^{Y537C} line corroborates that which was previously described (Martin et al., 2017), and that the adaptations conferring palbociclib-resistance in the HCC1428 LTED^{PalboR} line were not dependent on a change in *PIK3CA* mutational status.

Chapter 5 Use of high-throughput screens to probe for common vulnerabilities in models of endocrine resistance

5.1 Introduction

High-throughput screens (HTS) have become one of the most common approaches to drug discovery in the pharmaceutical industry over the last two decades. The advances in technology such as robotic automation, liquid handling, miniaturisation, and large-scale data analysis have resulted in the ability to screen thousands of compounds against a specific target in one day (Fox et al., 1999, Szymanski et al., 2012). The concept of HTS has extended beyond drug compound discovery, to RNA interference screens (Stockwell and Mittnacht, 2017), and genome editing using CRISPR-Cas9 screens (Korkmaz et al., 2019), to examine the effect of loss-of-function of specific genes, thus making HTS a useful experimental design for hit discovery.

5.1.1 Characteristics of a good HTS

The purpose of HTS is to identify hits that are active against a specific target (which may range from a protein to a cellular model). These hits may then be developed further into a viable lead compound after further optimisation for potency and selectivity. The initial screen, which may involve thousands of drugs or silencing agents, must therefore be simple to perform, homogeneous in how the models are handled, robust in quality control, and reproducible (Bronson D, 2001). In designing the screens performed in this project (as discussed in Sections 5.2.1 and 5.2.2), these principles have been employed to reduce the numbers of false hit identification.

5.1.2 Aims and hypothesis

The aim of this part of the project was to subject cell lines from different molecular backgrounds), but which all demonstrated endocrine resistance (as described in chapter 4), to drug and siRNA HTS in order to identify any common 'Achilles heels' that might mediate resistance across the different cell lines. The hypothesis underlying this was that there may be key molecular pathways common to all endocrine-resistant cell lines, and that by targeting these pathways, endocrine-resistance might be overcome. A secondary aim was to compare and contrast the hits between the palbociclib-sensitive

and palbociclib-resistant cell lines, to determine which targets might be important in mediating palbociclib-resistance. It was also recognised that some of the hits common to all cell lines might be those vital to cell survival, and these would be filtered out at the analysis stage.

The hypothesis underlying performing the screens in 2D and 3D was that 3D culture allows for the establishment of oxygen and nutrient gradients that exist *in vivo* (as discussed in section 1.5) and that by carrying out the screens in 3D, this might identify targets mediating endocrine-resistance that are not evident when the experiments are performed in 2D culture.

5.2 Results

In brief, each of the screens performed consist of exposing the cells to drugs or small-interfering RNAs (siRNAs) for a set time period in multi-well plates. The viability of the cells was then assessed with CellTiter-Glo. Positive and negative control wells were present on each plate, and Z-prime (Zhang et al., 1999) calculated for each plate as a measure of assay quality. Z-prime describes the separation of the distributions between the positive and negative controls, and only plates with Z-prime≥0.5 were taken for further analysis. Each assay was performed with three biological replicates to reduce the risk of false hit identification. A robust Z-score (Malo et al., 2006) was calculated from these three independent biological replicates for each compound or siRNA to describe the effect of that treatment on the viability of the cells. Whereas a Z-score describes the number of standard deviations away from the plate mean for each readout value, a robust Z-score utilises the plate median and the median absolute deviation, allowing the effect of outliers to be minimised (Malo et al., 2006). Therefore, a robust Z-score of -2 indicates the treatment has resulted in reduction of cell viability in that well two standard deviations away from the median cell viability observed in that plate.

5.2.1 Design of the 2D screens

The siRNA screens were designed using the Dharmacon ON-TARGETplus siRNA Library – Human Protein Kinases (G-103505, Horizon). This library consists of SMARTpools of siRNA targeting 709 protein kinases. The library was supplemented with non-targeting siRNA (siNTC), and siRNA against *PLK1* as negative and positive controls respectively.

The library was distributed over ten 96-well plates, and this 2D screen was performed by Dr Joanna Nikitorowicz-Buniak, as part of another project.

The drug screen was designed using a kinase inhibitor library from SelleckChem (L1200) comprising 378 drugs whose bioactivity and safety had already been confirmed. Eighteen additional drugs with known activity and characterised through previous work in the laboratory group (Ribas et al., 2018, Ribas et al., 2015, Weir et al., 2016), positive controls (staurosporin), and negative controls (DMSO vehicle) were added to the library, and the cell lines were screened at three concentrations of the compounds.

5.2.2 Design of the 3D screens

Following completion of the 2D screens, preliminary work was performed regarding how best to set up the screens using 3D tumour spheroid models. Initial attempts were made to design screens using 384-well ultra-low attachment plates, using the liquid overlay and centrifugation method (described in Section 2.2.1.3), as this strategy would confer time and cost savings by using fewer plates, but still retaining the aim of studying the cancer cells in a 3D model, with the attendant hypoxia and nutrient gradients (Meehan et al., 2017), and accurate reflection of *in vivo* signalling (Swietach et al., 2008, Cesarz et al., 2016).

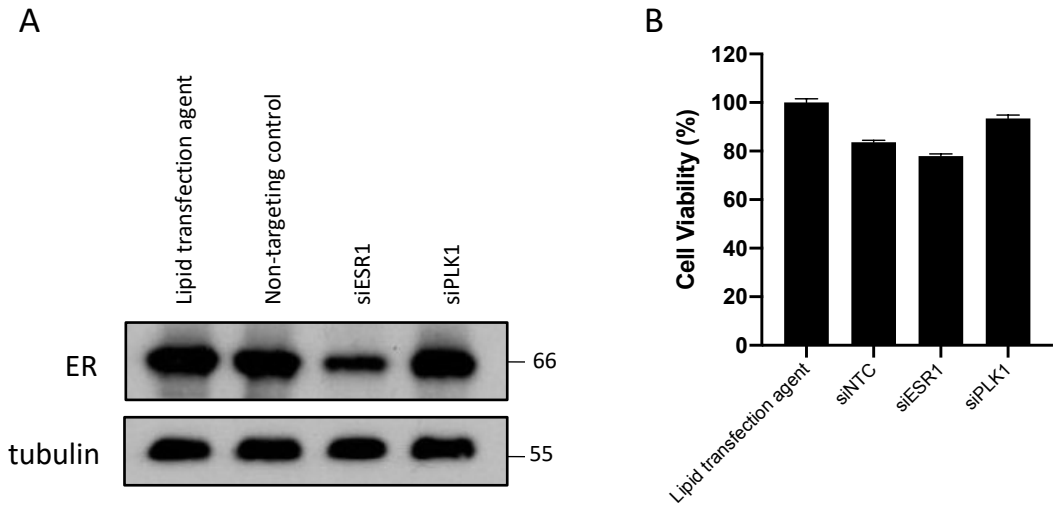

Figure 5.1 Trialling generation of spheroids in 384-well ultra-low attachment plates. 2500 cells/well were seeded in 384-well ultra-low attachment plates and spheroids formed using the liquid overlay and centrifugation method as described in section 2.2.1.3. **(A) Western blot of whole cell extracts of MCF7 LTED^{Y537C} spheroids.** MCF7 LTED^{Y537C} spheroid models were seeded with initial seeding density of 2500 cells/well in 384-well plates, and reverse transfected with 25nM SMARTpool siRNA targeting *ESR1*, *PLK1*, and non-targeting control. Spheroids were formed, extracted, lysed, and probed for ER to assess effectivity of *ESR1* knockdown after 5 days. Blots show abundance of ER in MCF7 LTED^{Y537C} spheroid models. Molecular weights listed in kilodaltons (kDa) **(B) Viability of MCF7 LTED^{Y537C} spheroids following siRNA treatment**. MCF7 LTED^{Y537C} spheroids were reverse transfected with siRNAs targeting *ESR1*, *PLK1*, and NTC as described above. Cell viability was assessed using the CellTiter-Glo assay after 6 days. Data represent percentage of viable cells compared to lipid transfection agent alone. Error bars represent means ±SEM (n=2 biological replicates, n=70 technical replicates.

It was possible to generate spheroids using the LTED cell lines in 384-well ultra-low attachment plates. The reverse transfection protocol from the 2D siRNA screens performed in 96-well plates was adapted to the 384-well plates. Lower levels of ER were seen in the spheroids treated with siRNA targeting *ESR1* when compared to non-targeting control (Figure 5.1A). However, the CellTiter-Glo assay to measure cell viability generated unexpected results (Figure 5.1B). Knockdown of *PLK1*, which is typically used as a positive control due to its essential cellular function, did not appear to have an impact on spheroid viability. Furthermore, phenotypically the spheroids appeared as expected, with disintegration and necrotic debris observed in those spheroids treated with siRNA targeting *PLK1*, and compact viable spheroid formation observed in those exposed to siNTC.

Due to the visual appearance of the spheroids, and Western blotting demonstrating *ESR1* knockdown, it was theorised that the CellTiter-Glo assay was not reflecting successful reverse transfection because the CellTiter-Glo reagent had not penetrated the compact spheroids as effectively as the disintegrating spheroids. Consequently, there was more available ATP for the assay in the siPLK1 knockouts, than in those treated with siNTC, and thus a higher luminescence reading. Attempts were then made to improve CellTiter-Glo penetration by evaporating the media prior to adding the reagent, or by placing the plates on an oscillator (rather than an orbital shaker) to increase the shearing force generated within the wells, unfortunately with no success.

An imaged-based assessment of viability was then trialled to assess the spheroid viability by using the CeligoS Imaging Cytometer, utilising a dual staining method to capture populations of cell death (using propidium iodide) and cell viability (using Calcein AM). Unfortunately this was also not successful, as it was not possible to create a mask on the CeligoS that captured both the siNTC and siPLK1 spheroid phenotypes. Further investigation revealed that this was due to the type of ultra-low attachment plates being used, and background marks in the plastic being detected by the CeligoS as cellular material. The alternative plates were prohibitively costly, and so the decision was taken to perform the 3D screens in 96-well ultra-low attachment plates.

Pilot experiments demonstrated an increase in luminescence readings with increasing cell seeding number (Figure 5.2A) and consistent readings with only 8% variability between wells when the same cell seeding number was used (Figure 5.2B). Furthermore, CellTiter-Glo results of siRNA knockdown using siPLK1 and siNTC siRNAs, and of drug treatment, gave the expected results when compared to those obtained in the 384-well plates (Figures 5.2C, D). Therefore, spheroids cultured in 96-well ultra-low attachment plates were chosen as the 3D models to be used in the 3D HTS.

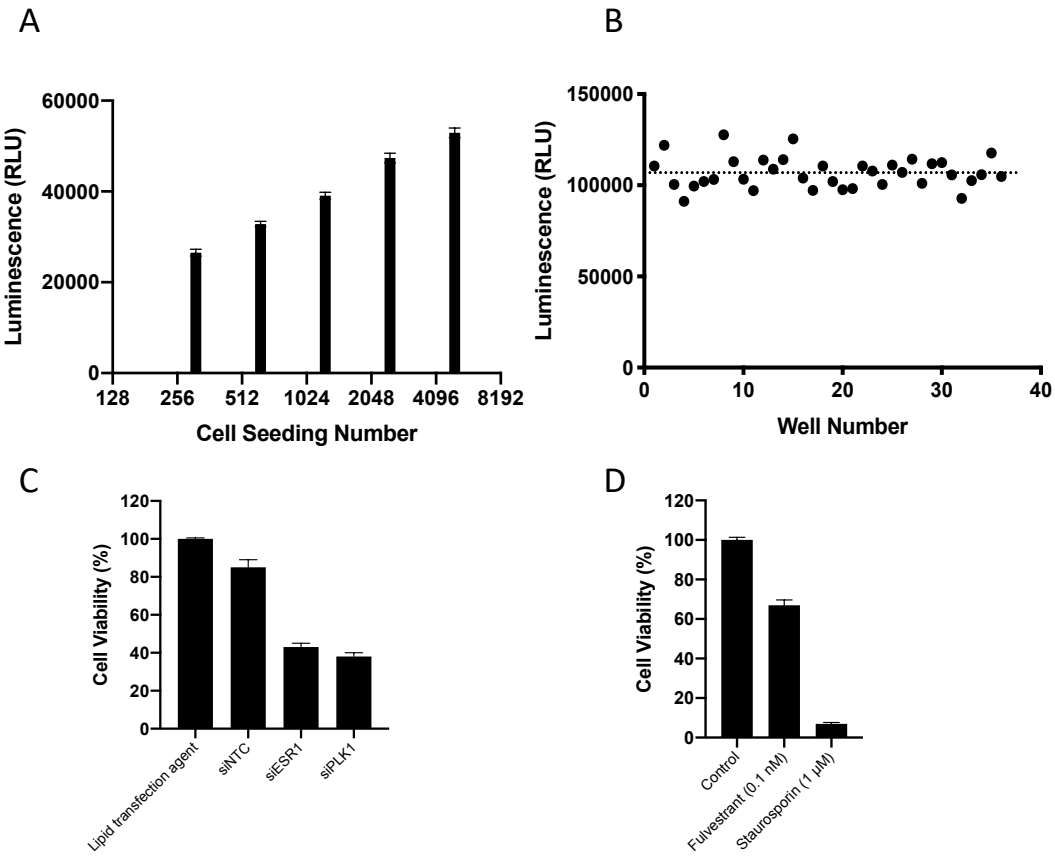

Figure 5.2 Optimisation of CellTiter-Glo assay for 3D spheroid culture in 96-well plates. (A) Changes in luminescence values according to cell seeding number. Spheroids were formed from MCF7 LTED^{Y537C} cells in 96-well plates with varying initial cell seeding number. Cell viability was assessed using CellTiter-Glo on day 7. Data represent mean luminescence values SEM (n=2 biological replicates, n= 16 technical replicates). **(B) Assessment of luminescence variability**. 36 spheroids were formed from MCF7 LTED^{Y537C} cells with identical initial cell seeding number. Cell viability was assessed on day 7 using CellTiter-Glo. The scatter plot demonstrates each luminescence reading, with the dotted line indicating mean luminescence value. **(C) Viability of spheroids following siRNA transfection**. Spheroids formed of MCF7 LTED^{Y537C} cells were reverse transfected with siRNA targeting *ESR1*, *PLK1*, and NTC. Cell viability was assessed using the CellTiter-Glo assay after 7 days. Data represent percentage of viable cells compared to lipid transfection agent alone. Error bars represent means ±SEM (n=1 biological replicate, n=16 technical replicates). **(D) Viability of spheroids following drug treatment**. Fulvestrant, staurosporin, or DMSO vehicle were aliquoted into ultra-low attachment 96-well 3D culture plates to achieve the final concentrations shown. 2500 cells/well of the MCF7 LTED^{Y537C} cell line were dispensed into each well and spheroids formed as described above. Viability was assessed using CellTiter-Glo assay after 7 days. Data represent percentage of viable cells compared to vehicle control. Error bars represent means ±SEM (n=1 biological replicates, n=12 technical replicates).

The final stage in optimising the design of the 3D screens was to clarify whether pre-treating the plates, i.e. adding the drug to the well in advance of cell seeding, would affect spheroid formation, or the response of the spheroids to the drugs. Therefore, pilot dose-response assays using the SERD fulvestrant were performed in the cell lines MCF7, MCF7 LTED^{WT}, and MCF7 LTED^{Y537C}. In the pretreated plates, fulvestrant had been dispensed into the well prior to cell seeding. In the non-pretreated plates, the spheroids were allowed to form before drug treatment. In both cases, spheroids were exposed to fulvestrant for 7 days, with no change of media. Cell viability was assessed using the CellTiter-Glo assay following 7 days of drug exposure (Figure 5.3).

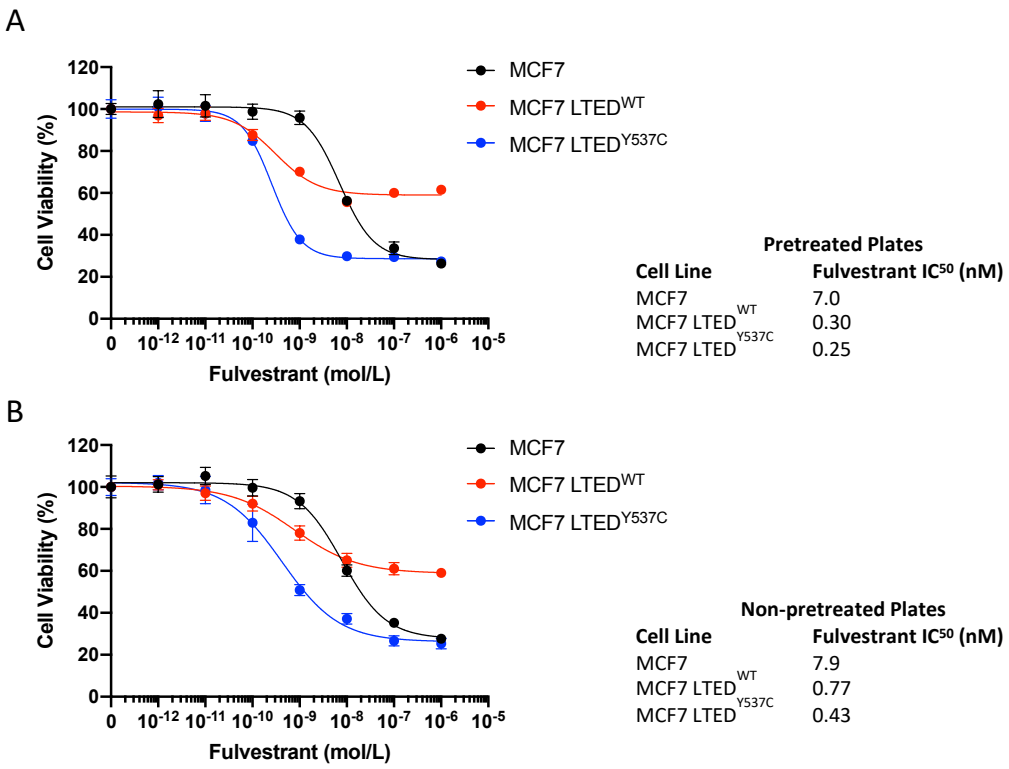

Figure 5.3 Effect of fulvestrant on spheroid cell viability. Dose-response graphs showing the effect of escalating concentrations of fulvestrant on MCF7, MCF7 LTED^{WT}, and MCF7 LTED^{Y537C} spheroids **(A) Pretreated plates.** Escalating concentrations of fulvestrant were aliquoted into ultra-low attachment 96-well 3D culture plates. 2500 cells/well were dispensed into each well, and spheroids formed by the liquid overlay and centrifugation method. Cells were incubated for 7 days, and viability assessed using CellTiter-Glo. Data represent percentage of viable cells compared with vehicle control. Error bars represent means ±SEM (n=2 biological replicates, n=6 technical replicates). Table shows IC_{50} values for each cell line. **(B) Non-pretreated plates**. 2500 cells/well were dispensed into each well, and spheroids formed by the liquid overlay and centrifugation method. After 72 hours, escalating doses of fulvestrant were used to treat the spheroids. After exposure to fulvestrant for 7 days, cell viability was assessed using CellTiter-Glo. Data represent percentage of viable cells compared with vehicle control. Error bars represent means ±SEM (n=2 biological replicates, n=6 technical replicates). Table shows IC_{50} values for each cell line.

Equivalent results were obtained with both approaches, with no significant difference found between the results (2-way ANOVA, data not shown). Therefore, the choice was made to proceed with the pretreated plate model for carrying out the 3D drug screens. Although this does not truly reflect the situation in vivo, where tumours are formed prior to being exposed to drug treatment, this method allowed for a degree of automation of the screens, as the drugs could be dispensed into the plates using the Hamilton liquid handler, rather than being dispensed by hand once the spheroids had formed, reducing the probability of human error. The drugs chosen to be taken forward into 3D screening were determined by the results of the 2D screen, and are described in Section 5.2.7.

Having thus confirmed the experimental models to be used, the 3D screening plates were formed as described in the Methods (Sections 2.2.4.1 and 2.2.6.1) and the screens were performed.

5.2.3 2D siRNA screens in cell lines modelling endocrine resistance

Eight cell lines were subjected to the 2D kinome library of 709 siRNAs (Figure 5.4A). The cell lines used were MCF7 LTED^{WT}, MCF7 LTED^{Y537C}, HCC1428 LTED, SUM44 LTED^{Y537S}, T47D LTED, and ZR75.1 LTED, which model endocrine resistance, and MCF7 LTED^{PalboR}, and HCC1428 LTED^{PalboR}, which model endocrine- and palbociclib-resistant disease. The experimental work was performed as part of a separate project, and the results kindly shared by Dr Joanna Nikitorowicz-Buniak, but the analysis described below was carried out in this project. A threshold robust Z-score of -2 was set to determine the targets classified as a hit, and comparisons between the different cell lines were drawn. Of note, there were no siRNAs generating a robust Z-score of -2 or lower with the HCC1428 LTED^{PalboR} cells.

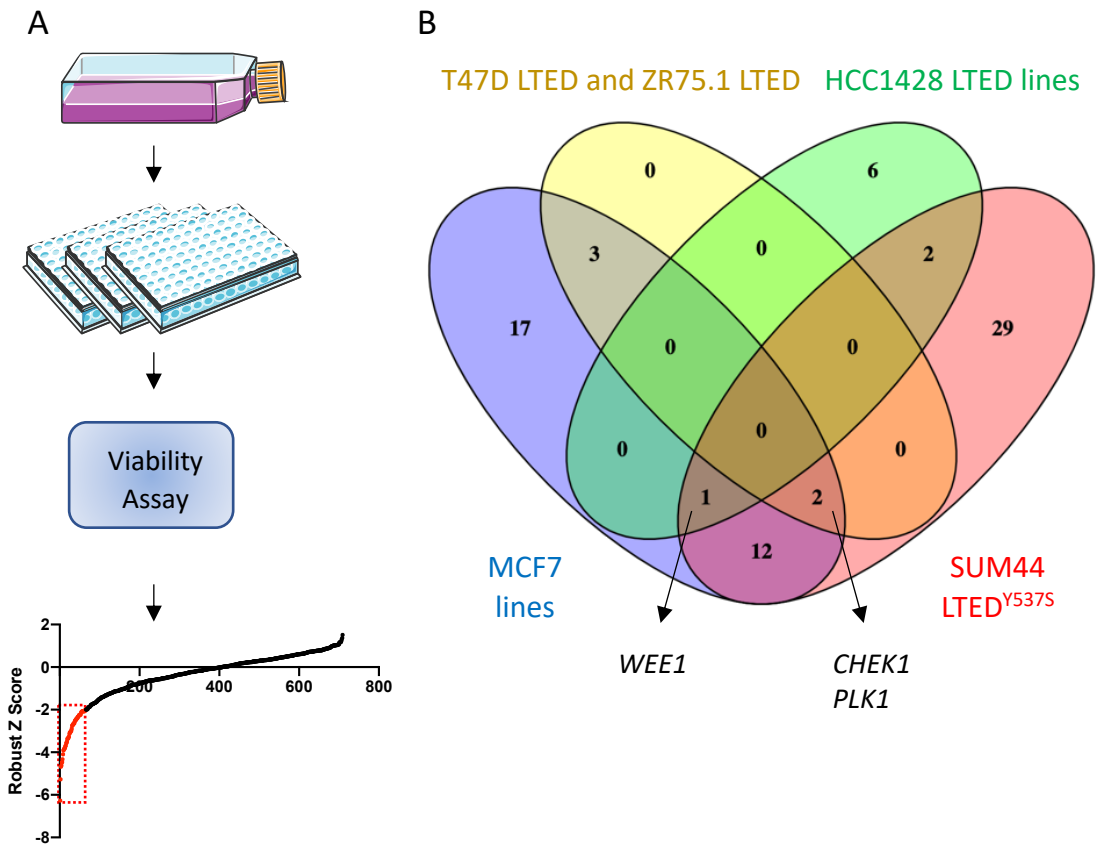

Figure 5.4 Identifying hits in 2D siRNA screens. (A) Multiple cell line models of endocrine resistance were subjected to siRNA kinome library screening in 2D. Cells were reverse transfected with siRNA in 96-well 2D culture plates and cell viability was assessed on day 7 using CellTiter-Glo. Following assessment of assay quality through calculation of Z-prime, robust Z scores were calculated for the effect of each siRNA using the R package cellHTS2. Hits were defined as those with a robust Z-score of ≤-2. n=3 biological replicates. **(B)** Venn diagram showing number of hits, with hits common to three of the four groups of cell lines listed.

5.2.3.1 Intersection of all cell lines in 2D

The significant hits generated from all 2D siRNA screens were intersected to identify whether there were targets common to all cell lines (Figure 5.4B). There were no targets common across all lines compared, but there were three hits common to three of the four groups shown (*WEE1*, *CHEK1*, and *PLK1*). These results highlight the importance of cell cycle checkpoints in the proliferation of these cancer cell lines.

5.2.3.2 Comparison of MCF7 LTED^{WT} and MCF7 LTED^{Y537C} in 2D

The results of the 2D siRNA screens in the MCF7 LTED^{WT} and MCF7 LTED^{Y537C} cell lines were compared to examine the effect of the mutant ER (ER^{MUT}) (Figure 5.5). Pathway

analysis of the targets was performed using STRING-db (Szklarczyk et al., 2015). Common vulnerabilities included siRNAs involved in cell cycle and phosphatidylinositol signalling. While phosphatidylinositol signalling and the PI3K-AKT pathway remained key in the MCF7 LTED^{WT} line, interestingly the PD-L1/PD-1 checkpoint pathway was highlighted in the hits private to the MCF7 LTED^{Y537C} line. While there have been findings that metastases expressing ER^{MUT} have been shown to have higher PD-L1-positive macrophages than those with wild-type ER (ER^{WT})(Williams et al., 2021), given that these experiments were performed using cancer cell lines, and not the associated tumour microenvironment, the significance of this result is unclear.

A

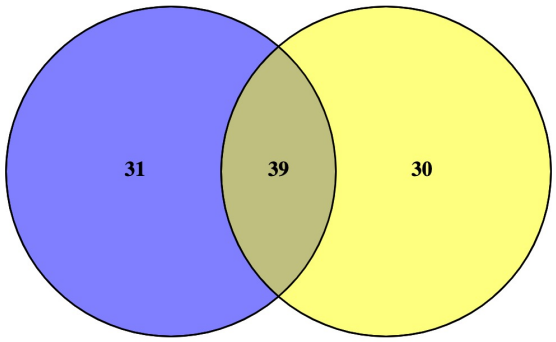

B

Common

KEGG Pathway	FDR
Cell cycle	2.38e-6
Phosphatidylinositol signalling	0.00012

MCF7 LTED^{WT}

KEGG Pathway	FDR
Phosphatidylinositol signalling	0.0039
PI3K-AKT signalling pathway	0.0039

MCF7 LTED^{Y537C}

KEGG Pathway	FDR
PD-L1 expression and PD-1 checkpoint pathway in cancer	2.55e-6
HIV-1 infection	0.00015

Figure 5.5 Identifying hits in 2D siRNA screens. (A) Venn diagram showing numbers of hits in the MCF7 LTED^{WT} and MCF7 LTED^{Y537C} 2D siRNA screens. **(B)** Top two key pathways and associated FDR identified from the shared hits, and pathways private to each cell line. Pathways were generated from STRING-db pathway analysis.

5.2.3.3 Probing for targets related to palbociclib-resistance in 2D

The results of the three MCF7 lines were compared, with the aim of identifying targets that may contribute to palbociclib resistance (Figure 5.6A). Examining the twenty-five shared hits highlighted cell cycle and PI3K-AKT signalling pathways as relevant (Figure 5.6B), but no pathways were identified when the siRNA targets private to MCF7 LTED^{PalboR} were submitted for pathway analysis. Literature review of the individual genes

that were only significant in the MCF7 LTED^{PalboR} line also did not reveal key mechanisms of palbociclib-resistance.

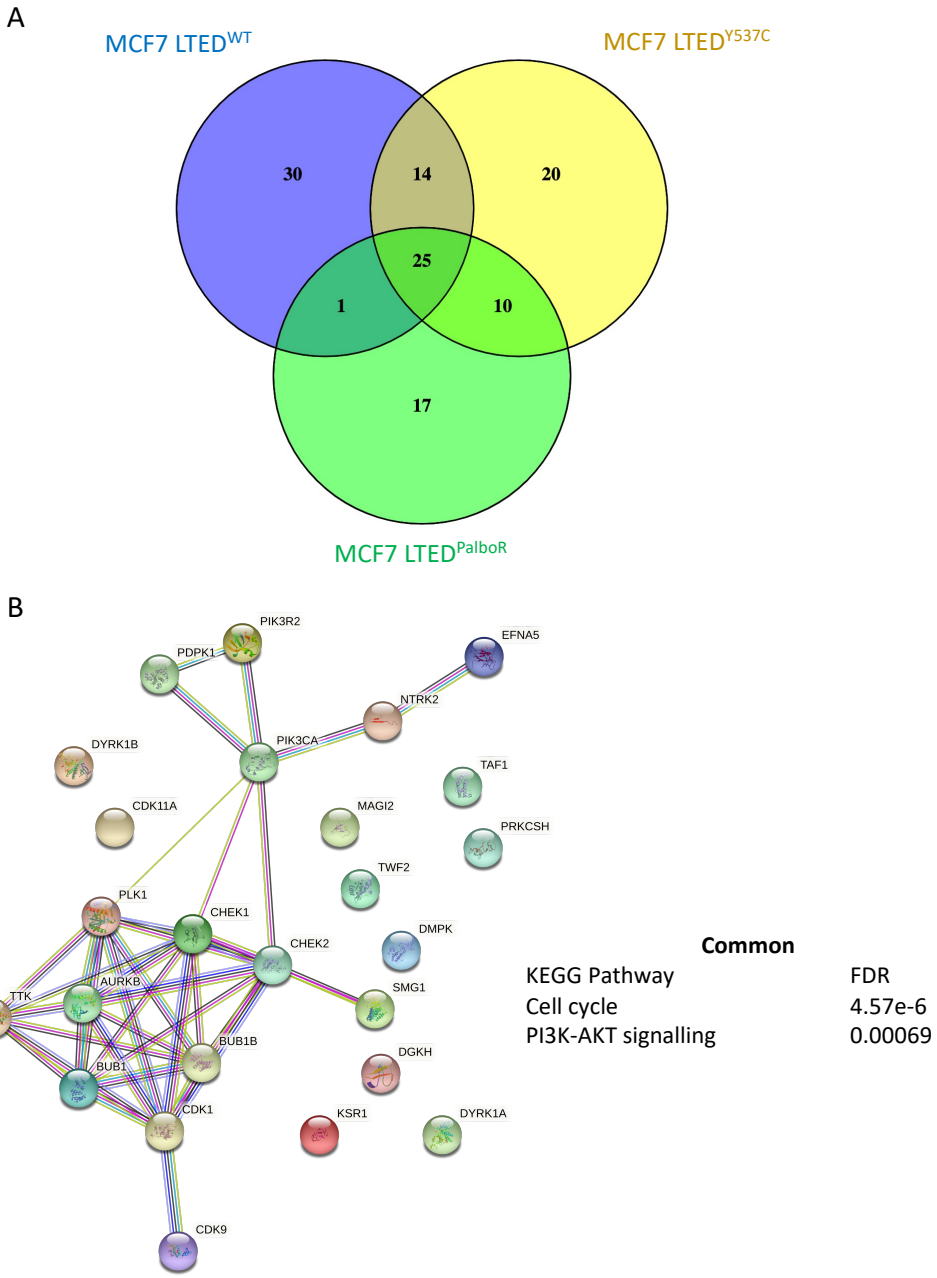

Figure 5.6 2D siRNA screen results of MCF7 LTED^{WT}, MCF7 LTED^{Y537C}, and MCF7 LTED^{PalboR}. (A) Venn diagram showing numbers of significant hits in the MCF7 LTED^{WT}, MCF7 LTED^{Y537C}, and MCF7 LTED^{PalboR} 2D siRNA screens. **(B)** Protein-protein interaction network of hits common to all MCF7 lines generated by STRING-db. Text box shows top two key pathways from these targets and associated FDR.

5.2.3.4 Probing for targets related to ER-loss in 2D

As discussed in Section 4.2.2, the cell lines T47D LTED and ZR75.1 LTED demonstrate loss of ER expression in their adaptation to oestrogen-deprived conditions. The results of the 2D siRNA screens for these two cell lines were therefore compared to look for novel shared vulnerabilities that may be typical of cancers that lose ER expression as a mechanism of endocrine resistance. Figure 5.7 demonstrates there were only five shared significant hits, all related to cell cycle checkpoints and the PI3K-AKT pathway. Furthermore, these are all also significant targets in cell lines retaining ER expression, and so no key targets that could shed light on the development of endocrine resistance in the specific ER loss context were identified in this study.

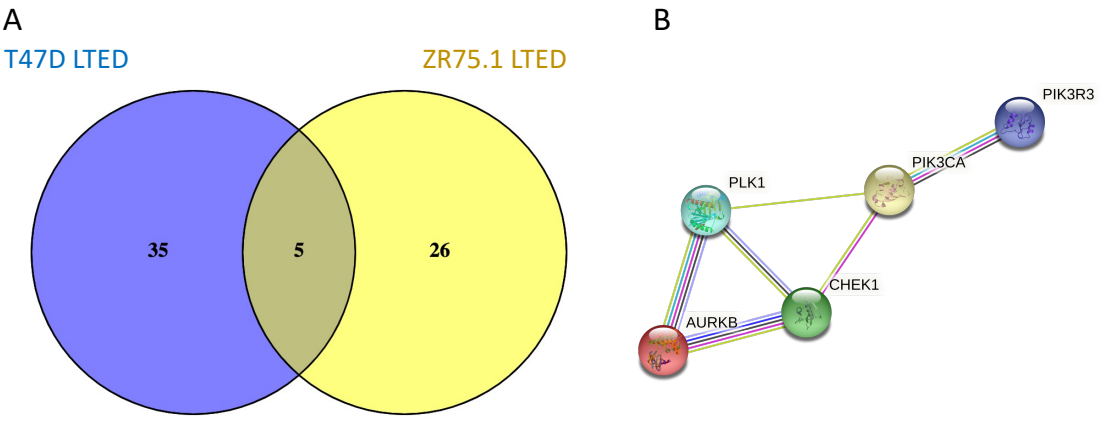

Figure 5.7 2D siRNA screen results of T47D LTED and ZR75.1 LTED. (A) Venn diagram illustrating numbers of significant targets in the T47D LTED and ZR75.1 LTED 2D siRNA screens. **(B)** Protein-protein interaction network of hits common to T47D LTED and ZR75.1 LTED cell lines generated by STRING-db

5.2.4 3D siRNA screens in cell lines modelling endocrine resistance

The same cell lines, with the exception of ZR75.1 LTED, were subjected to 3D screening using the kinome library of 709 siRNAs. The cell lines used were MCF7 LTED^{WT}, MCF7 LTED^{Y537C}, HCC1428 LTED, SUM44 LTED^{Y537S}, and T47D LTED, which model endocrine resistance, and MCF7 LTED^{PalboR}, and HCC1428 LTED^{PalboR}, which model endocrine- and palbociclib-resistant disease. Analysis was performed as per the protocol for the 2D siRNA screens as detailed in Section 2.2.14.1.

5.2.4.1 Intersection of all cell lines in 3D

The significant hits generated from all 3D siRNA screens were intersected to identify whether there were targets common to all cell lines (Figure 5.8). This identified inositol hexakisphosphate kinase 3 (*IP6K3*) as a common significant target in all cell lines. This protein is part of the inositol phosphokinase family, responsible for the conversion of inositol hexakisphosphate to diphosphoinositol pentakisphosphate, which are inositol pyrophosphates. IP6K3 has been primarily found in the brain (Saiardi et al., 2001) and muscle myotubules (Moritoh et al., 2016). Studies on *IP6K3* knockout mice suggest that IP6K3 may have an energy sensor role in muscle tissues, with these mice demonstrating improved glucose tolerance and reduced fat mass (Moritoh et al., 2016). Literature review did not reveal known associations between *IP6K3* and endocrine resistance. It is possible that IP6K3, through generating inositol pyrophosphate messenger molecules, is necessary for successful signalling in multiple pathways, resulting in its identification as a key hit.

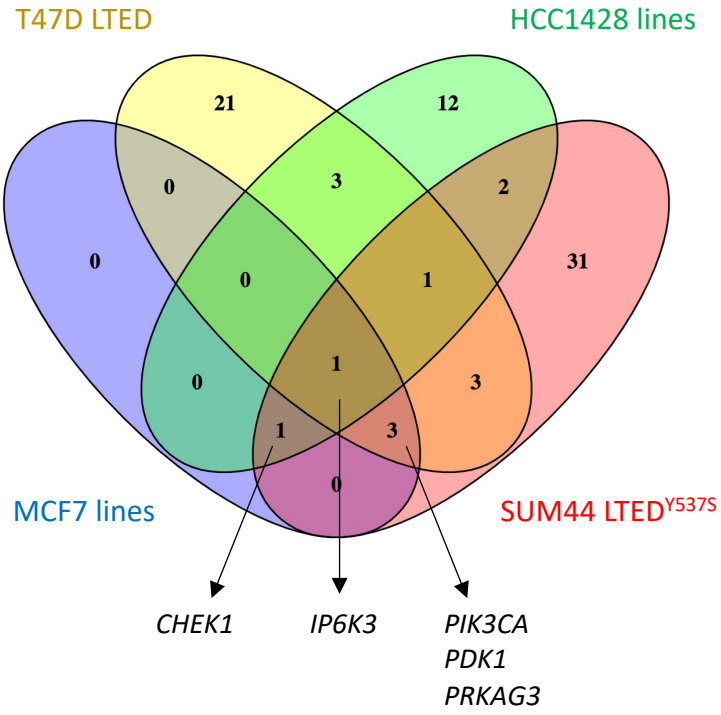

Figure 5.8 Identifying hits in 3D siRNA screens. Multiple models of endocrine resistance were subjected to siRNA kinome library screening in 3D. Cell viability was assessed on day 7 using CellTiter-Glo. Following assessment of assay quality through calculation of Z-prime, robust Z-scores were calculated for the effect of each siRNA using the R package cellHTS2. Those with a robust Z-score of ≤-2 were classified as hits. n=3 biological replicates. Venn diagram shows the number of hits, with targets common to all, or three of the groups listed.

CHEK1 was a significant hit in six of the seven cell lines, again suggesting that cell cycle checkpoints are a shared vulnerability in these cell lines. *PIK3CA*, *PDK1*, and protein kinase AMP-activated non-catalytic subunit gamma-3 (*PRKAG3*) were significant targets in all but the HCC1428 LTED lines. PRKAG3 is a regulatory subunit of AMPK-activated protein kinase (AMPK) and PI3Kα and PDK1 are key steps of PI3K signalling. This could suggest that the HCC1428 LTED lines are not as sensitive to perturbations of the PI3K-AKT signalling pathway, especially given that these lines do not carry an activating *PIK3CA* mutation (Table 4.2).

5.2.4.2 Comparison of MCF7 LTED^{WT} and MCF7 LTED^{Y537C} in 3D

The results of the 3D siRNA screens in the MCF7 LTED^{WT} and MCF7 LTED^{Y537C} cell lines were compared to examine whether different effects of the *ESR1* mutant receptor might be observed in 3D (Figure 5.9). Cell cycle pathways were again highlighted as common to both lines, and PI3K-AKT signalling was also identified up in the MCF7 LTED^{Y537C} cell line, but no pathways were identified when the hits private to MCF7 LTED^{WT} cells were submitted for analysis.

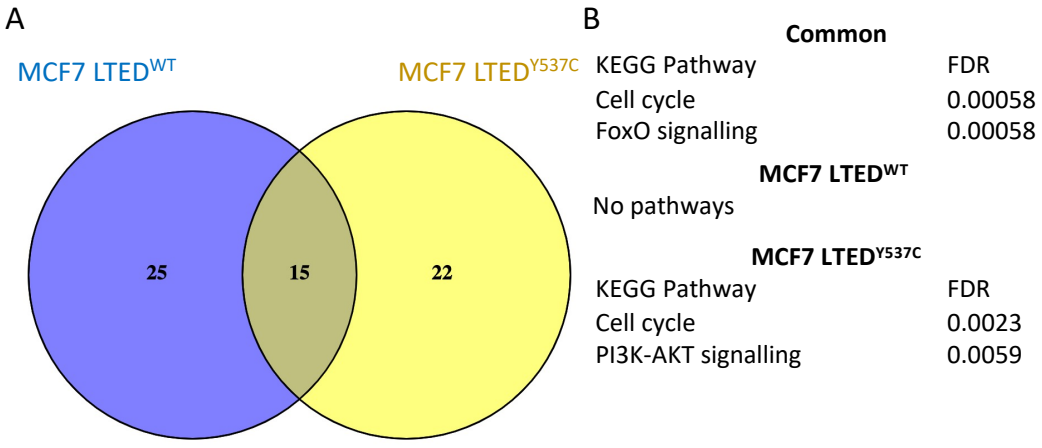

Figure 5.9 3D siRNA screen results of MCF7 LTED^{WT} and MCF7 LTED^{Y537C}. (A) Venn diagram showing numbers of hits in the MCF7 LTED^{WT} and MCF7 LTED^{Y537C} 3D siRNA screens. **(B)** Top two key pathways and associated FDR identified from the shared hits, and pathways private to each cell line. Pathways were generated from STRING-db pathway analysis

5.2.4.3 Probing for targets related to palbociclib-resistance in 3D

The results of the 3D siRNA screens for all three MCF7 lines were compared, with the aim of identifying targets that may contribute to palbociclib resistance (Figure 5.10). The common hits identified relate to PI3K signalling and cell cycle checkpoint control, and *PRKAG3* and *IP6K3* were also targets. Due to the small numbers of hits, no common pathways were found in pathway analysis. Literature review of the hits private to MCF7 LTED^{PalboR} did not reveal any known association with palbociclib-resistance, nor were any significant pathways identified through pathway analysis.

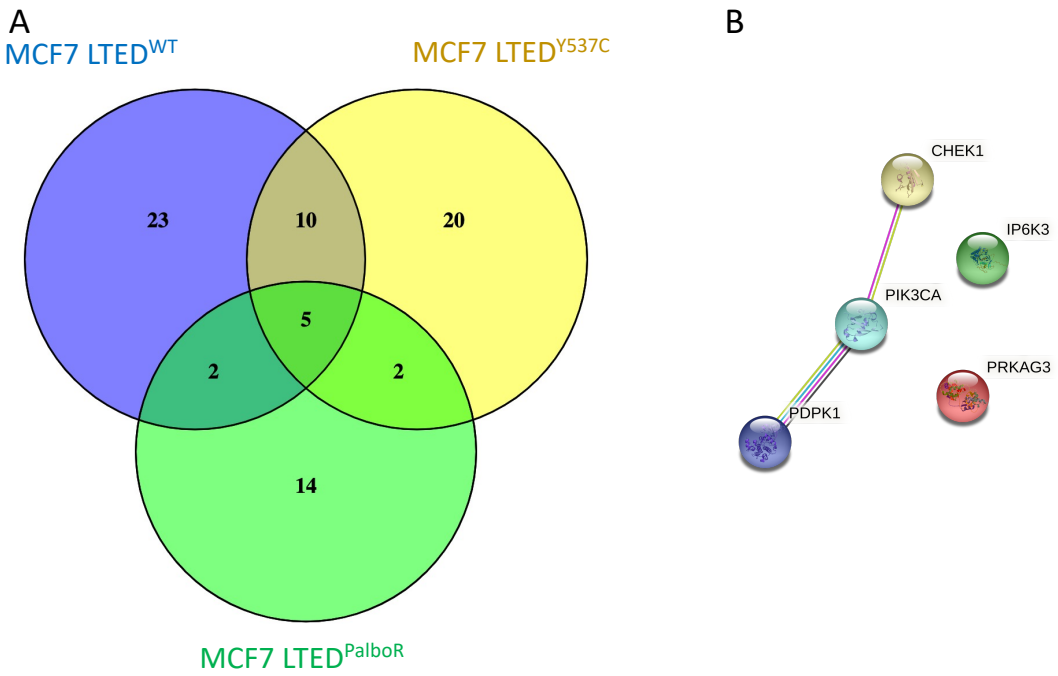

Figure 5.10 3D siRNA screen results of MCF7 LTED^{WT}, MCF7 LTED^{Y537C}, and MCF7 LTED^{PalboR}. (A) Venn diagram showing the number of hits in the MCF7 LTED^{WT}, MCF7 LTED^{Y537C}, and MCF7 LTED^{PalboR} 3D siRNA screens. **(B)** Protein-protein interaction network of hits common to all MCF7 lines, generated by STRING-db pathway analysis.

The 3D siRNA screen results for HCC1428 LTED and HCC1428 LTED^{PalboR} were also compared (Figure 5.11), and while mTOR and ErbB signalling were highlighted as key to survival in the HCC1428 LTED cell line, no pathways were identified from the common hits, or those only in the HCC1428 LTED^{PalboR} line. The pathways private to the HCC1428 LTED line are interesting in that mTOR signalling is downstream from PI3K, and ErbB signalling is upstream from PI3K, and these have been found to be significant, while

PIK3CA itself was not a hit. This could indicate there is crosstalk in these lines to circumvent *PIK3CA* to activate mTOR signalling.

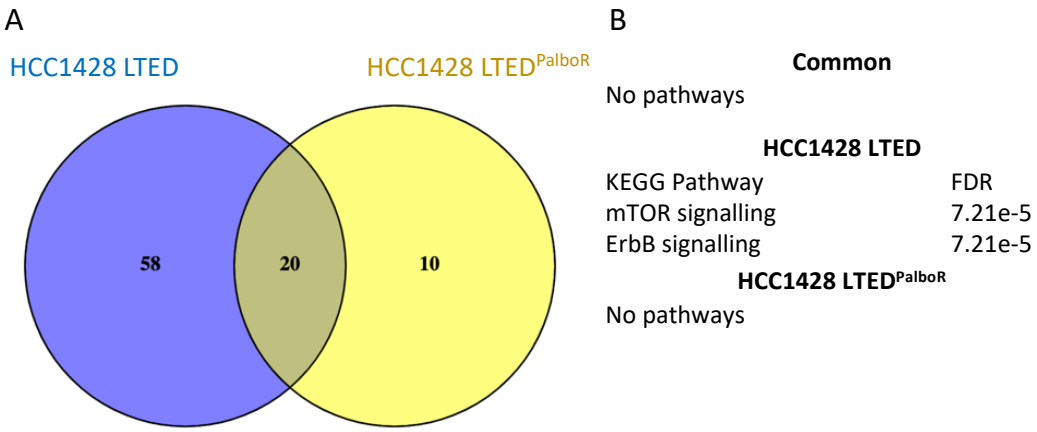

Figure 5.11 3D siRNA screen results of HCC1428 LTED and HCC1428 LTED^{PalboR}. (A) Venn diagram showing the number of hits in the HCC1428 LTED and HCC1428 LTED^{PalboR} 3D siRNA screens. **(B)** Top two key pathways and associated FDR identified from the shared hits, and pathways private to each cell line. Pathways were generated from STRING-db pathway analysis

Finally, the 3D siRNA screen results for the two palbociclib-resistant lines (MCF7 LTED^{PalboR} and HCC1428 LTED^{PalboR}) were compared to look for any shared vulnerabilities that might typify palbociclib-resistance. There were only two shared targets, *IP6K3*, and *CHEK1* (data not shown).

5.2.5 Comparison of 2D *vs* 3D siRNA screens

The results of the 2D and 3D siRNA screens demonstrate that cell cycle checkpoints, and PI3K-AKT signalling are common areas of sensitivity in these endocrine-resistant cell lines. The siRNA screens did not highlight potential mechanisms of palbociclib-resistance, or mechanisms of endocrine-resistance specific to cell lines that lose ER expression in oestrogen-deprived conditions. There were overall fewer significant targets identified in the 3D siRNA screens *vs* the 2D screens.

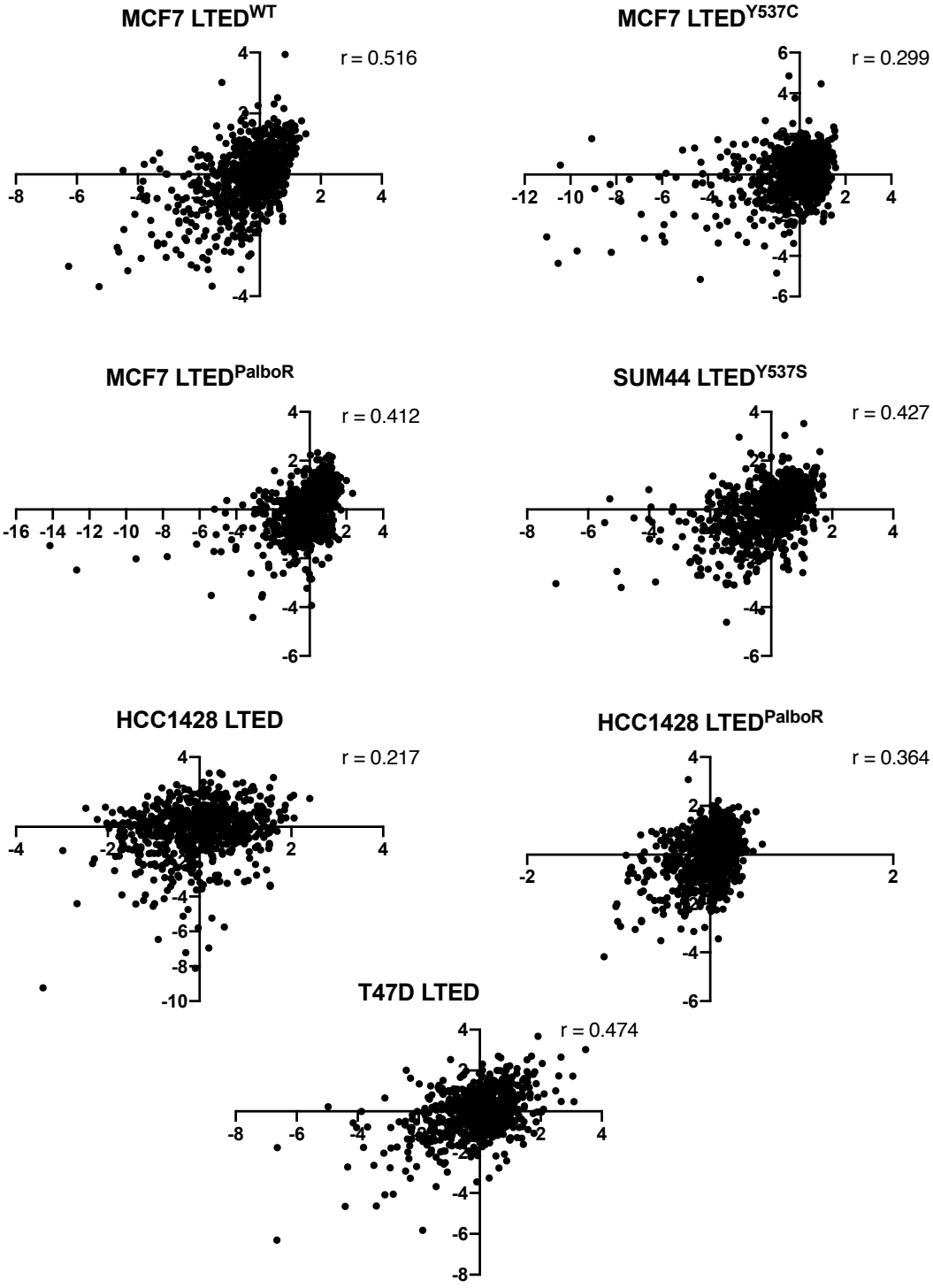

Figure 5.12 Correlation between 2D and 3D siRNA screens. Scatterplots of the robust Z-scores of each siRNA from the 2D (x-axis) and 3D (y-axis) screens. Pearson's r correlation coefficient is given for each cell line.

As one of the objectives of this project was to examine the use of 3D models to determine whether this method of culture might shed further light on the mechanisms of endocrine-resistance, the results obtained from the 2D and 3D siRNA screens were

compared (Figure 5.12). The Pearson's correlation coefficient ranges from 0.217 to 0.516. Given that the 2D and 3D screens were biologically independent replicates, carried out over eighteen months apart, this range of correlation coefficients indicates a modest correlation between the screening methods. Furthermore, the same key areas of vulnerability are highlighted in both the 2D and the 3D siRNA screens. The main notable difference is that the number of significant hits obtained from the 3D siRNA screens is lower than in the 2D siRNA screen for each cell line except HCC1428 LTED^{PalboR}. This suggests that performing screens in 3D could be used as a filtering mechanism to limit the number of potential hits to physiologically relevant targets, given that the actual pathways identified are the same in 2D and in 3D.

5.2.6 2D drug screens in cell lines modelling endocrine resistance

Seven LTED breast cancer cell lines were screened in triplicate against a library of 396 drugs, at four concentrations (0 nM, 10 nM, 100 nM, and 1000 nM). After five days, cell viability was measured using CellTiter-Glo. Following quality control assessment, robust Z-scores were calculated for each of the drugs in the library at the 1 μM concentration (Figure 5.13).

These plots of the 2D drug screen results demonstrate three broad areas were key to endocrine-resistance: the PI3K-AKT-mTOR pathway, as drugs targeting this pathway were significant in all cell lines; cell cycle checkpoints, as cyclin-dependent kinase (CDK) inhibitors were frequently identified; and ER-signalling, as SERDS were also recurrent hits. Representative drugs of each of these classes have been highlighted on Figure 5.13. However, it was noted that the range of robust Z-scores varied between the cell lines (from -15 to 5 in the MCF7 LTED^{WT} cell line, but -34 to 6 in the SUM44 LTED^{Y537S} cell line), and thus setting a threshold of robust Z-score ≤-2 to classify and compare hits was not considered appropriate. This patten was also seen in the calculations of robust Z-scores at the 10 nM and 100 nM doses (data not shown). Following discussion with bioinformaticians, a mean response score (a function of the cell viability results) was calculated for each drug, at each concentration, for each cell line. The threshold for a drug to be categorised as a hit was set at those causing ≥50% reduction in cell viability. A separate mean response score calculation, and hit selection, was performed at each of the three concentrations (10 nM, 100 nM, 1000 nM). At the 1000 nM dose, there

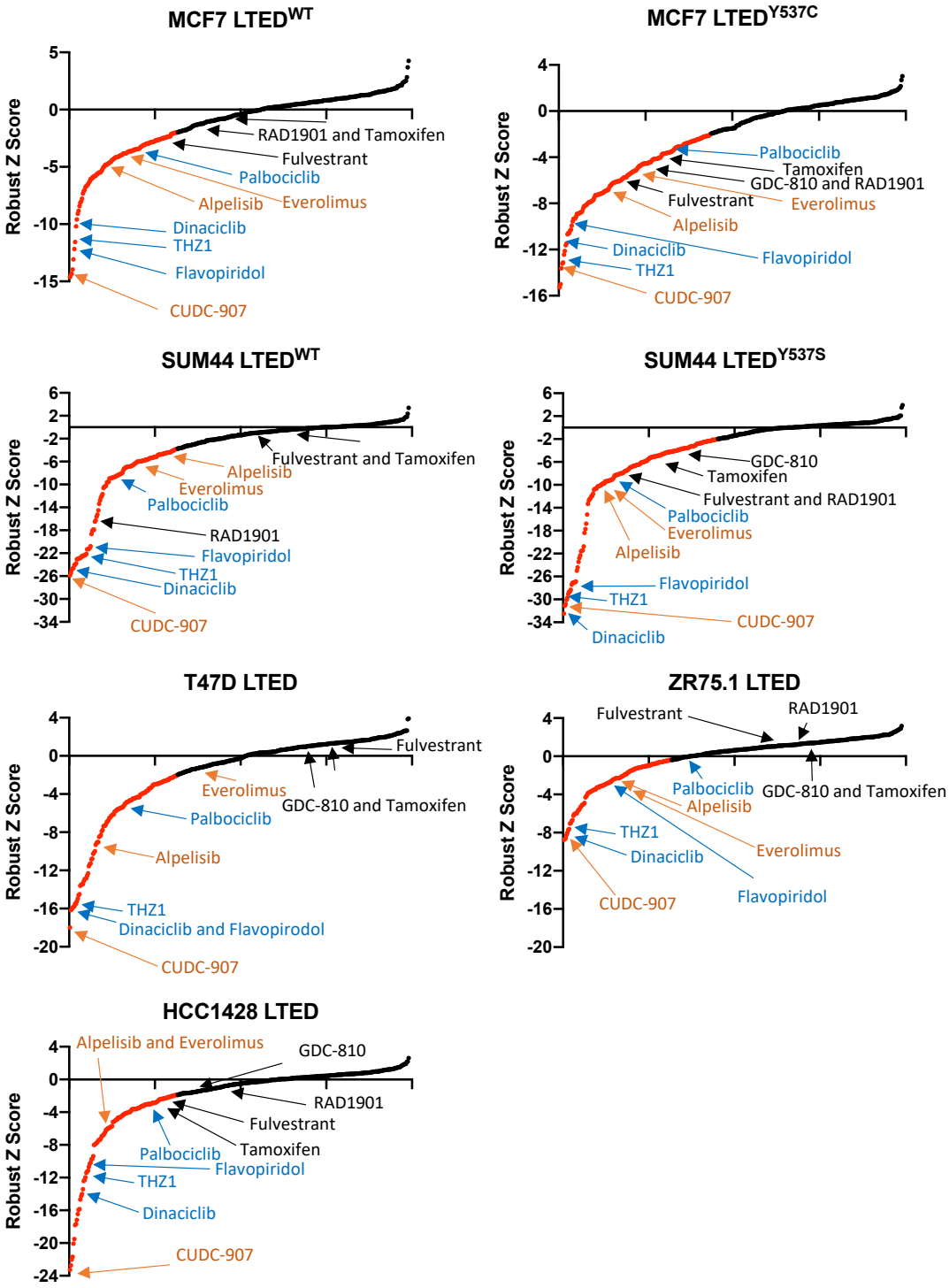

Figure 5.13 2D drug screen results at 1 μM in LTED breast cancer cell line models. Drugs (1 μM final concentration) were pre-aliquoted into 384-well 2D culture plates prior to seeding of 1200-2400 cells/well. Cell seeding number was adjusted to allow for ~80% confluence in the control wells at the end of the experiment. Cell viability was assessed using CellTiter-Glo after 5 days. Assay quality was assessed, and only those achieving Z-prime ≥0.5 were taken for further analysis. Robust Z-scores were calculated for the effect of each drug, at each concentration, using the R package CellHTS2. n=3 biological replicates. Plots represent robust Z-score rank order from low to high for each cell line tested, with drugs achieving a robust Z-score ≤-2 in red. Representative drugs of different classes have been highlighted. Black font indicates compounds targeting ER

(Tamoxifen, Fulvestrant, RAD1901, GDC-810). Blue font indicates compounds targeting cyclin-dependent kinases (CDKs) (THZ1: CDK7 inhibitor. Dinaciclib: CDKs 2, 1, 5, 9. Flavopiridol: CDKs 1, 2, 4, 6). Orange font indicates compounds targeting PI3K-AKT-mTOR pathway (CUDC-907: PI3Kα inhibitor. Alpelisib: PI3Kα inhibitor. Everolimus: mTOR inhibitor).

were ~100 hits for some cell lines, suggesting this dose was not sufficiently discriminatory for hit classification. Therefore, the results at 10 nM, and 100 nM were compared to find the common hits between related cell lines, and across all cell lines. When comparing all of the 2D drug screen results at 100 nM, compounds targeting the PI3K-AKT-mTOR pathway, and those acting on CDKs, were selected as hits in several cell lines (Figure 5.14), concordant with the pattern seen in the robust Z-score calculations (Figure 5.13)

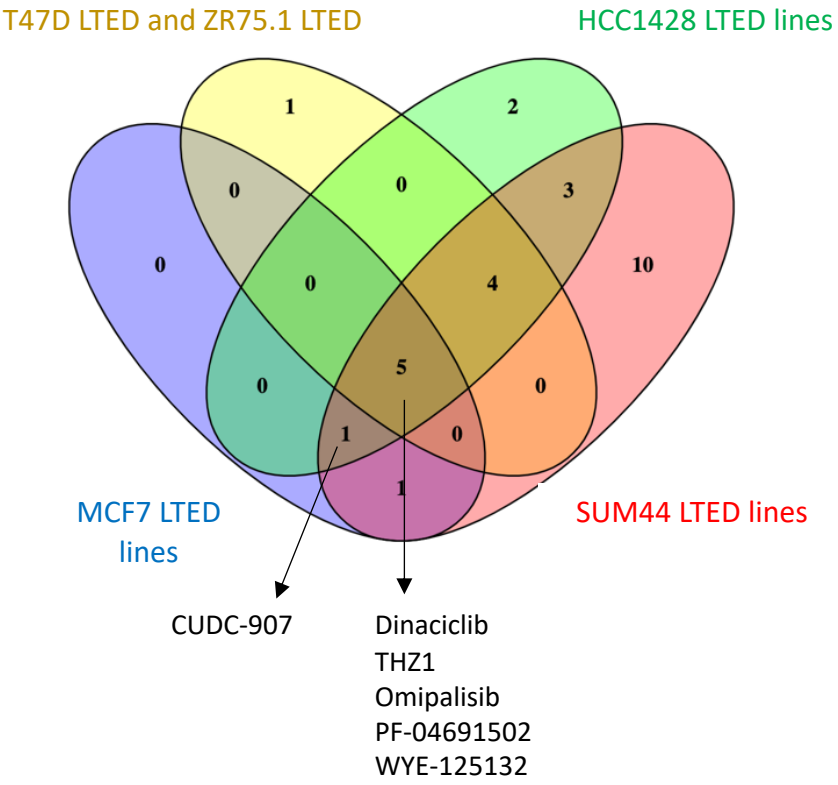

Figure 5.14 2D drug screen results at 100 nM in LTED breast cancer cell line models. 2D drug screens (final drug concentration 100 nM) were performed as described in Figure 5.13. Compounds causing ≥50% reduction in cell viability were classified as hits. Venn diagram shows the numbers of hits common to multiple cell lines at 100 nM, with targets that were common to three or four of the groups compared highlighted. CUDC-907: PI3Kα inhibitor. Dinaciclib: inhibitor of CDKs 2, 1, 5, 9. THZ1: CDK7 inhibitor. Omipalisib: dual PI3K/mTOR inhibitor. PF-04691502: dual PI3K/mTOR inhibitor. WYE-125132: mTOR inhibitor.

5.2.6.1 Comparison of 2D drug screen results at 10 nM identifies PI3K-AKT-mTOR pathway importance

At the lowest drug concentration in the screen (10 nM), all but one cell line (ZR75.1 LTED) demonstrated sensitivity to drugs targeting the PI3K-AKT-mTOR pathway, with the PI3Kα inhibitor CUDC-907, and the dual PI3K/mTOR inhibitor BGT226 being the most frequent hits (data not shown). Of the eighteen drugs that were classified as significant hits at the 10 nM concentration, twelve targeted this pathway, with the others being SERDs, and CDK inhibitors. This is in-keeping with the finding that the PI3K-AKT-mTOR pathway is the most frequently mutated in breast cancer, and of the relevance of cross-talk between ER and the PI3K-AKT-mTOR pathway, as discussed in Section 1.3.3.

5.2.6.2 Comparison of *ESR1*^{WT} and *ESR1*^{MUT} 2D drug screen results highlights the effect of the mutational status of ER on drug sensitivity

When comparing the difference between the LTED cell lines expressing ER^{WT} with those expressing ER^{MUT}, the most striking finding was that the ER^{MUT} models appear to show sensitivity to SERDs, while the ER^{WT} models do not (Figure 5.15). At 100 nM, the MCF7 LTED^{Y537C} models were sensitive to GDC810, RAD1901, and fulvestrant, and the MCF7 LTED^{WT} models were not (Figure 5.15A). Similarly, the SUM44 LTED^{Y537S} line was sensitive to fulvestrant, while the SUM44 LTED^{WT} was not (Figure 5.15B). Interestingly, when comparing SUM44 LTED^{Y537S} to MCF7 LTED^{Y537C}, while both were sensitive to fulvestrant, only MCF7 LTED^{Y537C} was sensitive to the other SERDs in the screen. The differential sensitivity of the lines expressing ER^{MUT} suggests that these cells continue to be dependent on ER-signalling for growth, while those expressing ER^{WT} are not. The different targets highlighted when comparing SUM44 LTED^{WT} *vs* SUM44 LTED^{Y537S} (EGFR, vascular endothelial growth factor receptor (VEGFR), and c-Met – data not shown) suggest that cell lines expressing ER^{WT} employ altered growth factor signalling to enable survival and proliferation in oestrogen-deprived conditions, while cell lines expressing ER^{MUT} utilise the constitutive activation of the ER^{MUT} to drive growth.

Furthermore, when comparing the ER^{Y537S} to ER^{Y537C} (Figure 5.15), although both demonstrate sensitivity to fulvestrant, ER^{Y537C} is also targeted by the other SERDs, RAD1901 and GDC810, suggesting a differential sensitivity between the mutations. This

has also been found in previous work (Toy et al., 2017), and suggests that some mutations may be more effective at promoting endocrine resistance than others. Given that there is a variation in prevalence of different *ESR1* mutations, with the D538 and Y537S mutations seen more frequently than Y537C (Fribbens et al., 2016), it is important to take this into account when considering strategies for overcoming endocrine-resistance in the clinic.

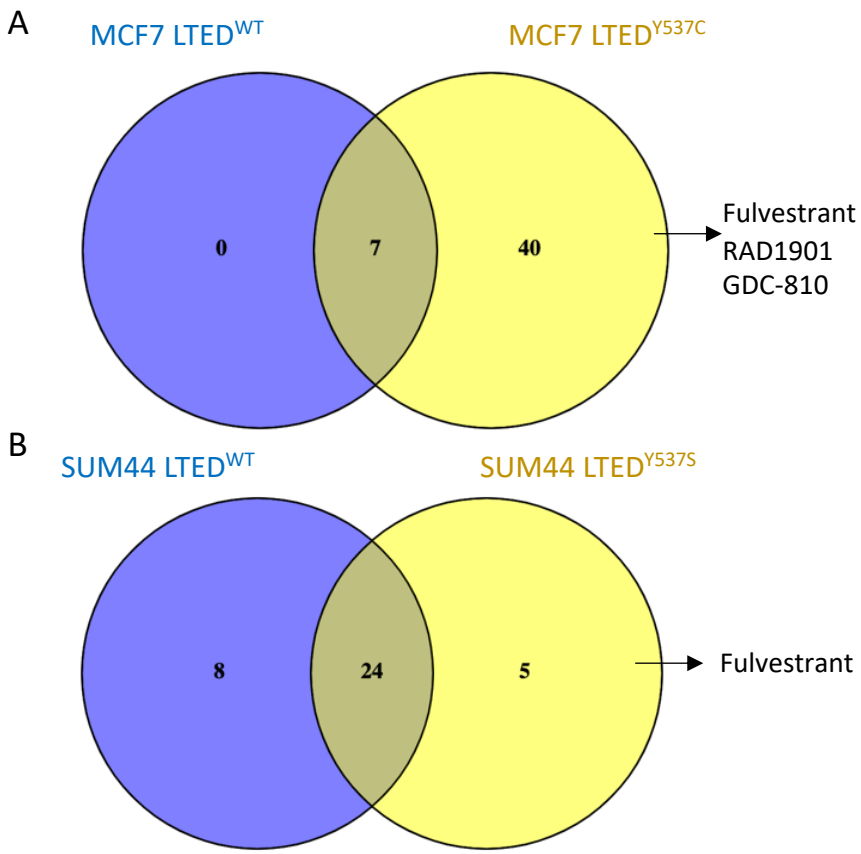

Figure 5.15 2D drug screen results at 100 nM in LTED breast cancer cell line models expressing ER^{WT} or ER^{MUT}. 2D drugs screens (final drug concentration 100 nM) were performed as described in Figure 5.13. Compounds causing ≥50% reduction in cell viability were classified as hits. Venn diagram shows numbers of hits shared and private to the named cell lines at 100 nM. **(A)** comparison of numbers of significant hits in the MCF7 LTED^{WT} and MCF7 LTED^{Y537C} cell lines. **(B)** comparison of numbers of significant hits in the SUM44 LTED^{WT} and SUM44 LTED^{Y537C} cell lines.

5.2.6.3 Cell cycle regulation

Several drugs targeting checkpoints in the cell cycle, such as CDKs, PLK1, CHK1, and Aurora kinases were detected as hits in the drug screen, at the 100 nM and 1 μM dosages (Figure 5.16; purple boxes). Interplay between cyclins and CDKs ensure an ordered progression through the cell cycle, controlled by a variety of cell signalling mechanisms, and deregulation of the cell cycle is a hallmark of cancer. The drug screen highlighted pan-CDK inhibitors, such as flavopiridol (targeting CDKs 1/2/4/6), dinaciclib (CDKs 2/1/5/9), and AT7519 (CDKs 1/2/4/6/9). These drugs can cause cell cycle arrest at multiple points, and targeting multiple CDKs is of interest as it may combat redundancy, but as will be discussed later in Section 6.4.3, the translation of these drugs from bench to clinic has been difficult.

The more selective inhibitor, THZ1, which targets CDK7, was also a hit across multiple models (Figure 5.14). As will be discussed further in Section 6.2, CDK7 plays a role in a myriad of biological processes, including control of the cell cycle, transcription initiation, and activation of ER. Therefore, by inhibiting the action of CDK7, not only is THZ1 disrupting progress through mitosis, but it may also interfere with ER-signalling pathways. Given that the ER^{MUT} cell lines have been shown to be sensitive to the disruption of ER-signalling mediated by SERDs, it could be hypothesised that combination therapy with CDK7 inhibitors and SERDs may provide a new therapeutic rationale for patients with an activating *ESR1* mutation.

There are several other checkpoints in the cell cycle which have been identified as potential targets. These include CHK1 and WEE1, components that prevent cells with DNA damage from passing the G_2/M checkpoint. Inhibitors of these can allow cell proliferation despite the presence of DNA damage, which can then result in mitotic catastrophe and tumour cell apoptosis (Castedo et al., 2004). Aurora kinases, which ensure the correct execution of cytokinesis, were also identified as targets. Overexpression of Aurora A can inactivate the spindle assembly checkpoint (Anand et al., 2003), and overexpression of Aurora B results in inappropriate chromosome separation, and therefore aneuploidy (Gonzalez-Loyola et al., 2015). Finally, PLK1 is necessary for the activation of cyclin B-CDK1 complexes, and is needed for re-entry into the cell cycle after G_2/M arrest as a result of DNA damage. As a result, inhibition of these

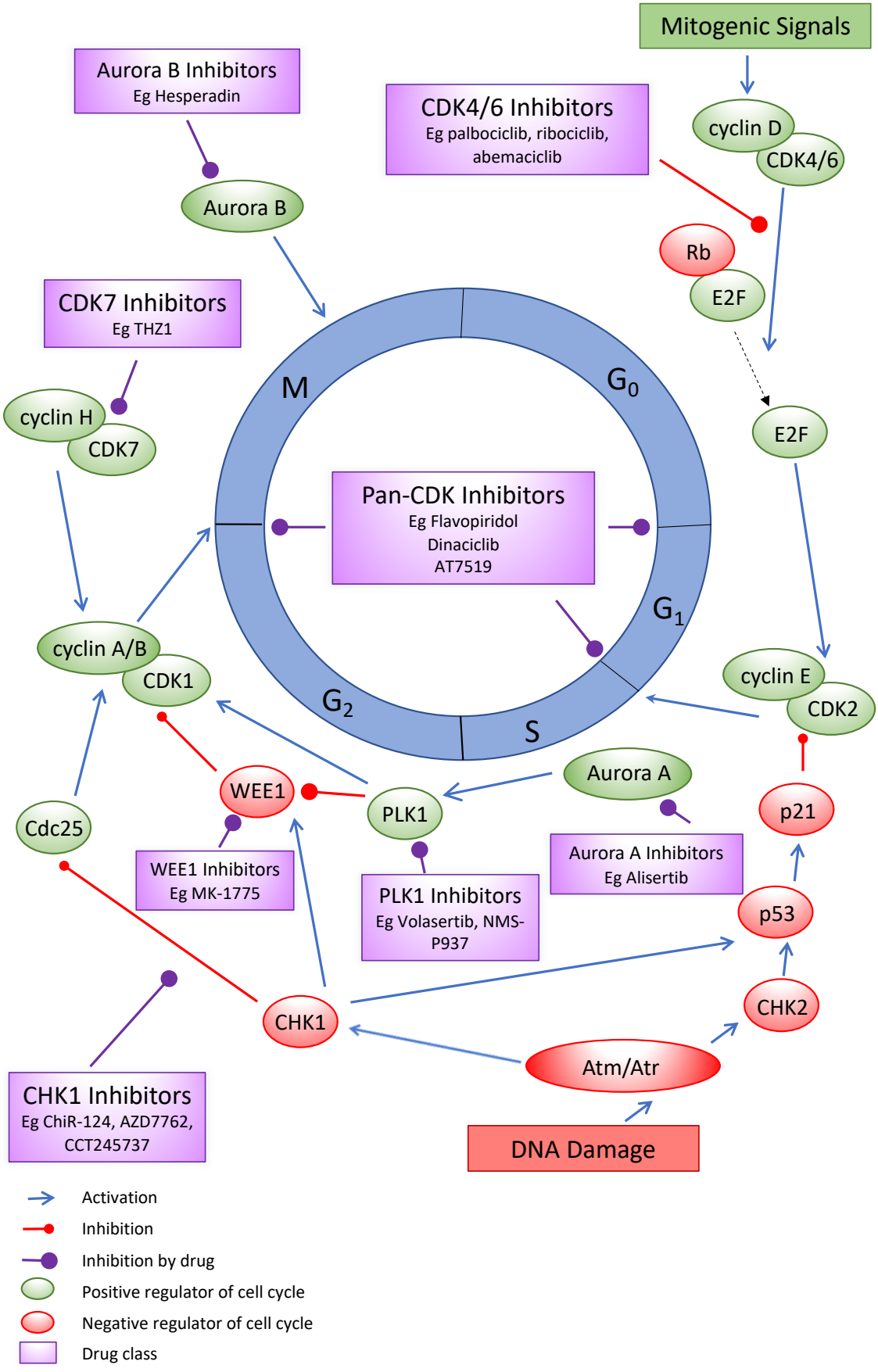

Figure 5.16 Schematic of cell cycle regulation by multiple kinases, and sites of drug action. Exit from the quiescent phase of G_0 by mitogenic signals is achieved through the formation of cyclin D-CDK4/6 complexes, which phosphorylate retinoblastoma (Rb) and

release E2F transcription factors. These activate the transcription of S-phase promoting genes such as *CCNE1*. Cyclin E-CDK2 complexes promote entry into S-phase. To enter mitosis, CDK1 must be phosphorylated by the cyclin H-CDK7 complex, and dephosphorylated by CDC-25. This is kept under regulation through ATM, CHK1, p53, and WEE1, which can stall the G_2-M checkpoint if DNA damage is detected. Upon recovery from DNA damage, PLK1 is necessary to overcome this cell cycle arrest and reactivate CDK1. Purple boxes indicate drugs that can act at the regulatory cell cycle checkpoints, that were classified as hits in the 2D drug screen at 100 nM or 1 μM in at least three of the seven cell lines.

important kinases can permit accumulation of chromosomal errors, and arrest the cell cycle. Some of the drugs highlighted as hits are in clinical trials for other malignancies, such as MK-1775 (a WEE1-inhibitor in phase 2 trials for ovarian malignancy (Oza et al., 2020)), volasertib (a PLK1-inhibitor in phase 3 trials for AML (Dohner et al., 2021)), and alisertib (an Aurora A-inhibitor kinase in phase I/II trials for solid cancers including advanced ER-positive breast cancer (O'Shaughnessy et al., 2021)). While there were significant grade 3/4 adverse effects encountered in these trials, nevertheless, the generally positive results with increase in overall survival are promising signs in the search for novel agents to target resistant disease.

5.2.7 3D drug screens in cell lines modelling endocrine resistance

The design of the 3D drug screen was informed by the results of the 2D drug screen. Seventy-one drugs were chosen to be taken into 3D screening because they targeted areas of interest highlighted in the 2D drug screens (Table 5.1). The decision was made to only screen at one drug concentration, as at least five concentrations would be necessary to fit a dose-response graph. The concentration chosen was 250 nM. This is because from the 2D drug screen, the 10 nM dose did not generate enough hits, but 1 μM was not discriminatory enough. As 100 nM is below the IC_{50} of many drugs used in clinical practice, such as palbociclib (FDA, 2014), the 250 nM dose was chosen. However, this did mean that the results of the 2D and 3D drug screens could not be directly compared.

Table 5.1: Compounds used in 3D screen, and their targets							
PI3K-AKT-mTOR		Hormonal Signalling		Cell Cycle Regulation		Growth Factor Signalling	
Drug	Target	Drug	Target	Drug	Target	Drug	Target
A674563	AKT1	Enobosarm	Androgen receptor	Alisertib	Aurora A	GDC0879	B-Raf
AZD5363/ capivasertib	AKT1/2/3	Enzalutamide	Androgen receptor	Aurora A Inhibitor 1	Aurora A	Nilotinib	Bcr-Abl
GSK690693	AKT1/2/3	H365 (SERCA)	ER	Flavopiridol	CDKs 1/2/4/6	A485	CREB-binding protein
MK2206	AKT1/2/3	Tamoxifen	ER	P-276-00/Riviciclib	CDKs 1/4/9	Gefitinib	EGFR
WYE-125132	mTOR	Fulvestrant	ER	Dinaciclib	CDKs 2/1/5/9	Lapatinib	EGFR
Everolimus	mTOR	RAD1901	ER	Abemaciclib	CDK 4/6	CUDC-101	EGFR
Sapinisertib	mTOR	GDC-910	ER	Palbociclib	CDK 4/6	PD168393	EGFR
Temsirolimus	mTOR	AZD9496	ER	SNS-032	CDK2	Ponatinib	FGFR1
Ridaforolimus	mTOR			BS-181	CDK 7	BGJ398	FGFR3
PF-04691502	PI3K			THZ1	CDK 7	Dovitinib	Flt1
BGT226	PI3K			NVP-2	CDK9	Neratinib	HER2
Omipalisib	PI3K			LDC00067	CDK9	BMS-754807	IGF-1R
Alpelisib	PI3Kα			CHIR-124	CHK1	Linsitinib	IGF-1R
CH5132799	PI3Kα			PF-477736	CHK1	Selumetinib	MAPK1
PIK-75	PI3Kα			Olaparib	PARP	Pimasertib	MAPK1/2
CUDC-907	PI3Kα			BI2536	PLK1	Binimetinib	MAPK1/2
				NMS-P937	PLK1	U0126	MAPK2
				GSK461364	PLK1	NVP-BVU972	MET
				Volarsertib	PLK1	Foretinib	MET
				MK1775	WEE1	SB203580	p38 MAPK
						Tyrphostin-9	PDGFR
						PP-121	PDGFR
						Sorafenib	Raf
						BBT-594	RET
						Crizotinib	ROS1
						Nintedanib	VEGFR1/2/3
						Sunitinib	VEGFR2

71 drugs used in 3D drug screen, classified by broad sites of action. Staurosporin was used as positive control, and DMSO vehicle as negative control.

Eight cell lines modelling endocrine resistance (MCF7 LTED^{WT}, MCF7 LTED^{Y537C}, MCF7 LTED^{PalboR}, SUM44 LTED^{WT}, SUM44 LTED^{Y537S}, HCC1428 LTED, HCC1428 LTED^{PalboR}, and T47D LTED) were screened against this 3D drug library. Two of the cell lines (MCF7 LTED^{PalboR}, and HCC1428 LTED^{PalboR}) also modelled palbociclib-resistant disease. Following assay quality assessment, where only assays with Z-prime≥0.5 were taken forward, robust Z-scores were calculated from three independent biological replicates to describe the effect of each drug on each cell line in 3D, at 250 nM. Robust Z-scores of ≤-1.65 were classified as hits (corresponding to *p*-value of 0.10). Due to the smaller numbers of targets identified, while the effect of the different *ESR1* mutations was examined, firm conclusions could not be drawn about their effect, and this data is not presented here.

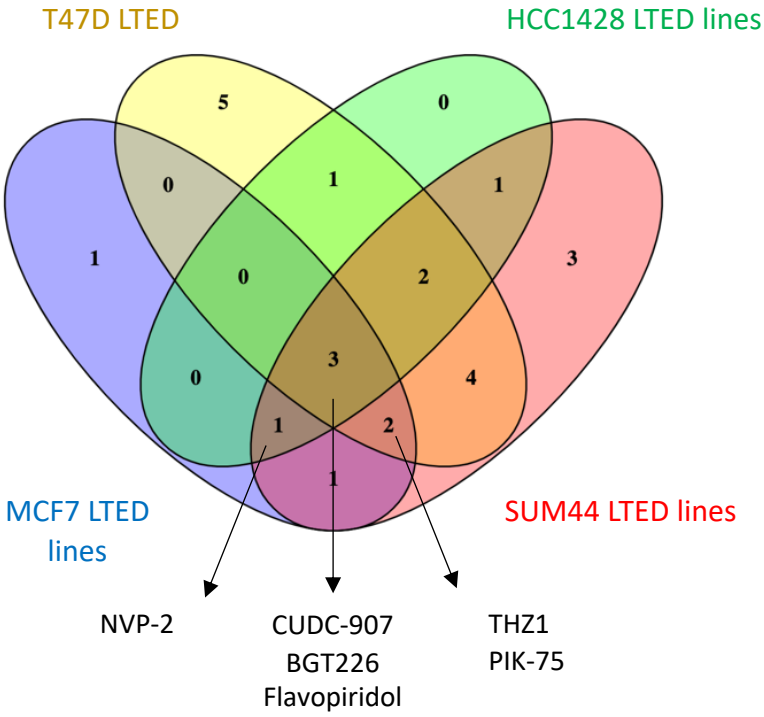

Figure 5.17 3D drug screen results of LTED breast cancer cell line models. Drugs (final concentration 250 nM) were pre-aliquoted into 96-well ultra-low attachment 3D drug screening plates, prior to seeding with 2500 cells/well. Cell viability was assessed using CellTiter-Glo after 7 days. Assay quality was assessed, and only those achieving Z-prime ≥0.5 were taken for further analysis. n=3 biological replicates. Robust Z-scores were calculated using the three independent replicates for each compound using the R package CellHTS2. Compounds with robust Z-score ≤-1.65 were classified as hits. Venn diagram shows the number of hits common to multiple cell lines, with targets that were common to three or four of the groups compared highlighted. NVP-2: CDK9 inhibitor. CUDC-907: PI3Kα inhibitor. BGT226: dual PI3K/mTOR inhibitor. Flavopiridol: inhibitor of CDKs 1, 2, 4, 6. THZ1: CDK7 inhibitor. PIK-75: PI3Kα inhibitor.

5.2.7.1 Comparison of 3D drug screen results for all cell lines

Figure 5.17 shows the number of compounds classed as significant hits common and private to the eight cell lines screened. As previously seen in the 2D drug screens, drugs affecting the PI3K-AKT-mTOR pathway cause a decrease in cell proliferation in all cell lines. The multi-CDK flavopiridol, which was also highlighted in the 2D drug screens, was also a common hit. Drugs that were significant hits in three of the four groups of cell lines compared were PIK-75, a PI3Kα inhibitor, the CDK7 inhibitor THZ1, and the CDK9 inhibitor NVP-2.

5.2.7.2 Comparison of 3D drug screen results of the palbociclib-sensitive and palbociclib-resistant lines

The significant hits between the palbociclib-sensitive MCF7 LTED^{Y537C} and HCC1428 LTED lines, and their palbociclib-resistant derivatives, were compared to look for potential mechanisms of palbociclib-resistance development (Figure 5.18A and 5.18B). While the palbociclib-resistant models retained their sensitivity to PI3Kα inhibitors, they were less sensitive to pan-PI3K inhibitors than the palbociclib-sensitive models. Comparison of the two palbociclib-resistant models indicates a shared common vulnerability are compounds targeting cell cycle control (Figure 5.18C).

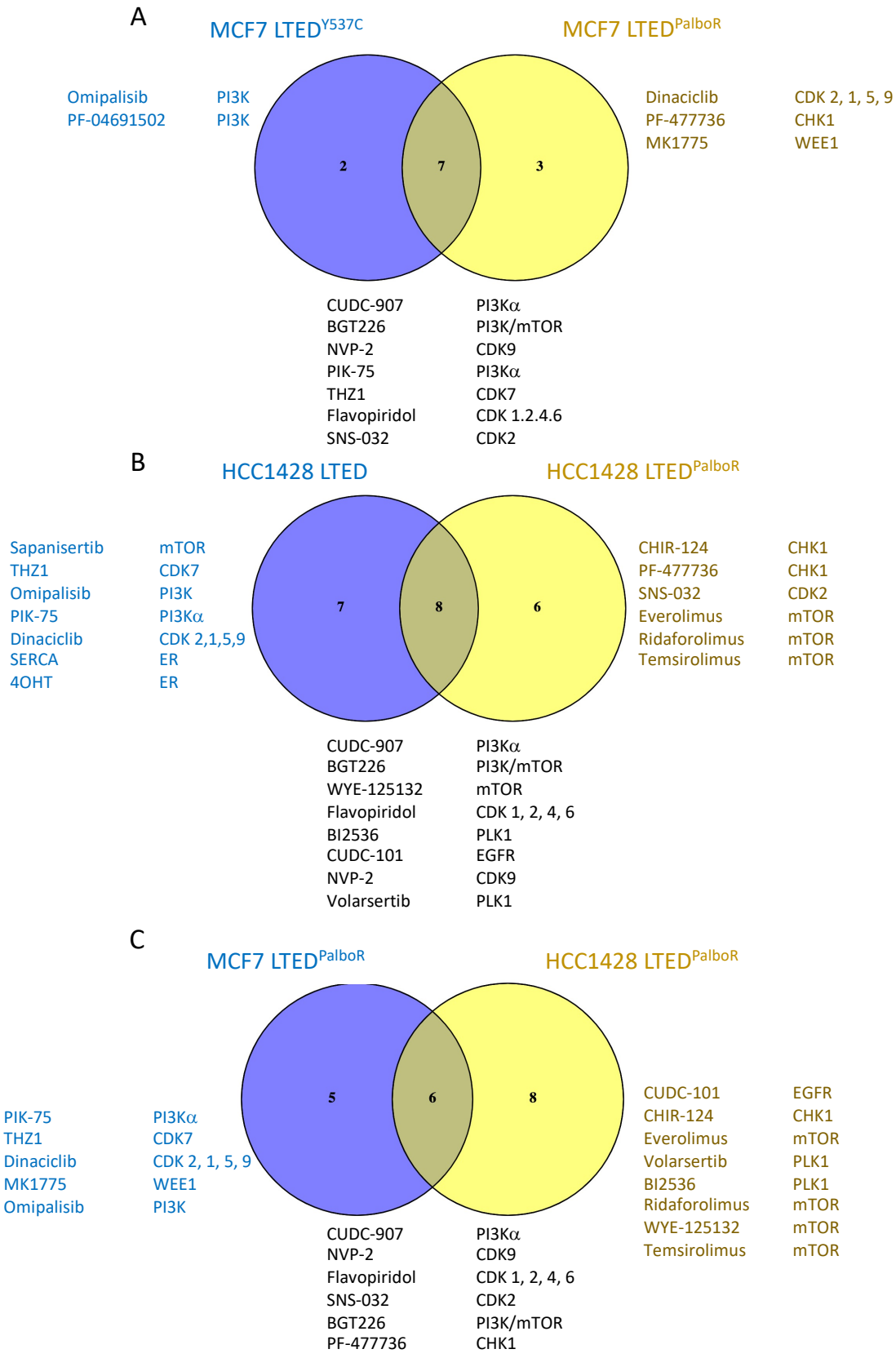

Figure 5.18 3D drug screen results of the palbociclib-sensitive LTED breast cancer cell lines, and their palbociclib-resistant derivatives. 3D drug screens (final concentration 250 nM) were performed as described in Figure 5.17. **(A)** Comparison of hits in the

palbociclib-sensitive MCF7 LTED^{Y537C} cell line, and its palbociclib-resistant derivative MCF7 LTED^{PalboR} cell line, in 3D. **(B)** Comparison of hits in the palbociclib-sensitive HCC1428 cell line, and its palbociclib-resistant derivative HCC1428 LTED^{PalboR} cell line, in 3D. **(C)** Comparison of the hits in the palbociclib-resistant cell lines MCF7 LTED^{PalboR} and HCC1428 LTED^{PalboR}.

5.3 Discussion

The use of the siRNA and drug screens has enabled the comparison of different models of endocrine-resistant disease, and the deconvolution of signalling pathways that are shared or private to the various cell lines. The comparison of the 2D and 3D models used in this study revealed that broadly similar results are achieved in both experimental contexts, but that the 3D models may provide another method of thresholding out false positives, as all key pathways identified in 2D were also seen in 3D.

When comparing the results for all the cell lines in the 3D siRNA screens, one target was identified as crucial in every cell line, *IP6K3*. This enzyme is needed to generate inositol pyrophosphate messenger molecules, and therefore it is likely that interfering with the expression of this gene resulted in the breakdown of signalling in multiple essential signalling pathways. As a result, given the presumed indiscriminate lethality of knocking down an enzyme required in multiple cellular functions, this target was not investigated further.

The siRNA and drug screens of these endocrine-resistant models have identified three key areas that may contribute to endocrine-resistance, and the results of the siRNA screens and drug screens corroborate each other. The PI3K-AKT-mTOR pathway is highlighted in all screens and is key for survival of these cell lines. Moreover, this pathway is also found to be significant in palbociclib-resistant models. This is in-keeping with the findings of the BYLieve trial (Rugo et al., 2021), which is looking to tackle the next obstacle in advanced ER-positive breast cancer – CDK4/6 inhibitor resistance. The inclusion criteria for this phase two trial were patients with ER-positive/HER2-negative disease, that had progressed on aromatase inhibitors and CDK4/6 inhibitors, and carried a *PIK3CA* mutation. The patients were treated with a combination of alpelisib, a PI3Kα inhibitor, and the SERD fulvestrant. With this combination, the trial met its primary endpoint of six months with no disease progression, and also showed increased

progression-free survival. This suggests that the findings of PI3Kα being a significant area of vulnerability in the 2D and 3D screens are valid.

Given the success of the BYLieve trial, and the considerable existing body of literature investigating the PI3K-AKT-mTOR pathway in breast cancer, I opted to choose CDK7 and CDK9, also identified in the screens, as the targets to investigate further. Given that cell cycle control was another frequently identified area of vulnerability, and that compounds targeting CDK7 and CDK9 appear to be active in both a wild-type and mutant *PIK3CA* setting, these CDKs were chosen as the hits for further validation

Chapter 6 Investigation of CDK7 and CDK9 as targets in breast cancer

6.1 Introduction

The aim of this project is to identify potential novel therapeutic targets in both the endocrine-resistant, and palbociclib-resistant setting. As described in Section 5.2.7.1, the drug screens identified THZ1, targeting CDK7, and NVP-2, targeting CDK9, as hits in the majority of the different cell lines modelling endocrine-resistance, and palbociclib-resistance. While these CDKs were not picked up as targets in many of the siRNA screens, the pathways that they play a role in were identified through pathway analysis of the siRNA screening data. Hence, CDK7 and CDK9 have been chosen for further investigation and validation. These studies were carried out in the MCF7, MCF7 LTED^{WT}, MCF7 LTED^{Y537C}, MCF7 LTED^{PalboR}, and HCC1428, HCC1428 LTED, HCC1428^{PalboR} cell lines (described in Section 4.2) to determine the effect of perturbing these targets in models of endocrine-sensitive, endocrine-resistant, and endocrine- and palbociclib-resistant disease.

6.2 CDK7

6.2.1 Structure and regulation of CDK7

CDK7 is a kinase comprising of 346 amino acids, with a molecular weight of ~40 kDa. The N-terminal region binds cyclin H, while the C-terminal region binds MAT1 (Figure 6.1A) (Rimel and Taatjes, 2018) This trimeric complex is called the CDK-activating kinase (CAK) complex, which has been termed a master regulator of the cell cycle, as will be discussed in Section 6.2. Cyclin H is crucial for CDK7 activity, and its association with CDK7 is enhanced by CDK7 phosphorylation at threonine-170 (T170) (Martinez et al., 1997). This CDK7-cyclin H complex is able to phosphorylate CDK2, but the addition of MAT1 to this binary complex, which stabilises the CAK complex, directs its kinase activity preferentially towards RNA polymerase II (RNA Pol II) (Larochelle et al., 2001). CDK7 may be phosphorylated at T170 by CDK1 and CDK2, and given that these are substrates of CDK7 itself, suggests the existence of a positive reinforcement loop (Garrett et al., 2001). The CAK complex itself may be activated through phosphorylation of cyclin H, which has been observed through autophosphorylation by CAK (Lolli et al., 2004), or by CK2 (Schneider et al., 2002).

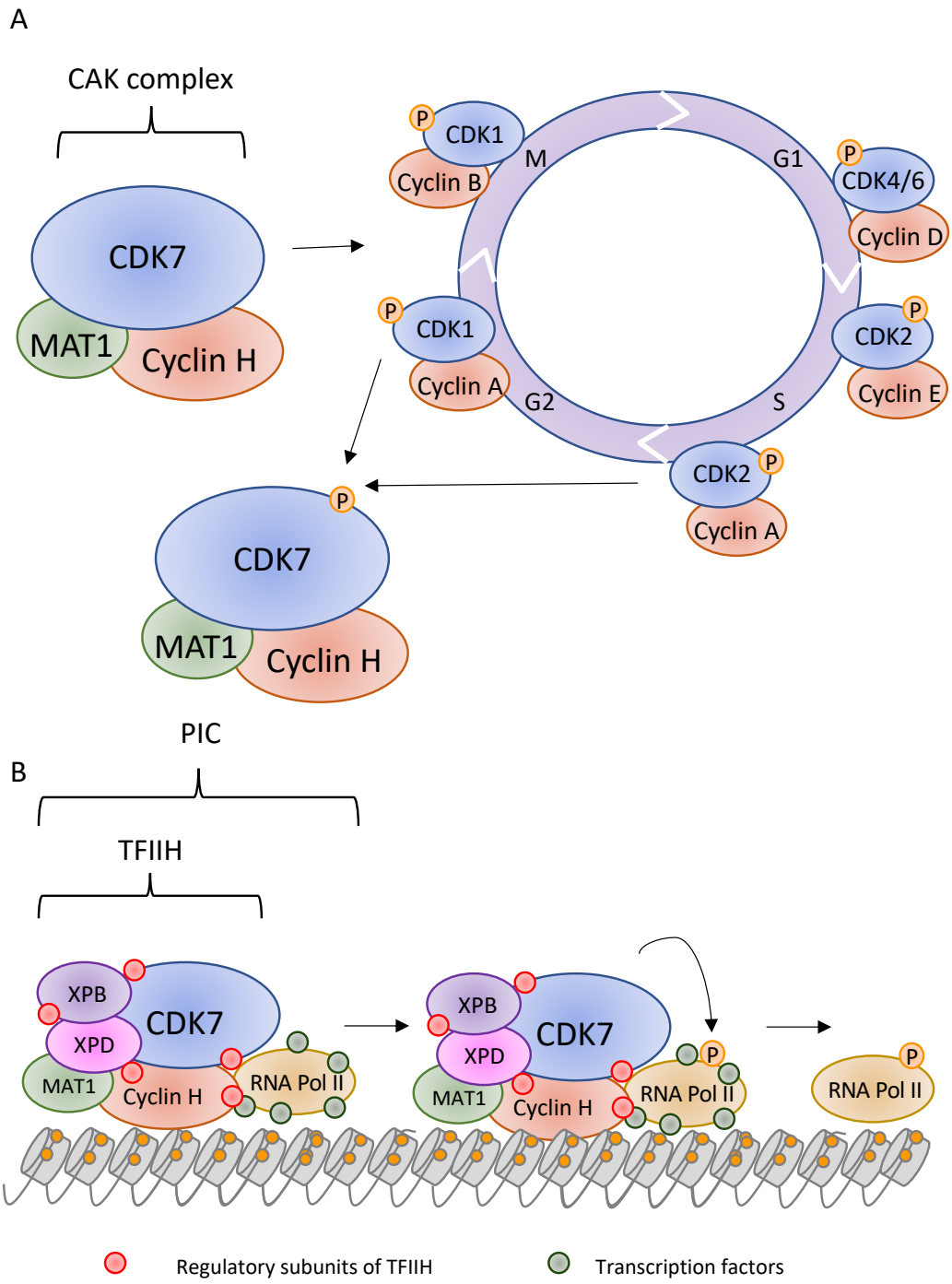

Figure 6.1 Role of CDK7. (A) Role of CDK7 in the cell cycle. CDK7 together with cyclin H and MAT1, form the CAK complex. The CAK complex can phosphorylate and activate multiple other CDKs, thus playing a regulatory role at multiple points in the cell cycle. G1 = gap phase 1, G2 = gap phase 2, M = mitosis, S = synthesis, P = phosphate. CDK1 and CDK2, as substrates of the CAK complex, can in turn phosphorylate and activate CDK7. **(B) Role of CDK7 in transcription.** CDK7, in the CAK complex, together with the two DNA helicases XPB and XPD (xeroderma pigmentosum proteins B and D), and other regulatory subunits form the heterodecameric transcription factor II H (TFIIH). The pre-initiation complex (PIC) is formed of TFIIH, RNA Polymerase II (RNA Pol II) and other transcription factors. It is through phosphorylation by CDK7 on Ser5 that RNA Pol II is released from the PIC and free to initiate transcription.

6.2.2 Role of CDK7 in the cell cycle

The control and progression of cells through the checkpoints in the cell cycle is regulated through the activity of several CDKs and their associated kinases. As illustrated in Figure 6.1A, the CAK complex is required to phosphorylate and activate CDKs 1, 2, 4, and 6, thus earning it the title of the master cell cycle regulator (Schachter and Fisher, 2013, Schachter et al., 2013, Bisteau et al., 2013). Inhibitors of CDK7 have been shown to delay S-phase by preventing CDK2 activation, and delay mitotic entry by preventing CDK1 activation (Patel et al., 2018). Furthermore, the control of the restriction point at which cells are committed to transit through the G_1/S checkpoint, the phosphorylation of retinoblastoma (Rb) (Mittnacht, 1998), is also indirectly governed by CDK7 activity. CDK4 and CDK6, activated via phosphorylation by CDK7, phosphorylate and inactivate Rb, releasing the previously bound transcription factors necessary to activate the transcription of S-phase genes. Inhibition of CDK7 has been shown to rapidly reduce CDK4 and CDK6 activity (Schachter et al., 2013), and as such can quickly perturb cell cycle progression.

6.2.3 Role of CDK7 in transcription

As well as its role in the cell cycle, CDK7 plays a key role in transcription. The CAK complex, together with two DNA helicases and other regulatory proteins, form the transcription factor complex TFIIH (Figure 6.1B) (Rimel and Taatjes, 2018). TFIIH associates with RNA Pol II, and other transcription factors, to form the pre-initiation complex (PIC), which governs the initiation of transcription. While anchored to the PIC, unphosphorylated RNA Pol II is not able to start transcription (Wong et al., 2014). CDK7 within TFIIH acts to phosphorylate RNA Pol II at serine-5, allowing the release of RNA Pol II from the PIC and initiation of transcription (Glover-Cutter et al., 2009). As will be discussed in Sections 6.3.1 and 6.3.2, CDK7 is also necessary for the productive elongation phase of transcription. Other regulatory roles of CDK7 in transcription include termination of transcription (Glover-Cutter et al., 2009), and the activation of CDK12 and CDK13 which can also phosphorylate RNA Pol II (Bosken et al., 2014, Liang et al., 2015).

In addition to its role in regulating the transcriptional machinery of the cell, CDK7 acts on several transcription factors to promote, or control their activity. With respect to ER-positive breast cancer, CDK7, when part of the TFIIH complex, is able to directly

phosphorylate ER at serine-118 in the presence of oestrogen (Chen et al., 2000b). This mechanism of ER activation, which is a key driver in the proliferation of ER-positive breast cancers, is inhibited by CDK7 inhibitors, especially within the *ESR1* mutant setting (Harrod et al., 2017), making this an attractive potential target in the setting of advanced ER^{MUT} breast cancer.

6.3 CDK9

6.3.1 Structure and regulation of CDK9

CDK9 is a cyclin dependent kinase that has two isoforms, with molecular weights of 42 kDa and 55 kDa. These different isoforms exist because there are two different promoters in the CDK9 gene. CDK_{42} is transcribed from a GC-rich promoter, while $CDK9_{55}$ is transcribed from a TATA-containing promoter. The $CDK9_{42}$ promoter has been found to have a higher constitutive activity (Shore et al., 2005), in keeping with the finding that in HeLa cells $CDK9_{55}$ is present at 10-20% of the level of $CDK9_{42}$ (Shore et al., 2003). CDK9 interacts with its cyclin partner, cyclin T, via its N-terminal lobe (Baumli et al., 2008) to form the complex Positive Transcription Elongation Factor (PTEF-b) (Figure 6.2). CDK9 has also been shown to associate with cyclin K, but this complex has a lower level of activity than PTEF-b (Fu et al., 1999). The primary role of PTEF-b is in transcription, as will be discussed in Section 6.3.2, and as the function of PTEF-b is essential for the transcription of a large programme of genes, its biological activity is highly regulated (Zhou et al., 2012).

The first mechanism is through sequestration: PTEF-b within the cell may be found reversibly sequestered in an inhibitory ribonucleoprotein complex, or in an active form bound to bromodomain containing 4 (BRD4) (Michels et al., 2004, Jang et al., 2005). The inhibitory complex is comprised of hexamethylene bisacetamide-inducible proteins (HEXIM 1 or 2), which are the main suppressors of PTEF-b function, and 7SK snRNA, a nuclear RNA that acts as a scaffold to mediate the interaction between the HEXIM proteins and PTEF-b. Intriguingly, phosphorylation of CDK9 at Thr186 (necessary for its kinase activity, as will be discussed in this section) is required for PTEF-b sequestration (Chen et al., 2004), suggesting that the inhibitory complex acts as a pool of active kinase, ready to undertake its transcriptional role. The mechanism by which PTEF-b is released

from the inhibitory complex remains unclear, but it has been shown that this process is dependent on BRD4 (Yang et al., 2005). BRD4 recruits JMJD6 to regions of chromatin where the inhibitory complex containing sequestered PTEF-b is anchored (Chang et al., 2007). JMJD6 is an arginine histone demethylase, which acts to dissociate the 7SK snRNA from the chromatin, allowing BRD4 and JMJD6 to interact with PTEF-b, and deliver it to RNA Pol II to play its role in transcription (Liu et al., 2013).

Phosphorylation of key residues in CDK9 is another method of regulating the activity of PTEF-b (Figure 6.2). As discussed earlier in this section, phosphorylation of threonine-186 in the T-loop of CDK9, which stimulates a conformational change in PTEF-b exposing the ATP and substrate binding sites (Baumli et al., 2008), is required for its enzymatic activity (Li et al., 2005). This crucial step is carried out by CDK7, further adding to its duties in transcriptional control (Larochelle et al., 2012). CDK7 is also able to phosphorylate CDK9 at serine-175, a step that promotes the interaction of cyclin T with BRD4 (Yang et al., 2005), which, as discussed above, is necessary for the recruitment of PTEF-b to RNA Pol II.

CDK9 and cyclin T may also be regulated by acetylation. Acetylation of lysine residues in cyclin T by the histone acetyl-transferase p300 aids in releasing PTEF-b from the inhibitory ribonucleoprotein complex (Cho et al., 2009). CDK9 has also been found to be acetylated on lysine residues, but conflicting reports as to whether this promotes CDK9 activity (Fu et al., 2007) or hinders it (Sabo et al., 2008).

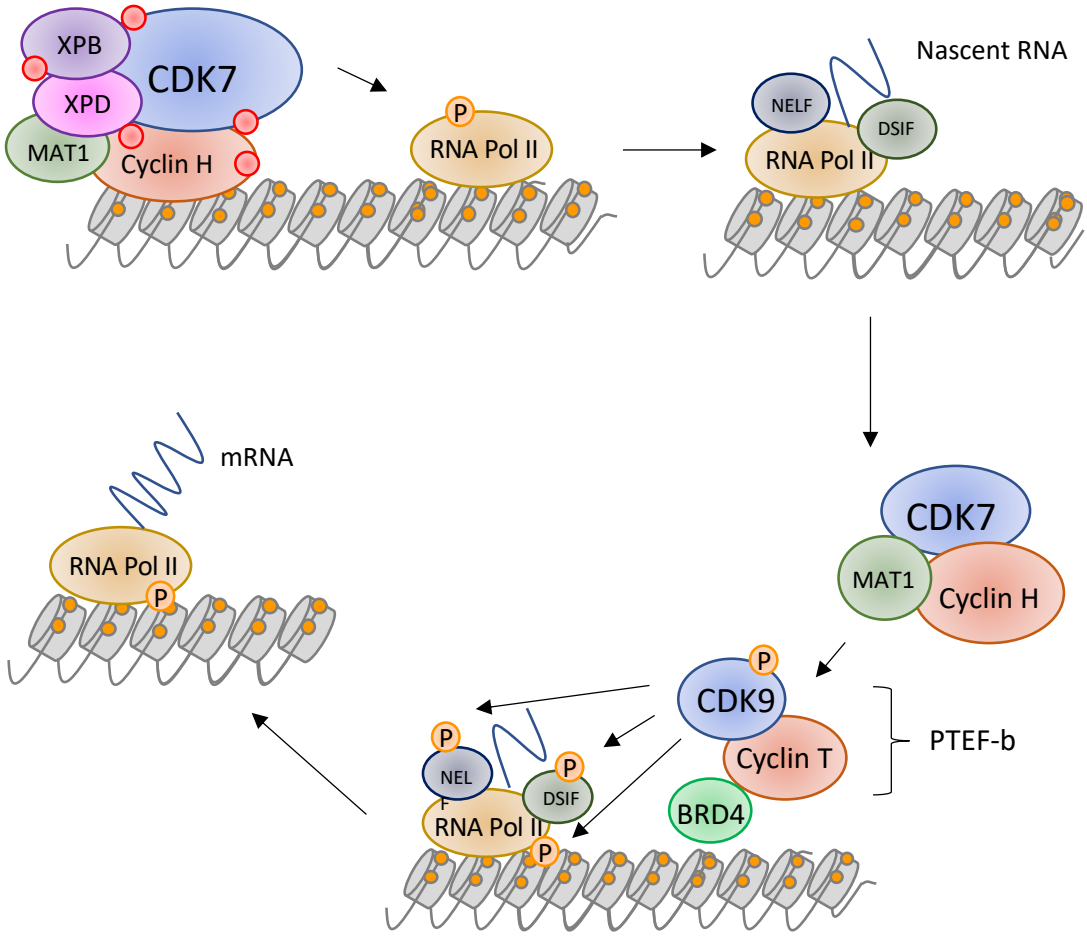

Figure 6.2 Role of CDK9 in transcription. Following activation by CDK7 in the TFIIH complex, RNA Pol II is held in a paused state after initiating transcription through interactions with DSIF (DRB sensitivity-inducing factor) and NELF (negative elongation factor). BRD4 recruits PTEF-b to these paused sites, CDK9 is activated through phosphorylation by CDK7, and activated CDK9 phosphorylates and removes the regulatory actions of these elements, as well as phosphorylating RNA Pol II at Ser2, facilitating productive mRNA elongation.

6.3.2 Role of CDK9 in transcription

As described in Section 6.2.3, the interactions between TFIIH (containing the CAK complex) and RNA Pol II are crucial for the initiation of transcription. Following the initiation phase, there is an elongation phase, and studies have shown that following the commencement of transcription, regulatory factors interact with RNA Pol II such that it cannot continue transcription beyond 20-50 nucleotides of the nascent mRNA (Marshall et al., 1996), and it is paused at the proximal promoter regions. These factors are DSIF (DRB sensitivity-inducing factor) (Wada et al., 1998) and NELF (negative elongation factor) (Yamaguchi et al., 1999). As illustrated in Figure 6.2, CDK9 as part of the PTEF-b complex, and having been activated through phosphorylation, is recruited by BRD4 to

sites where RNA Pol II is paused having initiated transcription (Itzen et al., 2014). PTEF-b then phosphorylates NELF, which releases it from RNA Pol II (Fujinaga et al., 2004), and phosphorylates DSIF, changing it to a positive elongation factor (Peterlin and Price, 2006). Concurrently, PTEF-b phosphorylates RNA Pol II at serine-2 (Ni et al., 2004). This is needed for the recruitment of elongation factors, spliceosomes, and other pre-mRNA processing factors (Gu et al., 2013, Li et al., 2003) to allow for productive elongation of mRNA.

In addition to its primary role in the elongation phase of transcription, CDK9 is also active in transcription initiation and termination. CRISPR-Cas9-based inhibition of CDK9 was found to cause a high degree of RNA Pol II pausing, but also limited the frequency of new transcription initiation (Gressel et al., 2017). Other studies using inhibitors of CDK9 found that RNA Pol II that managed to escape the promoter-proximal pausing caused by the inhibitors then went on to terminate transcription prematurely (Laitem et al., 2015).

6.3.3 Additional roles of CDK9

While CDK9 has primarily been considered a transcriptional CDK rather than related to cell cycle regulation, it does play a role in the cell cycle in that PTEF-b is required for the expression of key G_1-associated genes needed for cell cycle progression (Yang et al., 2008). PTEF-b has also been implicated in the cellular differentiation programmes of muscle cells (Simone et al., 2002), lymphocytes (Bellan et al., 2004), and neurons (De Falco et al., 2005). Finally, CDK9 may have a role in DNA repair when complexed with cyclin K. Following DNA damage, p53 has been shown to upregulate cyclin K transcription (Mori et al., 2002), and the use of siRNA to silence expression demonstrated that reduction of CDK9 and cyclin K, but not cyclin T, compromised the cell cycle in response to replication stress (Yu et al., 2010).

6.4 CDK7 and CDK9 in cancer

The concept of targeting CDKs, given their essential role in cellular homeostasis, may on first regard seem fruitless. Indeed, as will be discussed in Section 6.4.3, the first CDK inhibitors were unsuccessful due to their narrow therapeutic window. However, several cancers display features of transcriptional addiction – the need to maintain high levels

of certain survival proteins for proliferation and survival. Furthermore, many putative mechanisms of resistance to therapy involve bypassing cell cycle checkpoints where CDKs play a key role. Therefore, a tempting hypothesis exists whereby cancers, if found to be reliant on the activities of CDK7 or CDK9, could selectively be targeted by inhibitors against these CDKs.

6.4.1 Evidence for targeting CDK7 in cancer

CDK7 expression has been found to be upregulated in a range of different cancer types (Bartkova et al., 1996), including breast (Patel et al., 2016), stomach (Wang et al., 2016), and oral squamous cell carcinoma (Jiang et al., 2019). In breast cancer, while expression of *CDK7* and other components of the CAK complex correlates with improved patient survival in ER-positive disease (Patel et al., 2016), in TNBC, *CDK7* expression is associated with a worse prognosis (Li et al., 2017). Clinical studies have also suggested *CDK7* may be a valid target in advanced breast cancer, with encouraging efficacy seen with the combination of the CDK7 inhibitor ICEC0942/samuraciclib, and fulvestrant (Howell et al., 2021). Poorer outcomes in a variety of other cancers have also been associated with *CDK7* expression (Jiang et al., 2019, Tsang et al., 2019, Meng et al., 2018). These tumours with higher levels of *CDK7* expression may therefore be more sensitive to CDK7 inhibition, given its myriad of cellular roles, and therefore targeting CDK7 has been explored as a new area of therapy, as will be discussed in Section 6.4.4.

6.4.2 Evidence for targeting CDK9 in cancer

The link between CDK9 and cancers was first highlighted in haematological malignancies involving the rearrangement of a histone methyltransferase, named mixed-lineage leukaemia (MLL). MLL has several different rearrangements (Meyer et al., 2009), with the majority of the fusion proteins serving to act as nuclear transcription factors that recruit PTEF-b and promote transcription elongation (Lin et al., 2010), particularly of *HOXA* and *MEIS1* genes that block differentiation and drive proliferation (Muntean and Hess, 2012). PTEF-b also plays a role in the pathogenesis of acute myeloid leukaemia (AML). AML cells require high levels of the anti-apoptotic protein myeloid cell leukaemia-1 (MCL-1) (Glaser et al., 2012) for survival, but this protein has a very short half-life. As such, continuous activation of PTEF-b is necessary to maintain high levels of

transcription, and inhibition of CDK9 has been shown to reduce MCL-1 expression and demonstrate anti-cancer activity in AML mouse models (Lucking et al., 2017). The links between CDK9 and solid cancers such as breast cancer have not been as extensively characterised, but there is evidence suggesting breast cancers are reliant on CDK9. The transcription factor MYB, often overexpressed in ER-positive breast cancer, is a regulator of the key survival proteins cyclin E1 and BCL-2 (Mitra et al., 2016). One downstream pathway of ER-mediated signalling is to recruit PTEF-b to MYB promoter regions (Mitra et al., 2012). PTEF-b-mediated overexpression of the transcription factor MYC was also shown to be associated with oestrogen-independent growth of cell lines that had been developed to model hormone therapy resistance (Sengupta et al., 2014). CDK9 activity has also been linked to TNBCs. Gene expression studies of TNBCs demonstrated a cluster of TNBC-specific genes upon which the TNBCs were highly dependent for survival (Wang et al., 2015). The continuous transcription of these genes was driven by large clustered enhancer regions, densely occupied by transcriptional machinery, and so called super-enhancers (Hnisz et al., 2013). Consequently, cancers that are highly dependent on super-enhancer driven transcription of certain genes for survival, may be exquisitely sensitive to inhibitors targeting transcription.

6.4.3 History of targeting CDKs

Initial efforts to develop inhibitors of CDKs resulted in compounds that were active against multiple CDKs. The first pan-CDK inhibitor to enter clinical trials was flavopiridol, which showed activity against CDKs 1, 2, 4, 6, 7, and 9 (Senderowicz et al., 1998). This was then followed by the multi-CDK inhibitors seliciclib and dinaciclib. Unfortunately, these either had too high a toxicity profile, or did not perform better than the standard therapy at the time. It is likely that the lack of selectivity of these multi-CDK inhibitors has resulted in their inability to be translated from bench to bedside, given the key importance that CDKs play in normal cellular function. As such, subsequent work focused on enhancing the selectivity of CDK-targeting compounds. This proved fruitful in the development of CDK 4/6 inhibitors, as described in Section 1.1.5.4, suggesting that there is the potential for clinical success of selective inhibitors of other CDKs as well.

6.4.4 Current trials targeting CDK7

The first highly selective CDK7 inhibitor developed with BS-181. Although this was found to reduce CDK7 phosphorylation, and the growth of cancer cell lines and xenografts (which supports the hypothesis that CDK7 is a potential therapeutic drug target for cancer), it had poor bioavailability and cell permeability to proceed as a viable drug candidate (Ali et al., 2009). Through the development of BS-181 analogues, an orally bioavailable CDK7 inhibitor ICEC0942 was created (Patel et al., 2018). ICEC0942 was found to be active against a panel of cancer cell lines, in ER-positive breast cancer animal models and is now in phase 1/2 clinical trials (NCT03363893). In August 2021, a collaboration was announced to evaluate the combination of ICEC0942 with a novel SERD, giredestrant, to treat ER-positive/HER2-negative, palbociclib-resistant disease.

In a similar fashion to BS-181 and ICEC0942, another pair of selective CDK7 inhibitors are THZ1 and SY-1365. THZ1 is a covalent CDK7 inhibitor, has been shown to have favourable activity in several cancer types (Chipumuro et al., 2014, Kwiatkowski et al., 2014), and has been used as an interrogative tool compound in examining CDK7 function (Ebmeier et al., 2017), but also been found to inhibit CDK12 and CDK13. As such, SY-1365 was developed from THZ1 (Hu et al., 2019), and entered phase 1 trials for advanced solid tumours including breast and ovarian cancer (NCT03134638), but this trial was terminated early due to poor clinical activity and tolerability data. This company has now developed a new oral CDK7 inhibitor, SY-5609, which is now in phase I trials for advanced breast and small-cell lung cancer (NCT04247126).

6.4.5 Current trials targeting CDK9

Following favourable results in *in vitro* experiments and animal models of AML (Lucking et al., 2017), TNBC (Brisard et al., 2018), and oesophageal cancer (Veeranki et al., 2019), BAY1143572 is now being evaluated in phase I trials involving acute leukaemia (NCT02345382) and advanced gastric cancer, TNBC, or diffuse large B-cell lymphoma refractory to other therapies (NCT01938638), with results yet to be published.

AZD4573 is another selective CDK9 inhibitor, and has been found to cause extensive apoptosis in a diverse panel of haematological cancer cell lines, and induce regression of tumour growth in PDX models of AML (Cidado et al., 2020). Consequently, the drug is

now being examined in two phase 2 trials for advanced haematological malignancies (NCT03263637 and NCT04630756).

6.5 Results

6.5.1 Effect of targeting CDK7 using siRNA

To examine the effects of CDK7 on breast cancer cell viability in more detail, siRNA targeting CDK7 was used. The protocol for siRNA transfection was assessed to ensure effective knockdown. Each cell line was reverse transfected using siRNAs targeting CDK7 (siCDK7) or non-targeting control siRNAs (NTC). RTqPCR was used to examine the expression of *CDK7* in the treated cells (Figure 6.3A), while Western blotting was used to probe for the CDK7 protein (Figure 6.3B). The results of the qPCR show 80-90% reduction in *CDK7* expression across the cell lines. This is corroborated by evidence of reduction in *CDK7* expression in the Western blots shown, although the knockdown appears to be slightly less successful in the HCC1428 LTED and HCC1428 LTED^{PalboR} lines than in the MCF7 lines.

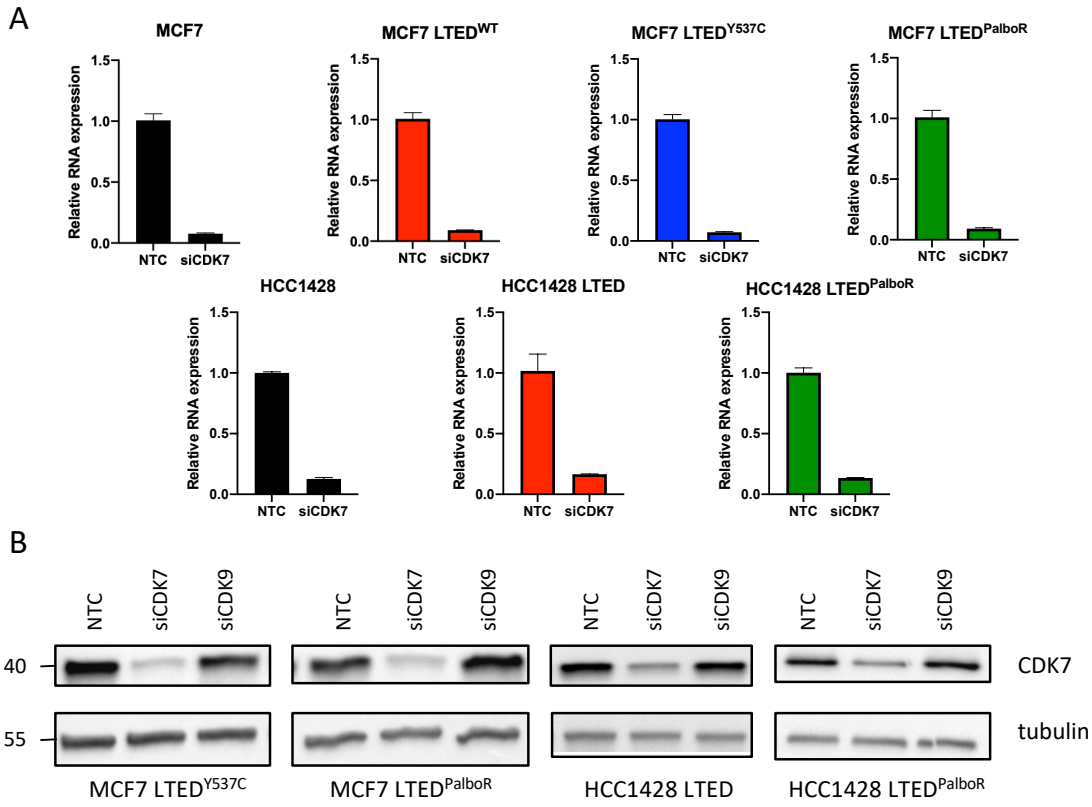

Figure 6.3 CDK7 knockdown using siRNA. (A) RTqPCR. 1x10^6 cells were reverse transfected with 25 nM SMARTpool siRNA targeting CDK7, or NTC, in 6cm plates. RNA was extracted 24 hours after transfection and RTqPCR performed. Barplots represent *CDK7* expression in cell lines transfected with siRNA targeting CDK7 (siCDK7) relative to non-targeting control (NTC). MCF7 lines: n=2 biological replicates, n=3 technical replicates, error bars represent means ±SEM. HCC1428 lines: n=1 biological replicate,

n=3 technical replicates, error bars represent SEM of 3 technical replicates. **(B) Western blotting** 5x10^5 cells of each cell line were reverse transfected with 25 nM SMARTpool siRNA targeting NTC/CDK7, or 10 nM siRNA targeting CDK9. Media was changed after 24 hours, and protein was extracted 4 days after transfection. Western blots show abundance of CDK7 in the MCF7 LTED^{Y537C}, MCF7 LTED^{PalboR}, HCC1428 LTED, and HCC1428 LTED^{PalboR} lines following transfection with siRNA targeting CDK7, CDK9, or NTC. Molecular weights of the proteins shown in kDa.

The effect of CDK7 knockdown on cell viability in these lines was then assessed. Cell viability was assessed 4 days after siRNA transfection (Figure 6.4). These assays show no difference in cell viability as a result of CDK7 knockdown in any of the lines, except in HCC1428 LTED^{PalboR} where CDK7 knockdown appears to show an increase in viability. This is in-keeping with the results of the siRNA screens, as CDK7 was not a significant hit in any of these cell lines when subjected to the screen-based approach either. However, this is not consistent with the results seen with drugs targeting CDK7, either in the drug screens (Sections 5.2.6 and 5.2.7) or in individual drug assays as will be discussed in Section 6.5.3.

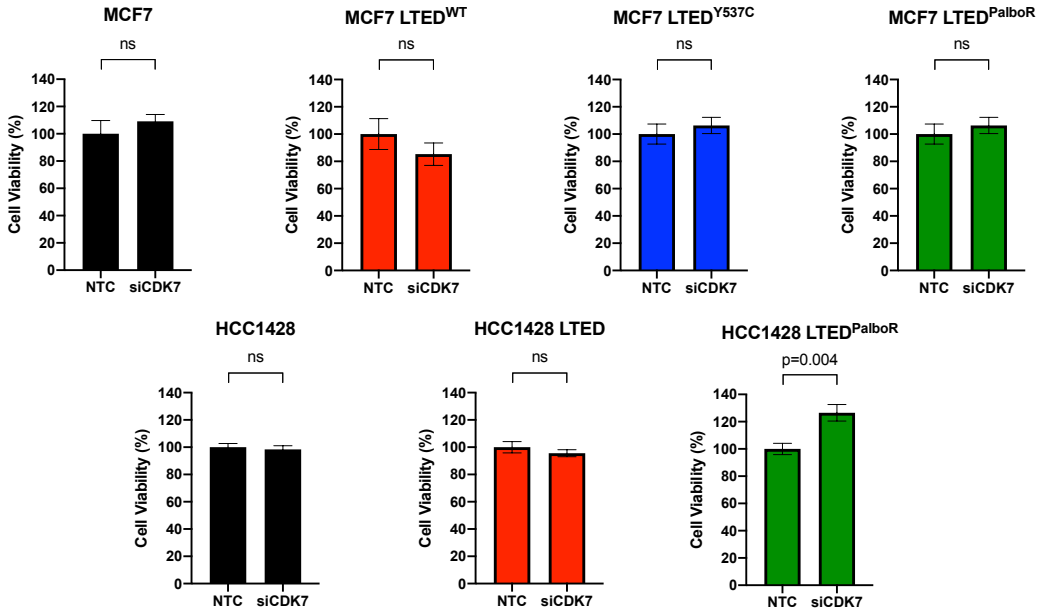

Figure 6.4 Effect of CDK7 knockdown by siRNA on cell viability. 4000-8000 cells were seeded in in 96-well plates and reverse transfected with 25 nM SMARTpool siRNA targeting CDK7 or NTC. Cell seeding number adjusted per line to allow for ~80% confluence in the control wells at the end of the experiment. Media was changed after 24 hours. Cell viability was assessed using CellTiter-Glo after 4 days. Barplots represent percentage cell viability in cell lines transfected with siRNA targeting CDK7 (siCDK7) relative to non-targeting control (NTC). MCF7 lines: n=2 biological replicates, n=6 technical replicates, error bars represent means ±SEM. HCC1428 lines: n=1 biological

replicate, n=8 technical replicates, error bars represent SEM of 8 technical replicates. Group means compared using one-way ANOVA, with Dunnett's post-hoc test to identify significant differences compared to NTC.

6.5.2 Effect of targeting CDK9 using siRNA

The effectiveness of CDK9 knockdown using siRNA targeting CDK9 (siCDK9) was also assessed using RTqPCR and Western blotting. Of note, transfecting the cells with 25 nM siCDK9 proved to be extremely toxic to the MCF7 cells (data not shown). As a result, a lower concentration of 10 nM siCDK9 was used, but all other experimental methods were identical to those used for knocking down CDK7. Figure 6.5A shows a 70-80% reduction in *CDK9* expression as assessed by RTqPCR in the MCF7, MCF7 LTED, and MCF7 LTED^{Y537C} lines. While only a 50% knockdown of *CDK9* expression was demonstrated in the MCF7 LTED^{PalboR} line, the Western blot in Figure 6.5B shows almost no expression of CDK9 protein in the MCF7 LTED^{PalboR} line. Furthermore, it appears that knocking down CDK7 decreases the expression of *CDK9*, although when this interaction was examined by RTqPCR, the opposite appeared to be true (data not shown). In the HCC1428 lines, CDK9 knockdown was not as effective as in the MCF7 lines as assessed by RTqPCR, but there is evidence of reduction in CDK9 protein levels in the Western blots.

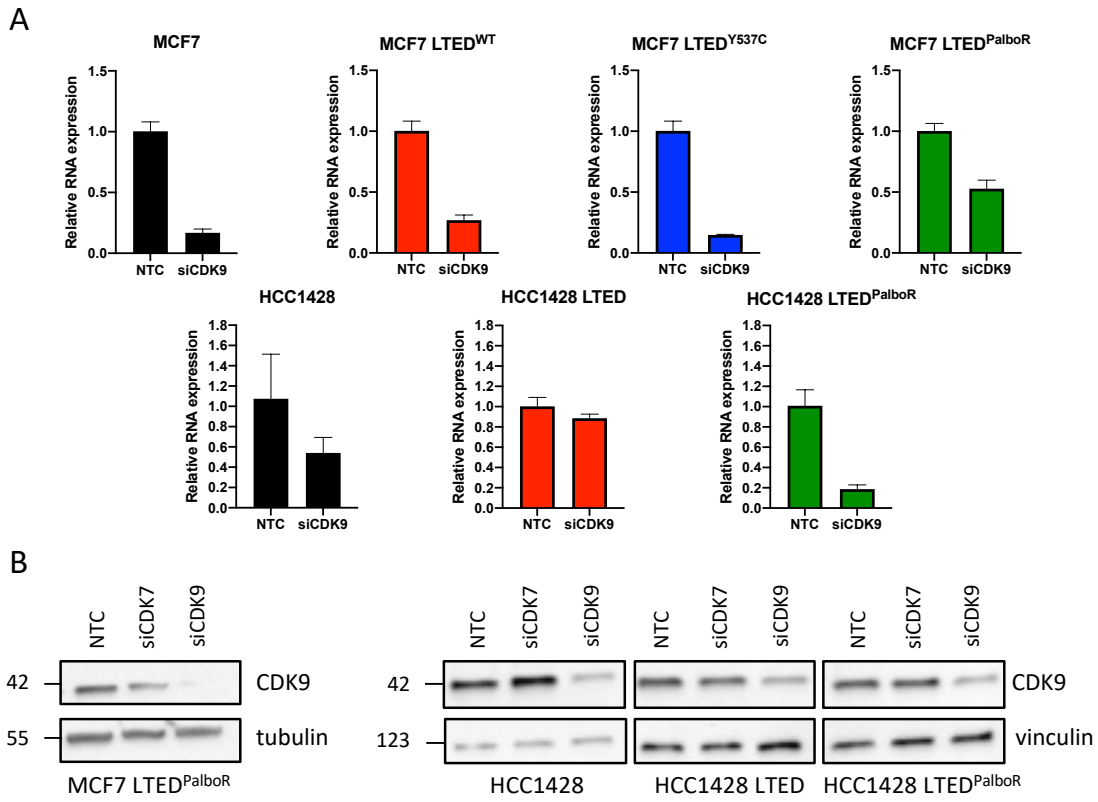

Figure 6.5: CDK9 knockdown using siRNA

Figure 6.5 CDK9 knockdown using siRNA (A) RTqPCR. $1x10^6$ cells were reverse transfected with 10 nM SMARTpool siRNA targeting CDK9, or 25 nM siNTC, in 6cm plates. RNA was extracted 24 hours after transfection and RTqPCR performed. Barplots represent *CDK9* expression in cell lines transfected with siRNA targeting CDK9 (siCDK9) relative to non-targeting control (NTC). MCF7 lines: n=2 biological replicates, n=3 technical replicates, error bars represent means ±SEM. HCC1428 lines: n=1 biological replicate, n=3 technical replicates, error bars represent SEM of 3 technical replicates. (**B) Western blotting**. $5x10^5$ cells of each cell line were reverse transfected with 25 nM SMARTpool siRNA targeting NTC/CDK7, or 10 nM siRNA targeting CDK9. Media was changed after 24 hours, and protein was extracted 4 days after transfection. Western blots show abundance of CDK9 in the MCF7 LTED^{PalboR}, HCC1428, HCC1428 LTED, and HCC1428 LTED^{PalboR} lines following transfection with siRNA targeting CDK7, CDK9, or NTC. Molecular weights of the proteins shown in kDa.

The effect of CDK9 knockdown on cell viability was assessed using the same protocol as described previously for CDK7, but using 10 nM siCDK9, with results shown in Figure 6.6. These cell viability assays show a significant reduction in viability for all cell lines following knockdown of CDK9, except in the HCC1428 LTED and HCC1428 LTED^{PalboR} lines. This could be a result of the less effective knockdown of CDK9 in these lines. However, it should be noted, in the siRNA screens (which used a concentration of 25 nM for each siRNA) *CDK9* was not a significant hit in the HCC1428 LTED or HCC1428 LTED^{PalboR} lines in 2D or in 3D.

The results of these siRNA knockdown experiments suggest that CDK7 would not be considered a valid target in terms of reducing proliferation in these lines, and that CDK9 is a valid target in some of these cell lines.

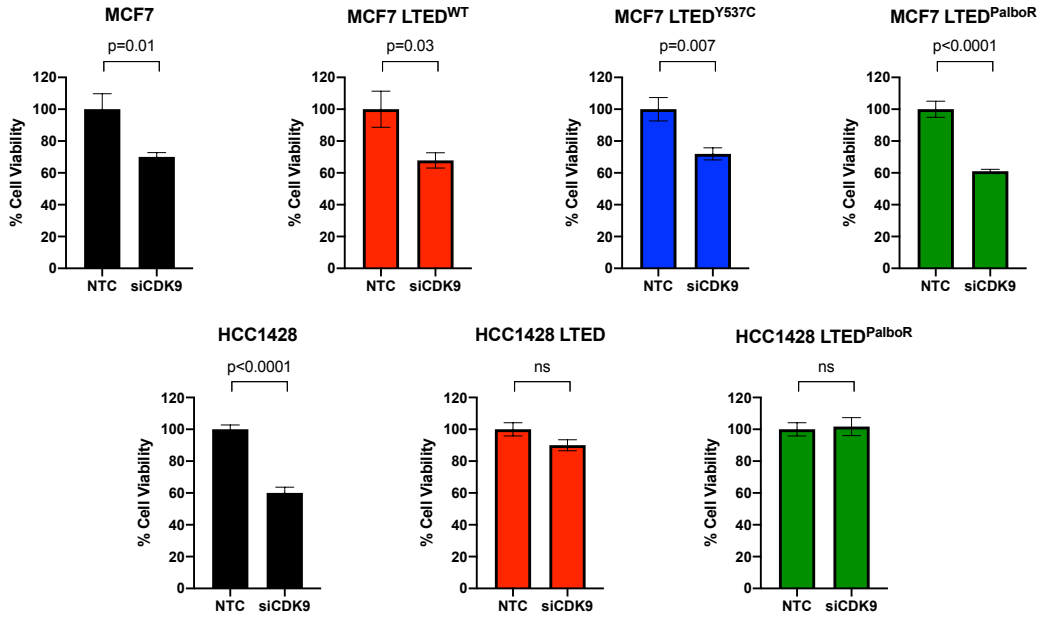

Figure 6.6 Effect of CDK9 knockdown by siRNA on cell viability. 4000-8000 cells were seeded in in 96-well plates and reverse transfected with 10 nM SMARTpool siRNA targeting CDK9, or 25 nM siNTC. Cell seeding number adjusted per line to allow ~80% confluence in the control wells at the end of the experiment. Barplots represent percentage cell viability in cell lines transfected with siRNA targeting CDK9 (siCDK9) relative to non-targeting control (NTC). MCF7 lines: n=2 biological replicates, n=6 technical replicates, error bars represent means ±SEM. HCC1428 lines: n=1 biological replicate, n=8 technical replicates, error bars represent SEM of 8 technical replicates. Group means compared using one-way ANOVA, with Dunnett's post-hoc test to identify significant differences compared to NTC.

6.5.3 Effect of pharmacological targeting of CDK7 in 2D culture

Cell proliferation assays using drugs to target CDK7 in the same breast cancer cell lines were run contemporaneously with the siRNA experiments. These results were different, and are shown in Figure 6.7 and Figure 6.8. The drugs used in these experiments were THZ1, and ICEC0942. THZ1, a tool compound often used to interrogate CDK7 function, was chosen as it has been well characterised in the literature. ICEC0942 was chosen due to its specificity, its oral bioavailability, and the fact that it has already entered human trials (Patel et al., 2018).

These results show that all of the cell lines are sensitive to THZ1, with similar IC_{50} values obtained for each cell line. The experiment for the HCC1428 LTED cell line warrants repeating, which unfortunately could not be carried out due to time constraints and shortage of tissue culture flasks post-Brexit. The findings are in contrast with those of Wang et al, who concluded that TNBCs, but not ER-positive cells, were sensitive to THZ1 inhibition (Wang et al., 2015), but corroborates with the subsequent findings of McDermott et all, who found that all subtypes of breast cancer were sensitive to THZ1 treatment (McDermott et al., 2020). There was no significant difference found in the response of the palbociclib-resistant cells when compared to their parental palbociclib-sensitive lines.

The results for ICEC0942 show a similar picture (Figure 6.8), with all cell lines found to be sensitive to this compound, except the HCC1428 LTED line. This result is surprising, given that the parental endocrine-sensitive cell line, and the derivative endocrine-resistant, palbociclib-resistant cell lines are both sensitive to ICEC0942. There was no significant difference in the dose-response curves between palbociclib-sensitive and palbociclib-resistant models in either cell line when tested by two-way ANOVA, but there was a significant difference in the IC_{50} values for the HCC1428 LTED and HCC1428 $LTED^{PalboR}$ lines as tested by comparing the sum-of-squares fit.

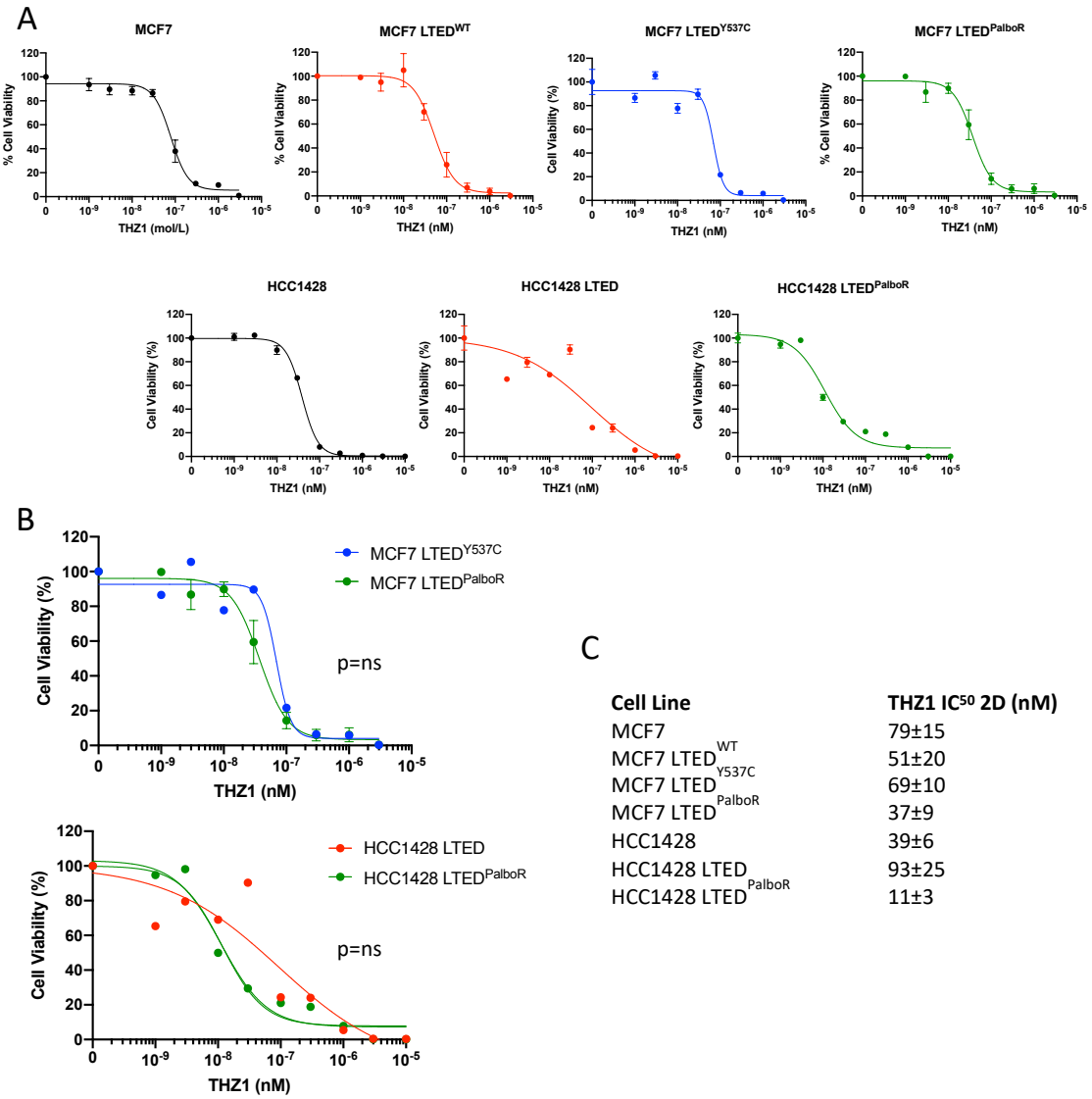

C

Cell Line	THZ1 IC^{50} 2D (nM)
MCF7	79±15
MCF7 $LTED^{WT}$	51±20
MCF7 $LTED^{Y537C}$	69±10
MCF7 $LTED^{PalboR}$	37±9
HCC1428	39±6
HCC1428 LTED	93±25
HCC1428 $LTED^{PalboR}$	11±3

Figure 6.7 Effect of THZ1 on cell proliferation (A) 4000-8000 cells were seeded in 2D 96-well plates (seeding number adjusted per line to allow ~80% confluence in the control wells at the end of the experiment). Cells were treated with THZ1 at 24 hours, with a second treatment at 72 hours. Cell viability was assessed using CellTiter-Glo after 7 days. Dose-response graphs show effect of escalating concentrations of THZ1 on viability of breast cancer cell lines. Data represent percentage of viable cells compared with vehicle control. MCF7 lines: n=2 biological replicates, n=4 technical replicates, error bars represent means ±SEM. HCC1428 lines: n=1 biological replicate, n=4 technical replicates, error bars represent SEM of 4 technical replicates. **(B)** Comparison of the effect of THZ1 on the palbociclib-sensitive MCF7 $LTED^{Y537C}$ and HCC1428 LTED cell lines, and their respective palbociclib-resistant derivatives. Data represent percentage of viable cells compared with vehicle control. MCF7 lines: n=2 biological replicates, n=4 technical replicates, error bars represent means ±SEM. HCC1428 lines: n=1 biological replicate, n=4 technical replicates, error bars represent SEM of 4 technical replicates. Difference in dose-response curves tested by two-way ANOVA. **(C)** IC_{50} values ± variance for THZ1 calculated from these experiments using 4-parameter non-linear regression.

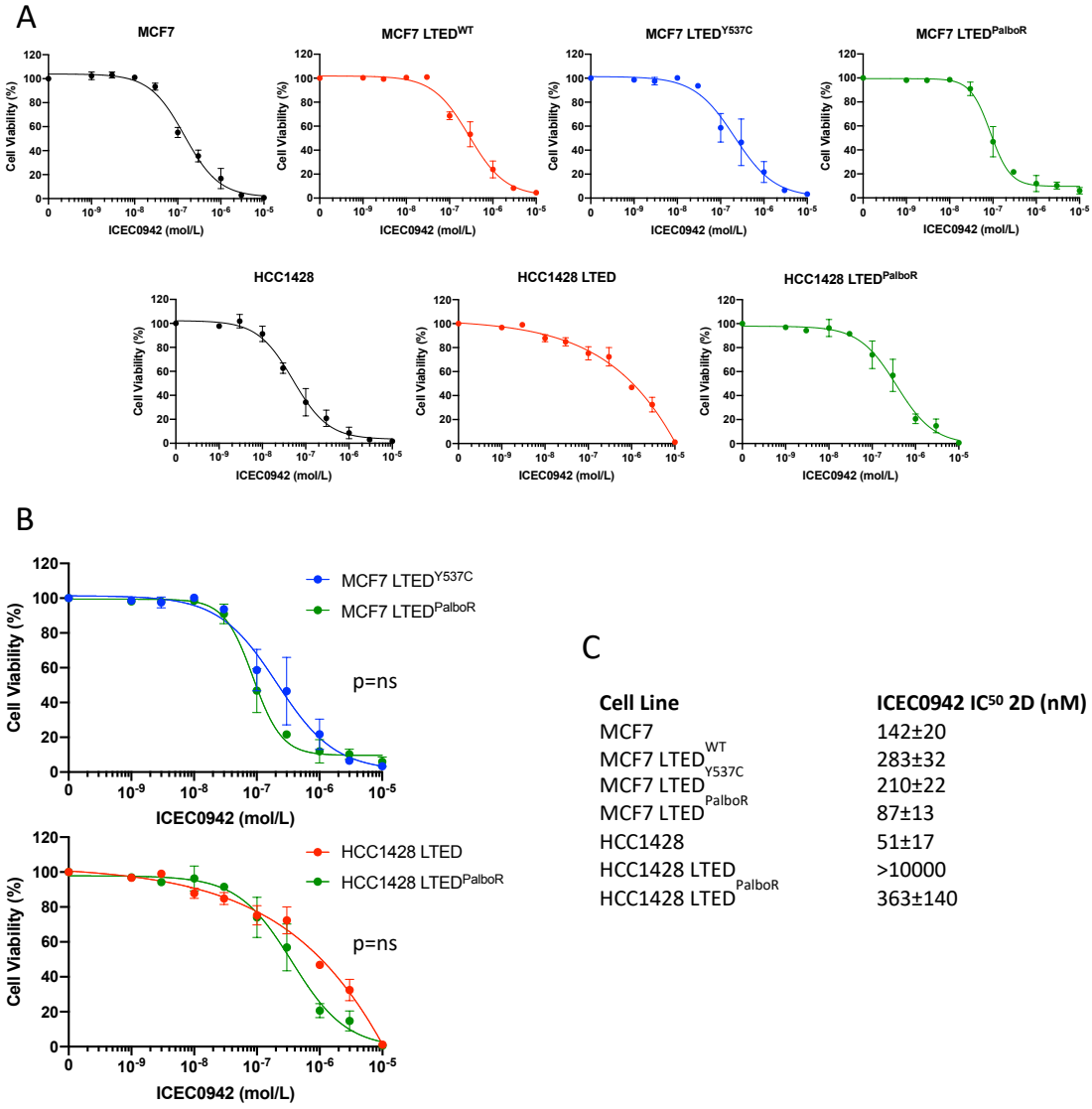

C

Cell Line	ICEC0942 IC^{50} 2D (nM)
MCF7	142±20
MCF7 LTED$_{Y537C}^{WT}$	283±32
MCF7 LTED^{PalboR}	210±22
HCC1428	87±13
HCC1428 LTED	51±17
HCC1428 LTED^{PalboR}	>10000
	363±140

Figure 6.8 Effect of ICEC0942 on cell proliferation (A) 4000-8000 cells were seeded in 2D 96-well plates (seeding number adjusted per line to allow ~80% confluence in the control wells at the end of the experiment). Cells were treated with ICEC0942 at 24 hours, with a second treatment at 72 hours. Cell viability was assessed using CellTiter-Glo after 7 days. Dose-response graphs show effect of escalating concentrations of ICEC0942 on viability of breast cancer cell lines. Data represent percentage of viable cells compared with vehicle control. MCF7 lines: n=3 biological replicates, n=4 technical replicates. HCC1428 lines: n=2 biological replicates, n=4 technical replicates. Error bars represent means ±SEM. **(B)** Comparison of the effect of ICEC0942 on the palbociclib-sensitive MCF7 LTED^{Y537C} and HCC1428 LTED cell lines, and their respective palbociclib-resistant derivatives. Data represent percentage of viable cells compared with vehicle control. MCF7 lines: n=3 biological replicates, n=4 technical replicates. HCC1428 lines: n=2 biological replicates, n=4 technical replicates. Error bars represent means ±SEM. Difference in dose-response curves tested by two-way ANOVA. **(C)** IC_{50} values ± variance for ICEC0942 calculated from these experiments using 4-parameter non-linear regression.

6.5.4 Effect of pharmacological targeting of CDK9 in 2D culture

Cell proliferation assays were performed in 2D using the CDK9 inhibitors NVP-2 and AZD4573. NVP-2 was chosen due to its high specificity for CDK9 inhibition (Olson et al., 2018), and AZD4573 because it is currently in clinical trials for treatment of leukaemia as discussed in Section 6.4.5, and so has the potential to be repurposed for breast cancer treatment. The results of exposing the different cancer cell lines to escalating doses of NVP-2 and AZD4573 are shown in Figures 6.9 and 6.10. All of the cell lines are sensitive to low doses of these drugs, which largely corroborates the findings of the siRNA knockdown of CDK9. In comparing the palbociclib-sensitive and palbociclib-resistant cell lines, the palbociclib-resistant lines are either just as sensitive, or more sensitive to NVP-2 and AZD4573 (Figures 6.9C, 6.10C). In particular, the dose-response curve for the MCF7 LTED^{PalboR} line shows almost a 2-fold shift in sensitivity to AZD4573 when compared to MCF7 LTED^{Y537C}, although this did not meet the threshold for significance by two-way ANOVA.

These results suggest that the pathway governed by CDK9 is key to cell survival in multiple settings, and potentially is conserved throughout the development of endocrine-resistance and palbociclib-resistance.

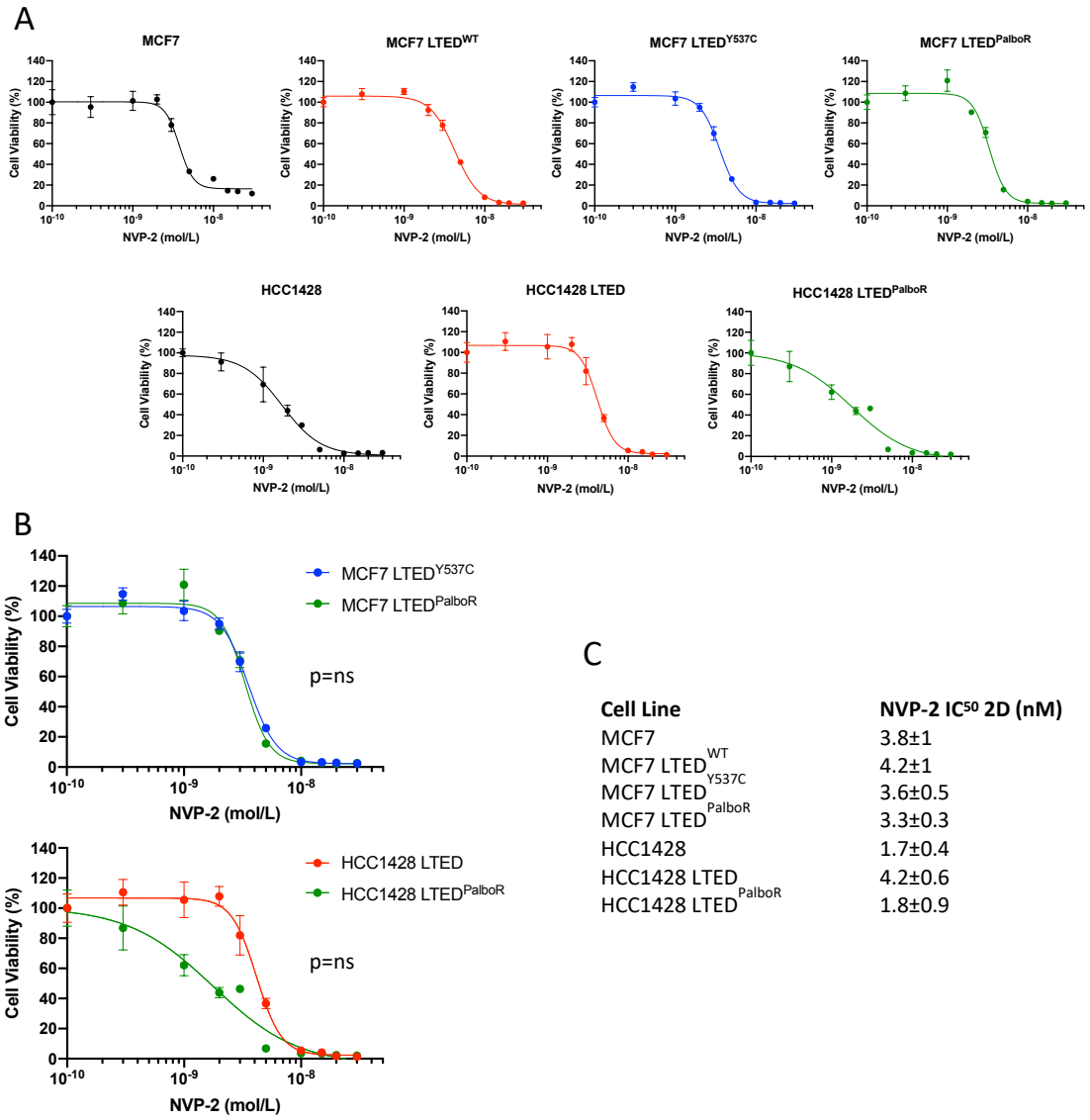

C

Cell Line	NVP-2 IC^{50} 2D (nM)
MCF7	3.8±1
MCF7 $LTED^{WT}_{Y537C}$	4.2±1
MCF7 $LTED^{PalboR}$	3.6±0.5
HCC1428	3.3±0.3
HCC1428 LTED	1.7±0.4
HCC1428 $LTED^{PalboR}$	4.2±0.6
	1.8±0.9

Figure 6.9 Effect of NVP-2 on cell proliferation (A) 4000-8000 cells were seeded in 2D 96-well plates (seeding number adjusted per line to allow ~80% confluence in the control wells at the end of the experiment). Cells were treated with NVP-2 at 24 hours, with a second treatment at 72 hours. Cell viability was assessed using CellTiter-Glo after 7 days. Dose-response graphs show effect of escalating concentrations of NVP-2 on viability of breast cancer cell lines. Data represent percentage of viable cells compared with vehicle control. n=1 biological replicate, n=4 technical replicates. Error bars represent SEM of 4 technical replicates. **(B)** Comparison of the effect of NVP-2 on the palbociclib-sensitive MCF7 $LTED^{Y537C}$ and HCC1428 LTED cell lines, and their respective palbociclib-resistant derivatives. Data represent percentage of viable cells compared with vehicle control. n=1 biological replicate, n=4 technical replicates, error bars represent SEM of 4 technical replicates. Difference in dose-response curves tested by two-way ANOVA. **(C)** IC_{50} values ± variance for NVP-2 calculated from these experiments using 4-parameter non-linear regression.

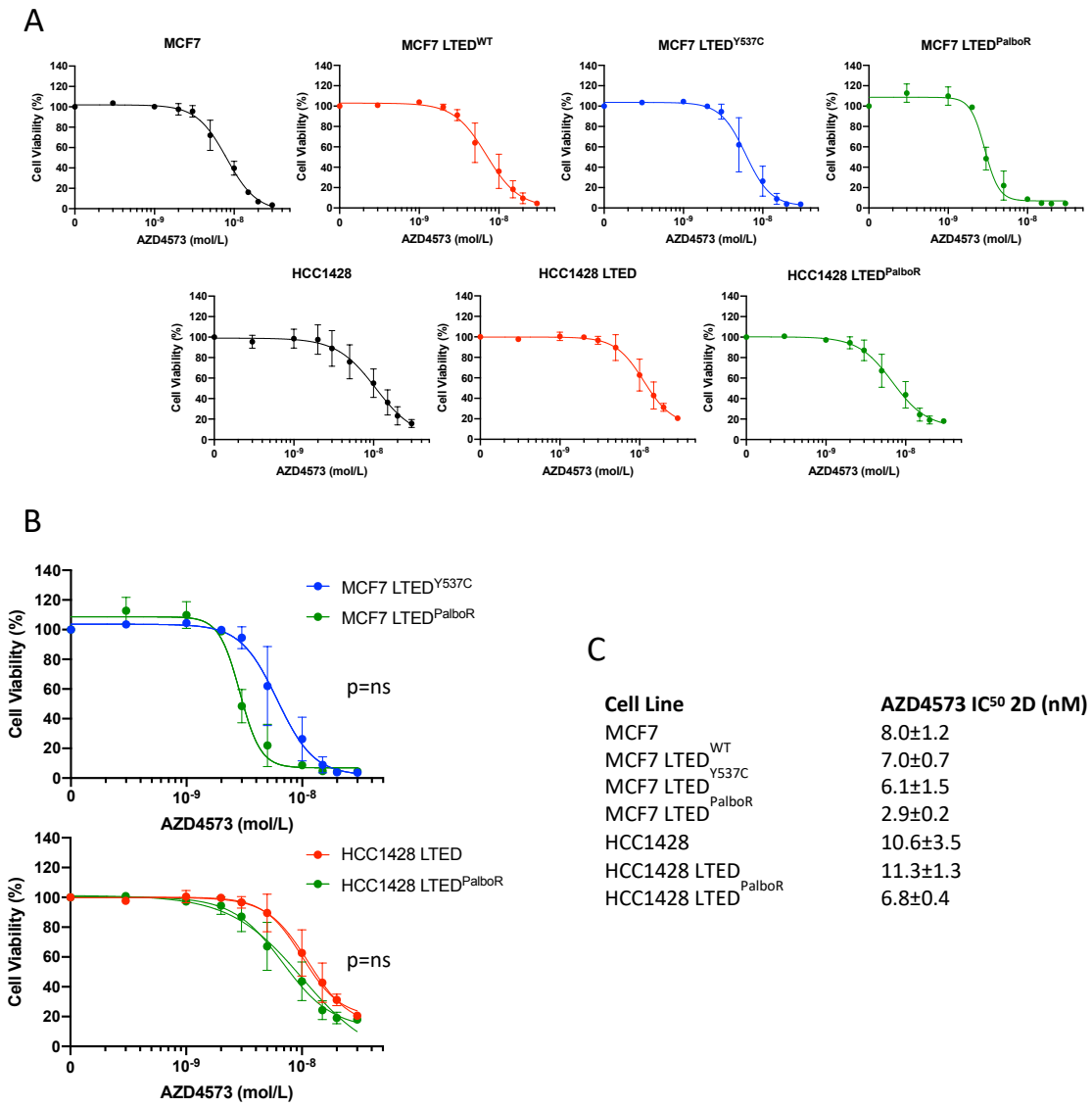

C

Cell Line	AZD4573 IC^{50} 2D (nM)
MCF7	8.0±1.2
MCF7 LTED^{WT}	7.0±0.7
MCF7 LTED^{Y537C}	6.1±1.5
MCF7 LTED^{PalboR}	2.9±0.2
HCC1428	10.6±3.5
HCC1428 LTED	11.3±1.3
HCC1428 LTED^{PalboR}	6.8±0.4

Figure 6.10 Effect of AZD4573 on cell proliferation (A) 4000-8000 cells were seeded in 2D 96-well plates (seeding number adjusted per line to allow ~80% confluence in the control wells at the end of the experiment). Cells were treated with AZD4573 at 24 hours, with a second treatment at 72 hours. Cell viability was assessed using CellTiter-Glo after 7 days. Dose-response graphs show effect of escalating concentrations of AZD4573 on viability of breast cancer cell lines. Data represent percentage of viable cells compared with vehicle control. n=2 biological replicates, n=4 technical replicates. Error bars represent means ±SEM. **(B)** Comparison of the effect of AZD4573 on the palbociclib-sensitive MCF7 LTED^{Y537C} and HCC1428 LTED cell lines, and their respective palbociclib-resistant derivatives. Data represent percentage of viable cells compared with vehicle control. MCF7 lines: n=2 biological replicates, n=4 technical replicates. Error bars represent means ±SEM. Difference in dose-response curves tested by two-way ANOVA. **(C)** IC_{50} values for AZD4573 calculated from these experiments using 4-parameter non-linear regression.

6.5.5 3D cell proliferation assays

To examine whether the effect of being in a 3D structure affected the sensitivity of these cells to perturbations in the CDK7 and CDK9 pathways, cell proliferation assays were also performed in 3D using spheroid models. Given the broadly correlative findings of the 2D and 3D siRNA screens discussed in Section 5.2.5, these 3D experiments were only performed using drugs to target CDK7 and CDK9. Due to time and cost constraints, only one drug was used for each target, with ICEC0942 and AZD4573, respectively, being chosen as likely to have the most clinical relevance as they are in clinical trials. Furthermore, the 3D assays were performed in the lines modelling endocrine-resistance and endocrine- and palbociclib-resistance only, given it is these cancer contexts that are the subject of this thesis. These 3D assays are a better approximation of a tumour *in vivo* than the 3D screens performed previously, as the cells were first allowed to aggregate into a 3D spheroid structure for 3 days, before being exposed to the drug. Furthermore, these spheroids received two drug treatments (at day 3 and day 6) before assessment of cell viability at day 10.

Figure 6.11 illustrates the effect of ICEC0942 targeting CDK7 in the 3D models. The results largely mirror those seen in 2D, with greater sensitivity to ICEC0942 observed in the MCF7 cell lines than in the HCC1428 lines. Interestingly, while the dose-response assay for HCC1428 LTED^{PalboR} in 2D generated a fairly typical sigmoidal curve, the results from the 3D assay suggest this line is insensitive to ICEC0942. Furthermore, the comparison of IC_{50} values obtained from the 2D and 3D drug assays (Figure 6.11B) shows that in all cases, the 3D models were less sensitive than when in 2D culture, as has been observed in other studies (Koch et al., 2021). These results highlight the potential value of testing drugs in a variety of models, in particular given the difference seen in the response of HCC1428 LTED^{PalboR} in 2D and 3D, but these experiments do warrant repeating as only one biological replicate was performed.

A

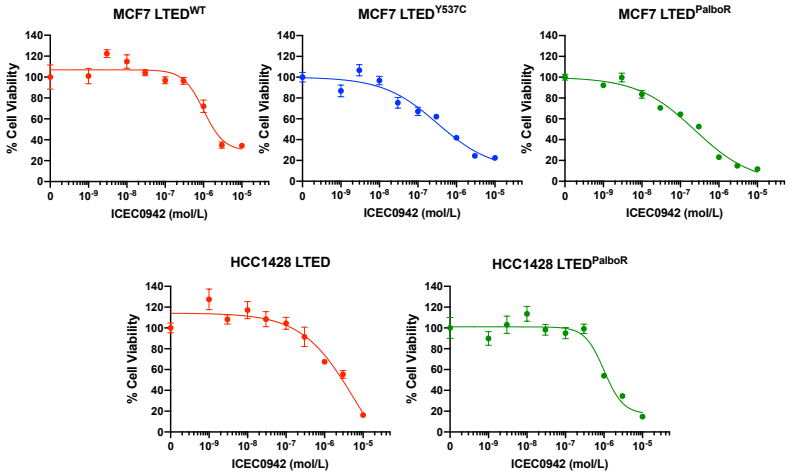

B

Cell Line	ICEC0942 3D IC^{50} (nM)	Cell Line	ICEC0942 IC^{50} 2D (nM)
MCF7 $LTED^{WT}$	1008±614	MCF7 $LTED^{WT}$	283±32
MCF7 $LTED^{Y537C}$	322±105	MCF7 $LTED^{Y537C}$	210±22
MCF7 $LTED^{PalboR}$	235±83	MCF7 $LTED^{PalboR}$	87±13
HCC1428 LTED	6457	HCC1428 LTED	>10000
HCC1428 $LTED^{PalboR}$	1004±412	HCC1428 $LTED^{PalboR}$	363±140

C

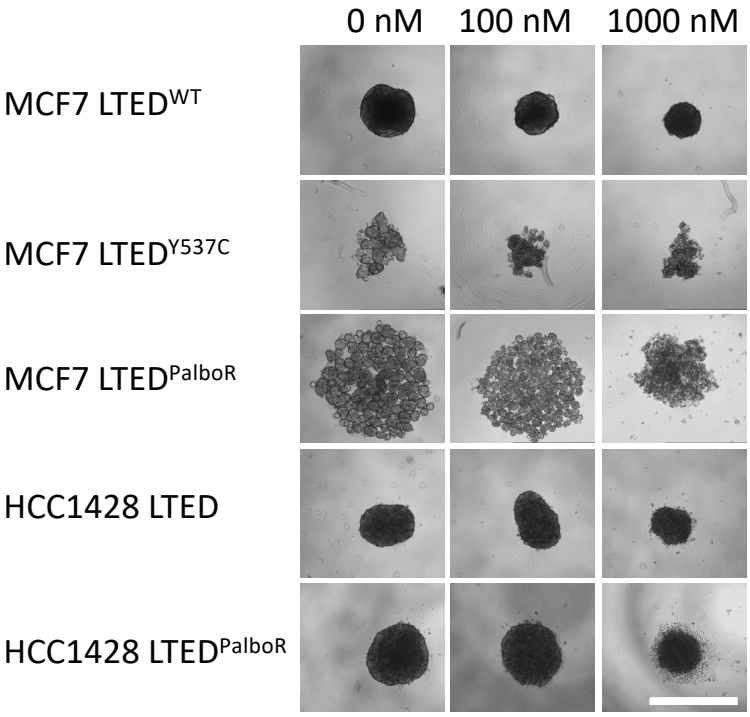

Figure 6.11 Effect of ICEC0942 on cell proliferation in 3D assays (A) 2500 cells were seeded in 96-well ultra-low attachment 3D culture plates, spheroids were formed as described in the methods. After 3 days, cells were treated with ICEC0942, with a second treatment at day 6. Cell viability was assessed using CellTiter-Glo on day 10 following spheroid formation. Dose-response graphs show effect of escalating concentrations of ICEC0942 on viability of breast cancer cell lines in 3D culture. Data represents percentage of viable cells compared with vehicle control. n = 1 biological replicate, and 4 technical replicates. Error bars represent SEM of 4 technical replicates **(B)** IC_{50} values ± variance for ICEC0942 calculated from these 3D experiments using 4-parameter non-linear regression, compared to the IC_{50} values from the 2D experiments (as shown in Figure 6.8) **(C)** Appearances of the spheroids at the end of the assay following treatment with 0 nM, 100 nM, or 1000 nM ICEC0942. Scale bars 1 mm.

A

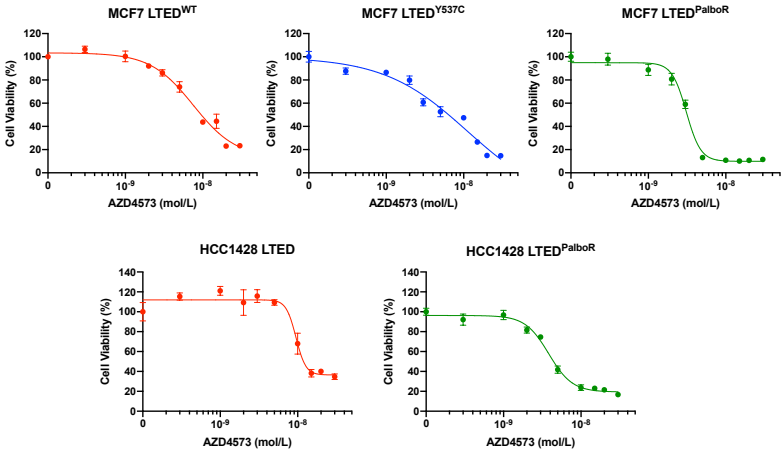

B

Cell Line	AZD4573 3D IC^{50} (nM)	Cell Line	AZD4573 IC^{50} 2D (nM)
MCF7 $LTED^{WT}$	7.6±4.2	MCF7 $LTED^{WT}$	7.0±0.7
MCF7 $LTED^{Y537C}$	11.1±5.8	MCF7 $LTED^{Y537C}$	6.1±1.5
MCF7 $LTED^{PalboR}$	3.1±0.3	MCF7 $LTED^{PalboR}$	2.9±0.2
HCC1428 LTED	9.5±2.0	HCC1428 LTED	11.3±1.3
HCC1428 $LTED^{PalboR}$	3.8±0.4	HCC1428 $LTED^{PalboR}$	6.8±0.4

C

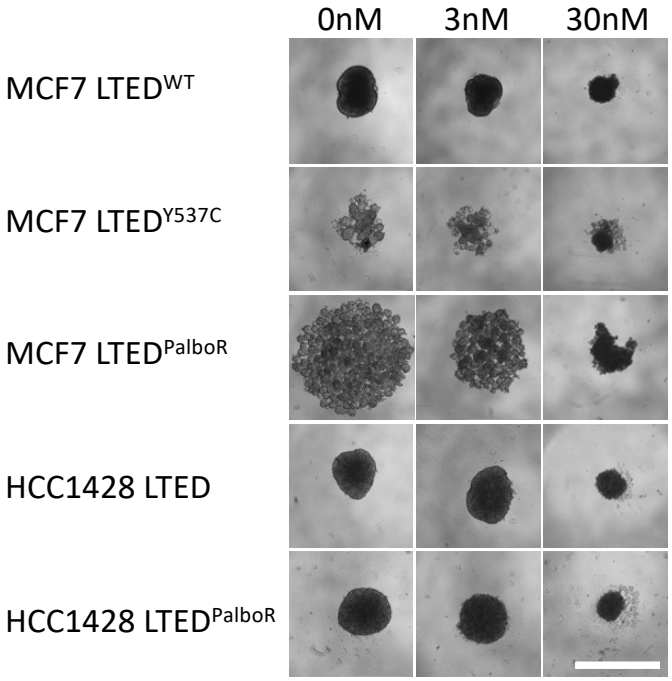

Figure 6.12 Effect of AZD4573 on cell proliferation in 3D assays (A) 2500 cells were seeded in 96-well ultra-low attachment 3D culture plates, and spheroids were formed as described in the methods. After 3 days, cells were treated with AZD4573, with a second treatment at day 6. Cell viability was assessed using CellTiter-Glo on day 10 following spheroid formation. Dose-response graphs show effect of escalating concentrations of AZD4573 on viability of breast cancer cell lines in 3D culture. Data represents percentage of viable cells compared with vehicle control. n = 1 biological replicate, and 4 technical replicates, error bars represent SEM of 4 technical replicates. **(B)** IC_{50} values for ICEC0942 calculated from these 3D experiments using 4-parameter non-linear regression, compared to the IC_{50} values from the 2D experiments (as shown in Figure 6.10). **(C)** Appearances of the spheroids at the end of the assay following treatment with 0 nM, 3 nM, or 30 nM ICEC0942. Scale bars 1 mm.

The outcome of treating the spheroid models with AZD4573 to target CDK9 is shown in Figure 6.12A. For this compound, the IC_{50} values obtained in 3D are similar to those in 2D (Figure 6.12B), and all of the cell lines were again found to be sensitive to AZD4573. In the MCF7 LTED^{PalboR} cells, the results are almost identical in 2D and in 3D, while in the HCC1428 LTED^{PalboR} cells, the 3D models are more sensitive to AZD4573 than the 2D models.

Figures 6.11D and 6.12D show the appearances of the different spheroid models at the end of treatment with the different doses of ICEC0942 and AZD4573. Unfortunately, these images are illustrative only, as it was not possible to create a mask that could accurately measure and track the growth of the spheroids on the Incucyte software. However, it is of note that with increasing doses of both drugs, a difference in the size of the spheroid can be observed in comparison with the control spheroids. Furthermore, central necrosis and disintegrating cellular debris can also be seen at the higher doses of ICEC0942 and AZD4573.

The results of the 2D and 3D drug assays suggest that these compounds developed to target CDK7 and CDK9 could be investigated further as potential new drugs to tackle endocrine-resistant and endocrine- and palbociclib-resistant disease. Furthermore, it is interesting to note that these drugs are able to inhibit proliferation in both an ER^{MUT} and an ER^{WT} setting. As discussed in Section 1.3.1, the presence of *ESR1* mutations predicts for shorter progression-free survival (Schiavon et al., 2015), shorter overall survival (Chandarlapaty et al., 2016), and studies have shown that the presence of activating *ESR1* mutations eliminates the endocrine therapy contribution of an AI in combination therapies (Fribbens et al., 2016). Similarly, ICEC0942 and AZD4573 have shown activity in both wild-type and mutant *PIK3CA* contexts (Section 4.2.4). Given that some of the most recent advances in treating resistant breast cancer are thus far limited to the *PIK3CA*-mutant setting (Rugo et al., 2021), it is important to find targets, such as CDK7 and CDK9, that demonstrate potential to be effective in multiple ER-positive breast cancer contexts.

6.5.6 Effect of combining target knockdown with palbociclib treatment

6.5.6.1 Combination studies in palbociclib-resistant cells

Further experiments were then designed to investigate whether CDK7 or CDK9 contributed to the mechanisms by which the palbociclib-resistant cells displayed resistance. The first way this was explored was by using siRNA to reduce the expression of the target CDKs in palbociclib-resistant cells, and then expose these cells to escalating doses of palbociclib. These experiments were performed using 2D culture.

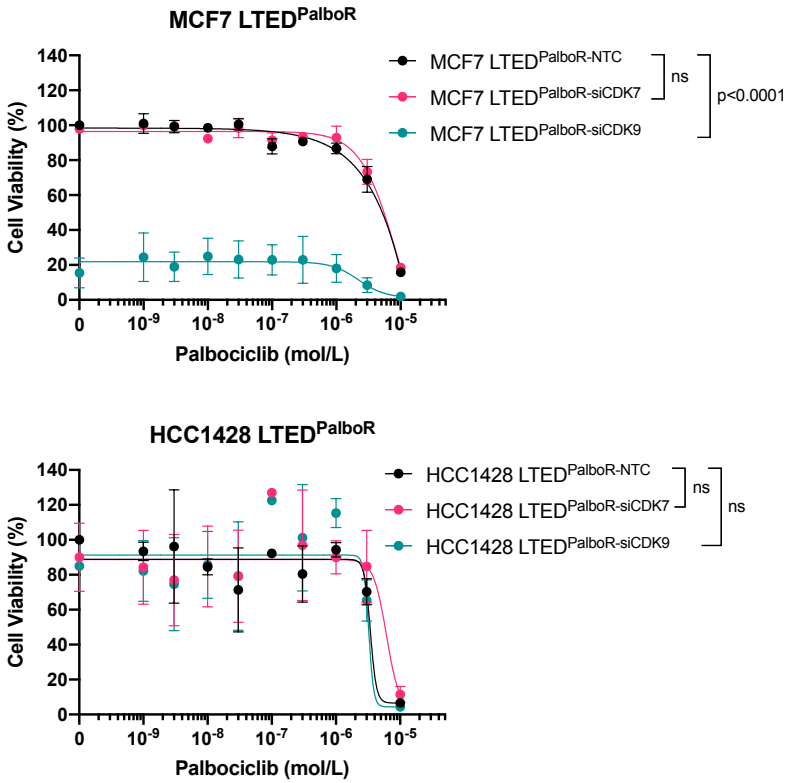

Figure 6.13 Effect of siRNA knockdown in combination with palbociclib on the viability of palbociclib-resistant cells. 5000 cells/well were reverse transfected with 25 nM siCDK7 or NTC, or 10 nM siCDK9 in 2D 96-well plates. The cells were treated with palbociclib after 24 hours, and again at 72 hours. Cell viability was assessed using CellTiter-Glo on day 7. Dose-response graphs showing effect of escalating concentrations of palbociclib on the viability of palbociclib-resistant breast cancer cell lines that had undergone knockdown of CDK7 and CDK9 using siRNAs. Data represents percentage of viable cells compared with vehicle control in the cells treated with NTC-siRNA. n = 2 biological replicates, and 3 technical replicates. Error bars represent means ±SEM. Difference in dose-response curves tested by two-way ANOVA, with *p*-value given for the difference in siRNA treatments

The results are shown in Figure 6.13, and do not suggest that CDK7 or CDK9 contribute to palbociclib-resistance, as knocking down either of these targets does not re-sensitise the cells to palbociclib. As seen previously in Section 6.5.1, knockdown of CDK7 does not affect the viability of either MCF7 LTED^{PalboR} of HCC1428 LTED^{PalboR} cell lines. Knockdown of CDK9 has a significant effect on the viability of the MCF7 LTED^{PalboR} cell line, but not on the HCC1428 LTED^{PalboR} cell lines. These siRNA knockdown studies would therefore suggest little role for combination therapy of palbociclib and agents targeting CDK7 and CDK9. However, this is in direct contrast to the results from combination drug studies, which were run concurrently.

In order to examine the effect of combining palbociclib with pharmaceutical agents targeting CDK7 and CDK9, the palbociclib-resistant lines were treated with either palbociclib and ICEC0942, or palbociclib and AZD4573, in escalating doses of both agents, initially in 2D culture. The cell viability was assessed using CellTiter-Glo, and the results inputted into SynergyFinder (Ianevski et al., 2020). This programme utilises the cell viability readouts to calculate the synergy score for the 2 agents based on the Bliss independence model (BLISS, 1939). This model compares the observed response to the combination of drugs with the predicted combination response, where the predicted response is based on the assumption that there is no effect of drug-drug interactions. While there are no absolute thresholds for the scores generated by this software (termed Bliss synergy score), scores of 0-10 are highly suggestive of an additive effect, while scores of >10 are indicative of a synergistic effect.

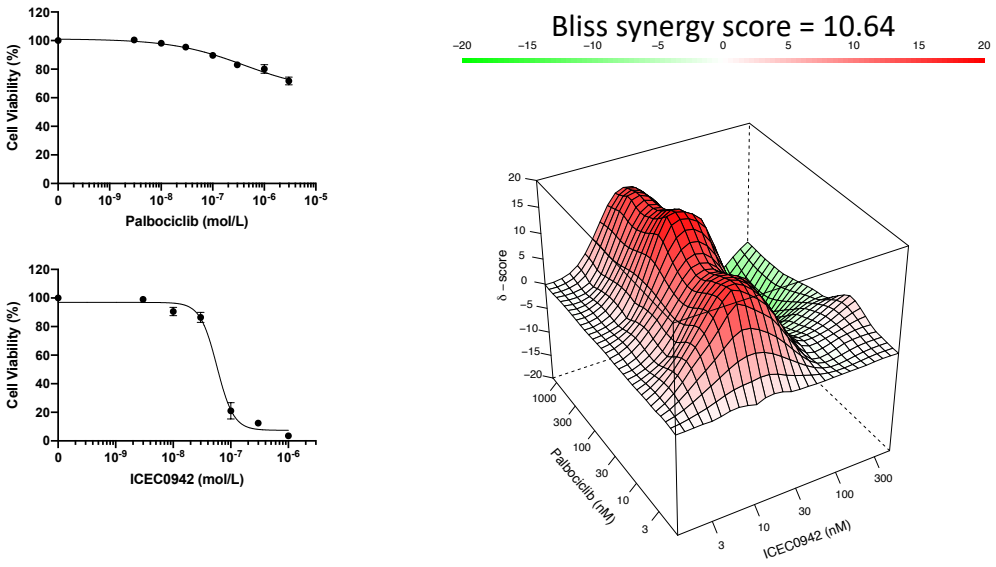

Figure 6.14 Synergy plot of MCF7 LTED^{PalboR} cells treated in 2D with ICEC0942 and palbociclib. 5000 cells/well of MCF7 LTED^{PalboR} were seeded in 2D 96-well plates. After 24 hours they were treated with escalating doses of palbociclib and ICEC0942, with a second treatment at 72 hours. Cell viability was assessed using CellTiter-Glo on day 7. The dose-response curves for the drugs individually are displayed on the left, with data representing percentage of viable cells compared with vehicle control. n=3 biological replicates, n=3 technical replicates. Error bars represent means ±SEM. The synergy plot on the right illustrates the synergy score from the combination of the two drugs, using the mean values of the 3 independent biological replicates. The Bliss synergy score references the most synergistic area of the plot.

Figures 6.14 and 6.15 show the effect of treating MCF7 LTED^{PalboR} cells, in 2D culture, with a combination of palbociclib and ICEC0942, and palbociclib and AZD4573, respectively. The data presented in Figure 6.14 suggest that ICEC0942 is able to synergise with palbociclib at doses below its IC_{50} value, with greatest synergism seen between 10-30 nM of ICEC0942 and 50-150 nM of palbociclib. A greater level of synergism is seen between palbociclib and AZD4573 (Figure 6.15), with a synergy score of nearly 20. The greatest synergism is seen at the IC_{50} value of AZD4573 (approx. 3 nM) and between 300-3000 nM palbociclib. The mean plasma concentration of palbociclib at steady-state is 116 ng/mL (259 nM) (FDA, 2014) and so it can be seen that synergism may be achieved at or near *in vivo* concentrations of palbociclib for the MCF7 LTED^{PalboR} cells.

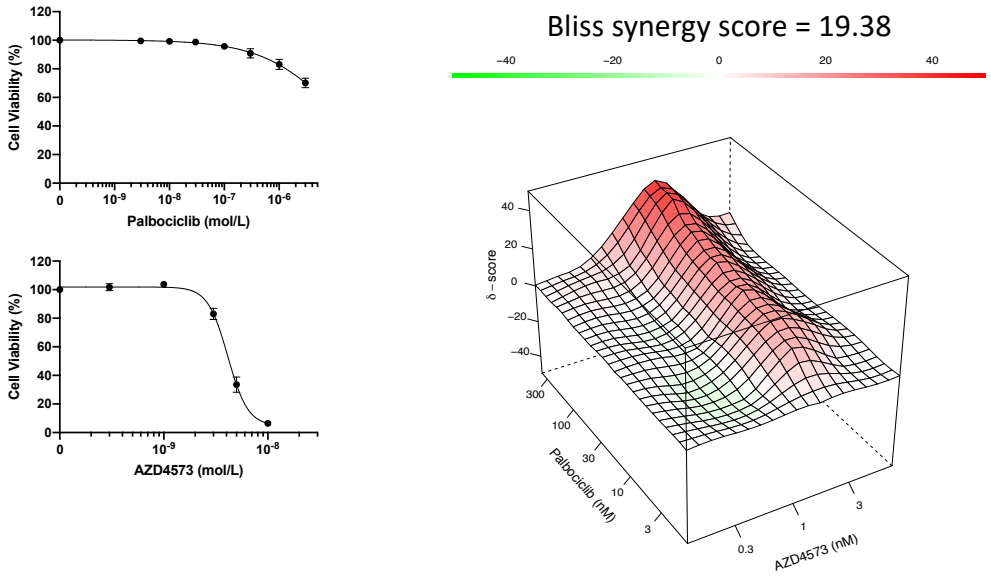

Figure 6.15 Synergy plot of MCF7 LTED^{PalboR} cells treated in 2D with AZD4573 and palbociclib. 5000 cells/well of MCF7 LTED^{PalboR} were seeded in 2D 96-well plates. After 24 hours they were treated with escalating doses of palbociclib and AZD4573, with a second treatment at 72 hours. Cell viability was assessed using CellTiter-Glo on day 7. The dose-response curves for the drugs individually are displayed on the left, with data representing percentage of viable cells compared with vehicle control. n=3 biological replicates, n=3 technical replicates. Error bars represent means ±SEM The synergy plot on the right illustrates the synergy score from the combination of the two drugs, using the mean values of the 3 independent biological replicates. The Bliss synergy score references the most synergistic area of the plot.

The results are quite different in the HCC1428 LTED^{PalboR} cells, with no true evidence of synergy observed (Figures 6.16 and 6.17). Given that the IC_{50} for ICEC0942 in the HCC1428 LTED^{PalboR} cells is higher than that observed in the MCF7 LTED^{PalboR} line, this is perhaps to be expected for the combination of ICEC0942 and palbociclib. It is worth noting that in the combination drug studies, the dose-response curve to AZD4573 alone is quite different to those in the single drug experiments (Figure 6.10A). This may be because, for logistical reasons, the combination studies were performed before the single drug experiments in the HCC1428 LTED^{PalboR} line. Therefore, it is possible that the cells had not quite reached their exponential phase of proliferation at the time the combination studies were performed, accounting for the apparent lack of sensitivity in these assays, which could account for the lack of synergism seen. Ideally, the combination treatments of AZD4573 and palbociclib would have been repeated with fresh HCC1428 LTED^{PalboR} cells in their exponential phase of growth, but this was not possible due to time constraints.

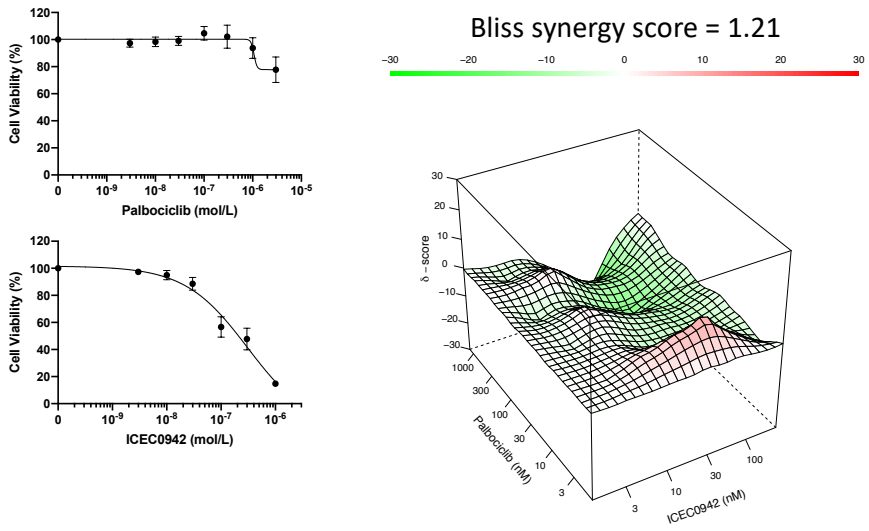

Figure 6.16 Synergy plot of HCC1428 LTED^{PalboR} cells treated in 2D with ICEC0942 and palbociclib. 5000 cells/well of HCC1428 LTED^{PalboR} were seeded in 2D 96-well plates. After 24 hours they were treated with escalating doses of palbociclib and ICEC0942, with a second treatment at 72 hours. Cell viability was assessed using CellTiter-Glo on day 7. The dose-response curves for the drugs individually are displayed on the left, with data representing percentage of viable cells compared with vehicle control. n=2 biological replicates, n=3 technical replicates. Error bars represent means ±SEM. The synergy plot on the right illustrates the synergy score from the combination of the two drugs, using the mean values of the 2 independent biological replicates. The Bliss synergy score references the most synergistic area of the plot.

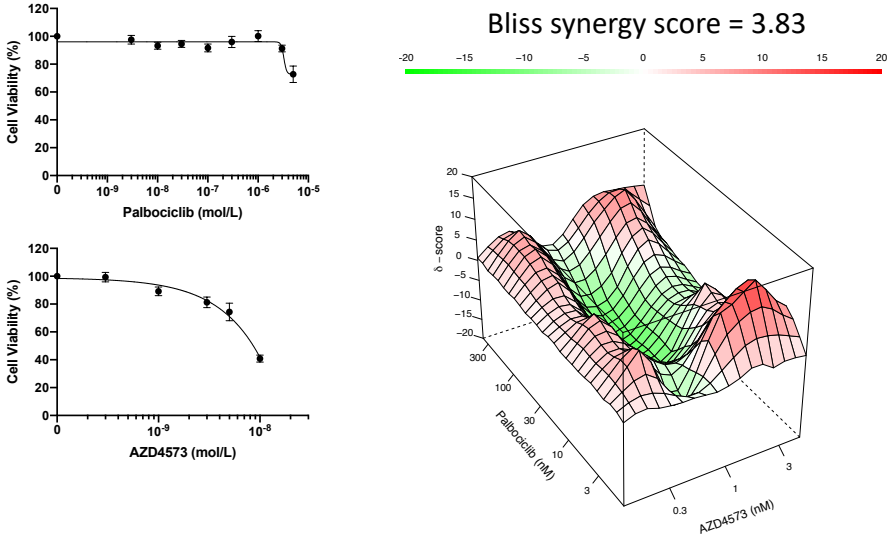

Figure 6.17 Synergy plot of HCC1428 LTED^{PalboR} cells treated in 2D with AZD4573 and palbociclib. 5000 cells/well of HCC1428 LTED^{PalboR} were seeded in 2D 96-well plates. After 24 hours they were treated with escalating doses of palbociclib and AZD4573, with a second treatment at 72 hours. Cell viability was assessed using CellTiter-Glo on day 7. The dose-response curves for the drugs individually are displayed on the left, with data representing percentage of viable cells compared with vehicle control. n=2 biological replicates, n=3 technical replicates. Error bars represent means ±SEM. The synergy plot

on the right illustrates the synergy score from the combination of the two drugs, using the mean values of the 2 independent biological replicates. The Bliss synergy score references the most synergistic area of the plot.

The combination drug studies suggest synergism could be achieved to treat some palbociclib-resistant disease by using drugs that have been designed to target CDK7 and CDK9. This is at odds with the findings of the siRNA-treated cells exposed to palbociclib. One explanation for this is that the outcomes of the drug assays are mediated through off-target effects of the drugs, and not through inhibiting CDK7 or CDK9. However, the compounds chosen for these assays were selected for their high specificity to CDK7 and CDK9. Another possibility is that the level of knockdown achieved by siRNA transfection is insufficient to accomplish synergism with palbociclib, as the Western blots in Figures 6.3B and 6.5B do show some residual CDK7 and CDK9 expression. Finally, the lack of synergism seen with siRNA treatment could be because siRNAs are relatively short-lived. Similarly, palbociclib does not act immediately, and requires longer experiments to demonstrate its full effect. This is seen in the Wellcome Sanger Institute's genomics of drug sensitivity in cancer database (Yang et al., 2013). Their screening assays are run for 72 hours, with one palbociclib treatment, and calculated an IC_{50} of 43 μM for MCF7 cells. An improved assay would be to transfect shRNAs into palbociclib-resistant cells to achieve a more sustained knockdown of CDK7 and CDK9, allowing for a longer time course to assess the effect of palbociclib.

To explore whether this synergism could be related to the mechanisms by which the palbociclib-resistant cells developed palbociclib resistance, the combination drug studies were carried out in the cell lines modelling endocrine-resistant, palbociclib-sensitive disease.

6.5.6.2 Combination studies in palbociclib-sensitive cells

Combination drug assays using ICEC0942/palbociclib, or AZD4573/palbociclib were performed in the MCF7 LTED^{WT}, MCF7 LTED^{Y537C}, HCC1428 LTED cell lines in 2D, with the results shown in Figures 6.18 to Figures 6.23. In the MCF7 lines treated with ICEC0942 and palbociclib, there is evidence of an additive, but not synergistic effect. By

comparison, in the HCC1428 LTED cells there is no strong evidence of an additive or synergistic effect.

Contrastingly, for the AZD4573/palbociclib combination in the palbociclib-sensitive MCF7 lines, the synergy scores greater than ten are suggestive of a synergistic effect, albeit weaker than that seen in the MCF7 LTED^{PalboR} cells, which could indicate a palbociclib-resistance mechanism reliant on CDK9. There is no clear evidence of synergism or additivity in the HCC1428 LTED line using the AZD4573/palbociclib combination.

Interestingly, the areas of highest additivity for both ICEC0942 and AZD4573 occur at subtherapeutic concentrations of palbociclib (between 30-100 nM) Furthermore, the greatest additivity in the ICEC0942/palbociclib combination occurs at a 30 nM ICEC0942, which is below the IC_{50} value for ICEC0942 in both MCF7 LTED^{WT} and MCF7 LTED^{Y537C} lines. Although conclusions that can be drawn from these assays are limited as only one biological replicate could be performed, this suggests that effective inhibition of cancer growth could occur at low doses of both agents, which is one of the key aims of combination therapy, as this can result in fewer treatment side-effects.

The results of the combination drug assays in the palbociclib-sensitive cells indicate that there could be a role for combination therapy of agents targeting CDK7 or CDK9 with CDK4/6 inhibitors in certain cancer contexts. The difference in synergy scores between the MCF7 LTED^{Y537C} and MCF7 LTED^{PalboR} lines suggests CDK9 may play a role in the palbociclib-resistance pathways.

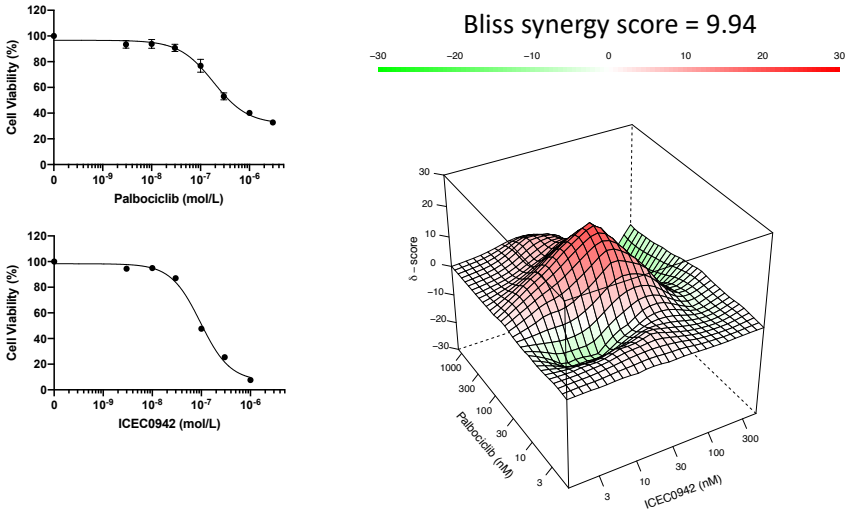

Figure 6.18 Synergy plot of MCF7 LTED^{WT} cells treated in 2D with ICEC0942 and palbociclib. 3000 cells/well of MCF7 LTED^{WT} were seeded in 2D 96-well plates. After 24 hours they were treated with escalating doses of palbociclib and ICEC0942, with a second treatment at 72 hours. Cell viability was assessed using CellTiter-Glo on day 7. The dose-response curves for the drugs individually are displayed on the left, with data representing percentage of viable cells compared with vehicle control. n=1 biological replicate, n=3 technical replicates. Error bars represent SEM of 3 technical replicates. The synergy plot on the right illustrates the synergy score from the combination of the two drugs. The Bliss synergy score references the most synergistic area of the plot.

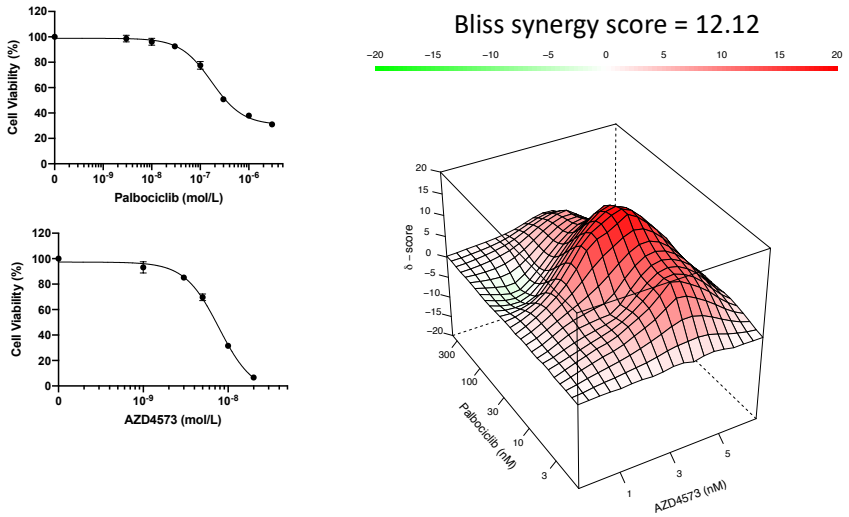

Figure 6.19 Synergy plot of MCF7 LTED^{WT} cells treated in 2D with AZD4573 and palbociclib. 3000 cells/well of MCF7 LTED^{WT} were seeded in 2D 96-well plates. After 24 hours they were treated with escalating doses of palbociclib and AZD4573, with a second treatment at 72 hours. Cell viability was assessed using CellTiter-Glo on day 7. The dose-response curves for the drugs individually are displayed on the left, with data representing percentage of viable cells compared with vehicle control. n=1 biological replicate, n=3 technical replicates. Error bars represent SEM of 3 technical replicates. The synergy plot on the right illustrates the synergy score from the combination of the two drugs. The Bliss synergy score references the most synergistic area of the plot.

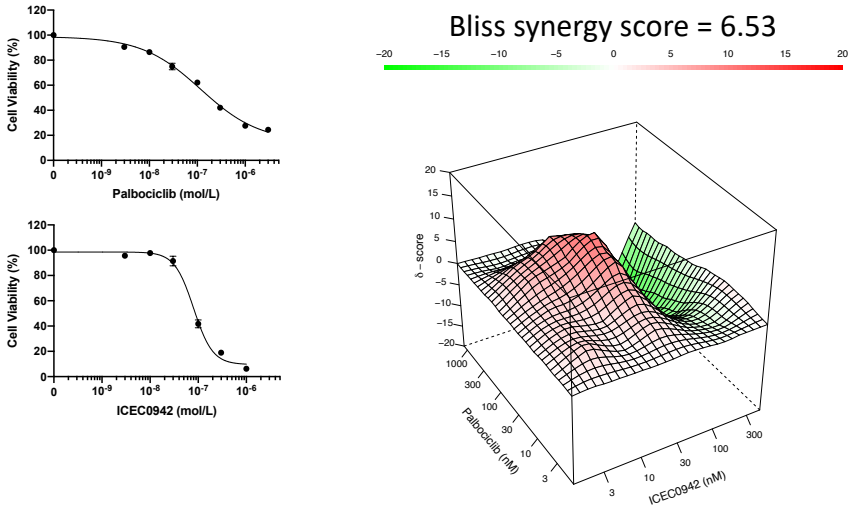

Figure 6.20 Synergy plot of MCF7 LTED^{Y537C} cells treated in 2D with ICEC0942 and palbociclib. 3000 cells/well of MCF7 LTED^{Y537C} were seeded in 2D 96-well plates. After 24 hours they were treated with escalating doses of palbociclib and ICEC0942, with a second treatment at 72 hours. Cell viability was assessed using CellTiter-Glo on day 7. The dose-response curves for the drugs individually are displayed on the left, with data representing percentage of viable cells compared with vehicle control. n=1 biological replicate, n=3 technical replicates. Error bars represent SEM of 3 technical replicates. The synergy plot on the right illustrates the synergy score from the combination of the two drugs. The Bliss synergy score references the most synergistic area of the plot.

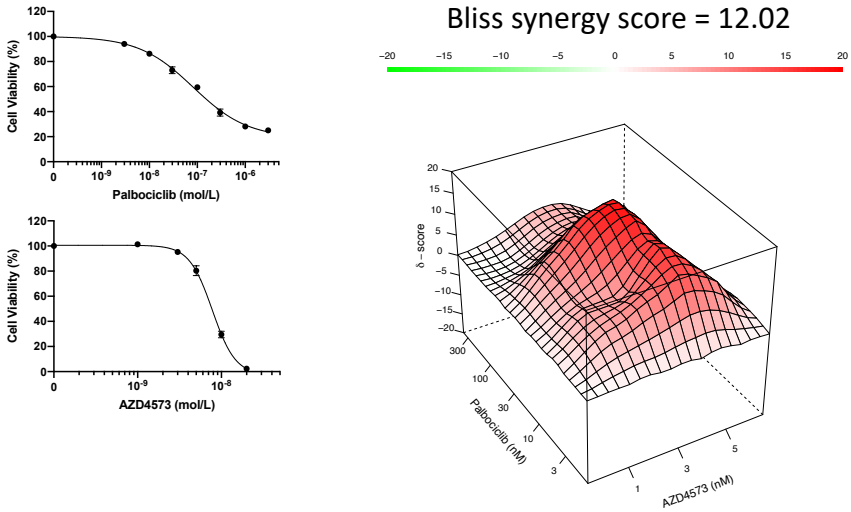

Figure 6.21 Synergy plot of MCF7 LTED^{Y537C} cells treated in 2D with AZD4573 and palbociclib. 3000 cells/well of MCF7 LTED^{Y537C} were seeded in 2D 96-well plates. After 24 hours they were treated with escalating doses of palbociclib and AZD4573, with a second treatment at 72 hours. Cell viability was assessed using CellTiter-Glo on day 7. The dose-response curves for the drugs individually are displayed on the left, with data representing percentage of viable cells compared with vehicle control. n=1 biological replicate, n=3 technical replicates. Error bars represent SEM of 3 technical replicates. The synergy plot on the right illustrates the synergy score from the combination of the two drugs. The Bliss synergy score references the most synergistic area of the plot

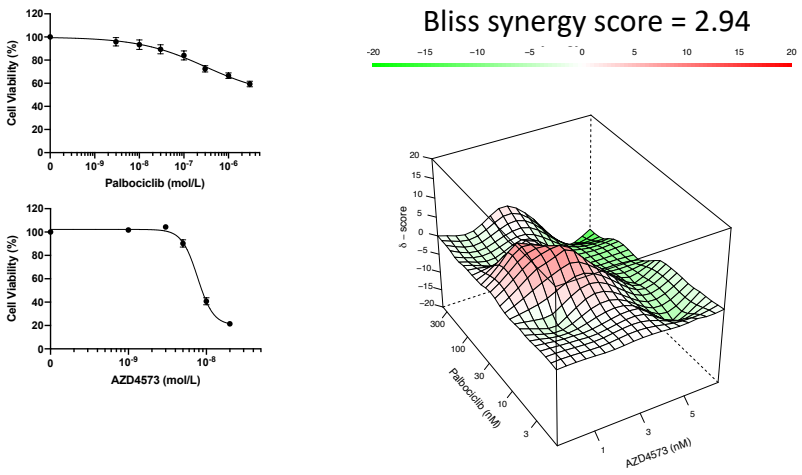

Figure 6.22 Synergy plot of HCC1428 LTED cells treated in 2D with ICEC0942 and palbociclib. 5000 cells/well of HCC1428 LTED were seeded in 2D 96-well plates. After 24 hours they were treated with escalating doses of palbociclib and ICEC0942, with a second treatment at 72 hours. Cell viability was assessed using CellTiter-Glo on day 7. The dose-response curves for the drugs individually are displayed on the left, with data representing percentage of viable cells compared with vehicle control. n=1 biological replicate, n=3 technical replicates. Error bars represent SEM of 3 technical replicates. The synergy plot on the right illustrates the synergy score from the combination of the two drugs. The Bliss synergy score references the most synergistic area of the plot.

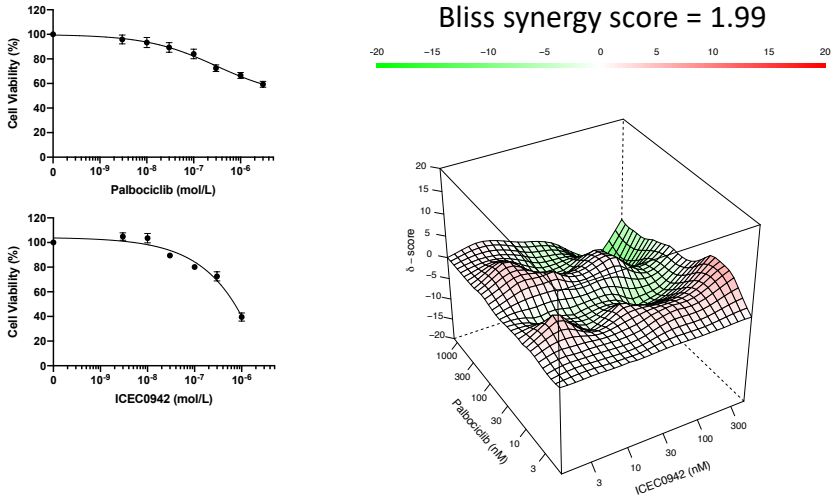

Figure 6.23 Synergy plot of HCC1428 LTED cells treated in 2D with AZD4573 and palbociclib. 5000 cells/well of HCC1428 LTED were seeded in 2D 96-well plates. After 24 hours they were treated with escalating doses of palbociclib and AZD4573, with a second treatment at 72 hours. Cell viability was assessed using CellTiter-Glo on day 7. The dose-response curves for the drugs individually are displayed on the left, with data representing percentage of viable cells compared with vehicle control. n=1 biological replicate, n=3 technical replicates. Error bars represent SEM of 3 technical replicates. The synergy plot on the right illustrates the synergy score from the combination of the two drugs. The Bliss synergy score references the most synergistic area of the plot

6.5.6.3 Combination studies in MCF10A cells

Given that combination therapies do have the potential for toxic side-effects, and in particular given the cytotoxic activity observed in AZD4573 at very low doses, combination assays in the non-tumorigenic mammary epithelial line MCF10A were carried out. The ICEC0942/palbociclib combination results are shown in Figure 6.24, and the AZD4573/palbociclib results in Figure 6.25. These results show high synergy scores for both drugs, and in the case of ICEC0942/palbociclib, greater evidence of synergy than in the MCF7 LTED^{PalboR} cell lines. This suggests that there may be too narrow a toxicity window to make this drug combination a viable option. However, it should be noted that the synergism in the MCF10A cells occurs at higher doses of both ICEC0942 and AZD4573 (30 nM and 7.5 nM, respectively) than in the MCF7 LTED^{PalboR} lines. Therefore, it is possible that with careful dosing of both of these agents, activity against cancer cell proliferation could be achieved without significant effects on normal tissue.

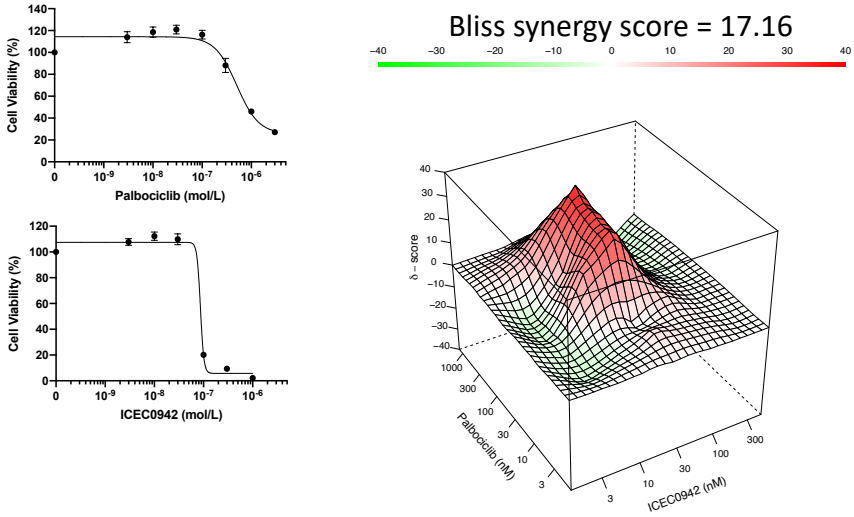

Figure 6.24 Synergy plot of MCF10A cells treated in 2D with ICEC0942 and palbociclib. 800 cells/well of MCF10A were seeded in 2D 96-well plates. After 24 hours they were treated with escalating doses of palbociclib and ICEC0942, with a second treatment at 72 hours. Cell viability was assessed using CellTiter-Glo on day 7. The dose-response curves for the drugs individually are displayed on the left, with data representing percentage of viable cells compared with vehicle control. n=1 biological replicate, n=3 technical replicates. Error bars represent SEM of 3 technical replicates. The synergy plot on the right illustrates the synergy score from the combination of the two drugs. The Bliss synergy score references the most synergistic area of the plot.

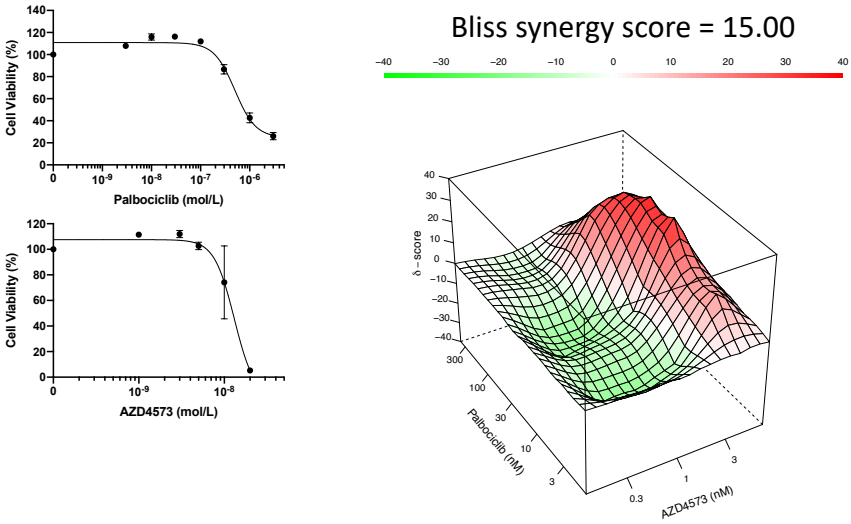

Figure 6.25 Synergy plot of MCF10A cells treated in 2D with AZD4573 and palbociclib. 800 cells/well of MCF10A were seeded in 2D 96-well plates. After 24 hours they were treated with escalating doses of palbociclib and AZD4573, with a second treatment at 72 hours. Cell viability was assessed using CellTiter-Glo on day 7. The dose-response curves for the drugs individually are displayed on the left, with data representing percentage of viable cells compared with vehicle control. n=1 biological replicate, n=3 technical replicates. Error bars represent SEM of 3 technical replicates. The synergy plot on the right illustrates the synergy score from the combination of the two drugs. The Bliss synergy score references the most synergistic area of the plot.

6.5.6.4 Combination studies in 3D

Finally, the combination drug assays were performed in the 3D spheroid models of MCF7 LTED^{PalboR} cells to examine whether the findings of synergism could be replicated in this context. Given the lack of synergism seen in the HCC1428 LTED^{PalboR} cells in 2D culture, and the time and cost constraints, the experiment were not repeated in this cell line in 3D. The results from the MCF7 LTED^{PalboR} 3D combination assays are shown in Figures 6.26 and 6.27.

The synergy plots show that for the ICEC0942/palbociclib combination, there is an additive effect seen, and this is observed at lower doses than the IC_{50} values for the individual drugs (30-100 nM for palbociclib, and 10-30 nM ICEC0942), suggesting that while synergism may not be achievable, an additive effect could be obtained at doses that carry a lower risk of side effects from these therapies.

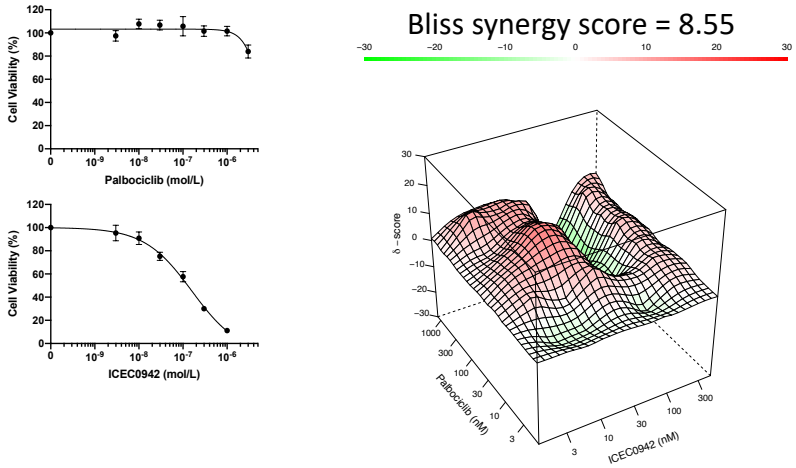

Figure 6.26 Synergy plot of MCF7 LTED^{PalboR} cells treated in 3D with ICEC0942 and palbociclib. 2500 cells/well were seeded in 96-well ultra-low attachment 3D culture plates, spheroids were formed as described in the methods. After 3 days, cells were treated with escalating doses of palbociclib and ICEC0942, with a second treatment at day 6. Cell viability was assessed using CellTiter-Glo on day 10 following spheroid formation. The dose-response curves for the drugs individually are displayed on the left, with data representing percentage of viable cells compared with vehicle control. n=1 biological replicate, n=3 technical replicates. Error bars represent SEM of 3 technical replicates. The synergy plot on the right illustrates the synergy score from the combination of the two drugs. The Bliss synergy score references the most synergistic area of the plot.

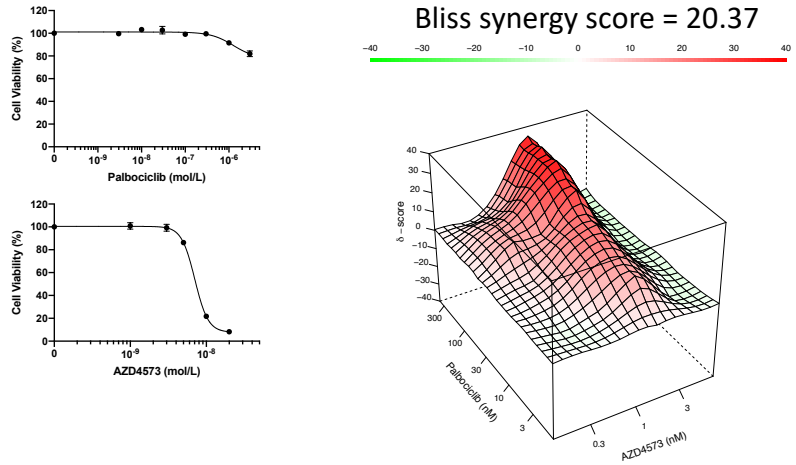

Figure 6.27 Synergy plot of MCF7 LTED^{PalboR} cells treated in 3D with AZD4573 and palbociclib. 2500 cells/well were seeded in 96-well ultra-low attachment 3D culture plates, spheroids were formed as described in the methods. After 3 days, cells were treated with escalating doses of palbociclib and AZD4573, with a second treatment at day 6. Cell viability was assessed using CellTiter-Glo on day 10 following spheroid formation. The dose-response curves for the drugs individually are displayed on the left, with data representing percentage of viable cells compared with vehicle control. n=1 biological replicate, n=3 technical replicates. Error bars represent SEM of 3 technical replicates. The synergy plot on the right illustrates the synergy score from the combination of the two drugs. The Bliss synergy score references the most synergistic area of the plot.

Figure 6.27 demonstrates that synergism is seen in the AZD4573/palbociclib combination, as it was in the 2D combination drug studies, with a higher synergy score obtained. Peak synergy is observed at palbociclib doses >100 nM, and AZD4573 doses of 3 nM. This lends further evidence to the theory that combination therapy of AZD4573, targeting CDK9, and palbociclib targeting CDK4/6, could be a viable option in palbociclib-resistant disease.

6.5.6.5 Conclusions of combination drug studies

The aim of the combination studies was to examine whether CDK7 and/or CDK9 contributed to the palbociclib-resistance mechanisms displayed in the cells modelling this treatment context. If this were the case, it would be expected that transfection with siRNAs targeting CDK7 or CDK9 would re-sensitise the palbociclib-resistant cells to palbociclib treatment. This was not observed, with possible explanations for this outlined in Section 6.5.6.1.

The combination drug studies in the HCC1428 LTED^{PalboR} line indicate that neither CDK7 nor CDK9 play a significant role in the development of palbociclib-resistance in this cell line, as little additivity or synergy was observed. The results of the single drug and combination studies also suggest that CDK7 may not play a significant role in cell survival in this line, given that it is fairly insensitive to ICEC0942. This would be surprising given its myriad of cellular functions. It is noted that HCC1428 LTED^{PalboR} is sensitive to THZ1, but this could be attributed to off-target effects of THZ1. It would be intriguing to repeat these assays with another specific CDK7 inhibitor in this cell line. HCC1428 LTED^{PalboR} is sensitive to CDK9 inhibition by AZD4573, but there does not appear to be additional benefit conferred by combination therapy.

The results of the combination treatments in the MCF7 LTED^{PalboR} line imply that there could be a role for combining CDK4/6 inhibitors with targeted therapy against CDK7 or CDK9, and that synergy could be achieved with doses lower than the IC_{50} values observed for the drugs individually. Furthermore, when considering the AZD4573/palbociclib combination, the higher synergy scores obtained in the MCF7

LTED^{PalboR} line when compared to the palbociclib-sensitive line it was derived from suggest that CDK9 could play a key role in the development of palbociclib resistance.

Overall, it should be noted that these combination assays are not truly reflective of the clinical scenario facing patients with advanced ER-positive breast cancer. They are not usually treated with CDK4/6 inhibitors alone (although abemaciclib has been licensed in the US for use as monotherapy based on the results of the MONARCH1 trial (Dickler et al., 2017)) but with CDK4/6 inhibitors in combination with an AI or a SERD. Furthermore, the findings of the combination studies in the "normal" breast epithelial line imply the presence of a narrow therapeutic window before toxicity may occur. These factors are currently being addressed in animal studies. The effect of AZD4573 monotherapy, and in combination with fulvestrant and palbociclib, will be evaluated in PDX models of palbociclib-resistant ER-positive breast cancer, through a collaboration with Dr Elisabetta Marangoni at the Institut Curie, with the aim of comparing the responses to standard treatment of fulvestrant and palbociclib.

6.5.7 Exploring the mechanism of action of ICEC0942 and AZD4573 in models of resistant breast cancer

The actions of the CDK7 inhibitor ICEC0942 and the CDK9 inhibitor AZD4573 have been characterised in MCF7 lines and MV-4-11 lines (Patel et al., 2018, Cidado et al., 2020), but not in resistant models of ER-positive breast cancer. Consequently, experiments were designed to examine the effects of these drugs on the same targets in the endocrine- and palbociclib-resistant cell lines. In addition, given the synergy observed with palbociclib treatment in both palbociclib-sensitive and palbociclib-resistant models, the effects of these drugs on some of the known mechanisms of palbociclib-resistance were evaluated. These two lines of enquiry were explored through Western blotting for endpoint proteins, and while experiments remain ongoing, some results are shown here.

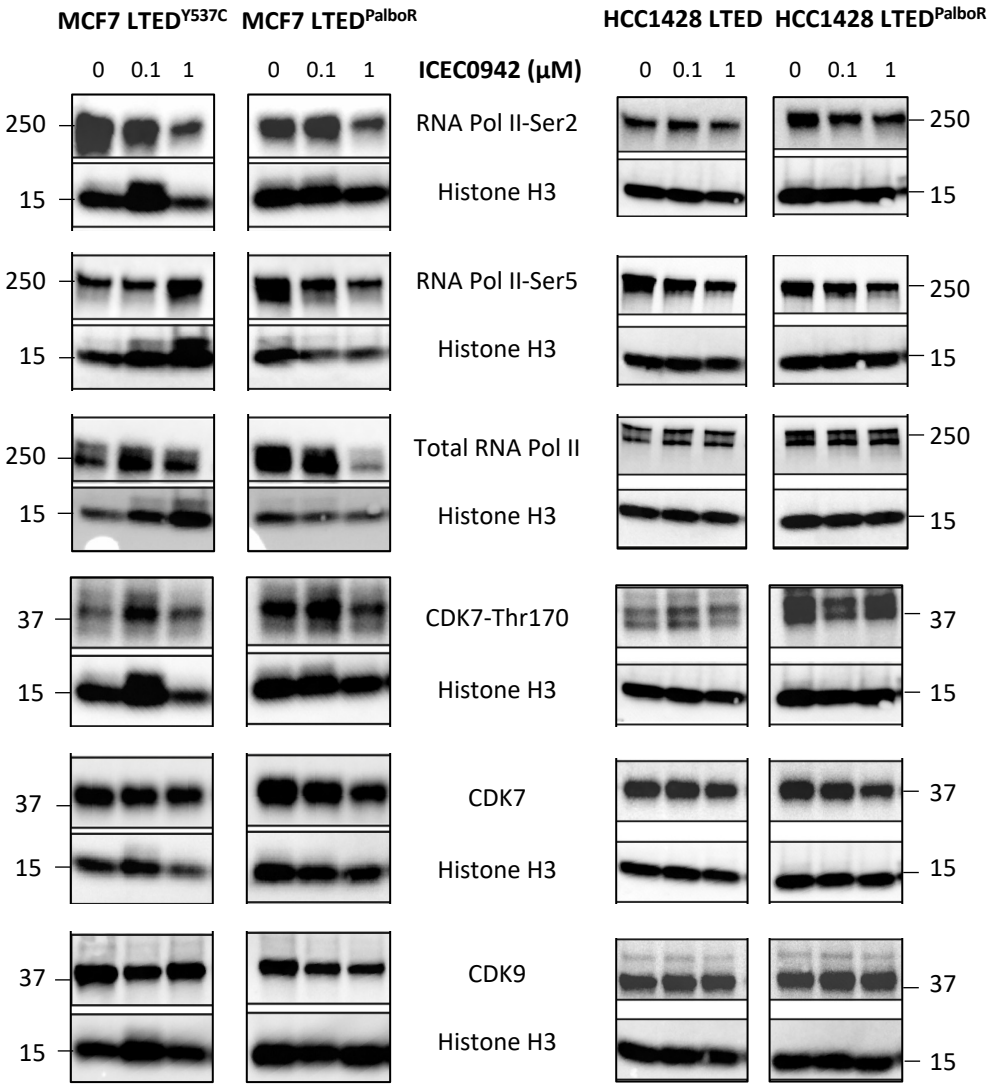

Figure 6.28. Western blots examining mechanism of action of ICEC0942 in palbociclib-sensitive and palbociclib-resistant models. 2-5 x 10^6 cells of the cell lines shown were seeded in 10 cm plates. After 24 hours, media was aspirated, and cells were treated with ICEC0942 at the concentrations shown. After 24 hours of exposure to ICEC0942, the cells were harvested and lysed, and Western blots were performed. The MCF7 LTED^{Y537C} line and its palbociclib-resistant derivative were run on the same gel, as were the HCC1428 LTED and its derivative. Histone H3 loading controls from each gel are shown below each blot. Positions of the protein ladder are indicated in kDa. Molecular weights: RNA Pol II: 250 kDa; CDK7: 40 kDa; CDK9: 42 kDa; Histone H3: 15 kDa.

6.5.7.1 Mechanism of action of ICEC0942

As a CDK7 inhibitor, ICEC0942 has been shown to inhibit the phosphorylation of RNA Pol II at serine-5 in a dose-dependent manner (Patel et al., 2018), without any effect on cellular levels of CDK7, phosphorylated CDK7, or total RNA Pol II. Therefore, Western blots were designed to probe for RNA Pol II phosphorylated at serine-5, total RNA Pol II, CDK7, and CDK7 phosphorylated at threonine-170. RNA Pol II phosphorylation at serine-

2 was also probed for, to assess the selectivity of ICEC0942 for CDK7 over CDK9. These assays were performed in the endocrine-resistant palbociclib-sensitive cell lines, and their palbociclib-resistant derivatives (MCF7 LTED^{Y537C}, MCF7 LTED^{PalboR}, HCC1428 LTED, and HCC1428 LTED^{PalboR}). The cells were treated with escalating doses of ICEC0942 (0 nM, 100 nM, 1000 nM, and 10000 nM) for 24 hours, prior to cell lysis and protein extraction (Figure 6.28). Treatment at 10000 nM ICEC0942 resulted in significant cell death and subsequent difficulties with protein quantification and loading, and so results for this highest dose are not shown.

In the MCF7 LTED^{PalboR} cells, treatment with ICEC0942 shows a reduction in total RNA Pol II, and therefore the effect of ICEC0942 on phosphorylation of RNA Pol II is difficult to interpret, but a reduction of phosphorylation of RNA Pol II at both serine-2 and serine-5 was observed. In the MCF7 LTED^{Y537C} cells, ICEC0942 did not affect the levels of total RNA Pol II, and interestingly, an increase in serine-5 phosphorylation, and a decrease in serine-2 phosphorylation was observed.

In both HCC1428 LTED cell lines, total RNA Pol II and serine-2 phosphorylated RNA Pol II levels were not affected by ICEC0942 treatment. A reduction in serine-5 phosphorylation was observed, which is in-keeping with previous studies of ICEC0942 (Patel et al., 2018).

Levels of CDK7, phosphorylated CDK7, and CDK9 were unaffected by ICEC0942 treatment in all four cell lines. In all Western blotting assays, the palbociclib-sensitive and palbociclib-resistant cell lysates were run on the same gel and exposed for the same length of time. Comparing the levels of CDK7 between palbociclib-sensitive and palbociclib-resistant cell lines in the untreated lanes, there is a higher level of total CDK7 in the palbociclib-resistant cell lines, which is concordant with previous RTqPCR findings (Pancholi et al., 2020), and higher levels of phosphorylated CDK7, suggesting this may be an adaptation conferring palbociclib-resistance.

6.5.7.2 Mechanism of action of AZD4573

AZD4573 is able to inhibit the phosphorylation of RNA Pol II at serine-2 in a dose-dependent manner (Cidado et al., 2020). Therefore, Western blots were run to probe

for RNA Pol II phosphorylated at serine-2, and at serine-5 (to assess for specificity of CDK9 inhibition), as well as total RNA Pol II and CDK9 levels. The cells were treated with escalating doses of AZD4573 (0 nM, 3 nM, 10 nM, and 20 nM) for 24 hours, prior to cell lysis and protein extraction (Figure 6.29). Treatment with 20 nM AZD4573 resulted in the same problems as the highest dose of ICEC0942, and so these results are not shown.

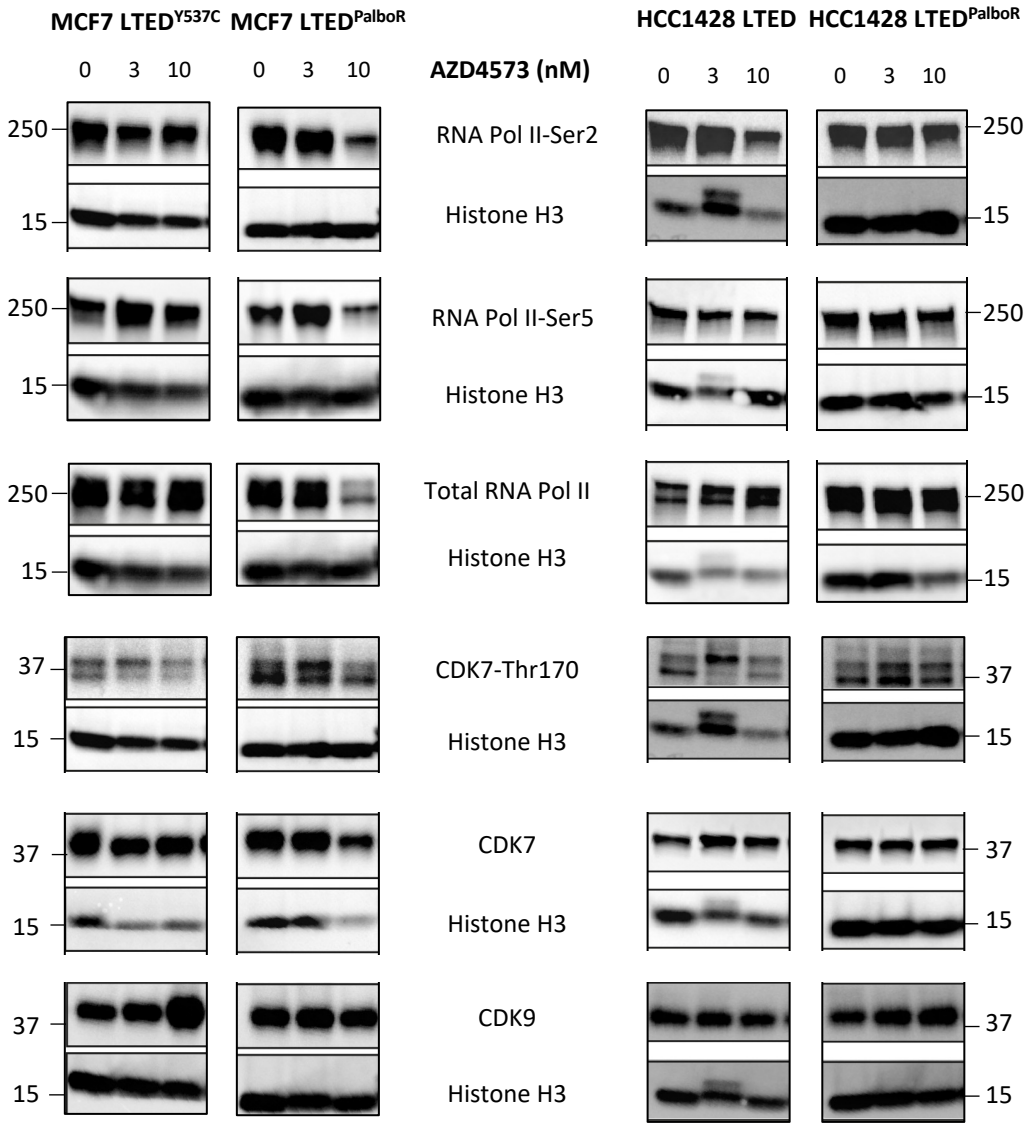

Figure 6.29. Western blots examining mechanism of action of AZD4573 in palbociclib-sensitive and palbociclib-resistant models. 2-5 x 10^6 cells of the cell lines shown were seeded in 10 cm plates. After 24 hours, media was aspirated, and cells were treated with AZD4573 at the concentrations shown. After 24 hours of exposure to AZD4573, the cells were harvested and lysed, and Western blots were performed. The MCF7 LTED^{Y537C} line and its palbociclib-resistant derivative were run on the same gel, as were the HCC1428 LTED and its derivative. Histone H3 loading controls from each gel are shown below each blot. Positions of the protein ladder are indicated in kDa. Molecular weights: RNA Pol II: 250 kDa; CDK7: 40 kDa; CDK9: 42 kDa; Histone H3: 15 kDa

In the MCF7 LTED^{PalboR} cells, AZD4573 was shown to reduce the total levels of RNA Pol II, and so the reduction in serine-2 and serine-5 phosphorylation also observed is difficult to interpret. In the MCF7 LTED^{Y537C} cell lines, no change in total RNA Pol II levels, or RNA Pol II phosphorylation was observed. In both the HCC1428 LTED cell lines, AZD4573 only reduced serine-2 phosphorylation of RNA Pol II, and did not affect serine-5 phosphorylation, or total RNA Pol II levels (although the difference in loading controls for this blot must be borne in mind), as has been previously observed in haematological cancer cell lines (Cidado et al., 2020).

Treatment with AZD4573 did not affect the levels of CDK7 or phosphorylated CDK7 in any of the cell lines examined (although the variable loading of the CDK7 blot for the MCF7 LTED^{PalboR} cells must be considered). While AZD4573 treatment did not affect the level of CDK9 in the MCF7 LTED^{PalboR} cells, or either of the HCC1428 LTED cell lines, a higher level of CDK9 was observed following 10 nM AZD4573 in MCF7 LTED^{Y537C}, which warrants repetition.

6.5.7.3 Exploring mechanisms of synergism with palbociclib

In the MCF7 LTED^{PalboR} cell lines, there was evidence of synergy in both the ICEC0942/palbociclib and the AZD4573/palbociclib combination experiments in 2D (Figures 6.14, 6.15), and the AZD4573/palbociclib combination experiments in 3D (Figure 6.27) cell viability assays. There was no evidence of synergy observed in the HCC1428 LTED^{PalboR} cell line for either of the two CDK inhibitors. Western blotting experiments were therefore designed to examine the effect of these drugs on known mechanisms of palbociclib resistance.

Rb is considered one of the key biomarkers of sensitivity to CDK4/6 inhibitor therapy (O'Leary et al., 2016), given that it is the primary target of CDK4/6 inhibitors. Rb loss or inactivation has been suggested in multiple preclinical studies as a driver of CDK4/6 inhibitor resistance (Dean et al., 2012, Witkiewicz and Knudsen, 2014), as with its loss of action, the inhibition of CDK4/6 has little effect, and E2F transcription factors remain active, resulting in dysregulation of the G_1/S checkpoint. Additionally, Rb-phosphorylation is an indirect marker of CDK7 activity, as CDK7 phosphorylates and

activates CDK4/6. In the study characterising ICEC0942 (Patel et al., 2018), Rb phosphorylation was reduced by ICEC0942 treatment, but total Rb was unchanged. Therefore, experiments to assess levels of total and phosphorylated-Rb, to examine the effect of both ICEC0942 and AZD4573 on Rb activity, are underway.

Cyclin E also plays a key role at the G_1/S checkpoint. Cyclin E forms a complex with CDK2, Rb is phosphorylated and the inhibitory action of Rb on E2F transcription factors is lost. Overexpression of *CCNE1*, which encodes cyclin E, is another recognised mechanism of CDK4/6 inhibitor resistance, as this mechanism also circumvents the regulatory control of Rb (Herrera-Abreu et al., 2016, Taylor-Harding et al., 2015). In previous studies using the palbociclib-resistant models described in this thesis, it was reported that there was lower expression of cyclin E in the palbociclib-sensitive models in comparison to their palbociclib-resistant derivatives (Pancholi et al., 2020). The transcription factor MYB has been reported to activate the expression of *CCNE1* in colonic epithelium (Cheasley et al., 2015), and CDK9 inhibitors have been shown to downregulate the expression of *MYB* through their inhibition of transcription (Mitra et al., 2016). Therefore, Western blots were designed to probe for cyclin E and MYB, to evaluate whether synergy of the CDK7/9 inhibitors with palbociclib is mediated through the downregulation of *CCNE1* expression (Figure 6.30).

In both the MCF7 LTED cell lines, treatment with AZD4573 reduced the levels of the transcription factor MYB, but not of cyclin E. In the HCC1428 LTED cell lines, cells treated with AZD4573 appeared to show increased levels of MYB. There also appeared to be an increase in levels of cyclin E, although the difference in loading between the HCC1428 LTED and HCC1428 LTED^{PalboR} lines makes this difficult to compare. Treatment with ICEC0942 did not affect MYB levels in the MCF7 LTED cell lines, or the HCC1428 LTED^{PalboR} cells, but reduced MYB levels following ICEC0942 treatment in the HCC1428 LTED cells was observed. Cyclin E expression was unaffected by ICEC0942 treatment in the HCC1428 LTED cell lines, and the MCF7 LTED^{PalboR} cells, but increased cyclin E was observed after ICEC0942 treatment in the MCF7 LTED^{Y537C} cells. When comparing the results for the untreated palbociclib-sensitive and palbociclib-resistant cell lines, there were increased levels of MYB and cyclin E in the palbociclib-resistant models compared

to those that are sensitive, indicating a potential role for these proteins in palbociclib-resistance mechanisms.

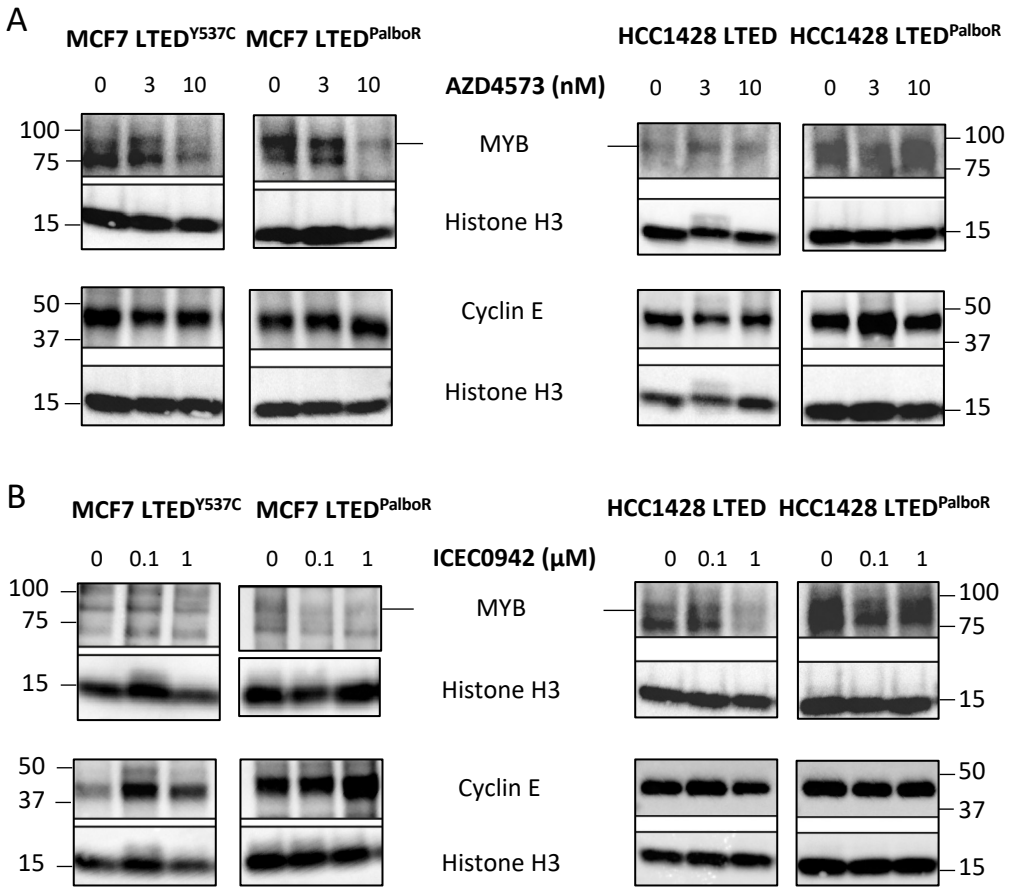

Figure 6.30. Western blots investigating cyclin E as a mechanism of synergy with palbociclib. (A) AZD4573 treatment(B) ICEC0942 treatment. Palbociclib-sensitive and palbociclib-resistant cells were treated with the relevant drug as described in Figures 6.28 and 6.29, harvested and lysed, and Western blots were performed. Histone H3 loading controls from each gel are shown below each blot. Positions of the protein ladder are indicated in kDa. Molecular weights: MYB: 80 kDa (line indicates position of MYB); Cyclin E: 48 kDa; Histone H3: 15 kDa

CDK4 and *CDK6* overexpression have also been reported to mediate CDK4/6 inhibitor resistance in pre-clinical models (Olanich et al., 2015, Cen et al., 2012, Yang et al., 2017). Given that both CDK7 and CDK9 have roles in transcription, it is possible that inhibition of their activities could reduce the levels of CDK4 and CDK6, contributing to synergy with palbociclib, and so these CDKs were probed for (Figure 6.31). In the MCF7 LTED cell lines, a decreased level of CDK4 was observed at the high 10 nM dose of AZD4573, but no effect of AZD4573 was seen on CDK6 levels. AZD4573 did not affect the levels of CDK4

or CDK6 in either of the HCC1428 LTED cell lines. ICEC0942 did not affect levels of CDK4 in the HCC1428 LTED cell lines, or in the MCF7 LTED^{Y537C} cells. A lower level of CDK4 was observed at the 10 nM dose of ICEC0942 in the MCF7 LTED^{PalboR} cell line. Interestingly, ICEC0942 treatment was shown to increase CDK6 levels from baseline in both of the MCF7 LTED lines, but no effect on CDK6 levels was seen in either of the HCC1428 LTED lines with ICEC0942 treatment. Examining the ICEC0942 blot for the HCC1428 LTED cell lines, the untreated lanes show that there was a higher level of CDK4 at baseline in the palbociclib-resistant cells. The levels of CDK6 were higher in the palbociclib-resistant cells than in the palbociclib-sensitive MCF7 LTED cell lines, in line with what has previously been shown (Pancholi et al., 2020), although the loading makes this difficult to interpret.

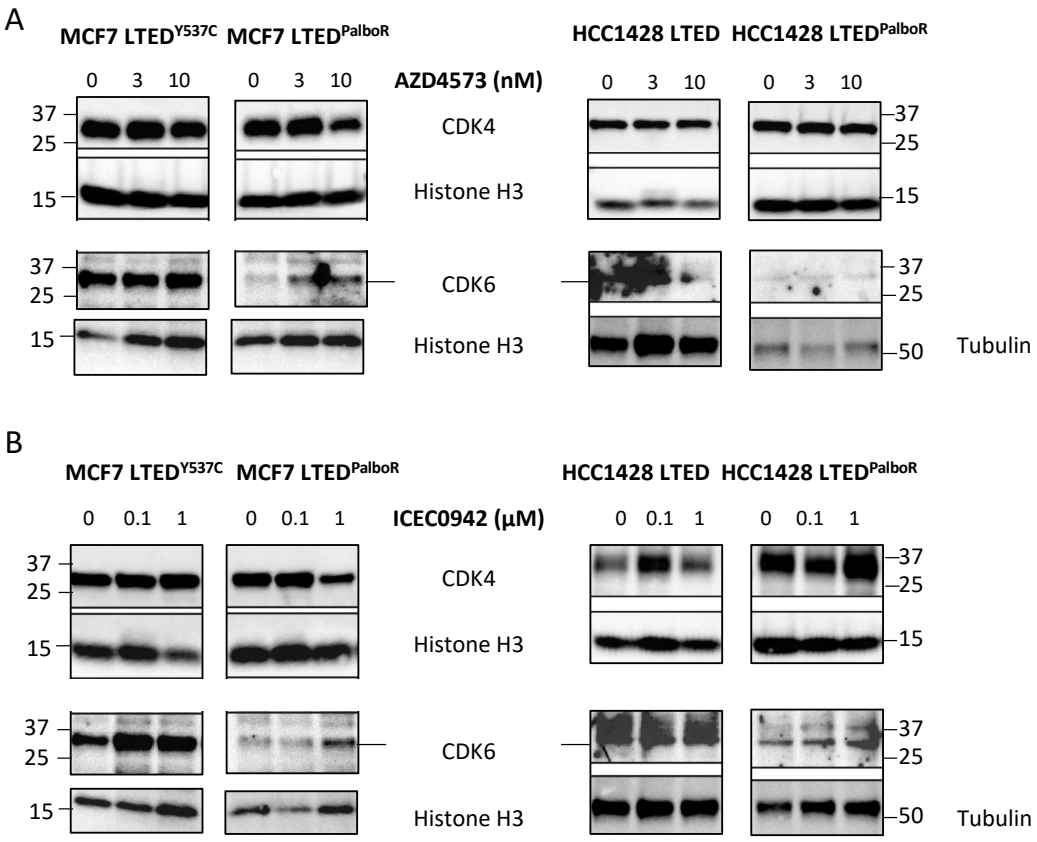

Figure 6.31. Western blots investigating CDK4 and CDK6 as mechanisms of synergy with palbociclib. (A) AZD4573 treatment. (B) ICEC0942 treatment. Palbociclib-sensitive and palbociclib-resistant cells were treated with the relevant drug as described in Figures 6.28 and 6.29, harvested and lysed, and Western blots were performed. Loading controls from each gel are shown below each blot. Histone H3 was used as loading control for all except the HCC1428 LTED^{PalboR} cell line, for which tubulin was used. Positions of the protein ladder are indicated in kDa. Molecular weights: CDK4: 30 kDa; CDK6: 36 kDa (line indicates position of CDK6); tubulin: 55 kDa; Histone H3: 15 kDa.

6.6 Discussion

CDK7 and CDK9 were selected for further investigation following their identification as hits from the 2D and 3D drug and siRNA screens in cell lines in a variety of molecular backgrounds. Treatments with NVP-2 and AZD4573, which target CDK9, were effective at inhibiting cell proliferation in parental, endocrine-resistant, and palbociclib-resistant cell lines in 2D culture (Figures 6.9, 6.10). AZD4573 treatment was also found to be effective in the endocrine-resistant models in 3D (Figure 6.12). THZ1, targeting CDK7, was also effective in all cell lines (Figure 6.7), and another CDK7 inhibitor, ICEC0942, inhibited cell proliferation in all models except the HCC1428 LTED cell line (Figure 6.8).

In 3D culture, neither the HCC1428 LTED or HCC1428 LTED^{PalboR} cell lines were sensitive to ICEC0942 treatment (Figure 6.11), but the MCF7 cell lines showed reduced proliferation. Interestingly, silencing of *CDK7* expression by using siRNA did not impact on cell viability, (discussed further in Section 7.3). CDK9 knockdown was effective at reducing cell viability in the MCF7 cell lines, and the parental HCC1428 cell line, but not the endocrine-resistant derivatives.

To examine whether CDK7 or CDK9 play a role in the mechanisms conferring palbociclib-resistance, two approaches were used. While using siRNAs to silence the expression of *CDK7* or *CDK9* did not alter the sensitivity of the palbociclib-resistant models to palbociclib (Figure 6.13), combination treatment of palbociclib/ICEC0942 and palbociclib/AZD4573 showed synergy in the MCF7 LTED^{PalboR} line in 2D (Figure 6.14, 6.15), and the palbociclib/AZD4573 combination also showed synergy in 3D in the MCF7 LTED^{PalboR} line (Figure 6.27). No evidence of synergy by combination treatment was observed in the HCC1428 LTED^{PalboR} lines. These results suggest that different cell signalling pathways that confer palbociclib-resistance could be in place in the different models.

Western blots evaluating the mechanism of action, and possible pathways that could explain the synergism observed were performed. Due to time constraints, these assays are still ongoing and have yet to be repeated using independent samples. Consequently, conclusions drawn are preliminary. The blots examining the mechanism of action of ICEC0942 (Figure 6.28) have not shown the specificity for inhibition of RNA Pol II serine-5 phosphorylation that has previously been reported (Patel et al., 2018), as effects on serine-2 phosphorylation observed as well. Similarly, AZD4573 was found to inhibit serine-2 phosphorylation selectively in some cell lines, but not in all (Figure 6.29). These findings call into question the specificity of the drug treatments for their respective CDK targets.

In comparing the untreated lanes for the palbociclib-sensitive and palbociclib-resistant models, higher levels of CDK7, phosphorylated CDK7, MYB, and cyclin E were seen in palbociclib-resistant models. Additionally, increased levels of CDK4 were seen in the HCC1428 LTED^{PalboR} cell line when compared to HCC1428 LTED cells. This indicates a role

for these proteins in contributing to palbociclib resistance. However, the effects of the drug treatments on these proteins do not logically lead to the synergism observed in the combination drug studies, save that of AZD4573 and ICEC0942 reducing CDK4 levels in the MCF7 LTED^{PalboR} cells. This could indicate that are there other alternative signalling pathways impacted by AZD4573 and ICEC0942 that the palbociclib-resistant cells are reliant upon. Alternatively, given that the drugs both have actions on transcription, it is possible that the design of the experiment did not optimally reflect their mechanism of action. AZD4573 has been observed to have an effect on RNA Pol II phosphorylation six hours after treatment (Cidado et al., 2020), and so a time-course assay would be better placed to examine for the transcriptional impact of these drugs.

While further studies are required to unpick the mechanisms by which ICEC0942 and AZD4573 have been shown to synergise with palbociclib in palbociclib-resistant cells, the data in this chapter suggest that CDK7 and CDK9 are intriguing potential targets for the treatment of endocrine-resistant, palbociclib-resistant ER-positive breast cancer.

Chapter 7 Final discussion and future perspectives

Breast cancer is a leading cause of mortality for women worldwide, and one of the most significant challenges for its treatment is that of endocrine-resistant disease. While in ER-negative breast cancer the risk of recurrence peaks in year two following diagnosis (Bushnell et al., 2021), those with ER-positive disease often relapse later, with 20% of women with ER-positive disease having a recurrence fifteen years or more after the initial diagnosis (Pan et al., 2017). In this intervening time period, patients will have become older, more frail, and may have additional comorbidities, lowering their resilience to withstand chemotherapeutic treatments and their associated toxicity profiles. Given that endocrine therapies are generally well-tolerated (Ohno, 2016), the problem of endocrine resistance becomes even more pertinent, as if the mechanisms conferring resistance were understood, they could be targeted such that endocrine therapy could be re-administered as a viable treatment option. Failing that, if common 'Achilles heels' displayed by endocrine-resistant tumours could be identified, targeted therapies against these nodes could become a next step in treatment for patients with endocrine-resistant disease. Indeed, CDK4/6 inhibitors are a prime example of such targeted therapy, but unfortunately resistance to CDK4/6 inhibitors is becoming the next hurdle in the treatment of advanced ER-positive breast cancer to be surpassed.

One of the consistent challenges in unpicking the mechanisms by which endocrine-resistance develops is the considerable heterogeneity displayed within the umbrella term of ER-positive breast cancer (Clarke et al., 2015). The majority of *in vitro* work on ER-positive breast cancer has been performed using MCF7 cells, with over fifty thousand entries on PubMed. While this is logical, given the paucity of ER-positive breast cancer lines available to researchers seeking to model response to hormone therapy (in comparison to ER-negative lines), one cell line cannot represent the behaviour of all ER-positive breast cancer. Furthermore, while cells growing in a 2D monolayer on plastic with uniform nutrient and oxygen conditions do not accurately reflect the results of *in vivo* studies or clinical trials (Sahai and Marshall, 2003), ER-positive PDX models have a low establishment rate, and take many months to develop (see Section 1.5.2), and therefore do not lend themselves to high-throughput discovery approaches.

The aim of this project was to investigate mechanisms contributing to endocrine resistance. This was undertaken by two approaches: first, RNA-sequencing of longitudinally-paired clinical samples before AI therapy and following relapse after AI therapy to examine the transcriptional changes that had occurred; and second by subjecting a variety of pre-clinical models of ER-positive breast cancer to high throughput screens to identify common nodes of vulnerability, using 2D and 3D cell culture to try and better capture the conditions tumours are subject to *in vivo*.

In summary, the data presented in this thesis are that transcriptional profiling of pre- and post-AI clinical samples did not reveal one key target as a proliferative driver of AI-resistant progression, but an overall trend towards a more aggressive phenotype in the post-AI samples. The results from the high-throughput screens have shown three common areas of vulnerability in the models of endocrine-resistance (a) ER-signalling, (b) PI3K-AKT-mTOR pathway, and (c) CDK-dependent pathways, with CDK7 and CDK9 being investigated further as potential therapeutic targets in endocrine-resistant and palbociclib-resistant models.

7.1 Characterisation of paired patient samples – findings and limitations

The ability to perform biopsies of the same tumour over time is an important but logistically tricky approach to learn how breast cancer may change and evolve within a patient. The cohort of paired samples examined in this study is therefore rare and valuable, hence why it was chosen for further investigation, despite the paucity of key drivers identified in a previous study on this sample set (Lopez-Knowles et al., 2019). This previous study performed mutational profiling of 16 key breast cancer genes and RNA expression analysis of 209 genes using a custom NanoString panel. These 209 genes comprised reference genes, the PAM50 geneset and selected genes involved in steroid hormone synthesis, ER targets, receptor tyrosine kinases, cell proliferation, apoptosis, and cell signalling. It was hypothesised that key drivers of AI-resistant progression may have been missed due to the limited profiling performed. However, even increasing the cohort size from the 209 genes examined by Nanostring to the whole transcriptome did not identify transcriptional pathways common to post-AI samples. That said, the RNA-seq analysis did corroborate the heterogeneity of samples within this set seen in earlier

studies (Arnedos et al., 2014, Lopez-Knowles et al., 2019), and revealed that it is the luminal A samples that undergo the greatest change following AI therapy (Figure 3.3). Overall, in the luminal A subtypes there is a drive towards upregulated expression of pro-proliferative MYC targets and MTORC1 signalling from pre-AI to post-AI, and maintained high expression of these pathways in the luminal B and HER2-positive subtypes. These findings lend validity to the findings of the drug and siRNA screens, as the common vulnerabilities identified (PI3K-AKT-mTOR, and CDK-dependent signalling) all impact on these pro-proliferative pathways. The high degree of heterogeneity observed may also contribute to the lack of key significant drivers promoting progression. For example, in Figure 3.6, an observable difference can be noted in the average $\log_2$ expression of genes involved in the early oestrogen response hallmark pathway between the pre- and post-AI samples of luminal A and luminal B samples, but this does not achieve significance by Mann-Whitney testing. This suggests the existence of sub-groups within the luminal A and luminal B samples, that may have had a different response to AI therapy. It would be intriguing to investigate this further, by performing further analyses within the sub-groups, but runs the risk of low sample numbers confounding the findings.

The conclusions that can be drawn from the sequencing data are necessarily limited by (a) the variation in the patient cohort with regards to when the biopsies were taken in relation to their AI therapy (Section 3.3.1.1), and (b) the quality of the RNA obtained from FFPE material that was submitted for library preparation (Section 3.3.1.2). Furthermore, with the FDR being set at ≤0.1, and low numbers of differentially expressed genes identified, reservations must be kept regarding the strength of the conclusions drawn from these results. A study with standardised biopsy collection protocols with a larger number of patients to allow for subgroup analyses would be better placed to answer the question of whether there are common genetic or transcriptional changes that occur on AI therapy in the clinic to mediate resistance.

7.2 Use of a screen-based approach to target discovery – findings and limitations

As discussed in Section 5.1, screens are a powerful tool to test for vulnerabilities against a large number of different compounds or gene expression interference mechanisms,

generating results rapidly and under homogeneous conditions. By interrogating the results of these screens, a picture of important pathways may be built.

Given that the heterogeneity of ER-positive disease is one of the obstacles to deconvoluting endocrine-resistance mechanisms, cell line models with a range of molecular backgrounds were subjected to these screens to try and better encompass the diversity of ER-positive disease. The LTED models chosen demonstrate E2-independence, and therefore reflect the clinical picture of patients who have relapsed on AI-therapy but are still sensitive to SERDs. The results of the screens highlighted ER-signalling, PI3K-AKT-mTOR signalling, and cell cycle regulation as the common nodes of vulnerability in the LTED models, with the latter two pathways also selected as hits in the palbociclib-resistant cell line models.

Sensitivity to perturbation of ER-signalling was predominantly highlighted in the 2D drug screen, with the finding that the cell lines with an activating mutation in ER were more sensitive to SERDs than those expressing an ER^{WT}, suggesting a reliance on constitutive ER activity in cells expressing ER^{MUT}. This finding is at odds with other studies suggesting that inhibition of ER^{MUT} cell proliferation requires higher concentrations of SERDS than those expressing ER^{WT} (Toy et al., 2013), although the Toy et al. study did not include the *ESR1*^{Y537C} model. In clinical practice there does not appear to be differential sensitivity to the SERD fulvestrant between ER^{WT} and ER^{MUT} breast cancers with no difference in progression-free survival observed (Turner et al., 2020). In the 3D drug screen, fulvestrant was only selected as a hit in one cell line (SUM44 LTED^{Y537S}, data not shown), with no differential sensitivity seen when comparing the MCF7 LTED^{WT} and MCF7 LTED^{Y537C} lines, supporting the assertion that the use of 3D models limits results to those of greater physiological relevance.

Pathways involving PI3K-AKT-mTOR signalling were selected as hits in the drug and siRNA screens, in both 2D and 3D culture. As discussed in Section 1.3.3, the cross-talk between ER and the PI3K-AKT-mTOR pathway has been extensively studied as a key mechanism of endocrine-resistance *in vitro*. Furthermore, there have been a plethora of trials evaluating drugs targeting the PI3K-AKT-mTOR pathway in endocrine-resistant breast cancer. These trials have assessed pan-PI3K inhibitors such as pictilisib (FERGI

study (Krop et al., 2016)), PI3Kα inhibitors such as buparlisib (BELLE2 study (Baselga et al., 2017)), alpelisib (SOLAR-1 study (Andre et al., 2019)) and taselisib (SANDPIPER study (Baselga et al., 2018)), AKT inhibitors such as capivasertib (FAKTION study, (Jones et al., 2020)), and mTOR inhibitors such as everolimus (BOLERO-2 study (Baselga et al., 2012). While most of these trials have shown potent anti-cancer effects, there have been difficulties with the toxicity profiles of these drugs. The success of the BYLieve study (Rugo et al., 2021), which showed progression-free survival in patients with AI-resistant, CDK4/6 inhibitor-resistant disease that carried a *PIK3CA* mutation is significant progress in the challenge of treating resistant ER-positive disease. Alpelisib, the PI3Kα inhibitor used in this trial, as well as many other agents targeting PI3K-signalling, were picked up as significant hits in the 2D and 3D drug screens, providing validity for the screening approach taken in this thesis. However, one of the inclusion criteria for the BYLieve study was the presence of a *PIK3CA* mutation. While *PIK3CA* mutations are seen in ~40% of ER-positive disease (Vasan et al., 2019a), this still leaves a majority of patients with advanced endocrine-resistant, CDK4/6 inhibitor-resistant disease with few options for further targeted treatment. Consequently, when picking the hits for further investigation and validation in this study, those that were common to lines that were both wild-type and mutant for *PIK3CA* were chosen.

As stated above, when comparing the 2D *vs.* 3D results, in both the drug and siRNA screens fewer significant hits were found in the 3D screens. However, the pathway analysis of the hits identified the same key signalling pathways in 2D and 3D, suggesting 3D screens may limit false positive hits. Correlation analyses between the 2D and 3D siRNA screens gave a Pearson r correlation coefficient ranging between 0.2 and 0.5 for the different cell lines. It is possible that had the 2D siRNA screens (performed by Dr Joanna Nikitorowicz-Buniak) and 3D siRNA screens (performed during this PhD project) been carried out at the same time (rather than eighteen months apart), by the same person, a greater degree of correlation might have been seen. It must be noted that no siRNA generated a robust Z-score ≤-2 in the 2D siRNA screen of the HCC1428 LTED^{PalboR} cell line and so these results could not be compared with the 2D siRNA screen results of HCC1428 LTED cells to examine for palbociclib resistance mechanisms, or with the 3D siRNA screen results of HCC1428 LTED^{PalboR} to look for changes that might occur in 3D culture. Experience gained during this PhD with culture of the HCC1428 LTED^{PalboR} cells

suggests that as they do take weeks to reach an exponential phase of growth, perhaps the 2D siRNA screens were performed by Dr Nikitorowicz-Buniak when the cells were still in a low proliferation phase, thus limiting the effect of RNA silencing.

There were also two design flaws in setting up the drug screens. In the 2D drug screen design, the aim was to screen several hundred compounds at multiple doses such that dose-response curves could be generated for each drug in each cell line. However, with only four dose points, this was not possible, and so the results at each concentration were analysed as separate screens (i.e. a screen at 10 nM, at 100 nM, and 1000 nM). The second flaw was in the drug dose used for the 3D drug screen. As many of the clinically relevant drugs used have an IC_{50} greater than 100 nM, but less than 1000 nM, the choice of using a 250 nM dose was made. This has meant that the results of the 2D and 3D drug screens could not be directly compared. Finally, it should be noted that while multicellular tumour spheroid models do generate gradients of hypoxia and nutrients not observed in 2D, they cannot capture a heterogeneous tumour in the same manner as organoids or PDXs, and cannot reflect the interactions with the extracellular matrix and stromal/immune cells. This represents the dichotomy of balancing accurate modelling of an *in vivo* tumour to reflect tumour biology with a screen-based approach that must be homogeneous and reproducible.

The aim of running the screens in many different endocrine-resistant cell lines, and under 2D and 3D culture conditions, was to identify hits that might be common nodes in key pathways mediating resistance. The fact that the screens picked up hits that are already targeted in the clinic suggests there was validity to this approach. However, by concentrating on the targets that were common to multiple cell lines, an opportunity has potentially been missed to compare and contrast the hits selected between the different lines, and thereby possibly identify pathways that are more important in one cell line than another. This was consciously done in order to find kinases that, if targeted, could ameliorate endocrine resistance in a wide variety of molecular contexts, but further work could be performed investigating hits that were selected for in only one cell line, and may therefore give further detail on the heterogenous methods by which endocrine resistance develops.

7.3 Validation of targets – findings and limitations

The targets chosen for further investigation were CDK7 and CDK9. While these were not frequently highlighted as hits in the siRNA screens (CDK7 was not significant in any of the 2D or 3D siRNA screens, CDK9 was significant in five cell lines in the 2D siRNA results, and one cell line in the 3D siRNA results), drugs targeting both of these CDKs were significant in the 2D and 3D screens. The CDK7 inhibitor THZ1 was significant in *PIK3CA*^{WT} and *PIK3CA*^{MUT} models in the 2D drug screen, and the CDK9 inhibitor NVP-2 was significant in both *PIK3CA* settings in the 3D drug screens, as well as sensitivity to these agents being observed in palbociclib-resistant models. Validation studies of these targets were performed using the CDK7 inhibitor ICEC0942, and the CDK9 inhibitor AZD4573 which are already in phase 1 trials, with the aim that should these drugs prove successful, repurposing them would be smoother. The two palbociclib-resistant models were both sensitive to the ICEC0942, as were all the endocrine-resistant models except HCC1428 LTED (Figure 6.8, 6.11). As yet it is unclear why the palbociclib-resistant HCC1428 LTED^{PalboR} (which is derived from the HCC1428 LTED line) and the parental HCC1428, should show sensitivity to ICEC0942 when the HCC1428 LTED line does not. Experiments to further investigate the mechanism of action of ICEC0942 in these cell lines are ongoing, with the aim of shedding light on the 2D and 3D dose-response assay results in the HCC1428 LTED line. All cell lines were sensitive to CDK9 inhibition by NVP-2 and AZD4573, and there was a promising finding of synergy between AZD4573 and palbociclib in the MCF7 LTED^{PalboR} model in both 2D and 3D culture (Figure 6.15, 6.27). Experiments to investigate the mechanism of action of AZD4573 in these cell lines may therefore further our understanding of the development of palbociclib-resistance. Support for targeting CDK9 in ER-positive breast cancer comes from the analyses of the MONARCH-E trial (Harbeck et al., 2021). This trial evaluated the role of the CDK4/6 inhibitor abemaciclib as adjuvant therapy in early breast cancer, and the improvement in invasive disease-free survival has resulted in FDA approval of abemaciclib as adjuvant therapy in early breast cancer with high proliferation markers. There have been other trials evaluating adjuvant CDK4/6 inhibitors in early breast cancer that have not shown significant improvement in invasive disease-free survival (PENELOPE-B (Loibl et al., 2021) and PALLAS (Mayer et al., 2021)). It has been suggested through examining the multiomics profiling of the different CDK4/6 inhibitors, that abemaciclib can target additional CDKs (one of which being CDK9) at clinically relevant concentrations (Hafner

et al., 2019), which may explain part of the success of abemaciclib in its adjuvant treatment of early breast cancer, in comparison to palbociclib.

The finding of synergy between the CDK9 inhibitor AZD4573 and palbociclib in the pre-clinical MCF7 LTED^{PalboR} model indicates a potential role for combination therapy for endocrine-resistant, palbociclib-resistant disease, which is currently being explored in animal studies. Specifically, through a collaboration with Dr Elisabetta Marangoni at the Institut Curie, a PDX model of palbociclib-resistant disease is being treated with AZD4573 alone, or in combination with fulvestrant and palbociclib, to examine whether this combination may be a viable option in resistant breast cancer.

A further interesting finding of the combination palbociclib/CDK7/9 inhibitor treatment experiments is that where additivity occurs in the palbociclib-sensitive models, it is at a lower concentration than the mean plasma concentration of palbociclib (FDA, 2014) (Figures 6.18, 6.19, 6.20, 6.21). This indicates that anti-proliferative effects could be achieved at lower palbociclib concentrations through combination therapy. This is important, given that a potential reason for the failure of the PALLAS trial to achieve significance was the palbociclib discontinuation rate of 42.2% due to adverse haematological effects. If the dose-sparing effect of combination treatment does translate from *in vitro* to *in vivo*, it would be of potential clinical relevance.

The discordance between the additivity and synergy seen in the combination drug studies, and the lack of re-sensitisation to palbociclib following siRNA treatment targeting CDK7 and CDK9 must be noted. One potential reason for this could be that the synergy is due to off-target effects of the drugs used. However, both ICEC0942 and AZD4573 were chosen for their selectivity and specificity for their targets. ICEC0942 is a small molecule inhibitor of CDK7 that binds reversibly to the ATP-binding site of CDK7, and while crystal structures of ICEC0942 bound to CDK7 are yet to be obtained, modelling studies have identified aspartate-155 as the residue that is likely to determine the selective binding of ICEC0942 to CDK7 (Hazel et al., 2017). Screening of ICEC0942 against a 117 kinase panel of various kinase classes confirmed CDK7 selectivity, with the next most sensitive CDK (CDK2) having an IC_{50} fifteen-fold higher than CDK7 (Patel et al., 2018). AZD4573 was identified through a structure-based drug discovery approach to

identify compounds showing high fidelity of binding to CDK9 (Barlaam et al., 2020). Kinase selectivity profiling of AZD4573 against a panel of 468 kinases showed high selectivity for CDK9, and notably AZD4573 exhibited >25-fold cellular selectivity for CDK9 over other CDKs in MCF7 cells (Cidado et al., 2020). Studies profiling the activity of ICEC0942 show that it is able to inhibit the key actions of CDK7, as increasing concentrations of ICEC0942 result in decreased phosphorylation of RNA-Pol II at serine-5, decreased phosphorylation of CDKs 1, 2, 4 and 6, and Rb, causing cells to be blocked through cell cycle progression, and decreased phosphorylation of ER at serine-118 (Patel et al., 2018). Similar studies investigating the activity of AZD4573 have shown that treatment with this compound inhibits the phosphorylation of RNA Pol II at serine-2, with inhibition of serine-5 phosphorylation only occurring at 200-fold higher concentrations (Cidado et al., 2020). No effect on the putative endpoints of multiple other CDKs were observed in this study. While the Western blots investigating the mechanism of action of ICEC0942 and AZD4573 (Figures 6.28, 6.29) have not shown the clear-cut specificity of inhibiting RNA Pol II at serine-5 and serine-2 respectively as has previously been published (Patel et al., 2018, Cidado et al., 2020), the time course for these experiments may have been too long. Therefore, the off-target effects of ICEC0942 and AZD4573 mediating the results seen in the combination drug studies is unlikely.

Another possible reason for the lack of effect observed after CDK7 and CDK9 siRNA transfection could be because the knockdown of the targets by siRNA was not sufficiently effective. Ideally, further optimisation of siRNA transfection, particularly in the HCC1428 lines, would have been carried out, through use of single siRNAs in the event that the SMARTpools contained ineffective siRNAs, or through the trial of alternative transfection agents, and repeats of siRNA knockdown followed by palbociclib treatment. Unfortunately, at the time of these experiments, there were significant delays in obtaining tissue culture flasks due to Brexit, and attempts to use other plastics were unsuccessful. In order to carry out validation studies of these targets without using pharmaceutical inhibition, alternative options would be to use shRNAs, or CRISPR-Cas9 editing to silence CDK7 and CDK9 expression in the MCF7 LTED^{PalboR} and HCC1428 LTED^{PalboR} lines, and then treat with palbociclib to examine whether silencing of these targets altered the palbociclib-resistant phenotype observed in these models.

As well as the ongoing experiments investigating how the mechanism of action of ICEC0942 and AZD4573 act to achieve synergy in the context of palbociclib treatment, future studies are required to examine the cellular response of palbociclib-resistant models to these drugs. Given that CDK7 is a master regulator of the cell cycle, cell cycle analysis using flow cytometry to examine the effects of ICEC0942 on how the palbociclib-resistant cell lines progress through the cell cycle should be performed. Cell-cycle analysis of HCT116 and MCF7 cells treated with ICEC0942 demonstrated induction of arrest at the G_2M checkpoint (Patel et al., 2018), and it would be intriguing to assess whether this effect persisted in the palbociclib-resistant derivatives. CDK9 is integral to transcription, and the hypothesis underlying targeting transcription in cancer is that certain cancers may be transcriptionally addicted to specific drivers (Section 6.4.2). Therefore, to examine if this is the case in these models of resistant breast cancer, transcriptomic profiling prior to and following AZD4573 treatment using RNA-seq may identify pathways specifically targeted by AZD4573 that the cells are reliant upon. Finally, given the successes of abemaciclib as adjuvant therapy in early breast cancer, and the hypothesis that this may be due to inhibition of CDKs beyond CDK4 and CDK6, it would be intriguing to assess whether the palbociclib-resistant models are also resistant to abemaciclib, and to assess the effect of combination therapy of abemaciclib with CDK7 and CDK9 inhibitors on these models.

7.4 Conclusions

The data presented in this thesis demonstrate that (a) there is significant heterogeneity with few key transcriptional driver pathways in endocrine-resistant clinical samples as determined by RNA-seq; and (b) there are three key areas of vulnerability common to multiple endocrine-resistant models – PI3K-AKT-mTOR signalling, ER-signalling, and CDK-dependent processes. Further investigation indicates that CDK7 and CDK9 are potential targets for therapy in both endocrine-resistant and palbociclib-resistant settings. Drug studies suggest that combination therapy of CDK7 or CDK9 inhibitors with palbociclib may be useful in endocrine-resistant and palbociclib-resistant disease, with the potential for palbociclib dose-reduction. Future studies are required to determine the mechanism of drug combination synergism in the context of palbociclib, and other

CDK4/6 inhibitor-resistant disease, and the potential for combination therapy in the clinic.

Chapter 8 Bibliography

(NICE), N. I. F. H. A. C. E. 2019. *Abemaciclib with an aromatase inhibitor for previously untreated, hormone receptor-positive, HER2-negative, locally advanced or metastatic breast cancer [TA563]* [Online]. Available: https://www.nice.org.uk/guidance/ta563/evidence [Accessed].

AFTIMOS, P., OLIVEIRA, M., IRRTHUM, A., FUMAGALLI, D., SOTIRIOU, C., GAL-YAM, E. N., ROBSON, M. E., NDOZENG, J., DI LEO, A., CIRUELOS, E. M., DE AZAMBUJA, E., VIALE, G., SCHEEPERS, E. D., CURIGLIANO, G., BLISS, J. M., REIS-FILHO, J. S., COLLEONI, M., BALIC, M., CARDOSO, F., ALBANELL, J., DUHEM, C., MARREAUD, S., ROMAGNOLI, D., ROJAS, B., GOMBOS, A., WILDIERS, H., GUERRERO-ZOTANO, A., HALL, P., BONETTI, A., LARSSON, K. F., DEGIORGIS, M., KHODAVERDI, S., GREIL, R., SVERRISDOTTIR, A., PAOLI, M., SEYLL, E., LOIBL, S., LINDERHOLM, B., ZOPPOLI, G., DAVIDSON, N. E., JOHANNSSON, O. T., BEDARD, P. L., LOI, S., KNOX, S., CAMERON, D. A., HARBECK, N., MONTOYA, M. L., BRANDAO, M., VINGIANI, A., CABALLERO, C., HILBERS, F. S., YATES, L. R., BENELLI, M., VENET, D. & PICCART, M. J. 2021. Genomic and Transcriptomic Analyses of Breast Cancer Primaries and Matched Metastases in AURORA, the Breast International Group (BIG) Molecular Screening Initiative. *Cancer Discov,* 11**,** 2796-2811.

ALI, S., HEATHCOTE, D. A., KROLL, S. H., JOGALEKAR, A. S., SCHEIPER, B., PATEL, H., BRACKOW, J., SIWICKA, A., FUCHTER, M. J., PERIYASAMY, M., TOLHURST, R. S., KANNEGANTI, S. K., SNYDER, J. P., LIOTTA, D. C., ABOAGYE, E. O., BARRETT, A. G. & COOMBES, R. C. 2009. The development of a selective cyclin-dependent kinase inhibitor that shows antitumor activity. *Cancer Res,* 69**,** 6208-15.

ALOIA, A., PETROVA, E., TOMIUK, S., BISSELS, U., DEAS, O., SAINI, M., ZICKGRAF, F. M., WAGNER, S., SPAICH, S., SUTTERLIN, M., SCHNEEWEISS, A., REITBERGER, M., RUBERG, S., GERSTMAYER, B., AGORKU, D., KNOBEL, S., TERRANEGRA, A., FALLENI, M., SOLDATI, L., SPRICK, M. R., TRUMPP, A., JUDDE, J. G., BOSIO, A., CAIRO, S. & HARDT, O. 2015. The sialyl-glycolipid stage-specific embryonic antigen 4 marks a subpopulation of chemotherapy-resistant breast cancer cells with mesenchymal features. *Breast Cancer Res,* 17**,** 146.

ANAND, S., PENRHYN-LOWE, S. & VENKITARAMAN, A. R. 2003. AURORA-A amplification overrides the mitotic spindle assembly checkpoint, inducing resistance to Taxol. *Cancer Cell,* 3**,** 51-62.

ANDERSON, H., BULUN, S., SMITH, I. & DOWSETT, M. 2007. Predictors of response to aromatase inhibitors. *J Steroid Biochem Mol Biol,* 106**,** 49-54.

ANDRE, F., CIRUELOS, E., RUBOVSZKY, G., CAMPONE, M., LOIBL, S., RUGO, H. S., IWATA, H., CONTE, P., MAYER, I. A., KAUFMAN, B., YAMASHITA, T., LU, Y. S., INOUE, K., TAKAHASHI, M., PAPAI, Z., LONGIN, A. S., MILLS, D., WILKE, C., HIRAWAT, S., JURIC, D. & GROUP, S.-S. 2019. Alpelisib for PIK3CA-Mutated, Hormone Receptor-Positive Advanced Breast Cancer. *N Engl J Med,* 380**,** 1929-1940.

ANZICK, S. L., KONONEN, J., WALKER, R. L., AZORSA, D. O., TANNER, M. M., GUAN, X. Y., SAUTER, G., KALLIONIEMI, O. P., TRENT, J. M. & MELTZER, P. S. 1997. AIB1, a steroid receptor coactivator amplified in breast and ovarian cancer. *Science,* 277**,** 965-8.

ARNEDOS, M., DRURY, S., AFENTAKIS, M., A'HERN, R., HILLS, M., SALTER, J., SMITH, I. E., REIS-FILHO, J. S. & DOWSETT, M. 2014. Biomarker changes associated with the development of resistance to aromatase inhibitors (AIs) in estrogen receptor-positive breast cancer. *Ann Oncol,* 25**,** 605-610.

ARONICA, S. M., KRAUS, W. L. & KATZENELLENBOGEN, B. S. 1994. Estrogen action via the cAMP signaling pathway: stimulation of adenylate cyclase and cAMP-regulated gene transcription. *Proc Natl Acad Sci U S A,* 91**,** 8517-21.

BAI, Y. & GIGUERE, V. 2003. Isoform-selective interactions between estrogen receptors and steroid receptor coactivators promoted by estradiol and ErbB-2 signaling in living cells. *Mol Endocrinol,* 17**,** 589-99.

BAIG, R. M., SANDERS, A. J., KAYANI, M. A. & JIANG, W. G. 2012. Association of Differentiation-Related Gene-1 (DRG1) with Breast Cancer Survival and in Vitro Impact of DRG1 Suppression. *Cancers (Basel),* 4**,** 658-72.

BAILEY, S. T., SHIN, H., WESTERLING, T., LIU, X. S. & BROWN, M. 2012. Estrogen receptor prevents p53-dependent apoptosis in breast cancer. *Proc Natl Acad Sci U S A,* 109**,** 18060-5.

BANDYOPADHYAY, S., PAI, S. K., HIROTA, S., HOSOBE, S., TAKANO, Y., SAITO, K., PIQUEMAL, D., COMMES, T., WATABE, M., GROSS, S. C., WANG, Y., RAN, S. & WATABE, K. 2004. Role of the putative tumor metastasis suppressor gene Drg-1 in breast cancer progression. *Oncogene,* 23**,** 5675-81.

BARDIA, A., AFTIMOS, P., BIHANI, T., ANDERSON-VILLALUZ, A. T., JUNG, J., CONLAN, M. G. & KAKLAMANI, V. G. 2019. EMERALD: Phase III trial of elacestrant (RAD1901) vs endocrine therapy for previously treated ER+ advanced breast cancer. *Future Oncology,* 15**,** 3209-3218.

BARDIA, A., KAKLAMANI, V., WILKS, S., WEISE, A., RICHARDS, D., HARB, W., OSBORNE, C., WESOLOWSKI, R., KARUTURI, M., CONKLING, P., BAGLEY, R. G., WANG, Y., CONLAN, M. G. & KABOS, P. 2021. Phase I Study of Elacestrant (RAD1901), a Novel Selective Estrogen Receptor Degrader, in ER-Positive, HER2-Negative Advanced Breast Cancer. *Journal of Clinical Oncology,* 39**,** 1360-1370.

BARLAAM, B., CASELLA, R., CIDADO, J., COOK, C., DE SAVI, C., DISHINGTON, A., DONALD, C. S., DREW, L., FERGUSON, A. D., FERGUSON, D., GLOSSOP, S., GREBE, T., GU, C., HANDE, S., HAWKINS, J., HIRD, A. W., HOLMES, J., HORSTICK, J., JIANG, Y., LAMB, M. L., MCGUIRE, T. M., MOORE, J. E., O'CONNELL, N., PIKE, A., PIKE, K. G., PROIA, T., ROBERTS, B., SAN MARTIN, M., SARKAR, U., SHAO, W., STEAD, D., SUMNER, N., THAKUR, K., VASBINDER, M. M., VARNES, J. G., WANG, J., WANG, L., WU, D., WU, L., YANG, B. & YAO, T. 2020. Discovery of AZD4573, a Potent and Selective Inhibitor of CDK9 That Enables Short Duration of Target Engagement for the Treatment of Hematological Malignancies. *J Med Chem,* 63**,** 15564-15590.

BARTKOVA, J., ZEMANOVA, M. & BARTEK, J. 1996. Expression of CDK7/CAK in normal and tumor cells of diverse histogenesis, cell-cycle position and differentiation. *Int J Cancer,* 66**,** 732-7.

BASAK, P., CHATTERJEE, S., BHAT, V., SU, A., JIN, H., LEE-WING, V., LIU, Q., HU, P., MURPHY, L. C. & RAOUF, A. 2018. Long Non-Coding RNA H19 Acts as an Estrogen Receptor Modulator that is Required for Endocrine Therapy Resistance in ER+ Breast Cancer Cells. *Cell Physiol Biochem,* 51**,** 1518-1532.

BASELGA, J., CAMPONE, M., PICCART, M., BURRIS, H. A., 3RD, RUGO, H. S., SAHMOUD, T., NOGUCHI, S., GNANT, M., PRITCHARD, K. I., LEBRUN, F., BECK, J. T., ITO, Y., YARDLEY, D., DELEU, I., PEREZ, A., BACHELOT, T., VITTORI, L., XU, Z., MUKHOPADHYAY, P., LEBWOHL, D. & HORTOBAGYI, G. N. 2012. Everolimus in postmenopausal hormone-receptor-positive advanced breast cancer. *N Engl J Med,* 366**,** 520-9.

BASELGA, J., DENT, S. F., CORTÉS, J., IM, Y.-H., DIÉRAS, V., HARBECK, N., KROP, I. E., VERMA, S., WILSON, T. R., JIN, H., WANG, L., SCHIMMOLLER, F., HSU, J. Y., HE, J.,

DELAURENTIIS, M., DRULLINSKY, P. & JACOT, W. 2018. Phase III study of taselisib (GDC-0032) + fulvestrant (FULV) v FULV in patients (pts) with estrogen receptor (ER)-positive, PIK3CA-mutant (MUT), locally advanced or metastatic breast cancer (MBC): Primary analysis from SANDPIPER. *Journal of Clinical Oncology,* 36**,** LBA1006-LBA1006.

BASELGA, J., IM, S. A., IWATA, H., CORTES, J., DE LAURENTIIS, M., JIANG, Z., ARTEAGA, C. L., JONAT, W., CLEMONS, M., ITO, Y., AWADA, A., CHIA, S., JAGIELLO-GRUSZFELD, A., PISTILLI, B., TSENG, L. M., HURVITZ, S., MASUDA, N., TAKAHASHI, M., VUYLSTEKE, P., HACHEMI, S., DHARAN, B., DI TOMASO, E., URBAN, P., MASSACESI, C. & CAMPONE, M. 2017. Buparlisib plus fulvestrant versus placebo plus fulvestrant in postmenopausal, hormone receptor-positive, HER2-negative, advanced breast cancer (BELLE-2): a randomised, double-blind, placebo-controlled, phase 3 trial. *Lancet Oncol,* 18**,** 904-916.

BAUMLI, S., LOLLI, G., LOWE, E. D., TROIANI, S., RUSCONI, L., BULLOCK, A. N., DEBRECZENI, J. E., KNAPP, S. & JOHNSON, L. N. 2008. The structure of P-TEFb (CDK9/cyclin T1), its complex with flavopiridol and regulation by phosphorylation. *EMBO J,* 27**,** 1907-18.

BEATSON, G. T. 1896. On the Treatment of Inoperable Cases of Carcinoma of the Mamma: Suggestions for a New Method of Treatment, with Illustrative Cases. *Trans Med Chir Soc Edinb,* 15**,** 153-179.

BEHBOD, F., KITTRELL, F. S., LAMARCA, H., EDWARDS, D., KERBAWY, S., HEESTAND, J. C., YOUNG, E., MUKHOPADHYAY, P., YEH, H. W., ALLRED, D. C., HU, M., POLYAK, K., ROSEN, J. M. & MEDINA, D. 2009. An intraductal human-in-mouse transplantation model mimics the subtypes of ductal carcinoma in situ. *Breast Cancer Res,* 11**,** R66.

BELLAN, C., DE FALCO, G., LAZZI, S., MICHELI, P., VICIDOMINI, S., SCHURFELD, K., AMATO, T., PALUMBO, A., BAGELLA, L., SABATTINI, E., BARTOLOMMEI, S., HUMMEL, M., PILERI, S., TOSI, P., LEONCINI, L. & GIORDANO, A. 2004. CDK9/CYCLIN T1 expression during normal lymphoid differentiation and malignant transformation. *J Pathol,* 203**,** 946-52.

BENEDETTI, L., CEREDA, M., MONTEVERDE, L., DESAI, N. & CICCARELLI, F. D. 2017. Synthetic lethal interaction between the tumour suppressor STAG2 and its paralog STAG1. *Oncotarget,* 8**,** 37619-37632.

BHATIA, S. N. & INGBER, D. E. 2014. Microfluidic organs-on-chips. *Nat Biotechnol,* 32**,** 760-72.

BIHANI, T., PATEL, H. K., ARLT, H., TAO, N., JIANG, H., BROWN, J. L., PURANDARE, D. M., HATTERSLEY, G. & GARNER, F. 2017. Elacestrant (RAD1901), a Selective Estrogen Receptor Degrader (SERD), Has Antitumor Activity in Multiple ER(+) Breast Cancer Patient-derived Xenograft Models. *Clin Cancer Res,* 23**,** 4793-4804.

BISTEAU, X., PATERNOT, S., COLLEONI, B., ECKER, K., COULONVAL, K., DE GROOTE, P., DECLERCQ, W., HENGST, L. & ROGER, P. P. 2013. CDK4 T172 phosphorylation is central in a CDK7-dependent bidirectional CDK4/CDK2 interplay mediated by p21 phosphorylation at the restriction point. *PLoS Genet,* 9**,** e1003546.

BJORNSTROM, L. & SJOBERG, M. 2005. Mechanisms of estrogen receptor signaling: convergence of genomic and nongenomic actions on target genes. *Mol Endocrinol,* 19**,** 833-42.

BLISS, C. I. 1939. THE TOXICITY OF POISONS APPLIED JOINTLY1. *Annals of Applied Biology,* 26**,** 585-615.

BOEHM, E. M., GILDENBERG, M. S. & WASHINGTON, M. T. 2016. The Many Roles of PCNA in Eukaryotic DNA Replication. *Enzymes,* 39**,** 231-54.

BOSCO, E. E., WANG, Y., XU, H., ZILFOU, J. T., KNUDSEN, K. E., ARONOW, B. J., LOWE, S. W. & KNUDSEN, E. S. 2007. The retinoblastoma tumor suppressor modifies the therapeutic response of breast cancer. *J Clin Invest,* 117**,** 218-28.

BOSKEN, C. A., FARNUNG, L., HINTERMAIR, C., MERZEL SCHACHTER, M., VOGEL-BACHMAYR, K., BLAZEK, D., ANAND, K., FISHER, R. P., EICK, D. & GEYER, M. 2014. The structure and substrate specificity of human Cdk12/Cyclin K. *Nat Commun,* 5**,** 3505.

BRISARD, D., ECKERDT, F., MARSH, L. A., BLYTH, G. T., JAIN, S., CRISTOFANILLI, M., HORIUCHI, D. & PLATANIAS, L. C. 2018. Antineoplastic effects of selective CDK9 inhibition with atuveciclib on cancer stem-like cells in triple-negative breast cancer. *Oncotarget,* 9**,** 37305-37318.

BRODIE, A., SABNIS, G. & MACEDO, L. 2007. Xenograft models for aromatase inhibitor studies. *J Steroid Biochem Mol Biol,* 106**,** 119-24.

BRONSON D, H. N., JANZEN WP, LISTER MS, MENKE K, WEGRZYN J 2001. Basic considerations in designing high-throughput screening assays. *In:* SEETHALA R, F. P. (ed.) *Handbook of Drug Screening.* New York: Marcel Decker.

BURNS, M. B., LACKEY, L., CARPENTER, M. A., RATHORE, A., LAND, A. M., LEONARD, B., REFSLAND, E. W., KOTANDENIYA, D., TRETYAKOVA, N., NIKAS, J. B., YEE, D., TEMIZ, N. A., DONOHUE, D. E., MCDOUGLE, R. M., BROWN, W. L., LAW, E. K. & HARRIS, R. S. 2013. APOBEC3B is an enzymatic source of mutation in breast cancer. *Nature,* 494**,** 366-70.

BURSTEIN, H. J., CIRRINCIONE, C. T., BARRY, W. T., CHEW, H. K., TOLANEY, S. M., LAKE, D. E., MA, C., BLACKWELL, K. L., WINER, E. P. & HUDIS, C. A. 2014. Endocrine therapy with or without inhibition of epidermal growth factor receptor and human epidermal growth factor receptor 2: a randomized, double-blind, placebo-controlled phase III trial of fulvestrant with or without lapatinib for postmenopausal women with hormone receptor-positive advanced breast cancer-CALGB 40302 (Alliance). *J Clin Oncol,* 32**,** 3959-66.

BUSHNELL, G. G., DESHMUKH, A. P., DEN HOLLANDER, P., LUO, M., SOUNDARARAJAN, R., JIA, D., LEVINE, H., MANI, S. A. & WICHA, M. S. 2021. Breast cancer dormancy: need for clinically relevant models to address current gaps in knowledge. *NPJ Breast Cancer,* 7**,** 66.

BUTT, A. J., MCNEIL, C. M., MUSGROVE, E. A. & SUTHERLAND, R. L. 2005. Downstream targets of growth factor and oestrogen signalling and endocrine resistance: the potential roles of c-Myc, cyclin D1 and cyclin E. *Endocr Relat Cancer,* 12 Suppl 1**,** S47-59.

CAGNET, S., ATACA, D., SFLOMOS, G., AOUAD, P., SCHUEPBACH-MALLEPELL, S., HUGUES, H., KRUST, A., AYYANAN, A., SCABIA, V. & BRISKEN, C. 2018. Oestrogen receptor alpha AF-1 and AF-2 domains have cell population-specific functions in the mammary epithelium. *Nat Commun,* 9**,** 4723.

CAMPBELL, R. A., BHAT-NAKSHATRI, P., PATEL, N. M., CONSTANTINIDOU, D., ALI, S. & NAKSHATRI, H. 2001. Phosphatidylinositol 3-kinase/AKT-mediated activation of estrogen receptor alpha: a new model for anti-estrogen resistance. *J Biol Chem,* 276**,** 9817-24.

CAMPONE, M., IM, S. A., IWATA, H., CLEMONS, M., ITO, Y., AWADA, A., CHIA, S., JAGIELLO-GRUSZFELD, A., PISTILLI, B., TSENG, L. M., HURVITZ, S., MASUDA, N., CORTES, J., DE LAURENTIIS, M., ARTEAGA, C. L., JIANG, Z., JONAT, W., LE

MOUHAER, S., SANKARAN, B., BOURDEAU, L., EL-HASHIMY, M., SELLAMI, D. & BASELGA, J. 2018. Buparlisib plus fulvestrant versus placebo plus fulvestrant for postmenopausal, hormone receptor-positive, human epidermal growth factor receptor 2-negative, advanced breast cancer: Overall survival results from BELLE-2. *Eur J Cancer,* 103**,** 147-154.

CANCEMI, P., BUTTACAVOLI, M., ROZ, E. & FEO, S. 2019. Expression of Alpha-Enolase (ENO1), Myc Promoter-Binding Protein-1 (MBP-1) and Matrix Metalloproteinases (MMP-2 and MMP-9) Reflect the Nature and Aggressiveness of Breast Tumors. *Int J Mol Sci,* 20.

CANCER GENOME ATLAS, N. 2012. Comprehensive molecular portraits of human breast tumours. *Nature,* 490**,** 61-70.

CANCER RESEARCH UK. 2020. *Breast Cancer Statistics* [Online]. Available: https://www.cancerresearchuk.org/health-professional/cancer-statistics/statistics-by-cancer-type/breast-cancer#heading-Zero [Accessed].

CAO, Y., ZHANG, W., JIN, Y. T. & ZOU, Q. 2020. Mining the Prognostic Value of HNRNPAB and Its Function in Breast Carcinoma. *Int J Genomics,* 2020**,** 3750673.

CARDOSO, F., HARBECK, N., FALLOWFIELD, L., KYRIAKIDES, S., SENKUS, E. & GROUP, E. G. W. 2012. Locally recurrent or metastatic breast cancer: ESMO Clinical Practice Guidelines for diagnosis, treatment and follow-up. *Ann Oncol,* 23 Suppl 7**,** vii11-9.

CARDOSO, F., KYRIAKIDES, S., OHNO, S., PENAULT-LLORCA, F., POORTMANS, P., RUBIO, I. T., ZACKRISSON, S., SENKUS, E. & CLINICALGUIDELINES@ESMO.ORG, E. G. C. E. A. 2019. Early breast cancer: ESMO Clinical Practice Guidelines for diagnosis, treatment and follow-updagger. *Ann Oncol,* 30**,** 1194-1220.

CARIOU, S., DONOVAN, J. C., FLANAGAN, W. M., MILIC, A., BHATTACHARYA, N. & SLINGERLAND, J. M. 2000. Down-regulation of p21WAF1/CIP1 or p27Kip1 abrogates antiestrogen-mediated cell cycle arrest in human breast cancer cells. *Proc Natl Acad Sci U S A,* 97**,** 9042-6.

CARPTEN, J. D., FABER, A. L., HORN, C., DONOHO, G. P., BRIGGS, S. L., ROBBINS, C. M., HOSTETTER, G., BOGUSLAWSKI, S., MOSES, T. Y., SAVAGE, S., UHLIK, M., LIN, A., DU, J., QIAN, Y. W., ZECKNER, D. J., TUCKER-KELLOGG, G., TOUCHMAN, J., PATEL, K., MOUSSES, S., BITTNER, M., SCHEVITZ, R., LAI, M. H., BLANCHARD, K. L. & THOMAS, J. E. 2007. A transforming mutation in the pleckstrin homology domain of AKT1 in cancer. *Nature,* 448**,** 439-44.

CARRACEDO, A., MA, L., TERUYA-FELDSTEIN, J., ROJO, F., SALMENA, L., ALIMONTI, A., EGIA, A., SASAKI, A. T., THOMAS, G., KOZMA, S. C., PAPA, A., NARDELLA, C., CANTLEY, L. C., BASELGA, J. & PANDOLFI, P. P. 2008. Inhibition of mTORC1 leads to MAPK pathway activation through a PI3K-dependent feedback loop in human cancer. *J Clin Invest,* 118**,** 3065-74.

CARROLL, J. S., LIU, X. S., BRODSKY, A. S., LI, W., MEYER, C. A., SZARY, A. J., EECKHOUTE, J., SHAO, W., HESTERMANN, E. V., GEISTLINGER, T. R., FOX, E. A., SILVER, P. A. & BROWN, M. 2005. Chromosome-wide mapping of estrogen receptor binding reveals long-range regulation requiring the forkhead protein FoxA1. *Cell,* 122**,** 33-43.

CARVALHO, M. R., BARATA, D., TEIXEIRA, L. M., GISELBRECHT, S., REIS, R. L., OLIVEIRA, J. M., TRUCKENMULLER, R. & HABIBOVIC, P. 2019. Colorectal tumor-on-a-chip system: A 3D tool for precision onco-nanomedicine. *Sci Adv,* 5**,** eaaw1317.

CASTANEDA, C. A., ANDRES, E., BARCENA, C., GOMEZ, H. L., CORTES-FUNES, H. & CIRUELOS, E. 2012. Behaviour of breast cancer molecular subtypes through tumour progression. *Clin Transl Oncol,* 14**,** 481-5.

CASTEDO, M., PERFETTINI, J. L., ROUMIER, T., ANDREAU, K., MEDEMA, R. & KROEMER, G. 2004. Cell death by mitotic catastrophe: a molecular definition. *Oncogene,* 23**,** 2825-37.

CEN, L., CARLSON, B. L., SCHROEDER, M. A., OSTREM, J. L., KITANGE, G. J., MLADEK, A. C., FINK, S. R., DECKER, P. A., WU, W., KIM, J. S., WALDMAN, T., JENKINS, R. B. & SARKARIA, J. N. 2012. p16-Cdk4-Rb axis controls sensitivity to a cyclin-dependent kinase inhibitor PD0332991 in glioblastoma xenograft cells. *Neuro Oncol,* 14**,** 870-81.

CERTO, M., DEL GAIZO MOORE, V., NISHINO, M., WEI, G., KORSMEYER, S., ARMSTRONG, S. A. & LETAI, A. 2006. Mitochondria primed by death signals determine cellular addiction to antiapoptotic BCL-2 family members. *Cancer Cell,* 9**,** 351-65.

CESARZ, Z., FUNNELL, J. L., GUAN, J. & TAMAMA, K. 2016. Soft Elasticity-Associated Signaling and Bone Morphogenic Protein 2 Are Key Regulators of Mesenchymal Stem Cell Spheroidal Aggregates. *Stem Cells Dev,* 25**,** 622-35.

CHAKRABARTY, A., SANCHEZ, V., KUBA, M. G., RINEHART, C. & ARTEAGA, C. L. 2012. Feedback upregulation of HER3 (ErbB3) expression and activity attenuates antitumor effect of PI3K inhibitors. *Proc Natl Acad Sci U S A,* 109**,** 2718-23.

CHAN, C. M., MARTIN, L. A., JOHNSTON, S. R., ALI, S. & DOWSETT, M. 2002. Molecular changes associated with the acquisition of oestrogen hypersensitivity in MCF-7 breast cancer cells on long-term oestrogen deprivation. *J Steroid Biochem Mol Biol,* 81**,** 333-41.

CHANDARLAPATY, S., CHEN, D., HE, W., SUNG, P., SAMOILA, A., YOU, D., BHATT, T., PATEL, P., VOI, M., GNANT, M., HORTOBAGYI, G., BASELGA, J. & MOYNAHAN, M. E. 2016. Prevalence of ESR1 Mutations in Cell-Free DNA and Outcomes in Metastatic Breast Cancer: A Secondary Analysis of the BOLERO-2 Clinical Trial. *JAMA Oncol,* 2**,** 1310-1315.

CHANDARLAPATY, S., SAWAI, A., SCALTRITI, M., RODRIK-OUTMEZGUINE, V., GRBOVIC-HUEZO, O., SERRA, V., MAJUMDER, P. K., BASELGA, J. & ROSEN, N. 2011. AKT inhibition relieves feedback suppression of receptor tyrosine kinase expression and activity. *Cancer Cell,* 19**,** 58-71.

CHANG, B., CHEN, Y., ZHAO, Y. & BRUICK, R. K. 2007. JMJD6 is a histone arginine demethylase. *Science,* 318**,** 444-7.

CHEASLEY, D., PEREIRA, L., SAMPURNO, S., SIEBER, O., JORISSEN, R., XU, H., GERMANN, M., YUQIAN, Y., RAMSAY, R. G. & MALATERRE, J. 2015. Defective Myb Function Ablates Cyclin E1 Expression and Perturbs Intestinal Carcinogenesis. *Mol Cancer Res,* 13**,** 1185-96.

CHEN, D., HUANG, S. M. & STALLCUP, M. R. 2000a. Synergistic, p160 coactivator-dependent enhancement of estrogen receptor function by CARM1 and p300. *J Biol Chem,* 275**,** 40810-6.

CHEN, D., RIEDL, T., WASHBROOK, E., PACE, P. E., COOMBES, R. C., EGLY, J. M. & ALI, S. 2000b. Activation of estrogen receptor alpha by S118 phosphorylation involves a ligand-dependent interaction with TFIIH and participation of CDK7. *Mol Cell,* 6**,** 127-37.

CHEN, H., LIN, R. J., SCHILTZ, R. L., CHAKRAVARTI, D., NASH, A., NAGY, L., PRIVALSKY, M. L., NAKATANI, Y. & EVANS, R. M. 1997. Nuclear receptor coactivator ACTR is a

novel histone acetyltransferase and forms a multimeric activation complex with P/CAF and CBP/p300. *Cell,* 90**,** 569-80.

CHEN, J. D. & EVANS, R. M. 1995. A transcriptional co-repressor that interacts with nuclear hormone receptors. *Nature,* 377**,** 454-7.

CHEN, R., YANG, Z. & ZHOU, Q. 2004. Phosphorylated positive transcription elongation factor b (P-TEFb) is tagged for inhibition through association with 7SK snRNA. *J Biol Chem,* 279**,** 4153-60.

CHIPUMURO, E., MARCO, E., CHRISTENSEN, C. L., KWIATKOWSKI, N., ZHANG, T., HATHEWAY, C. M., ABRAHAM, B. J., SHARMA, B., YEUNG, C., ALTABEF, A., PEREZ-ATAYDE, A., WONG, K. K., YUAN, G. C., GRAY, N. S., YOUNG, R. A. & GEORGE, R. E. 2014. CDK7 inhibition suppresses super-enhancer-linked oncogenic transcription in MYCN-driven cancer. *Cell,* 159**,** 1126-1139.

CHO, S., SCHROEDER, S., KAEHLCKE, K., KWON, H. S., PEDAL, A., HERKER, E., SCHNOELZER, M. & OTT, M. 2009. Acetylation of cyclin T1 regulates the equilibrium between active and inactive P-TEFb in cells. *EMBO J,* 28**,** 1407-17.

CIDADO, J., BOIKO, S., PROIA, T., FERGUSON, D., CRISCIONE, S. W., SAN MARTIN, M., POP-DAMKOV, P., SU, N., ROAMIO FRANKLIN, V. N., SEKHAR REDDY CHILAMAKURI, C., D'SANTOS, C. S., SHAO, W., SAEH, J. C., KOCH, R., WEINSTOCK, D. M., ZINDA, M., FAWELL, S. E. & DREW, L. 2020. AZD4573 Is a Highly Selective CDK9 Inhibitor That Suppresses MCL-1 and Induces Apoptosis in Hematologic Cancer Cells. *Clin Cancer Res,* 26**,** 922-934.

CIRILLO, L. A. & ZARET, K. S. 2004. Preparation of defined mononucleosomes, dinucleosomes, and nucleosome arrays in vitro and analysis of transcription factor binding. *Methods Enzymol,* 375**,** 131-58.

CLARKE, R., BRUNNER, N., KATZ, D., GLANZ, P., DICKSON, R. B., LIPPMAN, M. E. & KERN, F. G. 1989. The effects of a constitutive expression of transforming growth factor-alpha on the growth of MCF-7 human breast cancer cells in vitro and in vivo. *Mol Endocrinol,* 3**,** 372-80.

CLARKE, R., TYSON, J. J. & DIXON, J. M. 2015. Endocrine resistance in breast cancer--An overview and update. *Mol Cell Endocrinol,* 418 Pt 3**,** 220-34.

CLATOT, F., PERDRIX, A., AUGUSTO, L., BEAUSSIRE, L., DELACOUR, J., CALBRIX, C., SEFRIOUI, D., VIAILLY, P. J., BUBENHEIM, M., MOLDOVAN, C., ALEXANDRU, C., TENNEVET, I., RIGAL, O., GUILLEMET, C., LEHEURTEUR, M., GOUERANT, S., PETRAU, C., THERY, J. C., PICQUENOT, J. M., VEYRET, C., FREBOURG, T., JARDIN, F., SARAFAN-VASSEUR, N. & DI FIORE, F. 2016. Kinetics, prognostic and predictive values of ESR1 circulating mutations in metastatic breast cancer patients progressing on aromatase inhibitor. *Oncotarget,* 7**,** 74448-74459.

CORTES, J., CESCON, D. W., RUGO, H. S., NOWECKI, Z., IM, S. A., YUSOF, M. M., GALLARDO, C., LIPATOV, O., BARRIOS, C. H., HOLGADO, E., IWATA, H., MASUDA, N., OTERO, M. T., GOKMEN, E., LOI, S., GUO, Z., ZHAO, J., AKTAN, G., KARANTZA, V., SCHMID, P. & INVESTIGATORS, K.-. 2020. Pembrolizumab plus chemotherapy versus placebo plus chemotherapy for previously untreated locally recurrent inoperable or metastatic triple-negative breast cancer (KEYNOTE-355): a randomised, placebo-controlled, double-blind, phase 3 clinical trial. *Lancet,* 396**,** 1817-1828.

COSTA, E. C., MOREIRA, A. F., DE MELO-DIOGO, D., GASPAR, V. M., CARVALHO, M. P. & CORREIA, I. J. 2016. 3D tumor spheroids: an overview on the tools and techniques used for their analysis. *Biotechnol Adv,* 34**,** 1427-1441.

COTTU, P., MARANGONI, E., ASSAYAG, F., DE CREMOUX, P., VINCENT-SALOMON, A., GUYADER, C., DE PLATER, L., ELBAZ, C., KARBOUL, N., FONTAINE, J. J., CHATEAU-JOUBERT, S., BOUDOU-ROUQUETTE, P., ALRAN, S., DANGLES-MARIE, V., GENTIEN, D., POUPON, M. F. & DECAUDIN, D. 2012. Modeling of response to endocrine therapy in a panel of human luminal breast cancer xenografts. *Breast Cancer Res Treat,* 133**,** 595-606.

CRISTOFANILLI, M., TURNER, N. C., BONDARENKO, I., RO, J., IM, S. A., MASUDA, N., COLLEONI, M., DEMICHELE, A., LOI, S., VERMA, S., IWATA, H., HARBECK, N., ZHANG, K., THEALL, K. P., JIANG, Y., BARTLETT, C. H., KOEHLER, M. & SLAMON, D. 2016. Fulvestrant plus palbociclib versus fulvestrant plus placebo for treatment of hormone-receptor-positive, HER2-negative metastatic breast cancer that progressed on previous endocrine therapy (PALOMA-3): final analysis of the multicentre, double-blind, phase 3 randomised controlled trial. *Lancet Oncol,* 17**,** 425-439.

CUZICK, J., SESTAK, I., BAUM, M., BUZDAR, A., HOWELL, A., DOWSETT, M., FORBES, J. F. & INVESTIGATORS, A. L. 2010. Effect of anastrozole and tamoxifen as adjuvant treatment for early-stage breast cancer: 10-year analysis of the ATAC trial. *Lancet Oncol,* 11**,** 1135-41.

DAGOGO-JACK, I. & SHAW, A. T. 2018. Tumour heterogeneity and resistance to cancer therapies. *Nat Rev Clin Oncol,* 15**,** 81-94.

DAI, X., CHENG, H., BAI, Z. & LI, J. 2017. Breast Cancer Cell Line Classification and Its Relevance with Breast Tumor Subtyping. *J Cancer,* 8**,** 3131-3141.

DARBRE, P. D., CURTIS, S. & KING, R. J. 1984. Effects of estradiol and tamoxifen on human breast cancer cells in serum-free culture. *Cancer Res,* 44**,** 2790-3.

DE FALCO, G., BELLAN, C., D'AMURI, A., ANGELONI, G., LEUCCI, E., GIORDANO, A. & LEONCINI, L. 2005. Cdk9 regulates neural differentiation and its expression correlates with the differentiation grade of neuroblastoma and PNET tumors. *Cancer Biol Ther,* 4**,** 277-81.

DE LAURENTIIS, M., ARPINO, G., MASSARELLI, E., RUGGIERO, A., CARLOMAGNO, C., CIARDIELLO, F., TORTORA, G., D'AGOSTINO, D., CAPUTO, F., CANCELLO, G., MONTAGNA, E., MALORNI, L., ZINNO, L., LAURIA, R., BIANCO, A. R. & DE PLACIDO, S. 2005. A meta-analysis on the interaction between HER-2 expression and response to endocrine treatment in advanced breast cancer. *Clin Cancer Res,* 11**,** 4741-8.

DE LEEUW, R., FLACH, K., BENTIN TOALDO, C., ALEXI, X., CANISIUS, S., NEEFJES, J., MICHALIDES, R. & ZWART, W. 2013. PKA phosphorylation redirects ERalpha to promoters of a unique gene set to induce tamoxifen resistance. *Oncogene,* 32**,** 3543-51.

DEAN, J. L., MCCLENDON, A. K., HICKEY, T. E., BUTLER, L. M., TILLEY, W. D., WITKIEWICZ, A. K. & KNUDSEN, E. S. 2012. Therapeutic response to CDK4/6 inhibition in breast cancer defined by ex vivo analyses of human tumors. *Cell Cycle,* 11**,** 2756-61.

DENT, S., CORTES, J., IM, Y. H., DIERAS, V., HARBECK, N., KROP, I. E., WILSON, T. R., CUI, N., SCHIMMOLLER, F., HSU, J. Y., HE, J., DE LAURENTIIS, M., SOUSA, S., DRULLINSKY, P. & JACOT, W. 2021. Phase III randomized study of taselisib or placebo with fulvestrant in estrogen receptor-positive, PIK3CA-mutant, HER2-negative, advanced breast cancer: the SANDPIPER trial. *Ann Oncol,* 32**,** 197-207.

DHILLON, N. K. & MUDRYJ, M. 2002. Ectopic expression of cyclin E in estrogen responsive cells abrogates antiestrogen mediated growth arrest. *Oncogene,* 21**,** 4626-34.

DICKLER, M. N., TOLANEY, S. M., RUGO, H. S., CORTES, J., DIERAS, V., PATT, D., WILDIERS, H., HUDIS, C. A., O'SHAUGHNESSY, J., ZAMORA, E., YARDLEY, D. A., FRENZEL, M., KOUSTENIS, A. & BASELGA, J. 2017. MONARCH 1, A Phase II Study of Abemaciclib, a CDK4 and CDK6 Inhibitor, as a Single Agent, in Patients with Refractory HR(+)/HER2(-) Metastatic Breast Cancer. *Clin Cancer Res,* 23**,** 5218-5224.

DOHNER, H., SYMEONIDIS, A., DEEREN, D., DEMETER, J., SANZ, M. A., ANAGNOSTOPOULOS, A., ESTEVE, J., FIEDLER, W., PORKKA, K., KIM, H. J., LEE, J. H., USUKI, K., D'ARDIA, S., WON JUNG, C., SALAMERO, O., HORST, H. A., RECHER, C., ROUSSELOT, P., SANDHU, I., THEUNISSEN, K., THOL, F., DOHNER, K., TELEANU, V., DEANGELO, D. J., NAOE, T., SEKERES, M. A., BELSACK, V., GE, M., TAUBE, T. & OTTMANN, O. G. 2021. Adjunctive Volasertib in Patients With Acute Myeloid Leukemia not Eligible for Standard Induction Therapy: A Randomized, Phase 3 Trial. *Hemasphere,* 5**,** e617.

DONG, H., STROME, S. E., SALOMAO, D. R., TAMURA, H., HIRANO, F., FLIES, D. B., ROCHE, P. C., LU, J., ZHU, G., TAMADA, K., LENNON, V. A., CELIS, E. & CHEN, L. 2002. Tumor-associated B7-H1 promotes T-cell apoptosis: a potential mechanism of immune evasion. *Nat Med,* 8**,** 793-800.

DOWSETT, M., SMITH, I. E., EBBS, S. R., DIXON, J. M., SKENE, A., GRIFFITH, C., BOEDDINGHAUS, I., SALTER, J., DETRE, S., HILLS, M., ASHLEY, S., FRANCIS, S., WALSH, G. & A'HERN, R. 2006. Proliferation and apoptosis as markers of benefit in neoadjuvant endocrine therapy of breast cancer. *Clin Cancer Res,* 12**,** 1024s-1030s.

DROST, J. & CLEVERS, H. 2018. Organoids in cancer research. *Nat Rev Cancer,* 18**,** 407-418.

EBMEIER, C. C., ERICKSON, B., ALLEN, B. L., ALLEN, M. A., KIM, H., FONG, N., JACOBSEN, J. R., LIANG, K., SHILATIFARD, A., DOWELL, R. D., OLD, W. M., BENTLEY, D. L. & TAATJES, D. J. 2017. Human TFIIH Kinase CDK7 Regulates Transcription-Associated Chromatin Modifications. *Cell Rep,* 20**,** 1173-1186.

ELLIS, M. J., TAO, Y., LUO, J., A'HERN, R., EVANS, D. B., BHATNAGAR, A. S., CHAUDRI ROSS, H. A., VON KAMEKE, A., MILLER, W. R., SMITH, I., EIERMANN, W. & DOWSETT, M. 2008. Outcome prediction for estrogen receptor-positive breast cancer based on postneoadjuvant endocrine therapy tumor characteristics. *J Natl Cancer Inst,* 100**,** 1380-8.

FARMER, H., MCCABE, N., LORD, C. J., TUTT, A. N., JOHNSON, D. A., RICHARDSON, T. B., SANTAROSA, M., DILLON, K. J., HICKSON, I., KNIGHTS, C., MARTIN, N. M., JACKSON, S. P., SMITH, G. C. & ASHWORTH, A. 2005. Targeting the DNA repair defect in BRCA mutant cells as a therapeutic strategy. *Nature,* 434**,** 917-21.

FDA. 2014. *Clinical Pharmacology Review of Palbociclib (Ibrance)* [Online]. Available: https://www.accessdata.fda.gov/drugsatfda_docs/nda/2015/207103orig1s000clinpharmr.pdf [Accessed].

FINN, R. S., CROWN, J. P., LANG, I., BOER, K., BONDARENKO, I. M., KULYK, S. O., ETTL, J., PATEL, R., PINTER, T., SCHMIDT, M., SHPARYK, Y., THUMMALA, A. R., VOYTKO, N. L., FOWST, C., HUANG, X., KIM, S. T., RANDOLPH, S. & SLAMON, D. J. 2015. The cyclin-dependent kinase 4/6 inhibitor palbociclib in combination with letrozole versus letrozole alone as first-line treatment of oestrogen receptor-positive, HER2-negative, advanced breast cancer (PALOMA-1/TRIO-18): a randomised phase 2 study. *Lancet Oncol,* 16**,** 25-35.

FLANAGAN, J., QIAN, Y., GOUGH, S., ANDREOLI, M., BOOKBINDER, M., CADELINA, G., BRADLEY, J., ROUSSEAU, E., WILLARD, R., PIZZANO, J., CREWS, C., CREW, A.,

TAYLOR, I. & HOUSTON, J. 2019. Abstract P5-04-18: ARV-471, an oral estrogen receptor PROTAC degrader for breast cancer. *Cancer Research,* 79**,** P5-04-18-P5-04-18.

FOX, S., FARR-JONES, S. & YUND, M. A. 1999. High Throughput Screening for Drug Discovery: Continually Transitioning into New Technology. *J Biomol Screen,* 4**,** 183-186.

FRANKISH, A., DIEKHANS, M., FERREIRA, A. M., JOHNSON, R., JUNGREIS, I., LOVELAND, J., MUDGE, J. M., SISU, C., WRIGHT, J., ARMSTRONG, J., BARNES, I., BERRY, A., BIGNELL, A., CARBONELL SALA, S., CHRAST, J., CUNNINGHAM, F., DI DOMENICO, T., DONALDSON, S., FIDDES, I. T., GARCIA GIRON, C., GONZALEZ, J. M., GREGO, T., HARDY, M., HOURLIER, T., HUNT, T., IZUOGU, O. G., LAGARDE, J., MARTIN, F. J., MARTINEZ, L., MOHANAN, S., MUIR, P., NAVARRO, F. C. P., PARKER, A., PEI, B., POZO, F., RUFFIER, M., SCHMITT, B. M., STAPLETON, E., SUNER, M. M., SYCHEVA, I., USZCZYNSKA-RATAJCZAK, B., XU, J., YATES, A., ZERBINO, D., ZHANG, Y., AKEN, B., CHOUDHARY, J. S., GERSTEIN, M., GUIGO, R., HUBBARD, T. J. P., KELLIS, M., PATEN, B., REYMOND, A., TRESS, M. L. & FLICEK, P. 2019. GENCODE reference annotation for the human and mouse genomes. *Nucleic Acids Res,* 47**,** D766-D773.

FRASOR, J., WEAVER, A. E., PRADHAN, M. & MEHTA, K. 2008. Synergistic up-regulation of prostaglandin E synthase expression in breast cancer cells by 17beta-estradiol and proinflammatory cytokines. *Endocrinology,* 149**,** 6272-9.

FREEMAN, A. E. & HOFFMAN, R. M. 1986. In vivo-like growth of human tumors in vitro. *Proc Natl Acad Sci U S A,* 83**,** 2694-8.

FRIBBENS, C., O'LEARY, B., KILBURN, L., HREBIEN, S., GARCIA-MURILLAS, I., BEANEY, M., CRISTOFANILLI, M., ANDRE, F., LOI, S., LOIBL, S., JIANG, J., BARTLETT, C. H., KOEHLER, M., DOWSETT, M., BLISS, J. M., JOHNSTON, S. R. & TURNER, N. C. 2016. Plasma ESR1 Mutations and the Treatment of Estrogen Receptor-Positive Advanced Breast Cancer. *J Clin Oncol,* 34**,** 2961-8.

FRIEDEL, G., PASTORINO, U., GINSBERG, R. J., GOLDSTRAW, P., JOHNSTON, M., PASS, H., PUTNAM, J. B., TOOMES, H. & INTERNATIONAL REGISTRY OF LUNG METASTASES, L. E. 2002. Results of lung metastasectomy from breast cancer: prognostic criteria on the basis of 467 cases of the International Registry of Lung Metastases. *Eur J Cardiothorac Surg,* 22**,** 335-44.

FRIEDRICH, J., SEIDEL, C., EBNER, R. & KUNZ-SCHUGHART, L. A. 2009. Spheroid-based drug screen: considerations and practical approach. *Nat Protoc,* 4**,** 309-24.

FU, J., YOON, H. G., QIN, J. & WONG, J. 2007. Regulation of P-TEFb elongation complex activity by CDK9 acetylation. *Mol Cell Biol,* 27**,** 4641-51.

FU, T. J., PENG, J., LEE, G., PRICE, D. H. & FLORES, O. 1999. Cyclin K functions as a CDK9 regulatory subunit and participates in RNA polymerase II transcription. *J Biol Chem,* 274**,** 34527-30.

FUJINAGA, K., IRWIN, D., HUANG, Y., TAUBE, R., KUROSU, T. & PETERLIN, B. M. 2004. Dynamics of human immunodeficiency virus transcription: P-TEFb phosphorylates RD and dissociates negative effectors from the transactivation response element. *Mol Cell Biol,* 24**,** 787-95.

GAINOR, J. F., DARDAEI, L., YODA, S., FRIBOULET, L., LESHCHINER, I., KATAYAMA, R., DAGOGO-JACK, I., GADGEEL, S., SCHULTZ, K., SINGH, M., CHIN, E., PARKS, M., LEE, D., DICECCA, R. H., LOCKERMAN, E., HUYNH, T., LOGAN, J., RITTERHOUSE, L. L., LE, L. P., MUNIAPPAN, A., DIGUMARTHY, S., CHANNICK, C., KEYES, C., GETZ, G., DIAS-SANTAGATA, D., HEIST, R. S., LENNERZ, J., SEQUIST, L. V., BENES, C. H.,

IAFRATE, A. J., MINO-KENUDSON, M., ENGELMAN, J. A. & SHAW, A. T. 2016. Molecular Mechanisms of Resistance to First- and Second-Generation ALK Inhibitors in ALK-Rearranged Lung Cancer. *Cancer Discov,* 6**,** 1118-1133.

GARRETT, S., BARTON, W. A., KNIGHTS, R., JIN, P., MORGAN, D. O. & FISHER, R. P. 2001. Reciprocal activation by cyclin-dependent kinases 2 and 7 is directed by substrate specificity determinants outside the T loop. *Mol Cell Biol,* 21**,** 88-99.

GENNARI, R., MENARD, S., FAGNONI, F., PONCHIO, L., SCELSI, M., TAGLIABUE, E., CASTIGLIONI, F., VILLANI, L., MAGALOTTI, C., GIBELLI, N., OLIVIERO, B., BALLARDINI, B., DA PRADA, G., ZAMBELLI, A. & COSTA, A. 2004. Pilot study of the mechanism of action of preoperative trastuzumab in patients with primary operable breast tumors overexpressing HER2. *Clin Cancer Res,* 10**,** 5650-5.

GERLINGER, M., HORSWELL, S., LARKIN, J., ROWAN, A. J., SALM, M. P., VARELA, I., FISHER, R., MCGRANAHAN, N., MATTHEWS, N., SANTOS, C. R., MARTINEZ, P., PHILLIMORE, B., BEGUM, S., RABINOWITZ, A., SPENCER-DENE, B., GULATI, S., BATES, P. A., STAMP, G., PICKERING, L., GORE, M., NICOL, D. L., HAZELL, S., FUTREAL, P. A., STEWART, A. & SWANTON, C. 2014. Genomic architecture and evolution of clear cell renal cell carcinomas defined by multiregion sequencing. *Nat Genet,* 46**,** 225-233.

GILLET, J. P., CALCAGNO, A. M., VARMA, S., MARINO, M., GREEN, L. J., VORA, M. I., PATEL, C., ORINA, J. N., ELISEEVA, T. A., SINGAL, V., PADMANABHAN, R., DAVIDSON, B., GANAPATHI, R., SOOD, A. K., RUEDA, B. R., AMBUDKAR, S. V. & GOTTESMAN, M. M. 2011. Redefining the relevance of established cancer cell lines to the study of mechanisms of clinical anti-cancer drug resistance. *Proc Natl Acad Sci U S A,* 108**,** 18708-13.

GLASER, S. P., LEE, E. F., TROUNSON, E., BOUILLET, P., WEI, A., FAIRLIE, W. D., IZON, D. J., ZUBER, J., RAPPAPORT, A. R., HEROLD, M. J., ALEXANDER, W. S., LOWE, S. W., ROBB, L. & STRASSER, A. 2012. Anti-apoptotic Mcl-1 is essential for the development and sustained growth of acute myeloid leukemia. *Genes Dev,* 26**,** 120-5.

GLOVER-CUTTER, K., LAROCHELLE, S., ERICKSON, B., ZHANG, C., SHOKAT, K., FISHER, R. P. & BENTLEY, D. L. 2009. TFIIH-associated Cdk7 kinase functions in phosphorylation of C-terminal domain Ser7 residues, promoter-proximal pausing, and termination by RNA polymerase II. *Mol Cell Biol,* 29**,** 5455-64.

GOLDGAR, D. E., FIELDS, P., LEWIS, C. M., TRAN, T. D., CANNON-ALBRIGHT, L. A., WARD, J. H., SWENSEN, J. & SKOLNICK, M. H. 1994. A large kindred with 17q-linked breast and ovarian cancer: genetic, phenotypic, and genealogical analysis. *J Natl Cancer Inst,* 86**,** 200-9.

GOMPEL, A., SOMAI, S., CHAOUAT, M., KAZEM, A., KLOOSTERBOER, H. J., BEUSMAN, I., FORGEZ, P., MIMOUN, M. & ROSTENE, W. 2000. Hormonal regulation of apoptosis in breast cells and tissues. *Steroids,* 65**,** 593-8.

GONZALEZ-LOYOLA, A., FERNANDEZ-MIRANDA, G., TRAKALA, M., PARTIDA, D., SAMEJIMA, K., OGAWA, H., CANAMERO, M., DE MARTINO, A., MARTINEZ-RAMIREZ, A., DE CARCER, G., PEREZ DE CASTRO, I., EARNSHAW, W. C. & MALUMBRES, M. 2015. Aurora B Overexpression Causes Aneuploidy and p21Cip1 Repression during Tumor Development. *Mol Cell Biol,* 35**,** 3566-78.

GOTTLICHER, M., HECK, S. & HERRLICH, P. 1998. Transcriptional cross-talk, the second mode of steroid hormone receptor action. *J Mol Med (Berl),* 76**,** 480-9.

GRESSEL, S., SCHWALB, B., DECKER, T. M., QIN, W., LEONHARDT, H., EICK, D. & CRAMER, P. 2017. CDK9-dependent RNA polymerase II pausing controls transcription initiation. *Elife,* 6.

GROEBE, K. & MUELLER-KLIESER, W. 1991. Distributions of oxygen, nutrient, and metabolic waste concentrations in multicellular spheroids and their dependence on spheroid parameters. *Eur Biophys J,* 19**,** 169-81.

GU, B., EICK, D. & BENSAUDE, O. 2013. CTD serine-2 plays a critical role in splicing and termination factor recruitment to RNA polymerase II in vivo. *Nucleic Acids Res,* 41**,** 1591-603.

GU, H., TU, H., LIU, L., LIU, T., LIU, Z., ZHANG, W. & LIU, J. 2020. RSPO3 is a marker candidate for predicting tumor aggressiveness in ovarian cancer. *Ann Transl Med,* 8**,** 1351.

GUILLEN, K. P., FUJITA, M., BUTTERFIELD, A. J., SCHERER, S. D., BAILEY, M. H., CHU, Z., DEROSE, Y. S., ZHAO, L., CORTES-SANCHEZ, E., YANG, C.-H., TONER, J., WANG, G., QIAO, Y., HUANG, X., GREENLAND, J. A., VAHRENKAMP, J. M., LUM, D. H., FACTOR, R. E., NELSON, E. W., MATSEN, C. B., PORETTA, J. M., ROSENTHAL, R., BECK, A. C., BUYS, S. S., VAKLAVAS, C., WARD, J. H., JENSEN, R. L., JONES, K. B., LI, Z., OESTERREICH, S., DOBROLECKI, L. E., PATHI, S. S., WOO, X. Y., BERRETT, K. C., WADSWORTH, M. E., CHUANG, J. H., LEWIS, M. T., MARTH, G. T., GERTZ, J., VARLEY, K. E., WELM, B. E. & WELM, A. L. 2021. A breast cancer patient-derived xenograft and organoid platform for drug discovery and precision oncology. *bioRxiv***,** 2021.02.28.433268.

HAFNER, M., MILLS, C. E., SUBRAMANIAN, K., CHEN, C., CHUNG, M., BOSWELL, S. A., EVERLEY, R. A., LIU, C., WALMSLEY, C. S., JURIC, D. & SORGER, P. K. 2019. Multiomics Profiling Establishes the Polypharmacology of FDA-Approved CDK4/6 Inhibitors and the Potential for Differential Clinical Activity. *Cell Chem Biol,* 26**,** 1067-1080 e8.

HAIBE-KAINS, B., DESMEDT, C., LOI, S., CULHANE, A. C., BONTEMPI, G., QUACKENBUSH, J. & SOTIRIOU, C. 2012. A three-gene model to robustly identify breast cancer molecular subtypes. *J Natl Cancer Inst,* 104**,** 311-25.

HALL, A. E., LU, W. T., GODFREY, J. D., ANTONOV, A. V., PAICU, C., MOXON, S., DALMAY, T., WILCZYNSKA, A., MULLER, P. A. & BUSHELL, M. 2016. The cytoskeleton adaptor protein ankyrin-1 is upregulated by p53 following DNA damage and alters cell migration. *Cell Death Dis,* 7**,** e2184.

HAMILTON, E. P., PATEL, M. R., ARMSTRONG, A. C., BAIRD, R. D., JHAVERI, K., HOCH, M., KLINOWSKA, T., LINDEMANN, J. P. O., MORGAN, S. R., SCHIAVON, G., WEIR, H. M. & IM, S. A. 2018. A First-in-Human Study of the New Oral Selective Estrogen Receptor Degrader AZD9496 for ER(+)/HER2(-) Advanced Breast Cancer. *Clin Cancer Res,* 24**,** 3510-3518.

HANAHAN, D. & WEINBERG, R. A. 2000. The hallmarks of cancer. *Cell,* 100**,** 57-70.

HANAHAN, D. & WEINBERG, R. A. 2011. Hallmarks of cancer: the next generation. *Cell,* 144**,** 646-74.

HANSTEIN, B., ECKNER, R., DIRENZO, J., HALACHMI, S., LIU, H., SEARCY, B., KUROKAWA, R. & BROWN, M. 1996. p300 is a component of an estrogen receptor coactivator complex. *Proc Natl Acad Sci U S A,* 93**,** 11540-5.

HARBECK, N., RASTOGI, P., MARTIN, M., TOLANEY, S. M., SHAO, Z. M., FASCHING, P. A., HUANG, C. S., JALIFFE, G. G., TRYAKIN, A., GOETZ, M. P., RUGO, H. S., SENKUS, E., TESTA, L., ANDERSSON, M., TAMURA, K., DEL MASTRO, L., STEGER, G. G., KREIPE, H., HEGG, R., SOHN, J., GUARNERI, V., CORTES, J., HAMILTON, E., ANDRE, V., WEI,

R., BARRIGA, S., SHERWOOD, S., FORRESTER, T., MUNOZ, M., SHAHIR, A., SAN ANTONIO, B., NABINGER, S. C., TOI, M., JOHNSTON, S. R. D. & O'SHAUGHNESSY, J. 2021. Adjuvant Abemaciclib Combined With Endocrine Therapy for High-Risk Early Breast Cancer: Updated Efficacy and Ki-67 Analysis From the monarchE Study. *Ann Oncol*.

HARBST, K., LAUSS, M., CIRENAJWIS, H., ISAKSSON, K., ROSENGREN, F., TORNGREN, T., KVIST, A., JOHANSSON, M. C., VALLON-CHRISTERSSON, J., BALDETORP, B., BORG, A., OLSSON, H., INGVAR, C., CARNEIRO, A. & JONSSON, G. 2016. Multiregion Whole-Exome Sequencing Uncovers the Genetic Evolution and Mutational Heterogeneity of Early-Stage Metastatic Melanoma. *Cancer Res,* 76**,** 4765-74.

HARROD, A., FULTON, J., NGUYEN, V. T. M., PERIYASAMY, M., RAMOS-GARCIA, L., LAI, C. F., METODIEVA, G., DE GIORGIO, A., WILLIAMS, R. L., SANTOS, D. B., GOMEZ, P. J., LIN, M. L., METODIEV, M. V., STEBBING, J., CASTELLANO, L., MAGNANI, L., COOMBES, R. C., BULUWELA, L. & ALI, S. 2017. Genomic modelling of the ESR1 Y537S mutation for evaluating function and new therapeutic approaches for metastatic breast cancer. *Oncogene,* 36**,** 2286-2296.

HARTMAN, J., LAM, E. W., GUSTAFSSON, J. A. & STROM, A. 2009. Hes-6, an inhibitor of Hes-1, is regulated by 17beta-estradiol and promotes breast cancer cell proliferation. *Breast Cancer Res,* 11**,** R79.

HAZEL, P., KROLL, S. H., BONDKE, A., BARBAZANGES, M., PATEL, H., FUCHTER, M. J., COOMBES, R. C., ALI, S., BARRETT, A. G. & FREEMONT, P. S. 2017. Inhibitor Selectivity for Cyclin-Dependent Kinase 7: A Structural, Thermodynamic, and Modelling Study. *ChemMedChem,* 12**,** 372-380.

HERRERA-ABREU, M. T., PALAFOX, M., ASGHAR, U., RIVAS, M. A., CUTTS, R. J., GARCIA-MURILLAS, I., PEARSON, A., GUZMAN, M., RODRIGUEZ, O., GRUESO, J., BELLET, M., CORTES, J., ELLIOTT, R., PANCHOLI, S., BASELGA, J., DOWSETT, M., MARTIN, L. A., TURNER, N. C. & SERRA, V. 2016. Early Adaptation and Acquired Resistance to CDK4/6 Inhibition in Estrogen Receptor-Positive Breast Cancer. *Cancer Res,* 76**,** 2301-13.

HIDALGO, M., AMANT, F., BIANKIN, A. V., BUDINSKA, E., BYRNE, A. T., CALDAS, C., CLARKE, R. B., DE JONG, S., JONKERS, J., MAELANDSMO, G. M., ROMAN-ROMAN, S., SEOANE, J., TRUSOLINO, L. & VILLANUEVA, A. 2014. Patient-derived xenograft models: an emerging platform for translational cancer research. *Cancer Discov,* 4**,** 998-1013.

HIGGINS, M. J. & BASELGA, J. 2011. Targeted therapies for breast cancer. *Journal of Clinical Investigation,* 121**,** 3797-3803.

HILEY, C., DE BRUIN, E. C., MCGRANAHAN, N. & SWANTON, C. 2014. Deciphering intratumor heterogeneity and temporal acquisition of driver events to refine precision medicine. *Genome Biol,* 15**,** 453.

HNISZ, D., ABRAHAM, B. J., LEE, T. I., LAU, A., SAINT-ANDRE, V., SIGOVA, A. A., HOKE, H. A. & YOUNG, R. A. 2013. Super-enhancers in the control of cell identity and disease. *Cell,* 155**,** 934-47.

HOEFNAGEL, L. D., MOELANS, C. B., MEIJER, S. L., VAN SLOOTEN, H. J., WESSELING, P., WESSELING, J., WESTENEND, P. J., BART, J., SELDENRIJK, C. A., NAGTEGAAL, I. D., OUDEJANS, J., VAN DER VALK, P., VAN GILS, C. H., VAN DER WALL, E. & VAN DIEST, P. J. 2012. Prognostic value of estrogen receptor alpha and progesterone receptor conversion in distant breast cancer metastases. *Cancer,* 118**,** 4929-35.

HOLLERN, D. P., HONEYSETT, J., CARDIFF, R. D. & ANDRECHEK, E. R. 2014. The E2F transcription factors regulate tumor development and metastasis in a mouse model of metastatic breast cancer. *Mol Cell Biol,* 34**,** 3229-43.

HOLLESTELLE, A., NAGEL, J. H., SMID, M., LAM, S., ELSTRODT, F., WASIELEWSKI, M., NG, S. S., FRENCH, P. J., PEETERS, J. K., ROZENDAAL, M. J., RIAZ, M., KOOPMAN, D. G., TEN HAGEN, T. L., DE LEEUW, B. H., ZWARTHOFF, E. C., TEUNISSE, A., VAN DER SPEK, P. J., KLIJN, J. G., DINJENS, W. N., ETHIER, S. P., CLEVERS, H., JOCHEMSEN, A. G., DEN BAKKER, M. A., FOEKENS, J. A., MARTENS, J. W. & SCHUTTE, M. 2010. Distinct gene mutation profiles among luminal-type and basal-type breast cancer cell lines. *Breast Cancer Res Treat,* 121**,** 53-64.

HONG, H., KOHLI, K., TRIVEDI, A., JOHNSON, D. L. & STALLCUP, M. R. 1996. GRIP1, a novel mouse protein that serves as a transcriptional coactivator in yeast for the hormone binding domains of steroid receptors. *Proc Natl Acad Sci U S A,* 93**,** 4948-52.

HORTOBAGYI, G. N., STEMMER, S. M., BURRIS, H. A., YAP, Y. S., SONKE, G. S., PALUCH-SHIMON, S., CAMPONE, M., BLACKWELL, K. L., ANDRE, F., WINER, E. P., JANNI, W., VERMA, S., CONTE, P., ARTEAGA, C. L., CAMERON, D. A., PETRAKOVA, K., HART, L. L., VILLANUEVA, C., CHAN, A., JAKOBSEN, E., NUSCH, A., BURDAEVA, O., GRISCHKE, E. M., ALBA, E., WIST, E., MARSCHNER, N., FAVRET, A. M., YARDLEY, D., BACHELOT, T., TSENG, L. M., BLAU, S., XUAN, F., SOUAMI, F., MILLER, M., GERMA, C., HIRAWAT, S. & O'SHAUGHNESSY, J. 2016. Ribociclib as First-Line Therapy for HR-Positive, Advanced Breast Cancer. *N Engl J Med,* 375**,** 1738-1748.

HOWELL, A., ROBERTSON, J. F., QUARESMA ALBANO, J., ASCHERMANNOVA, A., MAURIAC, L., KLEEBERG, U. R., VERGOTE, I., ERIKSTEIN, B., WEBSTER, A. & MORRIS, C. 2002. Fulvestrant, formerly ICI 182,780, is as effective as anastrozole in postmenopausal women with advanced breast cancer progressing after prior endocrine treatment. *J Clin Oncol,* 20**,** 3396-403.

HOWELL, S. J., KREBS, M. G., LORD, S., KENNY, L., BAHL, A., CLACK, G., AINSCOW, E., ARKENAU, H. T., MANSI, J. L., PALMIERI, C., RICHARDS, P., JESELSOHN, R., MITRI, Z., GRADISHAR, W. J., SARDESAI, S., O'SHAUGHNESSY, J., LEHNERT, M., ALI, S., MCINTOSH, S. & COOMBES, R. C. 2021. 265P Study of samuraciclib (CT7001), a first-in-class, oral, selective inhibitor of CDK7, in combination with fulvestrant in patients with advanced hormone receptor positive HER2 negative breast cancer (HR+BC). *Annals of Oncology,* 32**,** S477-S478.

HU, S., MARINEAU, J. J., RAJAGOPAL, N., HAMMAN, K. B., CHOI, Y. J., SCHMIDT, D. R., KE, N., JOHANNESSEN, L., BRADLEY, M. J., ORLANDO, D. A., ALNEMY, S. R., REN, Y., CIBLAT, S., WINTER, D. K., KABRO, A., SPROTT, K. T., HODGSON, J. G., FRITZ, C. C., CARULLI, J. P., DI TOMASO, E. & OLSON, E. R. 2019. Discovery and Characterization of SY-1365, a Selective, Covalent Inhibitor of CDK7. *Cancer Res,* 79**,** 3479-3491.

HUI, R., FINNEY, G. L., CARROLL, J. S., LEE, C. S., MUSGROVE, E. A. & SUTHERLAND, R. L. 2002. Constitutive overexpression of cyclin D1 but not cyclin E confers acute resistance to antiestrogens in T-47D breast cancer cells. *Cancer Res,* 62**,** 6916-23.

IANEVSKI, A., GIRI, A. K. & AITTOKALLIO, T. 2020. SynergyFinder 2.0: visual analytics of multi-drug combination synergies. *Nucleic Acids Res,* 48**,** W488-W493.

IGNAR-TROWBRIDGE, D. M., NELSON, K. G., BIDWELL, M. C., CURTIS, S. W., WASHBURN, T. F., MCLACHLAN, J. A. & KORACH, K. S. 1992. Coupling of dual signaling pathways: epidermal growth factor action involves the estrogen receptor. *Proc Natl Acad Sci U S A,* 89**,** 4658-62.

IMPROTA-BREARS, T., WHORTON, A. R., CODAZZI, F., YORK, J. D., MEYER, T. & MCDONNELL, D. P. 1999. Estrogen-induced activation of mitogen-activated protein kinase requires mobilization of intracellular calcium. *Proc Natl Acad Sci U S A,* 96**,** 4686-91.

ITZEN, F., GREIFENBERG, A. K., BOSKEN, C. A. & GEYER, M. 2014. Brd4 activates P-TEFb for RNA polymerase II CTD phosphorylation. *Nucleic Acids Res,* 42**,** 7577-90.

IWAI, Y., ISHIDA, M., TANAKA, Y., OKAZAKI, T., HONJO, T. & MINATO, N. 2002. Involvement of PD-L1 on tumor cells in the escape from host immune system and tumor immunotherapy by PD-L1 blockade. *Proc Natl Acad Sci U S A,* 99**,** 12293-7.

JAMAL-HANJANI, M., WILSON, G. A., MCGRANAHAN, N., BIRKBAK, N. J., WATKINS, T. B. K., VEERIAH, S., SHAFI, S., JOHNSON, D. H., MITTER, R., ROSENTHAL, R., SALM, M., HORSWELL, S., ESCUDERO, M., MATTHEWS, N., ROWAN, A., CHAMBERS, T., MOORE, D. A., TURAJLIC, S., XU, H., LEE, S. M., FORSTER, M. D., AHMAD, T., HILEY, C. T., ABBOSH, C., FALZON, M., BORG, E., MARAFIOTI, T., LAWRENCE, D., HAYWARD, M., KOLVEKAR, S., PANAGIOTOPOULOS, N., JANES, S. M., THAKRAR, R., AHMED, A., BLACKHALL, F., SUMMERS, Y., SHAH, R., JOSEPH, L., QUINN, A. M., CROSBIE, P. A., NAIDU, B., MIDDLETON, G., LANGMAN, G., TROTTER, S., NICOLSON, M., REMMEN, H., KERR, K., CHETTY, M., GOMERSALL, L., FENNELL, D. A., NAKAS, A., RATHINAM, S., ANAND, G., KHAN, S., RUSSELL, P., EZHIL, V., ISMAIL, B., IRVIN-SELLERS, M., PRAKASH, V., LESTER, J. F., KORNASZEWSKA, M., ATTANOOS, R., ADAMS, H., DAVIES, H., DENTRO, S., TANIERE, P., O'SULLIVAN, B., LOWE, H. L., HARTLEY, J. A., ILES, N., BELL, H., NGAI, Y., SHAW, J. A., HERRERO, J., SZALLASI, Z., SCHWARZ, R. F., STEWART, A., QUEZADA, S. A., LE QUESNE, J., VAN LOO, P., DIVE, C., HACKSHAW, A., SWANTON, C. & CONSORTIUM, T. R. 2017. Tracking the Evolution of Non-Small-Cell Lung Cancer. *N Engl J Med,* 376**,** 2109-2121.

JANG, M. K., MOCHIZUKI, K., ZHOU, M., JEONG, H. S., BRADY, J. N. & OZATO, K. 2005. The bromodomain protein Brd4 is a positive regulatory component of P-TEFb and stimulates RNA polymerase II-dependent transcription. *Mol Cell,* 19**,** 523-34.

JENSEN, E. V. 1962. On the mechanism of estrogen action. *Perspect Biol Med,* 6**,** 47-59.

JESELSOHN, R., BUCHWALTER, G., DE ANGELIS, C., BROWN, M. & SCHIFF, R. 2015. ESR1 mutations-a mechanism for acquired endocrine resistance in breast cancer. *Nat Rev Clin Oncol,* 12**,** 573-83.

JESELSOHN, R., YELENSKY, R., BUCHWALTER, G., FRAMPTON, G., MERIC-BERNSTAM, F., GONZALEZ-ANGULO, A. M., FERRER-LOZANO, J., PEREZ-FIDALGO, J. A., CRISTOFANILLI, M., GOMEZ, H., ARTEAGA, C. L., GILTNANE, J., BALKO, J. M., CRONIN, M. T., JAROSZ, M., SUN, J., HAWRYLUK, M., LIPSON, D., OTTO, G., ROSS, J. S., DVIR, A., SOUSSAN-GUTMAN, L., WOLF, I., RUBINEK, T., GILMORE, L., SCHNITT, S., COME, S. E., PUSZTAI, L., STEPHENS, P., BROWN, M. & MILLER, V. A. 2014. Emergence of constitutively active estrogen receptor-alpha mutations in pretreated advanced estrogen receptor-positive breast cancer. *Clin Cancer Res,* 20**,** 1757-1767.

JIANG, L., HUANG, R., WU, Y., DIAO, P., ZHANG, W., LI, J., LI, Z., WANG, Y., CHENG, J. & YANG, J. 2019. Overexpression of CDK7 is associated with unfavourable prognosis in oral squamous cell carcinoma. *Pathology,* 51**,** 74-80.

JIANG, W., MCDONALD, D., HOPE, T. J. & HUNTER, T. 1999. Mammalian Cdc7-Dbf4 protein kinase complex is essential for initiation of DNA replication. *EMBO J,* 18**,** 5703-13.

JIN, Q., MAO, X., LI, B., GUAN, S., YAO, F. & JIN, F. 2015. Overexpression of SMARCA5 correlates with cell proliferation and migration in breast cancer. *Tumour Biol,* 36**,** 1895-902.

JOEL, P. B., SMITH, J., STURGILL, T. W., FISHER, T. L., BLENIS, J. & LANNIGAN, D. A. 1998. pp90rsk1 regulates estrogen receptor-mediated transcription through phosphorylation of Ser-167. *Mol Cell Biol,* 18**,** 1978-84.

JOHNSTON, S. R. & DOWSETT, M. 2003. Aromatase inhibitors for breast cancer: lessons from the laboratory. *Nat Rev Cancer,* 3**,** 821-31.

JOHNSTON, S. R. D., PLUARD, T. J., WANG, J. S., HAMILTON, E. P., JURIC, D., SCHOLZ, C. R., HNITECKI, E., GAO, L., CANTAGALLO, L., KORPAL, M., DESTENAVES, B., XIAO, J. A., ZHANG, Z., PIPAS, J. M. M., YU, L., SAHMOUD, T. & GUALBERTO, A. 2021. Phase 1b study of H3B-6545 in combination with palbociclib in women with metastatic estrogen receptor–positive (ER+), human epidermal growth factor receptor 2 (HER2)-negative breast cancer. *Journal of Clinical Oncology,* 39**,** e13025-e13025.

JONES, P. L. & SHI, Y. B. 2003. N-CoR-HDAC corepressor complexes: roles in transcriptional regulation by nuclear hormone receptors. *Curr Top Microbiol Immunol,* 274**,** 237-68.

JONES, R. H., CASBARD, A., CARUCCI, M., COX, C., BUTLER, R., ALCHAMI, F., MADDEN, T. A., BALE, C., BEZECNY, P., JOFFE, J., MOON, S., TWELVES, C., VENKITARAMAN, R., WATERS, S., FOXLEY, A. & HOWELL, S. J. 2020. Fulvestrant plus capivasertib versus placebo after relapse or progression on an aromatase inhibitor in metastatic, oestrogen receptor-positive breast cancer (FAKTION): a multicentre, randomised, controlled, phase 2 trial. *Lancet Oncol,* 21**,** 345-357.

JOSEPH, J. D., DARIMONT, B., ZHOU, W., ARRAZATE, A., YOUNG, A., INGALLA, E., WALTER, K., BLAKE, R. A., NONOMIYA, J., GUAN, Z., KATEGAYA, L., GOVEK, S. P., LAI, A. G., KAHRAMAN, M., BRIGHAM, D., SENSINTAFFAR, J., LU, N., SHAO, G., QIAN, J., GRILLOT, K., MOON, M., PRUDENTE, R., BISCHOFF, E., LEE, K. J., BONNEFOUS, C., DOUGLAS, K. L., JULIEN, J. D., NAGASAWA, J. Y., APARICIO, A., KAUFMAN, J., HALEY, B., GILTNANE, J. M., WERTZ, I. E., LACKNER, M. R., NANNINI, M. A., SAMPATH, D., SCHWARZ, L., MANNING, H. C., TANTAWY, M. N., ARTEAGA, C. L., HEYMAN, R. A., RIX, P. J., FRIEDMAN, L., SMITH, N. D., METCALFE, C. & HAGER, J. H. 2016. The selective estrogen receptor downregulator GDC-0810 is efficacious in diverse models of ER+ breast cancer. *Elife,* 5.

KAELIN, W. G., JR. 2009. Synthetic lethality: a framework for the development of wiser cancer therapeutics. *Genome Med,* 1**,** 99.

KATO, S., ENDOH, H., MASUHIRO, Y., KITAMOTO, T., UCHIYAMA, S., SASAKI, H., MASUSHIGE, S., GOTOH, Y., NISHIDA, E., KAWASHIMA, H., METZGER, D. & CHAMBON, P. 1995. Activation of the estrogen receptor through phosphorylation by mitogen-activated protein kinase. *Science,* 270**,** 1491-4.

KAUFMAN, B., MACKEY, J. R., CLEMENS, M. R., BAPSY, P. P., VAID, A., WARDLEY, A., TJULANDIN, S., JAHN, M., LEHLE, M., FEYEREISLOVA, A., REVIL, C. & JONES, A. 2009. Trastuzumab plus anastrozole versus anastrozole alone for the treatment of postmenopausal women with human epidermal growth factor receptor 2-positive, hormone receptor-positive metastatic breast cancer: results from the randomized phase III TAnDEM study. *J Clin Oncol,* 27**,** 5529-37.

KEIR, M. E., BUTTE, M. J., FREEMAN, G. J. & SHARPE, A. H. 2008. PD-1 and its ligands in tolerance and immunity. *Annu Rev Immunol,* 26**,** 677-704.

KHAN, S. A., ZHAO, F., SOLIN, L. J., GOLDSTEIN, L. J., CELLA, D., BASIK, M., GOLSHAN, M., JULIAN, T. B., POCKAJ, B. A., LEE, C. A., RAZAQ, W., SPARANO, J. A., BABIERA, G. V., DY, I. A., JAIN, S., SILVERMAN, P., FISHER, C., TEVAARWERK, A. J., WAGNER, L. I. & SLEDGE, G. W. 2020. A randomized phase III trial of systemic therapy plus early local therapy versus systemic therapy alone in women with de novo stage IV breast cancer: A trial of the ECOG-ACRIN Research Group (E2108). *Journal of Clinical Oncology,* 38**,** LBA2-LBA2.

KLIMCZAK, M., BIECEK, P., ZYLICZ, A. & ZYLICZ, M. 2019. Heat shock proteins create a signature to predict the clinical outcome in breast cancer. *Sci Rep,* 9**,** 7507.

KNOWLDEN, J. M., HUTCHESON, I. R., JONES, H. E., MADDEN, T., GEE, J. M., HARPER, M. E., BARROW, D., WAKELING, A. E. & NICHOLSON, R. I. 2003. Elevated levels of epidermal growth factor receptor/c-erbB2 heterodimers mediate an autocrine growth regulatory pathway in tamoxifen-resistant MCF-7 cells. *Endocrinology,* 144**,** 1032-44.

KOCH, J., MONCH, D., MAASS, A., GROMOLL, C., HEHR, T., LEIBOLD, T., SCHLITT, H. J., DAHLKE, M. H. & RENNER, P. 2021. Three dimensional cultivation increases chemo- and radioresistance of colorectal cancer cell lines. *PLoS One,* 16**,** e0244513.

KOEBERLE, D., RUHSTALLER, T., JOST, L., PAGANI, O., ZAMAN, K., VON MOOS, R., OEHLSCHLEGEL, C., CROWE, S., PILOP, C., THUERLIMANN, B. & SWISS GROUP FOR CLINICAL CANCER, R. 2011. Combination of trastuzumab and letrozole after resistance to sequential trastuzumab and aromatase inhibitor monotherapies in patients with estrogen receptor-positive, HER-2-positive advanced breast cancer: a proof-of-concept trial (SAKK 23/03). *Endocr Relat Cancer,* 18**,** 257-64.

KORKMAZ, G., MANBER, Z., LOPES, R., PREKOVIC, S., SCHUURMAN, K., KIM, Y., TEUNISSEN, H., FLACH, K., WIT, E., GALLI, G. G., ZWART, W., ELKON, R. & AGAMI, R. 2019. A CRISPR-Cas9 screen identifies essential CTCF anchor sites for estrogen receptor-driven breast cancer cell proliferation. *Nucleic Acids Res,* 47**,** 9557-9572.

KOUNDOUROS, N., KARALI, E., TRIPP, A., VALLE, A., INGLESE, P., PERRY, N. J. S., MAGEE, D. J., ANJOMANI VIRMOUNI, S., ELDER, G. A., TYSON, A. L., DORIA, M. L., VAN WEVERWIJK, A., SOARES, R. F., ISACKE, C. M., NICHOLSON, J. K., GLEN, R. C., TAKATS, Z. & POULOGIANNIS, G. 2020. Metabolic Fingerprinting Links Oncogenic PIK3CA with Enhanced Arachidonic Acid-Derived Eicosanoids. *Cell,* 181**,** 1596-1611 e27.

KOUSTENI, S., BELLIDO, T., PLOTKIN, L. I., O'BRIEN, C. A., BODENNER, D. L., HAN, L., HAN, K., DIGREGORIO, G. B., KATZENELLENBOGEN, J. A., KATZENELLENBOGEN, B. S., ROBERSON, P. K., WEINSTEIN, R. S., JILKA, R. L. & MANOLAGAS, S. C. 2001. Nongenotropic, sex-nonspecific signaling through the estrogen or androgen receptors: dissociation from transcriptional activity. *Cell,* 104**,** 719-30.

KROP, I. E., MAYER, I. A., GANJU, V., DICKLER, M., JOHNSTON, S., MORALES, S., YARDLEY, D. A., MELICHAR, B., FORERO-TORRES, A., LEE, S. C., DE BOER, R., PETRAKOVA, K., VALLENTIN, S., PEREZ, E. A., PICCART, M., ELLIS, M., WINER, E., GENDREAU, S., DERYNCK, M., LACKNER, M., LEVY, G., QIU, J., HE, J. & SCHMID, P. 2016. Pictilisib for oestrogen receptor-positive, aromatase inhibitor-resistant, advanced or metastatic breast cancer (FERGI): a randomised, double-blind, placebo-controlled, phase 2 trial. *Lancet Oncol,* 17**,** 811-821.

KRUEGER, F. 2019. Available: https://www.bioinformatics.babraham.ac.uk/projects/trim_galore/ [Accessed August 2019 2021].

KUMAR, V., GREEN, S., STACK, G., BERRY, M., JIN, J. R. & CHAMBON, P. 1987. Functional domains of the human estrogen receptor. *Cell,* 51**,** 941-51.

KUNZ-SCHUGHART, L. A., KREUTZ, M. & KNUECHEL, R. 1998. Multicellular spheroids: a three-dimensional in vitro culture system to study tumour biology. *Int J Exp Pathol,* 79**,** 1-23.

KUONG, K. J. & LOEB, L. A. 2013. APOBEC3B mutagenesis in cancer. *Nat Genet,* 45**,** 964-5.

KWIATKOWSKI, N., ZHANG, T., RAHL, P. B., ABRAHAM, B. J., REDDY, J., FICARRO, S. B., DASTUR, A., AMZALLAG, A., RAMASWAMY, S., TESAR, B., JENKINS, C. E., HANNETT, N. M., MCMILLIN, D., SANDA, T., SIM, T., KIM, N. D., LOOK, T., MITSIADES, C. S., WENG, A. P., BROWN, J. R., BENES, C. H., MARTO, J. A., YOUNG, R. A. & GRAY, N. S. 2014. Targeting transcription regulation in cancer with a covalent CDK7 inhibitor. *Nature,* 511**,** 616-20.

LAITEM, C., ZABOROWSKA, J., ISA, N. F., KUFS, J., DIENSTBIER, M. & MURPHY, S. 2015. CDK9 inhibitors define elongation checkpoints at both ends of RNA polymerase II-transcribed genes. *Nat Struct Mol Biol,* 22**,** 396-403.

LANGER, E. M., ALLEN-PETERSEN, B. L., KING, S. M., KENDSERSKY, N. D., TURNIDGE, M. A., KUZIEL, G. M., RIGGERS, R., SAMATHAM, R., AMERY, T. S., JACQUES, S. L., SHEPPARD, B. C., KORKOLA, J. E., MUSCHLER, J. L., THIBAULT, G., CHANG, Y. H., GRAY, J. W., PRESNELL, S. C., NGUYEN, D. G. & SEARS, R. C. 2019. Modeling Tumor Phenotypes In Vitro with Three-Dimensional Bioprinting. *Cell Rep,* 26**,** 608-623 e6.

LAROCHELLE, S., AMAT, R., GLOVER-CUTTER, K., SANSO, M., ZHANG, C., ALLEN, J. J., SHOKAT, K. M., BENTLEY, D. L. & FISHER, R. P. 2012. Cyclin-dependent kinase control of the initiation-to-elongation switch of RNA polymerase II. *Nat Struct Mol Biol,* 19**,** 1108-15.

LAROCHELLE, S., CHEN, J., KNIGHTS, R., PANDUR, J., MORCILLO, P., ERDJUMENT-BROMAGE, H., TEMPST, P., SUTER, B. & FISHER, R. P. 2001. T-loop phosphorylation stabilizes the CDK7-cyclin H-MAT1 complex in vivo and regulates its CTD kinase activity. *EMBO J,* 20**,** 3749-59.

LEE, J. J., LOH, K. & YAP, Y. S. 2015. PI3K/Akt/mTOR inhibitors in breast cancer. *Cancer Biol Med,* 12**,** 342-54.

LEE, Y. R., PARK, J., YU, H. N., KIM, J. S., YOUN, H. J. & JUNG, S. H. 2005. Up-regulation of PI3K/Akt signaling by 17beta-estradiol through activation of estrogen receptor-alpha, but not estrogen receptor-beta, and stimulates cell growth in breast cancer cells. *Biochem Biophys Res Commun,* 336**,** 1221-6.

LEHMANN, B. D., BAUER, J. A., CHEN, X., SANDERS, M. E., CHAKRAVARTHY, A. B., SHYR, Y. & PIETENPOL, J. A. 2011. Identification of human triple-negative breast cancer subtypes and preclinical models for selection of targeted therapies. *J Clin Invest,* 121**,** 2750-67.

LEWIS PHILLIPS, G. D., LI, G., DUGGER, D. L., CROCKER, L. M., PARSONS, K. L., MAI, E., BLATTLER, W. A., LAMBERT, J. M., CHARI, R. V., LUTZ, R. J., WONG, W. L., JACOBSON, F. S., KOEPPEN, H., SCHWALL, R. H., KENKARE-MITRA, S. R., SPENCER, S. D. & SLIWKOWSKI, M. X. 2008. Targeting HER2-positive breast cancer with trastuzumab-DM1, an antibody-cytotoxic drug conjugate. *Cancer Res,* 68**,** 9280-90.

LI, B., HOWE, L., ANDERSON, S., YATES, J. R., 3RD & WORKMAN, J. L. 2003. The Set2 histone methyltransferase functions through the phosphorylated carboxyl-terminal domain of RNA polymerase II. *J Biol Chem,* 278**,** 8897-903.

LI, B., NI CHONGHAILE, T., FAN, Y., MADDEN, S. F., KLINGER, R., O'CONNOR, A. E., WALSH, L., O'HURLEY, G., MALLYA UDUPI, G., JOSEPH, J., TARRANT, F., CONROY, E., GABER, A., CHIN, S. F., BARDWELL, H. A., PROVENZANO, E., CROWN, J., DUBOIS, T., LINN, S., JIRSTROM, K., CALDAS, C., O'CONNOR, D. P. & GALLAGHER, W. M. 2017. Therapeutic Rationale to Target Highly Expressed CDK7 Conferring Poor Outcomes in Triple-Negative Breast Cancer. *Cancer Res,* 77**,** 3834-3845.

LI, Q., PRICE, J. P., BYERS, S. A., CHENG, D., PENG, J. & PRICE, D. H. 2005. Analysis of the large inactive P-TEFb complex indicates that it contains one 7SK molecule, a dimer of HEXIM1 or HEXIM2, and two P-TEFb molecules containing Cdk9 phosphorylated at threonine 186. *J Biol Chem,* 280**,** 28819-26.

LI, W., NOTANI, D. & ROSENFELD, M. G. 2016. Enhancers as non-coding RNA transcription units: recent insights and future perspectives. *Nat Rev Genet,* 17**,** 207-23.

LIANG, K., GAO, X., GILMORE, J. M., FLORENS, L., WASHBURN, M. P., SMITH, E. & SHILATIFARD, A. 2015. Characterization of human cyclin-dependent kinase 12 (CDK12) and CDK13 complexes in C-terminal domain phosphorylation, gene transcription, and RNA processing. *Mol Cell Biol,* 35**,** 928-38.

LIBERZON, A., BIRGER, C., THORVALDSDOTTIR, H., GHANDI, M., MESIROV, J. P. & TAMAYO, P. 2015. The Molecular Signatures Database (MSigDB) hallmark gene set collection. *Cell Syst,* 1**,** 417-425.

LIN, C., SMITH, E. R., TAKAHASHI, H., LAI, K. C., MARTIN-BROWN, S., FLORENS, L., WASHBURN, M. P., CONAWAY, J. W., CONAWAY, R. C. & SHILATIFARD, A. 2010. AFF4, a component of the ELL/P-TEFb elongation complex and a shared subunit of MLL chimeras, can link transcription elongation to leukemia. *Mol Cell,* 37**,** 429-37.

LIN, R. Z. & CHANG, H. Y. 2008. Recent advances in three-dimensional multicellular spheroid culture for biomedical research. *Biotechnol J,* 3**,** 1172-84.

LIU, H., ZHANG, Z., HUANG, Y., WEI, W., NING, S., LI, J., LIANG, X., LIU, K. & ZHANG, L. 2021. Plasma HSP90AA1 Predicts the Risk of Breast Cancer Onset and Distant Metastasis. *Front Cell Dev Biol,* 9**,** 639596.

LIU, W., MA, Q., WONG, K., LI, W., OHGI, K., ZHANG, J., AGGARWAL, A. & ROSENFELD, M. G. 2013. Brd4 and JMJD6-associated anti-pause enhancers in regulation of transcriptional pause release. *Cell,* 155**,** 1581-1595.

LOGAN, S. K., FALASCA, M., HU, P. & SCHLESSINGER, J. 1997. Phosphatidylinositol 3-kinase mediates epidermal growth factor-induced activation of the c-Jun N-terminal kinase signaling pathway. *Mol Cell Biol,* 17**,** 5784-90.

LOI, S., HAIBE-KAINS, B., MAJJAJ, S., LALLEMAND, F., DURBECQ, V., LARSIMONT, D., GONZALEZ-ANGULO, A. M., PUSZTAI, L., SYMMANS, W. F., BARDELLI, A., ELLIS, P., TUTT, A. N., GILLETT, C. E., HENNESSY, B. T., MILLS, G. B., PHILLIPS, W. A., PICCART, M. J., SPEED, T. P., MCARTHUR, G. A. & SOTIRIOU, C. 2010. PIK3CA mutations associated with gene signature of low mTORC1 signaling and better outcomes in estrogen receptor-positive breast cancer. *Proc Natl Acad Sci U S A,* 107**,** 10208-13.

LOIBL, S., MARME, F., MARTIN, M., UNTCH, M., BONNEFOI, H., KIM, S. B., BEAR, H., MCCARTHY, N., MELE OLIVE, M., GELMON, K., GARCIA-SAENZ, J., KELLY, C. M., REIMER, T., TOI, M., RUGO, H. S., DENKERT, C., GNANT, M., MAKRIS, A., KOEHLER,

M., HUANG-BARTELETT, C., LECHUGA FREAN, M. J., COLLEONI, M., WERUTSKY, G., SEILER, S., BURCHARDI, N., NEKLJUDOVA, V. & VON MINCKWITZ, G. 2021. Palbociclib for Residual High-Risk Invasive HR-Positive and HER2-Negative Early Breast Cancer-The Penelope-B Trial. *J Clin Oncol,* 39**,** 1518-1530.

LOK, S. W., WHITTLE, J. R., VAILLANT, F., TEH, C. E., LO, L. L., POLICHENI, A. N., BERGIN, A. R. T., DESAI, J., FTOUNI, S., GANDOLFO, L. C., LIEW, D., LIU, H. K., MANN, G. B., MOODIE, K., MURUGASU, A., PAL, B., ROBERTS, A. W., ROSENTHAL, M. A., SHACKLETON, K., SILVA, M. J., SIOW, Z. R., SMYTH, G. K., TAYLOR, L., TRAVERS, A., YEO, B., YEUNG, M. M., BUJAK, A. Z., DAWSON, S. J., GRAY, D. H. D., VISVADER, J. E. & LINDEMAN, G. J. 2019. A Phase Ib Dose-Escalation and Expansion Study of the BCL2 Inhibitor Venetoclax Combined with Tamoxifen in ER and BCL2-Positive Metastatic Breast Cancer. *Cancer Discov,* 9**,** 354-369.

LOLLI, G., LOWE, E. D., BROWN, N. R. & JOHNSON, L. N. 2004. The crystal structure of human CDK7 and its protein recognition properties. *Structure,* 12**,** 2067-79.

LOPEZ-KNOWLES, E., PEARSON, A., SCHUSTER, G., GELLERT, P., RIBAS, R., YEO, B., CUTTS, R., BUUS, R., GARCIA-MURILLAS, I., HAYNES, B., MARTIN, L. A., SMITH, I., TURNER, N. & DOWSETT, M. 2019. Molecular characterisation of aromatase inhibitor-resistant advanced breast cancer: the phenotypic effect of ESR1 mutations. *Br J Cancer,* 120**,** 247-255.

LOVE, M. I., HUBER, W. & ANDERS, S. 2014. Moderated estimation of fold change and dispersion for RNA-seq data with DESeq2. *Genome Biol,* 15**,** 550.

LUCKING, U., SCHOLZ, A., LIENAU, P., SIEMEISTER, G., KOSEMUND, D., BOHLMANN, R., BRIEM, H., TEREBESI, I., MEYER, K., PRELLE, K., DENNER, K., BOMER, U., SCHAFER, M., EIS, K., VALENCIA, R., INCE, S., VON NUSSBAUM, F., MUMBERG, D., ZIEGELBAUER, K., KLEBL, B., CHOIDAS, A., NUSSBAUMER, P., BAUMANN, M., SCHULTZ-FADEMRECHT, C., RUHTER, G., EICKHOFF, J. & BRANDS, M. 2017. Identification of Atuveciclib (BAY 1143572), the First Highly Selective, Clinical PTEFb/CDK9 Inhibitor for the Treatment of Cancer. *ChemMedChem,* 12**,** 1776-1793.

LUPIEN, M., MEYER, C. A., BAILEY, S. T., EECKHOUTE, J., COOK, J., WESTERLING, T., ZHANG, X., CARROLL, J. S., RHODES, D. R., LIU, X. S. & BROWN, M. 2010. Growth factor stimulation induces a distinct ER(alpha) cistrome underlying breast cancer endocrine resistance. *Genes Dev,* 24**,** 2219-27.

LYNCH, T. J., BELL, D. W., SORDELLA, R., GURUBHAGAVATULA, S., OKIMOTO, R. A., BRANNIGAN, B. W., HARRIS, P. L., HASERLAT, S. M., SUPKO, J. G., HALUSKA, F. G., LOUIS, D. N., CHRISTIANI, D. C., SETTLEMAN, J. & HABER, D. A. 2004. Activating mutations in the epidermal growth factor receptor underlying responsiveness of non-small-cell lung cancer to gefitinib. *N Engl J Med,* 350**,** 2129-39.

MA, C. X., SANCHEZ, C. G. & ELLIS, M. J. 2009. Predicting endocrine therapy responsiveness in breast cancer. *Oncology (Williston Park),* 23**,** 133-42.

MA, Z. Q., SANTAGATI, S., PATRONE, C., POLLIO, G., VEGETO, E. & MAGGI, A. 1994. Insulin-like growth factors activate estrogen receptor to control the growth and differentiation of the human neuroblastoma cell line SK-ER3. *Mol Endocrinol,* 8**,** 910-8.

MABRY, K. M., PAYNE, S. Z. & ANSETH, K. S. 2016. Microarray analyses to quantify advantages of 2D and 3D hydrogel culture systems in maintaining the native valvular interstitial cell phenotype. *Biomaterials,* 74**,** 31-41.

MAK, H. Y., HOARE, S., HENTTU, P. M. & PARKER, M. G. 1999. Molecular determinants of the estrogen receptor-coactivator interface. *Mol Cell Biol,* 19**,** 3895-903.

MALO, N., HANLEY, J. A., CERQUOZZI, S., PELLETIER, J. & NADON, R. 2006. Statistical practice in high-throughput screening data analysis. *Nat Biotechnol,* 24**,** 167-75.

MARCOM, P. K., ISAACS, C., HARRIS, L., WONG, Z. W., KOMMARREDDY, A., NOVIELLI, N., MANN, G., TAO, Y. & ELLIS, M. J. 2007. The combination of letrozole and trastuzumab as first or second-line biological therapy produces durable responses in a subset of HER2 positive and ER positive advanced breast cancers. *Breast Cancer Res Treat,* 102**,** 43-9.

MARSHALL, N. F., PENG, J., XIE, Z. & PRICE, D. H. 1996. Control of RNA polymerase II elongation potential by a novel carboxyl-terminal domain kinase. *J Biol Chem,* 271**,** 27176-83.

MARTIN, L. A., FARMER, I., JOHNSTON, S. R., ALI, S., MARSHALL, C. & DOWSETT, M. 2003. Enhanced estrogen receptor (ER) alpha, ERBB2, and MAPK signal transduction pathways operate during the adaptation of MCF-7 cells to long term estrogen deprivation. *J Biol Chem,* 278**,** 30458-68.

MARTIN, L. A., GHAZOUI, Z., WEIGEL, M. T., PANCHOLI, S., DUNBIER, A., JOHNSTON, S. & DOWSETT, M. 2011. An in vitro model showing adaptation to long-term oestrogen deprivation highlights the clinical potential for targeting kinase pathways in combination with aromatase inhibition. *Steroids,* 76**,** 772-6.

MARTIN, L. A., RIBAS, R., SIMIGDALA, N., SCHUSTER, E., PANCHOLI, S., TENEV, T., GELLERT, P., BULUWELA, L., HARROD, A., THORNHILL, A., NIKITOROWICZ-BUNIAK, J., BHAMRA, A., TURGEON, M. O., POULOGIANNIS, G., GAO, Q., MARTINS, V., HILLS, M., GARCIA-MURILLAS, I., FRIBBENS, C., PATANI, N., LI, Z., SIKORA, M. J., TURNER, N., ZWART, W., OESTERREICH, S., CARROLL, J., ALI, S. & DOWSETT, M. 2017. Discovery of naturally occurring ESR1 mutations in breast cancer cell lines modelling endocrine resistance. *Nat Commun,* 8**,** 1865.

MARTINEZ, A. M., AFSHAR, M., MARTIN, F., CAVADORE, J. C., LABBE, J. C. & DOREE, M. 1997. Dual phosphorylation of the T-loop in cdk7: its role in controlling cyclin H binding and CAK activity. *EMBO J,* 16**,** 343-54.

MAYER, E. L., DUECK, A. C., MARTIN, M., RUBOVSZKY, G., BURSTEIN, H. J., BELLET-EZQUERRA, M., MILLER, K. D., ZDENKOWSKI, N., WINER, E. P., PFEILER, G., GOETZ, M., RUIZ-BORREGO, M., ANDERSON, D., NOWECKI, Z., LOIBL, S., MOULDER, S., RING, A., FITZAL, F., TRAINA, T., CHAN, A., RUGO, H. S., LEMIEUX, J., HENAO, F., LYSS, A., ANTOLIN NOVOA, S., WOLFF, A. C., VETTER, M., EGLE, D., MORRIS, P. G., MAMOUNAS, E. P., GIL-GIL, M. J., PRAT, A., FOHLER, H., METZGER FILHO, O., SCHWARZ, M., DUFRANE, C., FUMAGALLI, D., THEALL, K. P., LU, D. R., BARTLETT, C. H., KOEHLER, M., FESL, C., DEMICHELE, A. & GNANT, M. 2021. Palbociclib with adjuvant endocrine therapy in early breast cancer (PALLAS): interim analysis of a multicentre, open-label, randomised, phase 3 study. *Lancet Oncol,* 22**,** 212-222.

MCAULIFFE, P. F., MERIC-BERNSTAM, F., MILLS, G. B. & GONZALEZ-ANGULO, A. M. 2010. Deciphering the role of PI3K/Akt/mTOR pathway in breast cancer biology and pathogenesis. *Clin Breast Cancer,* 10 Suppl 3**,** S59-65.

MCCARTNEY, A., MIGLIACCIO, I., BONECHI, M., BIAGIONI, C., ROMAGNOLI, D., DE LUCA, F., GALARDI, F., RISI, E., DE SANTO, I., BENELLI, M., MALORNI, L. & DI LEO, A. 2019. Mechanisms of Resistance to CDK4/6 Inhibitors: Potential Implications and Biomarkers for Clinical Practice. *Front Oncol,* 9**,** 666.

MCCLAIN, M. R., PALOMAKI, G. E., NATHANSON, K. L. & HADDOW, J. E. 2005. Adjusting the estimated proportion of breast cancer cases associated with BRCA1 and BRCA2 mutations: public health implications. *Genet Med,* 7**,** 28-33.

MCDERMOTT, M. S. J., SHARKO, A. C., MUNIE, J., KASSLER, S., MELENDEZ, T., LIM, C. U. & BROUDE, E. V. 2020. CDK7 Inhibition is Effective in all the Subtypes of Breast Cancer: Determinants of Response and Synergy with EGFR Inhibition. *Cells,* 9.

MCKENNA, N. J., LANZ, R. B. & O'MALLEY, B. W. 1999. Nuclear receptor coregulators: cellular and molecular biology. *Endocr Rev,* 20**,** 321-44.

MEEHAN, J., WARD, C., TURNBULL, A., BUKOWSKI-WILLS, J., FINCH, A. J., JARMAN, E. J., XINTAROPOULOU, C., MARTINEZ-PEREZ, C., GRAY, M., PEARSON, M., MULLEN, P., SUPURAN, C. T., CARTA, F., HARRISON, D. J., KUNKLER, I. H. & LANGDON, S. P. 2017. Inhibition of pH regulation as a therapeutic strategy in hypoxic human breast cancer cells. *Oncotarget,* 8**,** 42857-42875.

MEHTA, R. S., BARLOW, W. E., ALBAIN, K. S., VANDENBERG, T. A., DAKHIL, S. R., TIRUMALI, N. R., LEW, D. L., HAYES, D. F., GRALOW, J. R., LIVINGSTON, R. B. & HORTOBAGYI, G. N. 2012. Combination anastrozole and fulvestrant in metastatic breast cancer. *N Engl J Med,* 367**,** 435-44.

MELISSARIDOU, S., WIECHEC, E., MAGAN, M., JAIN, M. V., CHUNG, M. K., FARNEBO, L. & ROBERG, K. 2019. The effect of 2D and 3D cell cultures on treatment response, EMT profile and stem cell features in head and neck cancer. *Cancer Cell Int,* 19**,** 16.

MENG, W., WANG, J., WANG, B., LIU, F., LI, M., ZHAO, Y., ZHANG, C., LI, Q., CHEN, J., ZHANG, L., TANG, Y. & MA, J. 2018. CDK7 inhibition is a novel therapeutic strategy against GBM both in vitro and in vivo. *Cancer Manag Res,* 10**,** 5747-5758.

MERENBAKH-LAMIN, K., BEN-BARUCH, N., YEHESKEL, A., DVIR, A., SOUSSAN-GUTMAN, L., JESELSOHN, R., YELENSKY, R., BROWN, M., MILLER, V. A., SARID, D., RIZEL, S., KLEIN, B., RUBINEK, T. & WOLF, I. 2013. D538G mutation in estrogen receptor-alpha: A novel mechanism for acquired endocrine resistance in breast cancer. *Cancer Res,* 73**,** 6856-64.

MEYER, C., KOWARZ, E., HOFMANN, J., RENNEVILLE, A., ZUNA, J., TRKA, J., BEN ABDELALI, R., MACINTYRE, E., DE BRAEKELEER, E., DE BRAEKELEER, M., DELABESSE, E., DE OLIVEIRA, M. P., CAVE, H., CLAPPIER, E., VAN DONGEN, J. J., BALGOBIND, B. V., VAN DEN HEUVEL-EIBRINK, M. M., BEVERLOO, H. B., PANZER-GRUMAYER, R., TEIGLER-SCHLEGEL, A., HARBOTT, J., KJELDSEN, E., SCHNITTGER, S., KOEHL, U., GRUHN, B., HEIDENREICH, O., CHAN, L. C., YIP, S. F., KRZYWINSKI, M., ECKERT, C., MORICKE, A., SCHRAPPE, M., ALONSO, C. N., SCHAFER, B. W., KRAUTER, J., LEE, D. A., ZUR STADT, U., TE KRONNIE, G., SUTTON, R., IZRAELI, S., TRAKHTENBROT, L., LO NIGRO, L., TSAUR, G., FECHINA, L., SZCZEPANSKI, T., STREHL, S., ILENCIKOVA, D., MOLKENTIN, M., BURMEISTER, T., DINGERMANN, T., KLINGEBIEL, T. & MARSCHALEK, R. 2009. New insights to the MLL recombinome of acute leukemias. *Leukemia,* 23**,** 1490-9.

MICHELS, A. A., FRALDI, A., LI, Q., ADAMSON, T. E., BONNET, F., NGUYEN, V. T., SEDORE, S. C., PRICE, J. P., PRICE, D. H., LANIA, L. & BENSAUDE, O. 2004. Binding of the 7SK snRNA turns the HEXIM1 protein into a P-TEFb (CDK9/cyclin T) inhibitor. *EMBO J,* 23**,** 2608-19.

MIKI, Y., SWENSEN, J., SHATTUCK-EIDENS, D., FUTREAL, P. A., HARSHMAN, K., TAVTIGIAN, S., LIU, Q., COCHRAN, C., BENNETT, L. M., DING, W. & ET AL. 1994. A strong candidate for the breast and ovarian cancer susceptibility gene BRCA1. *Science,* 266**,** 66-71.

MILLA-SANTOS, A., MILLA, L., PORTELLA, J., RALLO, L., PONS, M., RODES, E., CASANOVAS, J. & PUIG-GALI, M. 2003. Anastrozole versus tamoxifen as first-line therapy in

postmenopausal patients with hormone-dependent advanced breast cancer: a prospective, randomized, phase III study. *Am J Clin Oncol,* 26**,** 317-22.

MILLER, T. W., BALKO, J. M. & ARTEAGA, C. L. 2011. Phosphatidylinositol 3-kinase and antiestrogen resistance in breast cancer. *J Clin Oncol,* 29**,** 4452-61.

MILLER, T. W., HENNESSY, B. T., GONZALEZ-ANGULO, A. M., FOX, E. M., MILLS, G. B., CHEN, H., HIGHAM, C., GARCIA-ECHEVERRIA, C., SHYR, Y. & ARTEAGA, C. L. 2010. Hyperactivation of phosphatidylinositol-3 kinase promotes escape from hormone dependence in estrogen receptor-positive human breast cancer. *J Clin Invest,* 120**,** 2406-13.

MILLER, T. W., PEREZ-TORRES, M., NARASANNA, A., GUIX, M., STAL, O., PEREZ-TENORIO, G., GONZALEZ-ANGULO, A. M., HENNESSY, B. T., MILLS, G. B., KENNEDY, J. P., LINDSLEY, C. W. & ARTEAGA, C. L. 2009. Loss of Phosphatase and Tensin homologue deleted on chromosome 10 engages ErbB3 and insulin-like growth factor-I receptor signaling to promote antiestrogen resistance in breast cancer. *Cancer Res,* 69**,** 4192-201.

MITRA, P., PEREIRA, L. A., DRABSCH, Y., RAMSAY, R. G. & GONDA, T. J. 2012. Estrogen receptor-alpha recruits P-TEFb to overcome transcriptional pausing in intron 1 of the MYB gene. *Nucleic Acids Res,* 40**,** 5988-6000.

MITRA, P., YANG, R. M., SUTTON, J., RAMSAY, R. G. & GONDA, T. J. 2016. CDK9 inhibitors selectively target estrogen receptor-positive breast cancer cells through combined inhibition of MYB and MCL-1 expression. *Oncotarget,* 7**,** 9069-83.

MITTNACHT, S. 1998. Control of pRB phosphorylation. *Curr Opin Genet Dev,* 8**,** 21-7.

MOLLON, L. E., ANDERSON, E. J., DEAN, J. L., WARHOLAK, T. L., AIZER, A., PLATT, E. A., TANG, D. H. & DAVIS, L. E. 2020. A Systematic Literature Review of the Prognostic and Predictive Value of PIK3CA Mutations in HR(+)/HER2(-) Metastatic Breast Cancer. *Clin Breast Cancer,* 20**,** e232-e243.

MORI, T., ANAZAWA, Y., MATSUI, K., FUKUDA, S., NAKAMURA, Y. & ARAKAWA, H. 2002. Cyclin K as a direct transcriptional target of the p53 tumor suppressor. *Neoplasia,* 4**,** 268-74.

MORITOH, Y., OKA, M., YASUHARA, Y., HOZUMI, H., IWACHIDOW, K., FUSE, H. & TOZAWA, R. 2016. Inositol Hexakisphosphate Kinase 3 Regulates Metabolism and Lifespan in Mice. *Sci Rep,* 6**,** 32072.

MORRIS, K. V. & MATTICK, J. S. 2014. The rise of regulatory RNA. *Nat Rev Genet,* 15**,** 423-37.

MUNTEAN, A. G. & HESS, J. L. 2012. The pathogenesis of mixed-lineage leukemia. *Annu Rev Pathol,* 7**,** 283-301.

MURTAZA, M., DAWSON, S. J., TSUI, D. W., GALE, D., FORSHEW, T., PISKORZ, A. M., PARKINSON, C., CHIN, S. F., KINGSBURY, Z., WONG, A. S., MARASS, F., HUMPHRAY, S., HADFIELD, J., BENTLEY, D., CHIN, T. M., BRENTON, J. D., CALDAS, C. & ROSENFELD, N. 2013. Non-invasive analysis of acquired resistance to cancer therapy by sequencing of plasma DNA. *Nature,* 497**,** 108-12.

MURUGAESU, N., WILSON, G. A., BIRKBAK, N. J., WATKINS, T., MCGRANAHAN, N., KUMAR, S., ABBASSI-GHADI, N., SALM, M., MITTER, R., HORSWELL, S., ROWAN, A., PHILLIMORE, B., BIGGS, J., BEGUM, S., MATTHEWS, N., HOCHHAUSER, D., HANNA, G. B. & SWANTON, C. 2015. Tracking the genomic evolution of esophageal adenocarcinoma through neoadjuvant chemotherapy. *Cancer Discov,* 5**,** 821-831.

NATH, S. & DEVI, G. R. 2016. Three-dimensional culture systems in cancer research: Focus on tumor spheroid model. *Pharmacol Ther,* 163**,** 94-108.

NAVIN, N., KENDALL, J., TROGE, J., ANDREWS, P., RODGERS, L., MCINDOO, J., COOK, K., STEPANSKY, A., LEVY, D., ESPOSITO, D., MUTHUSWAMY, L., KRASNITZ, A., MCCOMBIE, W. R., HICKS, J. & WIGLER, M. 2011. Tumour evolution inferred by single-cell sequencing. *Nature,* 472**,** 90-4.

NEVE, R. M., CHIN, K., FRIDLYAND, J., YEH, J., BAEHNER, F. L., FEVR, T., CLARK, L., BAYANI, N., COPPE, J. P., TONG, F., SPEED, T., SPELLMAN, P. T., DEVRIES, S., LAPUK, A., WANG, N. J., KUO, W. L., STILWELL, J. L., PINKEL, D., ALBERTSON, D. G., WALDMAN, F. M., MCCORMICK, F., DICKSON, R. B., JOHNSON, M. D., LIPPMAN, M., ETHIER, S., GAZDAR, A. & GRAY, J. W. 2006. A collection of breast cancer cell lines for the study of functionally distinct cancer subtypes. *Cancer Cell,* 10**,** 515-27.

NEWMAN, B., MU, H., BUTLER, L. M., MILLIKAN, R. C., MOORMAN, P. G. & KING, M. C. 1998. Frequency of breast cancer attributable to BRCA1 in a population-based series of American women. *JAMA,* 279**,** 915-21.

NI, Z., SCHWARTZ, B. E., WERNER, J., SUAREZ, J. R. & LIS, J. T. 2004. Coordination of transcription, RNA processing, and surveillance by P-TEFb kinase on heat shock genes. *Mol Cell,* 13**,** 55-65.

NOWELL, P. C. 1976. The clonal evolution of tumor cell populations. *Science,* 194**,** 23-8.

O'LEARY, B., CUTTS, R. J., HUANG, X., HREBIEN, S., LIU, Y., ANDRE, F., LOIBL, S., LOI, S., GARCIA-MURILLAS, I., CRISTOFANILLI, M., BARTLETT, C. H. & TURNER, N. C. 2021. Circulating Tumor DNA Markers for Early Progression on Fulvestrant With or Without Palbociclib in ER+ Advanced Breast Cancer. *J Natl Cancer Inst,* 113**,** 309-317.

O'LEARY, B., FINN, R. S. & TURNER, N. C. 2016. Treating cancer with selective CDK4/6 inhibitors. *Nat Rev Clin Oncol,* 13**,** 417-30.

O'LONE, R., FRITH, M. C., KARLSSON, E. K. & HANSEN, U. 2004. Genomic targets of nuclear estrogen receptors. *Mol Endocrinol,* 18**,** 1859-75.

O'SHAUGHNESSY, J., MCINTYRE, K., WILKS, S., MA, L., BLOCK, M., ANDORSKY, D., DANSO, M., LOCKE, T., SCALES, A. & WANG, Y. 2021. Efficacy and Safety of Weekly Paclitaxel With or Without Oral Alisertib in Patients With Metastatic Breast Cancer: A Randomized Clinical Trial. *JAMA Netw Open,* 4**,** e214103.

OCANA, A. & PANDIELLA, A. 2020. Proteolysis targeting chimeras (PROTACs) in cancer therapy. *J Exp Clin Cancer Res,* 39**,** 189.

OHNO, S. 2016. Tolerability of Therapies Recommended for the Treatment of Hormone Receptor-Positive Locally Advanced or Metastatic Breast Cancer. *Clin Breast Cancer,* 16**,** 238-46.

OLANICH, M. E., SUN, W., HEWITT, S. M., ABDULLAEV, Z., PACK, S. D. & BARR, F. G. 2015. CDK4 Amplification Reduces Sensitivity to CDK4/6 Inhibition in Fusion-Positive Rhabdomyosarcoma. *Clin Cancer Res,* 21**,** 4947-59.

OLIVEROS, J. C. 2017-2015. *Venny. An interactive tool for comparings lists with Venn's diagrams* [Online]. Available: https://bioinfogp.cnb.csic.es/tools/venny/index.html [Accessed].

OLSON, C. M., JIANG, B., ERB, M. A., LIANG, Y., DOCTOR, Z. M., ZHANG, Z., ZHANG, T., KWIATKOWSKI, N., BOUKHALI, M., GREEN, J. L., HAAS, W., NOMANBHOY, T., FISCHER, E. S., YOUNG, R. A., BRADNER, J. E., WINTER, G. E. & GRAY, N. S. 2018. Pharmacological perturbation of CDK9 using selective CDK9 inhibition or degradation. *Nat Chem Biol,* 14**,** 163-170.

ONATE, S. A., TSAI, S. Y., TSAI, M. J. & O'MALLEY, B. W. 1995. Sequence and characterization of a coactivator for the steroid hormone receptor superfamily. *Science,* 270**,** 1354-7.

OTTO, A. M., PADDENBERG, R., SCHUBERT, S. & MANNHERZ, H. G. 1996. Cell-cycle arrest, micronucleus formation, and cell death in growth inhibition of MCF-7 breast cancer cells by tamoxifen and cisplatin. *J Cancer Res Clin Oncol,* 122**,** 603-12.

OWYONG, M., CHOU, J., VAN DEN BIJGAART, R. J., KONG, N., EFE, G., MAYNARD, C., TALMI-FRANK, D., SOLOMONOV, I., KOOPMAN, C., HADLER-OLSEN, E., HEADLEY, M., LIN, C., WANG, C. Y., SAGI, I., WERB, Z. & PLAKS, V. 2019. MMP9 modulates the metastatic cascade and immune landscape for breast cancer anti-metastatic therapy. *Life Sci Alliance,* 2.

OZA, A. M., ESTEVEZ-DIZ, M., GRISCHKE, E. M., HALL, M., MARME, F., PROVENCHER, D., UYAR, D., WEBERPALS, J. I., WENHAM, R. M., LAING, N., TRACY, M., FRESHWATER, T., LEE, M. A., LIU, J., QIU, J., ROSE, S., RUBIN, E. H. & MOORE, K. 2020. A Biomarker-enriched, Randomized Phase II Trial of Adavosertib (AZD1775) Plus Paclitaxel and Carboplatin for Women with Platinum-sensitive TP53-mutant Ovarian Cancer. *Clin Cancer Res,* 26**,** 4767-4776.

PAN, H., GRAY, R., BRAYBROOKE, J., DAVIES, C., TAYLOR, C., MCGALE, P., PETO, R., PRITCHARD, K. I., BERGH, J., DOWSETT, M., HAYES, D. F. & EBCTCG 2017. 20-Year Risks of Breast-Cancer Recurrence after Stopping Endocrine Therapy at 5 Years. *N Engl J Med,* 377**,** 1836-1846.

PANCHOLI, S., RIBAS, R., SIMIGDALA, N., SCHUSTER, E., NIKITOROWICZ-BUNIAK, J., RESSA, A., GAO, Q., LEAL, M. F., BHAMRA, A., THORNHILL, A., MORISSET, L., MONTAUDON, E., SOURD, L., FITZPATRICK, M., ALTELAAR, M., JOHNSTON, S. R., MARANGONI, E., DOWSETT, M. & MARTIN, L. A. 2020. Tumour kinome re-wiring governs resistance to palbociclib in oestrogen receptor positive breast cancers, highlighting new therapeutic modalities. *Oncogene,* 39**,** 4781-4797.

PATEL, H., ABDULJABBAR, R., LAI, C. F., PERIYASAMY, M., HARROD, A., GEMMA, C., STEEL, J. H., PATEL, N., BUSONERO, C., JERJEES, D., REMENYI, J., SMITH, S., GOMM, J. J., MAGNANI, L., GYORFFY, B., JONES, L. J., FULLER-PACE, F., SHOUSHA, S., BULUWELA, L., RAKHA, E. A., ELLIS, I. O., COOMBES, R. C. & ALI, S. 2016. Expression of CDK7, Cyclin H, and MAT1 Is Elevated in Breast Cancer and Is Prognostic in Estrogen Receptor-Positive Breast Cancer. *Clin Cancer Res,* 22**,** 5929-5938.

PATEL, H., PERIYASAMY, M., SAVA, G. P., BONDKE, A., SLAFER, B. W., KROLL, S. H. B., BARBAZANGES, M., STARKEY, R., OTTAVIANI, S., HARROD, A., ABOAGYE, E. O., BULUWELA, L., FUCHTER, M. J., BARRETT, A. G. M., COOMBES, R. C. & ALI, S. 2018. ICEC0942, an Orally Bioavailable Selective Inhibitor of CDK7 for Cancer Treatment. *Mol Cancer Ther,* 17**,** 1156-1166.

PATEL, H. K., TAO, N., LEE, K. M., HUERTA, M., ARLT, H., MULLARKEY, T., TROY, S., ARTEAGA, C. L. & BIHANI, T. 2019. Elacestrant (RAD1901) exhibits anti-tumor activity in multiple ER+ breast cancer models resistant to CDK4/6 inhibitors. *Breast Cancer Res,* 21**,** 146.

PATRO, R., DUGGAL, G., LOVE, M. I., IRIZARRY, R. A. & KINGSFORD, C. 2017. Salmon provides fast and bias-aware quantification of transcript expression. *Nat Methods,* 14**,** 417-419.

PEARSON, K. 1901. LIII. On lines and planes of closest fit to systems of points in space. *The London, Edinburgh, and Dublin Philosophical Magazine and Journal of Science,* 2**,** 559-572.

PELEKANOU, V., VILLARROEL-ESPINDOLA, F., SCHALPER, K. A., PUSZTAI, L. & RIMM, D. L. 2018. CD68, CD163, and matrix metalloproteinase 9 (MMP-9) co-localization in breast tumor microenvironment predicts survival differently in ER-positive and -negative cancers. *Breast Cancer Res,* 20**,** 154.

PEROU, C. M., SORLIE, T., EISEN, M. B., VAN DE RIJN, M., JEFFREY, S. S., REES, C. A., POLLACK, J. R., ROSS, D. T., JOHNSEN, H., AKSLEN, L. A., FLUGE, O., PERGAMENSCHIKOV, A., WILLIAMS, C., ZHU, S. X., LONNING, P. E., BORRESEN-DALE, A. L., BROWN, P. O. & BOTSTEIN, D. 2000. Molecular portraits of human breast tumours. *Nature,* 406**,** 747-52.

PETERLIN, B. M. & PRICE, D. H. 2006. Controlling the elongation phase of transcription with P-TEFb. *Mol Cell,* 23**,** 297-305.

PETZ, L. N., ZIEGLER, Y. S., LOVEN, M. A. & NARDULLI, A. M. 2002. Estrogen receptor alpha and activating protein-1 mediate estrogen responsiveness of the progesterone receptor gene in MCF-7 breast cancer cells. *Endocrinology,* 143**,** 4583-91.

PICCART-GEBHART, M. J., BURZYKOWSKI, T., BUYSE, M., SLEDGE, G., CARMICHAEL, J., LUCK, H. J., MACKEY, J. R., NABHOLTZ, J. M., PARIDAENS, R., BIGANZOLI, L., JASSEM, J., BONTENBAL, M., BONNETERRE, J., CHAN, S., BASARAN, G. A. & THERASSE, P. 2008. Taxanes alone or in combination with anthracyclines as first-line therapy of patients with metastatic breast cancer. *Journal of Clinical Oncology,* 26**,** 1980-1986.

POMMIER, Y., O'CONNOR, M. J. & DE BONO, J. 2016. Laying a trap to kill cancer cells: PARP inhibitors and their mechanisms of action. *Sci Transl Med,* 8**,** 362ps17.

PORTER, W., SAVILLE, B., HOIVIK, D. & SAFE, S. 1997. Functional synergy between the transcription factor Sp1 and the estrogen receptor. *Mol Endocrinol,* 11**,** 1569-80.

PRESTON-MARTIN, S., PIKE, M. C., ROSS, R. K., JONES, P. A. & HENDERSON, B. E. 1990. Increased cell division as a cause of human cancer. *Cancer Res,* 50**,** 7415-21.

PUYANG, X., FURMAN, C., ZHENG, G. Z., WU, Z. J., BANKA, D., AITHAL, K., AGOULNIK, S., BOLDUC, D. M., BUONAMICI, S., CALEB, B., DAS, S., ECKLEY, S., FEKKES, P., HAO, M. H., HART, A., HOUTMAN, R., IRWIN, S., JOSHI, J. J., KARR, C., KIM, A., KUMAR, N., KUMAR, P., KUZNETSOV, G., LAI, W. G., LARSEN, N., MACKENZIE, C., MARTIN, L. A., MELCHERS, D., MORIARTY, A., NGUYEN, T. V., NORRIS, J., O'SHEA, M., PANCHOLI, S., PRAJAPATI, S., RAJAGOPALAN, S., REYNOLDS, D. J., RIMKUNAS, V., RIOUX, N., RIBAS, R., SIU, A., SIVAKUMAR, S., SUBRAMANIAN, V., THOMAS, M., VAILLANCOURT, F. H., WANG, J., WARDELL, S., WICK, M. J., YAO, S., YU, L., WARMUTH, M., SMITH, P. G., ZHU, P. & KORPAL, M. 2018. Discovery of Selective Estrogen Receptor Covalent Antagonists for the Treatment of ERalpha(WT) and ERalpha(MUT) Breast Cancer. *Cancer Discov,* 8**,** 1176-1193.

RAUDVERE, U., KOLBERG, L., KUZMIN, I., ARAK, T., ADLER, P., PETERSON, H. & VILO, J. 2019. g:Profiler: a web server for functional enrichment analysis and conversions of gene lists (2019 update). *Nucleic Acids Res,* 47**,** W191-W198.

RAZANDI, M., PEDRAM, A., GREENE, G. L. & LEVIN, E. R. 1999. Cell membrane and nuclear estrogen receptors (ERs) originate from a single transcript: studies of ERalpha and ERbeta expressed in Chinese hamster ovary cells. *Mol Endocrinol,* 13**,** 307-19.

RAZAVI, P., CHANG, M. T., XU, G., BANDLAMUDI, C., ROSS, D. S., VASAN, N., CAI, Y., BIELSKI, C. M., DONOGHUE, M. T. A., JONSSON, P., PENSON, A., SHEN, R., PAREJA, F., KUNDRA, R., MIDDHA, S., CHENG, M. L., ZEHIR, A., KANDOTH, C., PATEL, R., HUBERMAN, K., SMYTH, L. M., JHAVERI, K., MODI, S., TRAINA, T. A., DANG, C., ZHANG, W., WEIGELT, B., LI, B. T., LADANYI, M., HYMAN, D. M., SCHULTZ, N., ROBSON, M. E., HUDIS, C., BROGI, E., VIALE, A., NORTON, L., DICKLER, M. N., BERGER, M. F., IACOBUZIO-DONAHUE, C. A., CHANDARLAPATY, S., SCALTRITI, M., REIS-FILHO, J. S., SOLIT, D. B., TAYLOR, B. S. & BASELGA, J. 2018. The Genomic Landscape of Endocrine-Resistant Advanced Breast Cancers. *Cancer Cell,* 34**,** 427-438 e6.

REYAL, F., GUYADER, C., DECRAENE, C., LUCCHESI, C., AUGER, N., ASSAYAG, F., DE PLATER, L., GENTIEN, D., POUPON, M. F., COTTU, P., DE CREMOUX, P., GESTRAUD, P., VINCENT-SALOMON, A., FONTAINE, J. J., ROMAN-ROMAN, S., DELATTRE, O., DECAUDIN, D. & MARANGONI, E. 2012. Molecular profiling of patient-derived breast cancer xenografts. *Breast Cancer Res,* 14**,** R11.

RIAZ, M., VAN JAARSVELD, M. T., HOLLESTELLE, A., PRAGER-VAN DER SMISSEN, W. J., HEINE, A. A., BOERSMA, A. W., LIU, J., HELMIJR, J., OZTURK, B., SMID, M., WIEMER, E. A., FOEKENS, J. A. & MARTENS, J. W. 2013. miRNA expression profiling of 51 human breast cancer cell lines reveals subtype and driver mutation-specific miRNAs. *Breast Cancer Res,* 15**,** R33.

RIBAS, R., PANCHOLI, S., GUEST, S. K., MARANGONI, E., GAO, Q., THULEAU, A., SIMIGDALA, N., POLANSKA, U. M., CAMPBELL, H., RANI, A., LICCARDI, G., JOHNSTON, S., DAVIES, B. R., DOWSETT, M. & MARTIN, L. A. 2015. AKT Antagonist AZD5363 Influences Estrogen Receptor Function in Endocrine-Resistant Breast Cancer and Synergizes with Fulvestrant (ICI182780) In Vivo. *Mol Cancer Ther,* 14**,** 2035-48.

RIBAS, R., PANCHOLI, S., RANI, A., SCHUSTER, E., GUEST, S. K., NIKITOROWICZ-BUNIAK, J., SIMIGDALA, N., THORNHILL, A., AVOGADRI-CONNORS, F., CUTLER, R. E., JR., LALANI, A. S., DOWSETT, M., JOHNSTON, S. R. & MARTIN, L. A. 2018. Targeting tumour re-wiring by triple blockade of mTORC1, epidermal growth factor, and oestrogen receptor signalling pathways in endocrine-resistant breast cancer. *Breast Cancer Res,* 20**,** 44.

RIEDL, A., SCHLEDERER, M., PUDELKO, K., STADLER, M., WALTER, S., UNTERLEUTHNER, D., UNGER, C., KRAMER, N., HENGSTSCHLAGER, M., KENNER, L., PFEIFFER, D., KRUPITZA, G. & DOLZNIG, H. 2017. Comparison of cancer cells in 2D vs 3D culture reveals differences in AKT-mTOR-S6K signaling and drug responses. *J Cell Sci,* 130**,** 203-218.

RIMEL, J. K. & TAATJES, D. J. 2018. The essential and multifunctional TFIIH complex. *Protein Sci,* 27**,** 1018-1037.

ROBINSON, D. R., WU, Y. M., VATS, P., SU, F., LONIGRO, R. J., CAO, X., KALYANA-SUNDARAM, S., WANG, R., NING, Y., HODGES, L., GURSKY, A., SIDDIQUI, J., TOMLINS, S. A., ROYCHOWDHURY, S., PIENTA, K. J., KIM, S. Y., ROBERTS, J. S., RAE, J. M., VAN POZNAK, C. H., HAYES, D. F., CHUGH, R., KUNJU, L. P., TALPAZ, M., SCHOTT, A. F. & CHINNAIYAN, A. M. 2013. Activating ESR1 mutations in hormone-resistant metastatic breast cancer. *Nat Genet,* 45**,** 1446-51.

ROBSON, M., IM, S. A., SENKUS, E., XU, B., DOMCHEK, S. M., MASUDA, N., DELALOGE, S., LI, W., TUNG, N., ARMSTRONG, A., WU, W., GOESSL, C., RUNSWICK, S. & CONTE, P. 2017. Olaparib for Metastatic Breast Cancer in Patients with a Germline BRCA Mutation. *N Engl J Med,* 377**,** 523-533.

RODRIGUES, J., HEINRICH, M. A., TEIXEIRA, L. M. & PRAKASH, J. 2021. 3D In Vitro Model (R)evolution: Unveiling Tumor-Stroma Interactions. *Trends Cancer,* 7**,** 249-264.

ROGATSKY, I., TROWBRIDGE, J. M. & GARABEDIAN, M. J. 1999. Potentiation of human estrogen receptor alpha transcriptional activation through phosphorylation of serines 104 and 106 by the cyclin A-CDK2 complex. *J Biol Chem,* 274**,** 22296-302.

ROWLEY, J. D. 1973. Letter: A new consistent chromosomal abnormality in chronic myelogenous leukaemia identified by quinacrine fluorescence and Giemsa staining. *Nature,* 243**,** 290-3.

RUFF, M., GANGLOFF, M., WURTZ, J. M. & MORAS, D. 2000. Estrogen receptor transcription and transactivation: Structure-function relationship in DNA- and ligand-binding domains of estrogen receptors. *Breast Cancer Res,* 2**,** 353-9.

RUGO, H. S., LEREBOURS, F., CIRUELOS, E., DRULLINSKY, P., RUIZ-BORREGO, M., NEVEN, P., PARK, Y. H., PRAT, A., BACHELOT, T., JURIC, D., TURNER, N., SOPHOS, N., ZARATE, J. P., ARCE, C., SHEN, Y. M., TURNER, S., KANAKAMEDALA, H., HSU, W. C. & CHIA, S. 2021. Alpelisib plus fulvestrant in PIK3CA-mutated, hormone receptor-positive advanced breast cancer after a CDK4/6 inhibitor (BYLieve): one cohort of a phase 2, multicentre, open-label, non-comparative study. *Lancet Oncol,* 22**,** 489-498.

SABBAH, M., COURILLEAU, D., MESTER, J. & REDEUILH, G. 1999. Estrogen induction of the cyclin D1 promoter: involvement of a cAMP response-like element. *Proc Natl Acad Sci U S A,* 96**,** 11217-22.

SABO, A., LUSIC, M., CERESETO, A. & GIACCA, M. 2008. Acetylation of conserved lysines in the catalytic core of cyclin-dependent kinase 9 inhibits kinase activity and regulates transcription. *Mol Cell Biol,* 28**,** 2201-12.

SACHS, N., DE LIGT, J., KOPPER, O., GOGOLA, E., BOUNOVA, G., WEEBER, F., BALGOBIND, A. V., WIND, K., GRACANIN, A., BEGTHEL, H., KORVING, J., VAN BOXTEL, R., DUARTE, A. A., LELIEVELD, D., VAN HOECK, A., ERNST, R. F., BLOKZIJL, F., NIJMAN, I. J., HOOGSTRAAT, M., VAN DE VEN, M., EGAN, D. A., ZINZALLA, V., MOLL, J., BOJ, S. F., VOEST, E. E., WESSELS, L., VAN DIEST, P. J., ROTTENBERG, S., VRIES, R. G. J., CUPPEN, E. & CLEVERS, H. 2018. A Living Biobank of Breast Cancer Organoids Captures Disease Heterogeneity. *Cell,* 172**,** 373-386 e10.

SAHA, S., DEY, S. & NATH, S. 2021. Steroid Hormone Receptors: Links With Cell Cycle Machinery and Breast Cancer Progression. *Front Oncol,* 11**,** 620214.

SAHAI, E. & MARSHALL, C. J. 2003. Differing modes of tumour cell invasion have distinct requirements for Rho/ROCK signalling and extracellular proteolysis. *Nat Cell Biol,* 5**,** 711-9.

SAIARDI, A., NAGATA, E., LUO, H. R., SNOWMAN, A. M. & SNYDER, S. H. 2001. Identification and characterization of a novel inositol hexakisphosphate kinase. *J Biol Chem,* 276**,** 39179-85.

SCHACHTER, M. M. & FISHER, R. P. 2013. The CDK-activating kinase Cdk7: taking yes for an answer. *Cell Cycle,* 12**,** 3239-40.

SCHACHTER, M. M., MERRICK, K. A., LAROCHELLE, S., HIRSCHI, A., ZHANG, C., SHOKAT, K. M., RUBIN, S. M. & FISHER, R. P. 2013. A Cdk7-Cdk4 T-loop phosphorylation cascade promotes G1 progression. *Mol Cell,* 50**,** 250-60.

SCHIAVON, G., HREBIEN, S., GARCIA-MURILLAS, I., CUTTS, R. J., PEARSON, A., TARAZONA, N., FENWICK, K., KOZAREWA, I., LOPEZ-KNOWLES, E., RIBAS, R., NERURKAR, A., OSIN, P., CHANDARLAPATY, S., MARTIN, L. A., DOWSETT, M., SMITH, I. E. & TURNER, N. C. 2015. Analysis of ESR1 mutation in circulating tumor

DNA demonstrates evolution during therapy for metastatic breast cancer. *Sci Transl Med,* 7**,** 313ra182.

SCHMID, P., CORTES, J., PUSZTAI, L., MCARTHUR, H., KUMMEL, S., BERGH, J., DENKERT, C., PARK, Y. H., HUI, R., HARBECK, N., TAKAHASHI, M., FOUKAKIS, T., FASCHING, P. A., CARDOSO, F., UNTCH, M., JIA, L., KARANTZA, V., ZHAO, J., AKTAN, G., DENT, R., O'SHAUGHNESSY, J. & INVESTIGATORS, K.-. 2020. Pembrolizumab for Early Triple-Negative Breast Cancer. *N Engl J Med,* 382**,** 810-821.

SCHNEIDER, E., KARTARIUS, S., SCHUSTER, N. & MONTENARH, M. 2002. The cyclin H/cdk7/Mat1 kinase activity is regulated by CK2 phosphorylation of cyclin H. *Oncogene,* 21**,** 5031-7.

SCHOLZ, A., TRUSS, M. & BEATO, M. 1998. Hormone-induced recruitment of Sp1 mediates estrogen activation of the rabbit uteroglobin gene in endometrial epithelium. *J Biol Chem,* 273**,** 4360-6.

SCHROLL, M. M., LIU, X., HERZOG, S. K., SKUBE, S. B. & HUMMON, A. B. 2016. Nutrient restriction of glucose or serum results in similar proteomic expression changes in 3D colon cancer cell cultures. *Nutr Res,* 36**,** 1068-1080.

SENDEROWICZ, A. M., HEADLEE, D., STINSON, S. F., LUSH, R. M., KALIL, N., VILLALBA, L., HILL, K., STEINBERG, S. M., FIGG, W. D., TOMPKINS, A., ARBUCK, S. G. & SAUSVILLE, E. A. 1998. Phase I trial of continuous infusion flavopiridol, a novel cyclin-dependent kinase inhibitor, in patients with refractory neoplasms. *J Clin Oncol,* 16**,** 2986-99.

SENGUPTA, S., BIARNES, M. C. & JORDAN, V. C. 2014. Cyclin dependent kinase-9 mediated transcriptional de-regulation of cMYC as a critical determinant of endocrine-therapy resistance in breast cancers. *Breast Cancer Res Treat,* 143**,** 113-24.

SFLOMOS, G., DORMOY, V., METSALU, T., JEITZINER, R., BATTISTA, L., SCABIA, V., RAFFOUL, W., DELALOYE, J. F., TREBOUX, A., FICHE, M., VILO, J., AYYANAN, A. & BRISKEN, C. 2016. A Preclinical Model for ERalpha-Positive Breast Cancer Points to the Epithelial Microenvironment as Determinant of Luminal Phenotype and Hormone Response. *Cancer Cell,* 29**,** 407-422.

SHANG, Y. 2006. Molecular mechanisms of oestrogen and SERMs in endometrial carcinogenesis. *Nat Rev Cancer,* 6**,** 360-8.

SHARIATI, M. & MERIC-BERNSTAM, F. 2019. Targeting AKT for cancer therapy. *Expert Opin Investig Drugs,* 28**,** 977-988.

SHORE, S. M., BYERS, S. A., DENT, P. & PRICE, D. H. 2005. Characterization of Cdk9(55) and differential regulation of two Cdk9 isoforms. *Gene,* 350**,** 51-8.

SHORE, S. M., BYERS, S. A., MAURY, W. & PRICE, D. H. 2003. Identification of a novel isoform of Cdk9. *Gene,* 307**,** 175-82.

SHOU, J., MASSARWEH, S., OSBORNE, C. K., WAKELING, A. E., ALI, S., WEISS, H. & SCHIFF, R. 2004. Mechanisms of tamoxifen resistance: increased estrogen receptor-HER2/neu cross-talk in ER/HER2-positive breast cancer. *J Natl Cancer Inst,* 96**,** 926-35.

SIEUWERTS, A. M., SCHRIJVER, W. A., DALM, S. U., DE WEERD, V., MOELANS, C. B., TER HOEVE, N., VAN DIEST, P. J., MARTENS, J. W. & VAN DEURZEN, C. H. 2017. Progressive APOBEC3B mRNA expression in distant breast cancer metastases. *PLoS One,* 12**,** e0171343.

SIKORA, M. J., JACOBSEN, B. M., LEVINE, K., CHEN, J., DAVIDSON, N. E., LEE, A. V., ALEXANDER, C. M. & OESTERREICH, S. 2016. WNT4 mediates estrogen receptor

signaling and endocrine resistance in invasive lobular carcinoma cell lines. *Breast Cancer Res,* 18**,** 92.

SIMONE, C., STIEGLER, P., BAGELLA, L., PUCCI, B., BELLAN, C., DE FALCO, G., DE LUCA, A., GUANTI, G., PURI, P. L. & GIORDANO, A. 2002. Activation of MyoD-dependent transcription by cdk9/cyclin T2. *Oncogene,* 21**,** 4137-48.

SLAMON, D. J., LEYLAND-JONES, B., SHAK, S., FUCHS, H., PATON, V., BAJAMONDE, A., FLEMING, T., EIERMANN, W., WOLTER, J., PEGRAM, M., BASELGA, J. & NORTON, L. 2001. Use of chemotherapy plus a monoclonal antibody against HER2 for metastatic breast cancer that overexpresses HER2. *N Engl J Med,* 344**,** 783-92.

SLEDGE, G. W., JR., TOI, M., NEVEN, P., SOHN, J., INOUE, K., PIVOT, X., BURDAEVA, O., OKERA, M., MASUDA, N., KAUFMAN, P. A., KOH, H., GRISCHKE, E. M., CONTE, P., LU, Y., BARRIGA, S., HURT, K., FRENZEL, M., JOHNSTON, S. & LLOMBART-CUSSAC, A. 2019. The Effect of Abemaciclib Plus Fulvestrant on Overall Survival in Hormone Receptor-Positive, ERBB2-Negative Breast Cancer That Progressed on Endocrine Therapy-MONARCH 2: A Randomized Clinical Trial. *JAMA Oncol*.

SMITH, I. E., WALSH, G., SKENE, A., LLOMBART, A., MAYORDOMO, J. I., DETRE, S., SALTER, J., CLARK, E., MAGILL, P. & DOWSETT, M. 2007. A phase II placebo-controlled trial of neoadjuvant anastrozole alone or with gefitinib in early breast cancer. *J Clin Oncol,* 25**,** 3816-22.

SORLIE, T. 2007. Molecular classification of breast tumors: toward improved diagnostics and treatments. *Methods Mol Biol,* 360**,** 91-114.

SPARANO, J. A., GRAY, R. J., MAKOWER, D. F., PRITCHARD, K. I., ALBAIN, K. S., HAYES, D. F., GEYER, C. E., JR., DEES, E. C., GOETZ, M. P., OLSON, J. A., JR., LIVELY, T., BADVE, S. S., SAPHNER, T. J., WAGNER, L. I., WHELAN, T. J., ELLIS, M. J., PAIK, S., WOOD, W. C., RAVDIN, P. M., KEANE, M. M., GOMEZ MORENO, H. L., REDDY, P. S., GOGGINS, T. F., MAYER, I. A., BRUFSKY, A. M., TOPPMEYER, D. L., KAKLAMANI, V. G., BERENBERG, J. L., ABRAMS, J. & SLEDGE, G. W., JR. 2018. Adjuvant Chemotherapy Guided by a 21-Gene Expression Assay in Breast Cancer. *N Engl J Med,* 379**,** 111-121.

SPRING, L. M., FELL, G., ARFE, A., SHARMA, C., GREENUP, R., REYNOLDS, K. L., SMITH, B. L., ALEXANDER, B., MOY, B., ISAKOFF, S. J., PARMIGIANI, G., TRIPPA, L. & BARDIA, A. 2020. Pathologic Complete Response after Neoadjuvant Chemotherapy and Impact on Breast Cancer Recurrence and Survival: A Comprehensive Meta-analysis. *Clin Cancer Res*.

STOCKWELL, S. R. & MITTNACHT, S. 2017. High-Content Imaging and RNAi Screens for Investigating Kinase Network Plasticity. *Methods Mol Biol,* 1636**,** 133-161.

SWIETACH, P., WIGFIELD, S., COBDEN, P., SUPURAN, C. T., HARRIS, A. L. & VAUGHAN-JONES, R. D. 2008. Tumor-associated carbonic anhydrase 9 spatially coordinates intracellular pH in three-dimensional multicellular growths. *J Biol Chem,* 283**,** 20473-83.

SZKLARCZYK, D., FRANCESCHINI, A., WYDER, S., FORSLUND, K., HELLER, D., HUERTA-CEPAS, J., SIMONOVIC, M., ROTH, A., SANTOS, A., TSAFOU, K. P., KUHN, M., BORK, P., JENSEN, L. J. & VON MERING, C. 2015. STRING v10: protein-protein interaction networks, integrated over the tree of life. *Nucleic Acids Res,* 43**,** D447-52.

SZYMANSKI, P., MARKOWICZ, M. & MIKICIUK-OLASIK, E. 2012. Adaptation of high-throughput screening in drug discovery-toxicological screening tests. *Int J Mol Sci,* 13**,** 427-52.

TAO, S., CHEN, Q., LIN, C. & DONG, H. 2020. Linc00514 promotes breast cancer metastasis and M2 polarization of tumor-associated macrophages via Jagged1-mediated notch signaling pathway. *J Exp Clin Cancer Res,* 39**,** 191.

TATE, J. G., BAMFORD, S., JUBB, H. C., SONDKA, Z., BEARE, D. M., BINDAL, N., BOUTSELAKIS, H., COLE, C. G., CREATORE, C., DAWSON, E., FISH, P., HARSHA, B., HATHAWAY, C., JUPE, S. C., KOK, C. Y., NOBLE, K., PONTING, L., RAMSHAW, C. C., RYE, C. E., SPEEDY, H. E., STEFANCSIK, R., THOMPSON, S. L., WANG, S., WARD, S., CAMPBELL, P. J. & FORBES, S. A. 2019. COSMIC: the Catalogue Of Somatic Mutations In Cancer. *Nucleic Acids Res,* 47**,** D941-D947.

TAYLOR-HARDING, B., ASPURIA, P. J., AGADJANIAN, H., CHEON, D. J., MIZUNO, T., GREENBERG, D., ALLEN, J. R., SPURKA, L., FUNARI, V., SPITERI, E., WANG, Q., ORSULIC, S., WALSH, C., KARLAN, B. Y. & WIEDEMEYER, W. R. 2015. Cyclin E1 and RTK/RAS signaling drive CDK inhibitor resistance via activation of E2F and ETS. *Oncotarget,* 6**,** 696-714.

TOKUNAGA, E., OKI, E., EGASHIRA, A., SADANAGA, N., MORITA, M., KAKEJI, Y. & MAEHARA, Y. 2008. Deregulation of the Akt pathway in human cancer. *Curr Cancer Drug Targets,* 8**,** 27-36.

TORA, L., WHITE, J., BROU, C., TASSET, D., WEBSTER, N., SCHEER, E. & CHAMBON, P. 1989. The human estrogen receptor has two independent nonacidic transcriptional activation functions. *Cell,* 59**,** 477-87.

TORISAWA, Y. S., TAKAGI, A., NASHIMOTO, Y., YASUKAWA, T., SHIKU, H. & MATSUE, T. 2007. A multicellular spheroid array to realize spheroid formation, culture, and viability assay on a chip. *Biomaterials,* 28**,** 559-66.

TOY, W., SHEN, Y., WON, H., GREEN, B., SAKR, R. A., WILL, M., LI, Z., GALA, K., FANNING, S., KING, T. A., HUDIS, C., CHEN, D., TARAN, T., HORTOBAGYI, G., GREENE, G., BERGER, M., BASELGA, J. & CHANDARLAPATY, S. 2013. ESR1 ligand-binding domain mutations in hormone-resistant breast cancer. *Nat Genet,* 45**,** 1439-45.

TOY, W., WEIR, H., RAZAVI, P., LAWSON, M., GOEPPERT, A. U., MAZZOLA, A. M., SMITH, A., WILSON, J., MORROW, C., WONG, W. L., DE STANCHINA, E., CARLSON, K. E., MARTIN, T. S., UDDIN, S., LI, Z., FANNING, S., KATZENELLENBOGEN, J. A., GREENE, G., BASELGA, J. & CHANDARLAPATY, S. 2017. Activating ESR1 Mutations Differentially Affect the Efficacy of ER Antagonists. *Cancer Discov,* 7**,** 277-287.

TSANG, F. H., LAW, C. T., TANG, T. C., CHENG, C. L., CHIN, D. W., TAM, W. V., WEI, L., WONG, C. C., NG, I. O. & WONG, C. M. 2019. Aberrant Super-Enhancer Landscape in Human Hepatocellular Carcinoma. *Hepatology,* 69**,** 2502-2517.

TURNER, N. C., ALARCON, E., ARMSTRONG, A. C., PHILCO, M., LOPEZ CHUKEN, Y. A., SABLIN, M. P., TAMURA, K., GOMEZ VILLANUEVA, A., PEREZ-FIDALGO, J. A., CHEUNG, S. Y. A., CORCORAN, C., CULLBERG, M., DAVIES, B. R., DE BRUIN, E. C., FOXLEY, A., LINDEMANN, J. P. O., MAUDSLEY, R., MOSCHETTA, M., OUTHWAITE, E., PASS, M., RUGMAN, P., SCHIAVON, G. & OLIVEIRA, M. 2019. BEECH: a dose-finding run-in followed by a randomised phase II study assessing the efficacy of AKT inhibitor capivasertib (AZD5363) combined with paclitaxel in patients with estrogen receptor-positive advanced or metastatic breast cancer, and in a PIK3CA mutant sub-population. *Ann Oncol,* 30**,** 774-780.

TURNER, N. C., SWIFT, C., KILBURN, L., FRIBBENS, C., BEANEY, M., GARCIA-MURILLAS, I., BUDZAR, A. U., ROBERTSON, J. F. R., GRADISHAR, W., PICCART, M., SCHIAVON, G., BLISS, J. M., DOWSETT, M., JOHNSTON, S. R. D. & CHIA, S. K. 2020. ESR1 Mutations and Overall Survival on Fulvestrant versus Exemestane in Advanced

Hormone Receptor-Positive Breast Cancer: A Combined Analysis of the Phase III SoFEA and EFECT Trials. *Clin Cancer Res,* 26**,** 5172-5177.

UMAYAHARA, Y., KAWAMORI, R., WATADA, H., IMANO, E., IWAMA, N., MORISHIMA, T., YAMASAKI, Y., KAJIMOTO, Y. & KAMADA, T. 1994. Estrogen regulation of the insulin-like growth factor I gene transcription involves an AP-1 enhancer. *J Biol Chem,* 269**,** 16433-42.

VAIDYA, J. S., BULSARA, M., BAUM, M., WENZ, F., MASSARUT, S., PIGORSCH, S., ALVARADO, M., DOUEK, M., SAUNDERS, C., FLYGER, H. L., EIERMANN, W., BREW-GRAVES, C., WILLIAMS, N. R., POTYKA, I., ROBERTS, N., BERNSTEIN, M., BROWN, D., SPERK, E., LAWS, S., SUTTERLIN, M., CORICA, T., LUNDGREN, S., HOLMES, D., VINANTE, L., BOZZA, F., PAZOS, M., LE BLANC-ONFROY, M., GRUBER, G., POLKOWSKI, W., DEDES, K. J., NIEWALD, M., BLOHMER, J., MCCREADY, D., HOEFER, R., KELEMEN, P., PETRALIA, G., FALZON, M., JOSEPH, D. J. & TOBIAS, J. S. 2020. Long term survival and local control outcomes from single dose targeted intraoperative radiotherapy during lumpectomy (TARGIT-IORT) for early breast cancer: TARGIT-A randomised clinical trial. *BMJ,* 370**,** m2836.

VAILLANT, F., MERINO, D., LEE, L., BRESLIN, K., PAL, B., RITCHIE, M. E., SMYTH, G. K., CHRISTIE, M., PHILLIPSON, L. J., BURNS, C. J., MANN, G. B., VISVADER, J. E. & LINDEMAN, G. J. 2013. Targeting BCL-2 with the BH3 mimetic ABT-199 in estrogen receptor-positive breast cancer. *Cancer Cell,* 24**,** 120-9.

VASAN, N., TOSKA, E. & SCALTRITI, M. 2019a. Overview of the relevance of PI3K pathway in HR-positive breast cancer. *Ann Oncol,* 30**,** x3-x11.

VASAN, N., TOSKA, E. & SCALTRITI, M. 2019b. Overview of the relevance of PI3K pathway in HR-positive breast cancer. *Ann Oncol,* 30 Suppl 10**,** x3-x11.

VEERANKI, O. L., TONG, Z., DOKEY, R., MEJIA, A., ZHANG, J., QIAO, Y., SINGH, P. K., KATKHUDA, R., MINO, B., TAILOR, R., CANALES, J. R., BASSETT, R., AJANI, J., WU, J. Y., KOPETZ, S., BLUM, M., HOFSTETTER, W., TETZLAFF, M., KRISHNAN, S., LIN, S. H. & MARU, D. 2019. Targeting cyclin-dependent kinase 9 by a novel inhibitor enhances radiosensitization and identifies Axl as a novel downstream target in esophageal adenocarcinoma. *Oncotarget,* 10**,** 4703-4718.

VENDITTI, M., IWASIOW, B., ORR, F. W. & SHIU, R. P. 2002. C-myc gene expression alone is sufficient to confer resistance to antiestrogen in human breast cancer cells. *Int J Cancer,* 99**,** 35-42.

VINCI, M., GOWAN, S., BOXALL, F., PATTERSON, L., ZIMMERMANN, M., COURT, W., LOMAS, C., MENDIOLA, M., HARDISSON, D. & ECCLES, S. A. 2012. Advances in establishment and analysis of three-dimensional tumor spheroid-based functional assays for target validation and drug evaluation. *BMC Biol,* 10**,** 29.

VLACHOGIANNIS, G., HEDAYAT, S., VATSIOU, A., JAMIN, Y., FERNANDEZ-MATEOS, J., KHAN, K., LAMPIS, A., EASON, K., HUNTINGFORD, I., BURKE, R., RATA, M., KOH, D. M., TUNARIU, N., COLLINS, D., HULKKI-WILSON, S., RAGULAN, C., SPITERI, I., MOORCRAFT, S. Y., CHAU, I., RAO, S., WATKINS, D., FOTIADIS, N., BALI, M., DARVISH-DAMAVANDI, M., LOTE, H., ELTAHIR, Z., SMYTH, E. C., BEGUM, R., CLARKE, P. A., HAHNE, J. C., DOWSETT, M., DE BONO, J., WORKMAN, P., SADANANDAM, A., FASSAN, M., SANSOM, O. J., ECCLES, S., STARLING, N., BRACONI, C., SOTTORIVA, A., ROBINSON, S. P., CUNNINGHAM, D. & VALERI, N. 2018. Patient-derived organoids model treatment response of metastatic gastrointestinal cancers. *Science,* 359**,** 920-926.

VON MINCKWITZ, G., HUANG, C. S., MANO, M. S., LOIBL, S., MAMOUNAS, E. P., UNTCH, M., WOLMARK, N., RASTOGI, P., SCHNEEWEISS, A., REDONDO, A., FISCHER, H. H.,

JACOT, W., CONLIN, A. K., ARCE-SALINAS, C., WAPNIR, I. L., JACKISCH, C., DIGIOVANNA, M. P., FASCHING, P. A., CROWN, J. P., WULFING, P., SHAO, Z., ROTA CAREMOLI, E., WU, H., LAM, L. H., TESAROWSKI, D., SMITT, M., DOUTHWAITE, H., SINGEL, S. M., GEYER, C. E., JR. & INVESTIGATORS, K. 2019. Trastuzumab Emtansine for Residual Invasive HER2-Positive Breast Cancer. *N Engl J Med,* 380**,** 617-628.

VOUTSADAKIS, I. A. 2000. Apoptosis and the pathogenesis of lymphoma. *Acta Oncol,* 39**,** 151-6.

WADA, T., TAKAGI, T., YAMAGUCHI, Y., FERDOUS, A., IMAI, T., HIROSE, S., SUGIMOTO, S., YANO, K., HARTZOG, G. A., WINSTON, F., BURATOWSKI, S. & HANDA, H. 1998. DSIF, a novel transcription elongation factor that regulates RNA polymerase II processivity, is composed of human Spt4 and Spt5 homologs. *Genes Dev,* 12**,** 343-56.

WAKELING, A. E., DUKES, M. & BOWLER, J. 1991. A potent specific pure antiestrogen with clinical potential. *Cancer Res,* 51**,** 3867-73.

WANG, J., XIE, S., YANG, J., XIONG, H., JIA, Y., ZHOU, Y., CHEN, Y., YING, X., CHEN, C., YE, C., WANG, L. & ZHOU, J. 2019. The long noncoding RNA H19 promotes tamoxifen resistance in breast cancer via autophagy. *J Hematol Oncol,* 12**,** 81.

WANG, Q., LI, M., ZHANG, X., HUANG, H., HUANG, J., KE, J., DING, H., XIAO, J., SHAN, X., LIU, Q., BAO, B. & YANG, L. 2016. Upregulation of CDK7 in gastric cancer cell promotes tumor cell proliferation and predicts poor prognosis. *Exp Mol Pathol,* 100**,** 514-21.

WANG, Y., ZHANG, T., KWIATKOWSKI, N., ABRAHAM, B. J., LEE, T. I., XIE, S., YUZUGULLU, H., VON, T., LI, H., LIN, Z., STOVER, D. G., LIM, E., WANG, Z. C., IGLEHART, J. D., YOUNG, R. A., GRAY, N. S. & ZHAO, J. J. 2015. CDK7-dependent transcriptional addiction in triple-negative breast cancer. *Cell,* 163**,** 174-86.

WEIR, H. M., BRADBURY, R. H., LAWSON, M., RABOW, A. A., BUTTAR, D., CALLIS, R. J., CURWEN, J. O., DE ALMEIDA, C., BALLARD, P., HULSE, M., DONALD, C. S., FERON, L. J., KAROUTCHI, G., MACFAUL, P., MOSS, T., NORMAN, R. A., PEARSON, S. E., TONGE, M., DAVIES, G., WALKER, G. E., WILSON, Z., ROWLINSON, R., POWELL, S., SADLER, C., RICHMOND, G., LADD, B., PAZOLLI, E., MAZZOLA, A. M., D'CRUZ, C. & DE SAVI, C. 2016. AZD9496: An Oral Estrogen Receptor Inhibitor That Blocks the Growth of ER-Positive and ESR1-Mutant Breast Tumors in Preclinical Models. *Cancer Res,* 76**,** 3307-18.

WILLIAMS, M. M., SPOELSTRA, N. S., ARNESEN, S., O'NEILL, K. I., CHRISTENSON, J. L., REESE, J., TORKKO, K. C., GOODSPEED, A., ROSAS, E., HANAMURA, T., SAMS, S. B., LI, Z., OESTERREICH, S., RIGGINS, R. B., JACOBSEN, B. M., ELIAS, A., GERTZ, J. & RICHER, J. K. 2021. Steroid Hormone Receptor and Infiltrating Immune Cell Status Reveals Therapeutic Vulnerabilities of ESR1-Mutant Breast Cancer. *Cancer Res,* 81**,** 732-746.

WITKIEWICZ, A. K. & KNUDSEN, E. S. 2014. Retinoblastoma tumor suppressor pathway in breast cancer: prognosis, precision medicine, and therapeutic interventions. *Breast Cancer Res,* 16**,** 207.

WOLFF, A. C., LAZAR, A. A., BONDARENKO, I., GARIN, A. M., BRINCAT, S., CHOW, L., SUN, Y., NESKOVIC-KONSTANTINOVIC, Z., GUIMARAES, R. C., FUMOLEAU, P., CHAN, A., HACHEMI, S., STRAHS, A., CINCOTTA, M., BERKENBLIT, A., KRYGOWSKI, M., KANG, L. L., MOORE, L. & HAYES, D. F. 2013. Randomized phase III placebo-controlled trial of letrozole plus oral temsirolimus as first-line endocrine therapy

in postmenopausal women with locally advanced or metastatic breast cancer. *J Clin Oncol,* 31**,** 195-202.

WONG, K. H., JIN, Y. & STRUHL, K. 2014. TFIIH phosphorylation of the Pol II CTD stimulates mediator dissociation from the preinitiation complex and promoter escape. *Mol Cell,* 54**,** 601-12.

WORLD CANCER RESEARCH FUND 2018. Breast Cancer Statistics.

WU, J., ZHANG, S., SHAN, J., HU, Z., LIU, X., CHEN, L., REN, X., YAO, L., SHENG, H., LI, L., ANN, D., YEN, Y., WANG, J. & WANG, X. 2016. Elevated HMGA2 expression is associated with cancer aggressiveness and predicts poor outcome in breast cancer. *Cancer Lett,* 376**,** 284-92.

XING, Y., LIN, N. U., MAURER, M. A., CHEN, H., MAHVASH, A., SAHIN, A., AKCAKANAT, A., LI, Y., ABRAMSON, V., LITTON, J., CHAVEZ-MACGREGOR, M., VALERO, V., PIHA-PAUL, S. A., HONG, D., DO, K. A., TARCO, E., RIALL, D., ETEROVIC, A. K., WULF, G. M., CANTLEY, L. C., MILLS, G. B., DOYLE, L. A., WINER, E., HORTOBAGYI, G. N., GONZALEZ-ANGULO, A. M. & MERIC-BERNSTAM, F. 2019. Phase II trial of AKT inhibitor MK-2206 in patients with advanced breast cancer who have tumors with PIK3CA or AKT mutations, and/or PTEN loss/PTEN mutation. *Breast Cancer Res,* 21**,** 78.

XU, B., GUAN, Z., SHEN, Z., TONG, Z., JIANG, Z., YANG, J., DESILVIO, M., RUSSO, M., LEIGH, M. & ELLIS, C. 2014. Association of phosphatase and tensin homolog low and phosphatidylinositol 3-kinase catalytic subunit alpha gene mutations on outcome in human epidermal growth factor receptor 2-positive metastatic breast cancer patients treated with first-line lapatinib plus paclitaxel or paclitaxel alone. *Breast Cancer Res,* 16**,** 405.

YAMAGUCHI, Y., TAKAGI, T., WADA, T., YANO, K., FURUYA, A., SUGIMOTO, S., HASEGAWA, J. & HANDA, H. 1999. NELF, a multisubunit complex containing RD, cooperates with DSIF to repress RNA polymerase II elongation. *Cell,* 97**,** 41-51.

YANG, C., LI, Z., BHATT, T., DICKLER, M., GIRI, D., SCALTRITI, M., BASELGA, J., ROSEN, N. & CHANDARLAPATY, S. 2017. Acquired CDK6 amplification promotes breast cancer resistance to CDK4/6 inhibitors and loss of ER signaling and dependence. *Oncogene,* 36**,** 2255-2264.

YANG, W., SOARES, J., GRENINGER, P., EDELMAN, E. J., LIGHTFOOT, H., FORBES, S., BINDAL, N., BEARE, D., SMITH, J. A., THOMPSON, I. R., RAMASWAMY, S., FUTREAL, P. A., HABER, D. A., STRATTON, M. R., BENES, C., MCDERMOTT, U. & GARNETT, M. J. 2013. Genomics of Drug Sensitivity in Cancer (GDSC): a resource for therapeutic biomarker discovery in cancer cells. *Nucleic Acids Res,* 41**,** D955-61.

YANG, Z., HE, N. & ZHOU, Q. 2008. Brd4 recruits P-TEFb to chromosomes at late mitosis to promote G1 gene expression and cell cycle progression. *Mol Cell Biol,* 28**,** 967-76.

YANG, Z., YIK, J. H., CHEN, R., HE, N., JANG, M. K., OZATO, K. & ZHOU, Q. 2005. Recruitment of P-TEFb for stimulation of transcriptional elongation by the bromodomain protein Brd4. *Mol Cell,* 19**,** 535-45.

YATES, L. R., GERSTUNG, M., KNAPPSKOG, S., DESMEDT, C., GUNDEM, G., VAN LOO, P., AAS, T., ALEXANDROV, L. B., LARSIMONT, D., DAVIES, H., LI, Y., JU, Y. S., RAMAKRISHNA, M., HAUGLAND, H. K., LILLENG, P. K., NIK-ZAINAL, S., MCLAREN, S., BUTLER, A., MARTIN, S., GLODZIK, D., MENZIES, A., RAINE, K., HINTON, J., JONES, D., MUDIE, L. J., JIANG, B., VINCENT, D., GREENE-COLOZZI, A., ADNET, P. Y., FATIMA, A., MAETENS, M., IGNATIADIS, M., STRATTON, M. R., SOTIRIOU, C.,

RICHARDSON, A. L., LONNING, P. E., WEDGE, D. C. & CAMPBELL, P. J. 2015. Subclonal diversification of primary breast cancer revealed by multiregion sequencing. *Nat Med,* 21**,** 751-9.

YU, D. S., ZHAO, R., HSU, E. L., CAYER, J., YE, F., GUO, Y., SHYR, Y. & CORTEZ, D. 2010. Cyclin-dependent kinase 9-cyclin K functions in the replication stress response. *EMBO Rep,* 11**,** 876-82.

YU, G., WANG, L. G., HAN, Y. & HE, Q. Y. 2012. clusterProfiler: an R package for comparing biological themes among gene clusters. *OMICS,* 16**,** 284-7.

YU, H. A., ARCILA, M. E., HELLMANN, M. D., KRIS, M. G., LADANYI, M. & RIELY, G. J. 2014. Poor response to erlotinib in patients with tumors containing baseline EGFR T790M mutations found by routine clinical molecular testing. *Ann Oncol,* 25**,** 423-8.

ZHANG, J. H., CHUNG, T. D. & OLDENBURG, K. R. 1999. A Simple Statistical Parameter for Use in Evaluation and Validation of High Throughput Screening Assays. *J Biomol Screen,* 4**,** 67-73.

ZHAO, X., RODLAND, E. A., TIBSHIRANI, R. & PLEVRITIS, S. 2015. Molecular subtyping for clinically defined breast cancer subgroups. *Breast Cancer Res,* 17**,** 29.

ZHAO, Y., SHEN, X., ZHU, Y., WANG, A., XIONG, Y., WANG, L., FEI, Y., WANG, Y., WANG, W., LIN, F. & LIANG, Z. 2019. Cathepsin L-mediated resistance of paclitaxel and cisplatin is mediated by distinct regulatory mechanisms. *J Exp Clin Cancer Res,* 38**,** 333.

ZHAO, Y. L., HAN, W. D., LI, Q., MU, Y. M., LU, X. C., YU, L., SONG, H. J., LI, X., LU, J. M. & PAN, C. Y. 2005. Mechanism of transcriptional regulation of LRP16 gene expression by 17-beta estradiol in MCF-7 human breast cancer cells. *J Mol Endocrinol,* 34**,** 77-89.

ZHENG, H. Q., ZHOU, Z., HUANG, J., CHAUDHURY, L., DONG, J. T. & CHEN, C. 2009. Kruppel-like factor 5 promotes breast cell proliferation partially through upregulating the transcription of fibroblast growth factor binding protein 1. *Oncogene,* 28**,** 3702-13.

ZHOU, Q., LI, T. & PRICE, D. H. 2012. RNA polymerase II elongation control. *Annu Rev Biochem,* 81**,** 119-43.

ZUNDELEVICH, A., DADIANI, M., KAHANA-EDWIN, S., ITAY, A., SELLA, T., GADOT, M., CESARKAS, K., FARAGE-BARHOM, S., SAAR, E. G., EYAL, E., KOL, N., PAVLOVSKI, A., BALINT-LAHAT, N., DICK-NECULA, D., BARSHACK, I., KAUFMAN, B. & GAL-YAM, E. N. 2020. ESR1 mutations are frequent in newly diagnosed metastatic and loco-regional recurrence of endocrine-treated breast cancer and carry worse prognosis. *Breast Cancer Res,* 22**,** 16.

Chapter 9 Appendix 1

9.1 Genes identified as hits in 2D siRNA screens

9.1.1 Comparison of all LTED cell lines (Fig 5.4B)

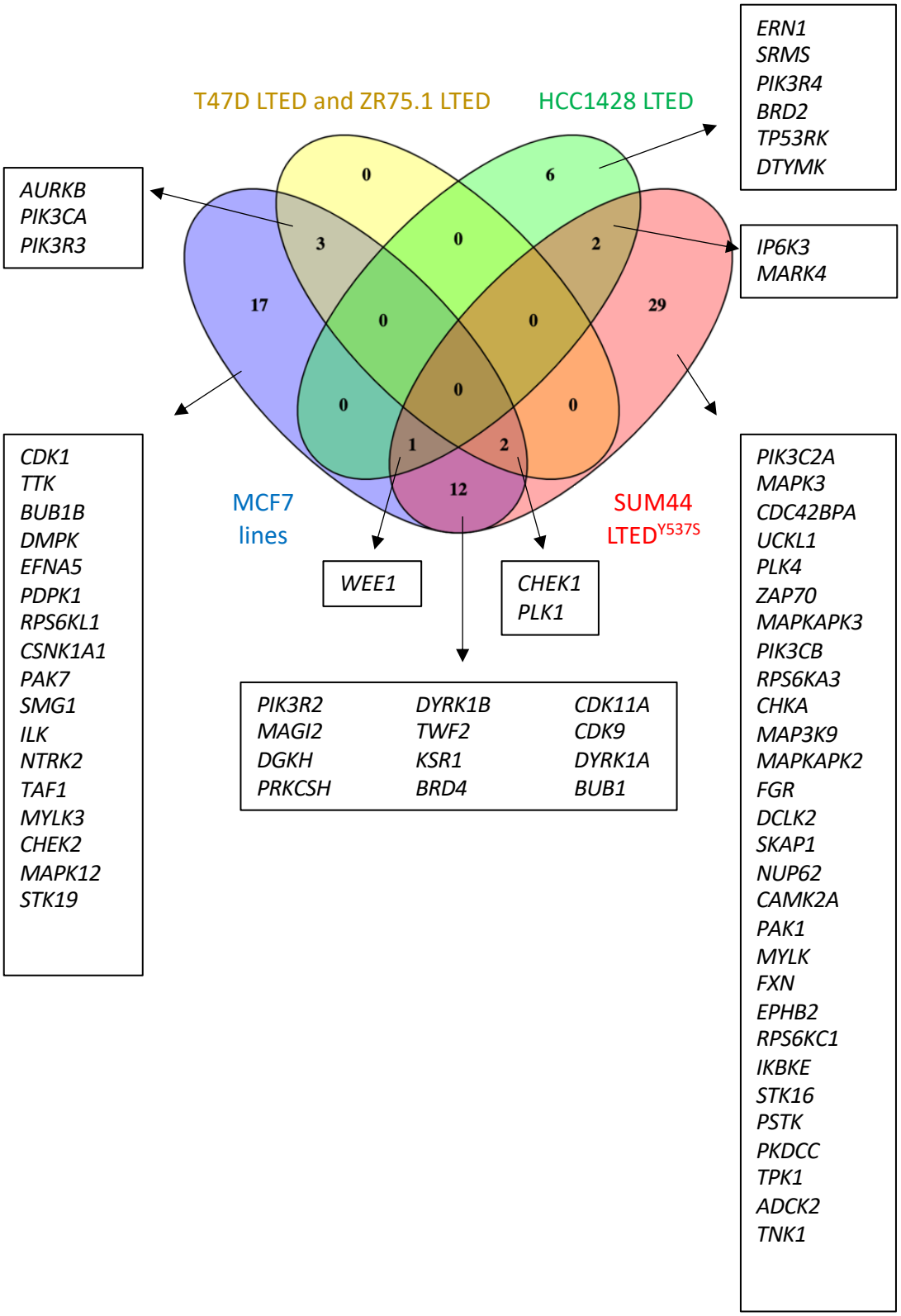

9.1.2 Comparison of MCF7 LTED^{WT} and MCF7 LTED^{Y537C} lines (Fig 5.5A)

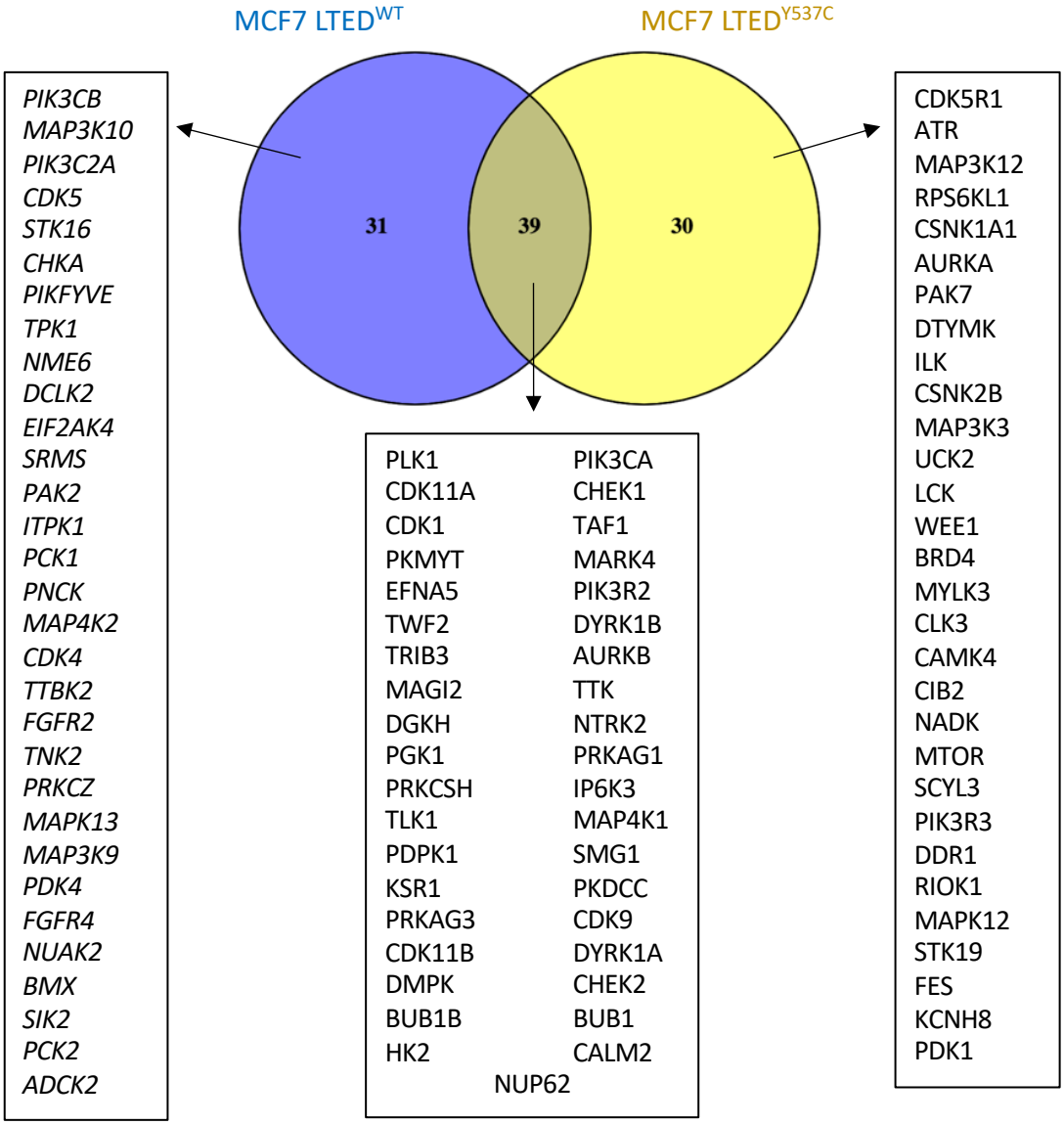

9.1.3 Comparison of all MCF7 LTED lines (Fig 5.6A)

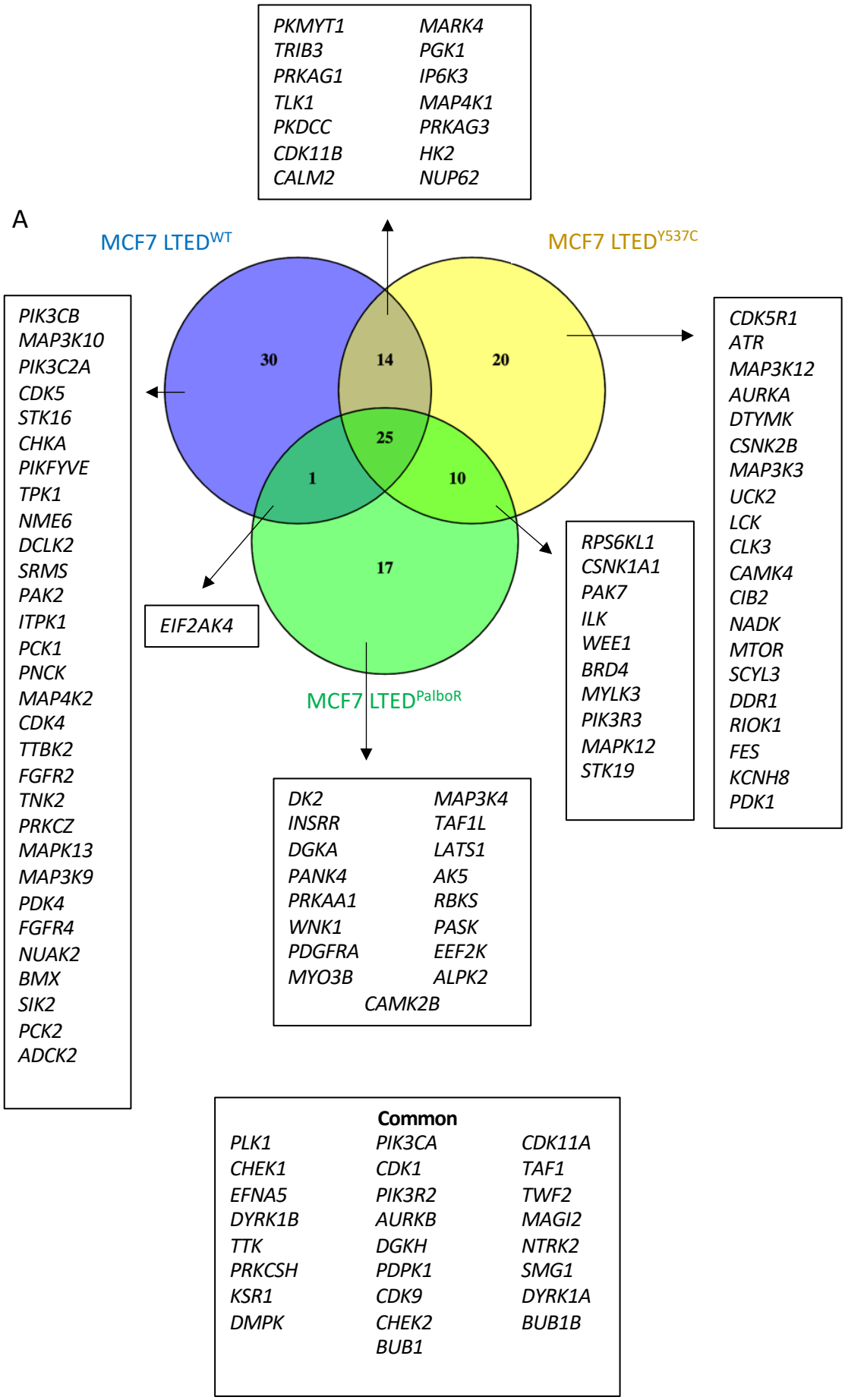

9.1.4 Comparison of T47D LTED and ZR75.1 LTED (Fig 5.7A)

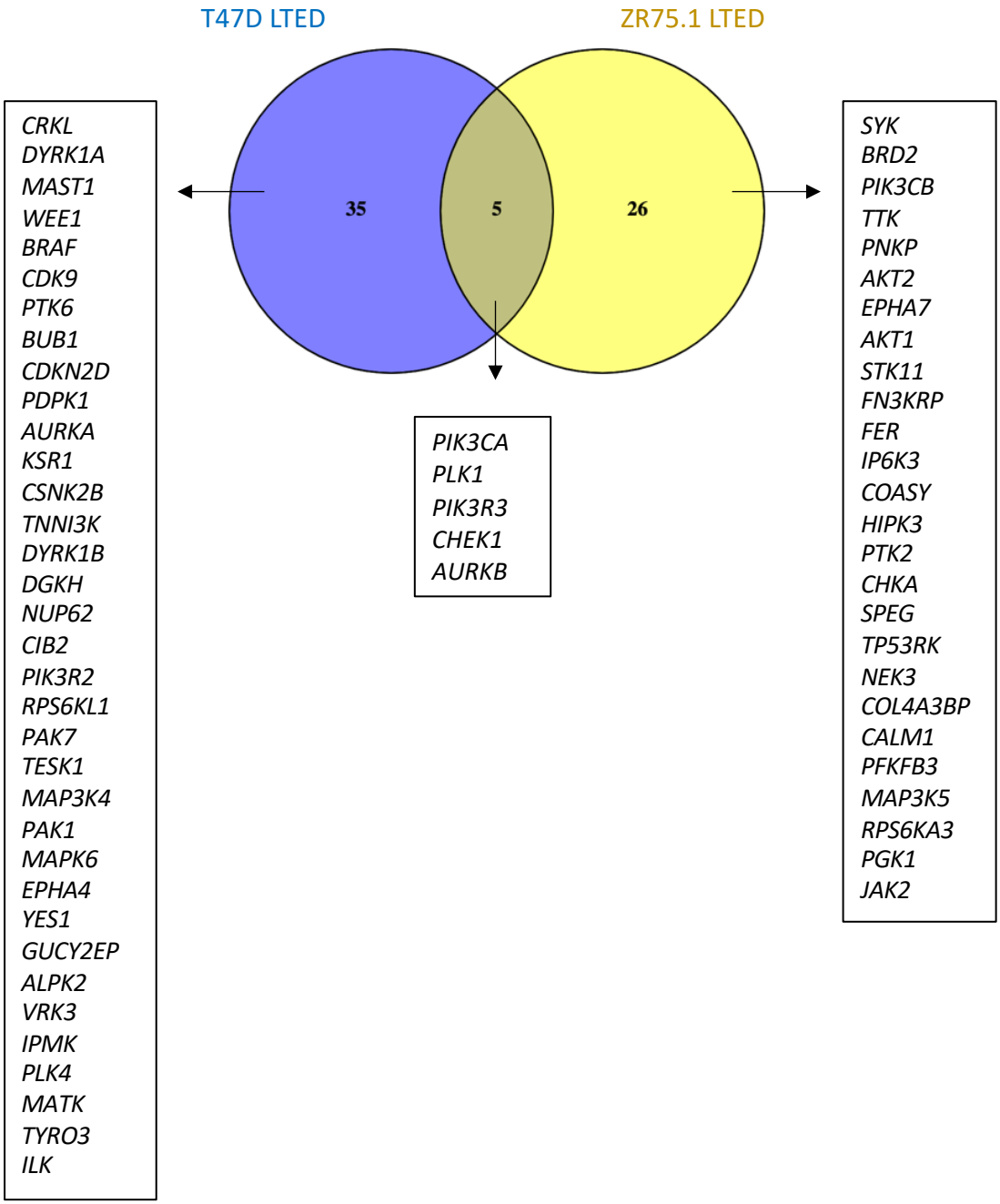

9.2 Genes identified as hits in 3D siRNA screens

9.2.1 Comparison of all LTED lines (Fig 5.8)

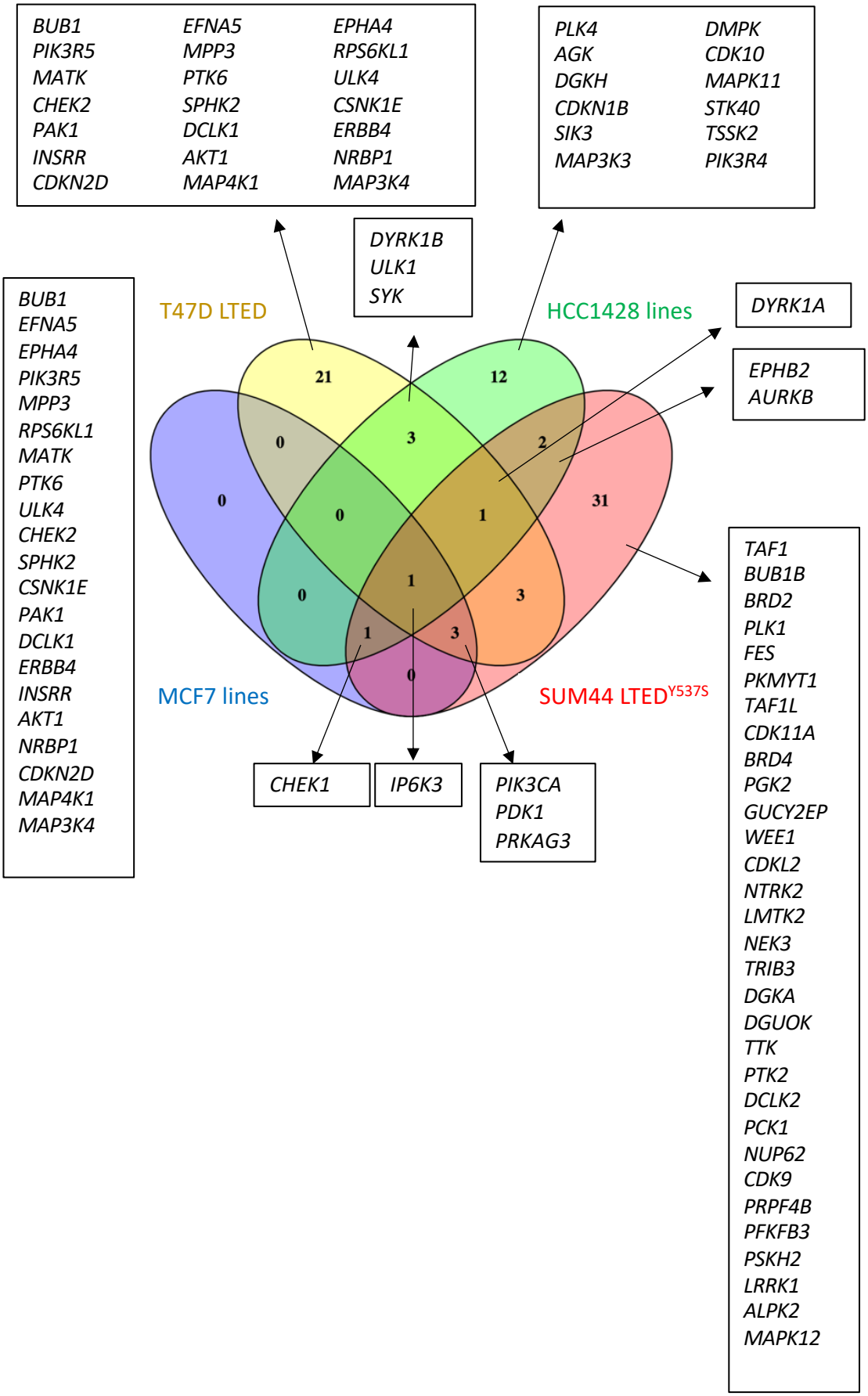

9.2.2 Comparison of MCF7 LTED^{WT} and MCF7 LTED^{Y537C} lines (Fig 5.9A)

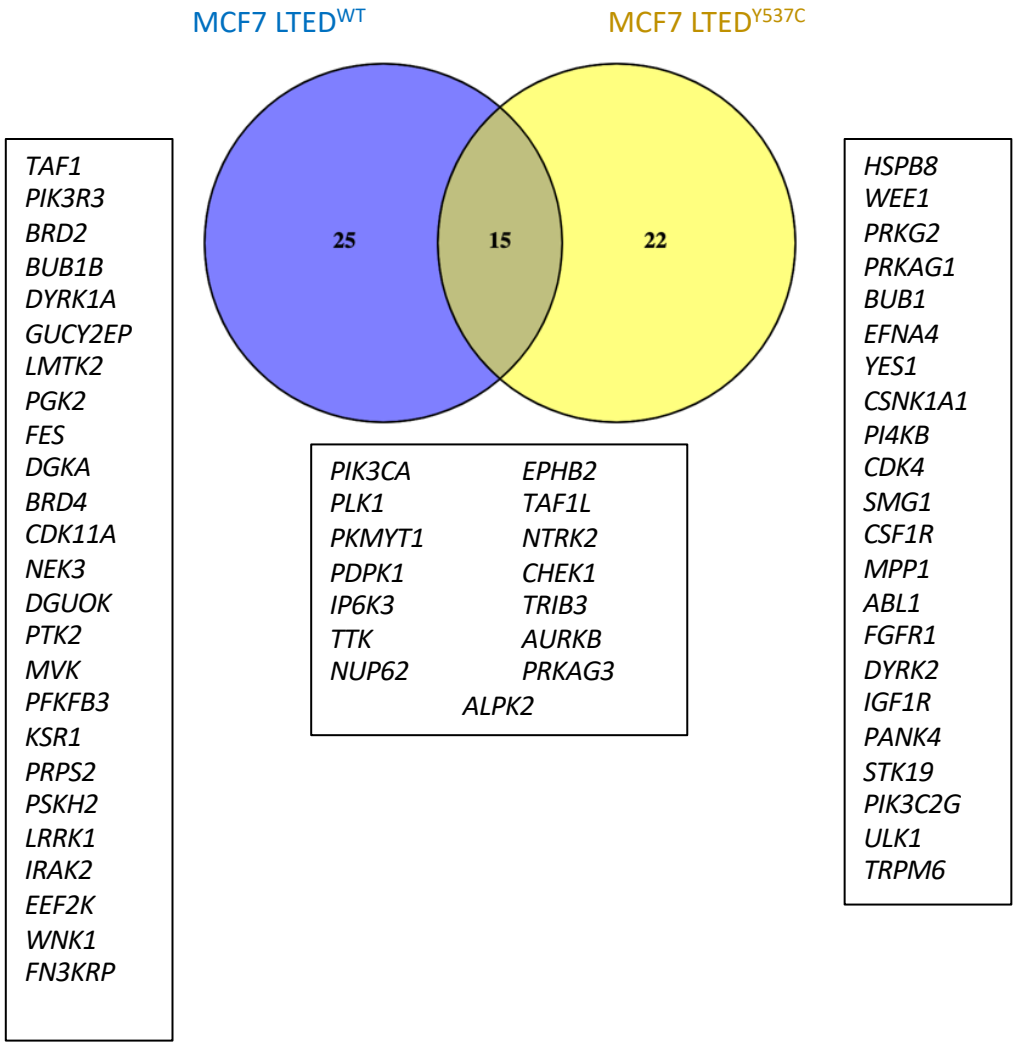

9.2.3 Comparison of all MCF7 LTED lines (Fig 5.10A)

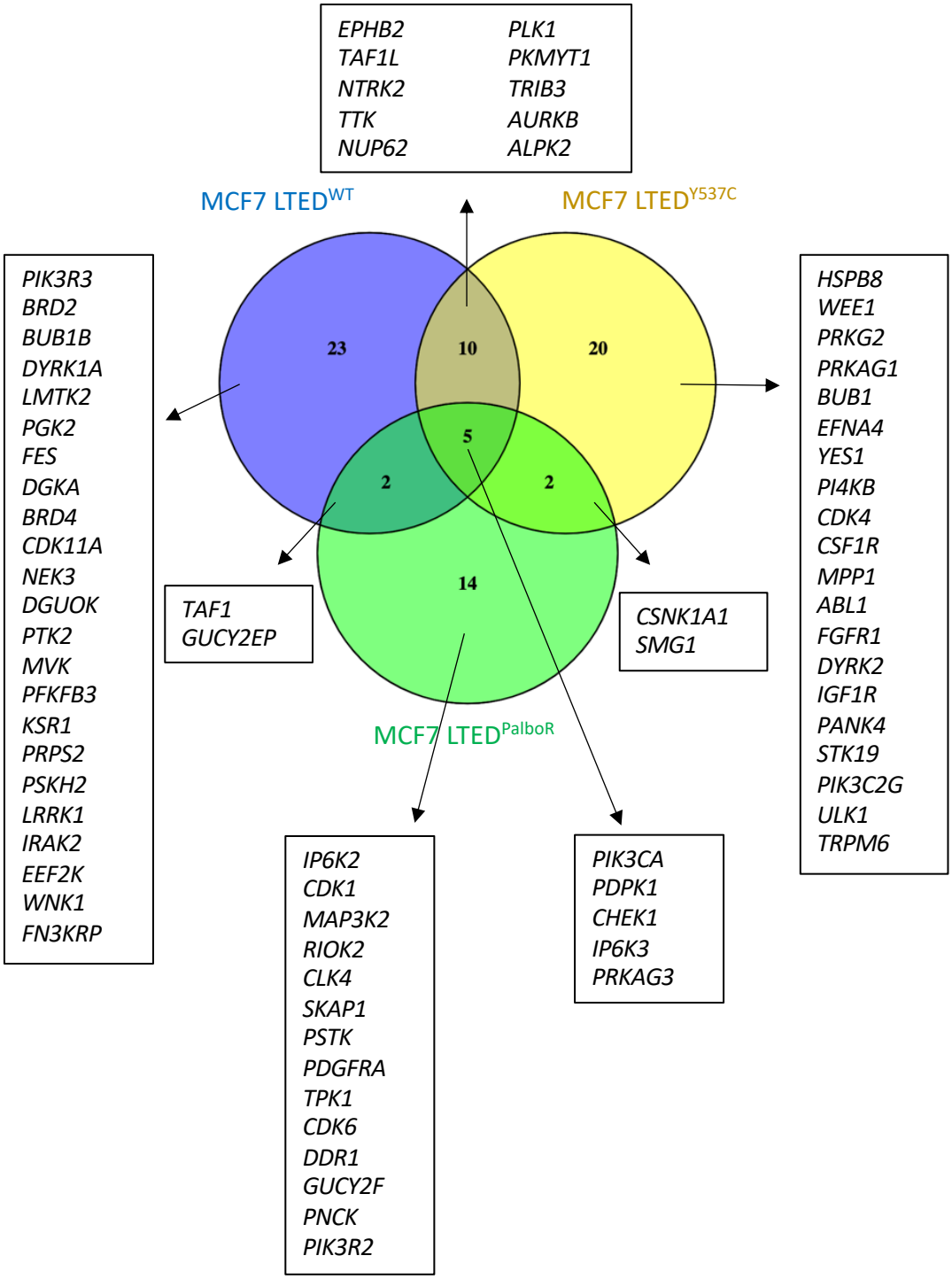

9.2.4 Comparison of HCC1428 LTED and HCC1428 LTED^{PalboR} (Fig 5.11A)

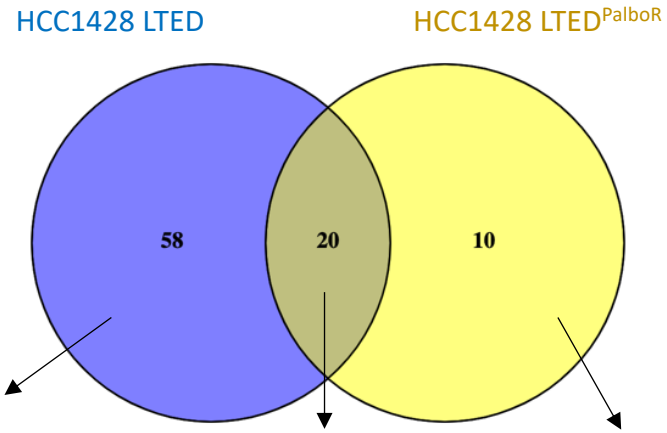

BUB1	TNNI3K
KCNH8	CDC42BPA
TYRO3	FGR
ERN1	MAPK3
PEAK1	TWF2
PTK6	TAF1
GAK	MTOR
STK11	DGKG
MAPKAPK3	PAK6
MOK	NUP62
PANK4	RPS6KA3
TNK2	KSR1
PLK1	IRAK2
LCK	HK2
FES	CIB2
GRK4	AK5
PIM2	PAK2
PKDCC	JAK2
BRSK2	PIK3C2A
LYN	GUCY2EP
CAMK1	IPPK
HIPK3	EEF2K
FGFRL1	SPHK2
RPS6KB1	MATK
RPS6KL1	EXOSC10
INSR	MYLK3
AKT3	DGUOK
PRKAR2B	STK16
PRPF4B	CMPK1

IP6K3
PLK4
DYRK1A
ULK1
DMPK
SYK
DYRK1B
EPHB2
AGK
CDK10
DGKH
MAPK11
CHEK1
CDKN1B
STK40
SIK3
TSSK2
MAP3K3
AURKB
PIK3R4

ERBB3
MYLK
RET
TESK1
COL4A3B
P
PBK
WEE1
MAPK6
MPP3
TP53RK

9.3 Drugs identified as hits in 2D screens

9.3.1 Comparison of all cell lines (Fig 5.14)

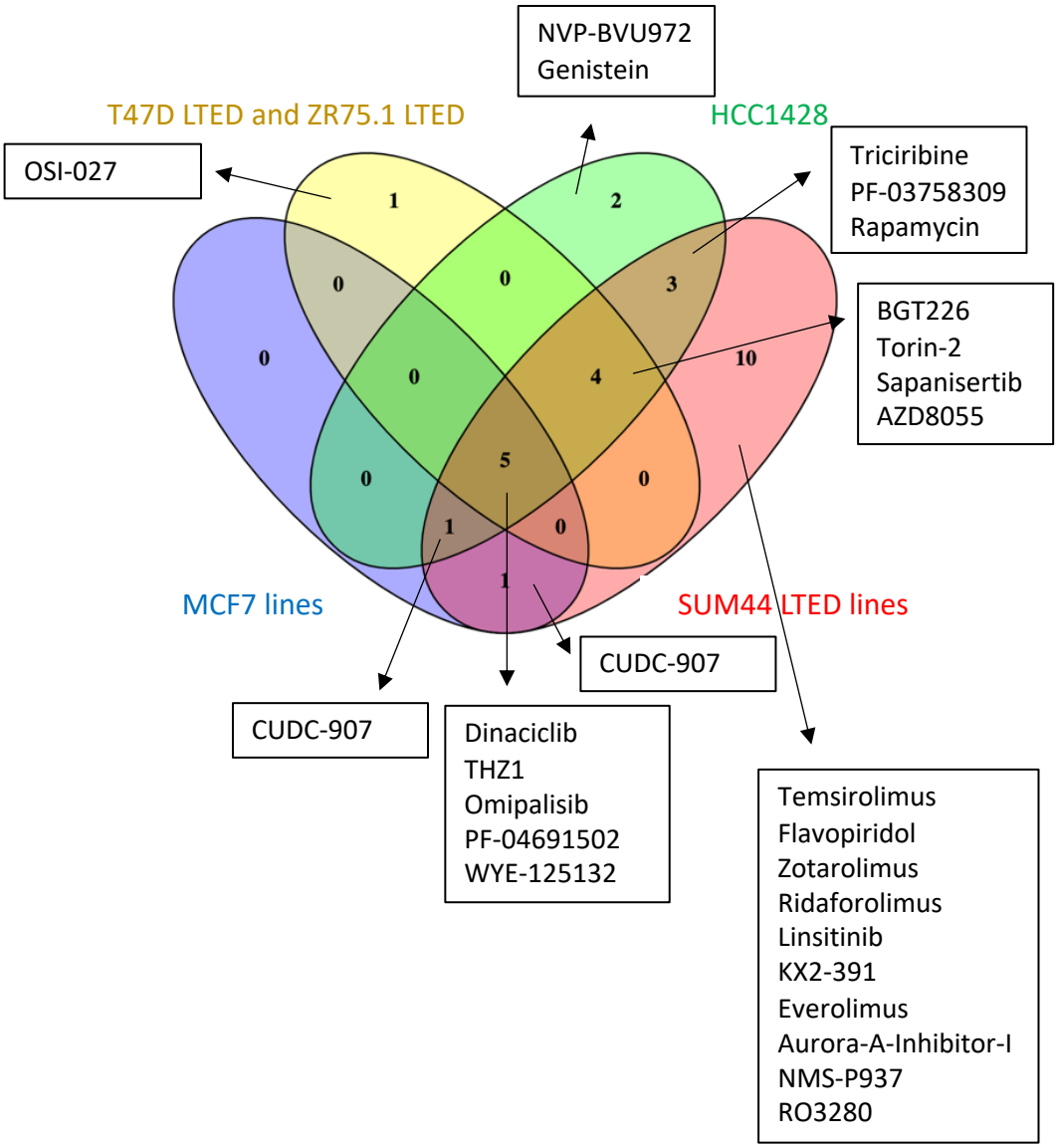

9.3.2 Comparison of MCF7 LTED^{WT} and MCF7 LTED^{Y537C} lines (Fig 5.15A)

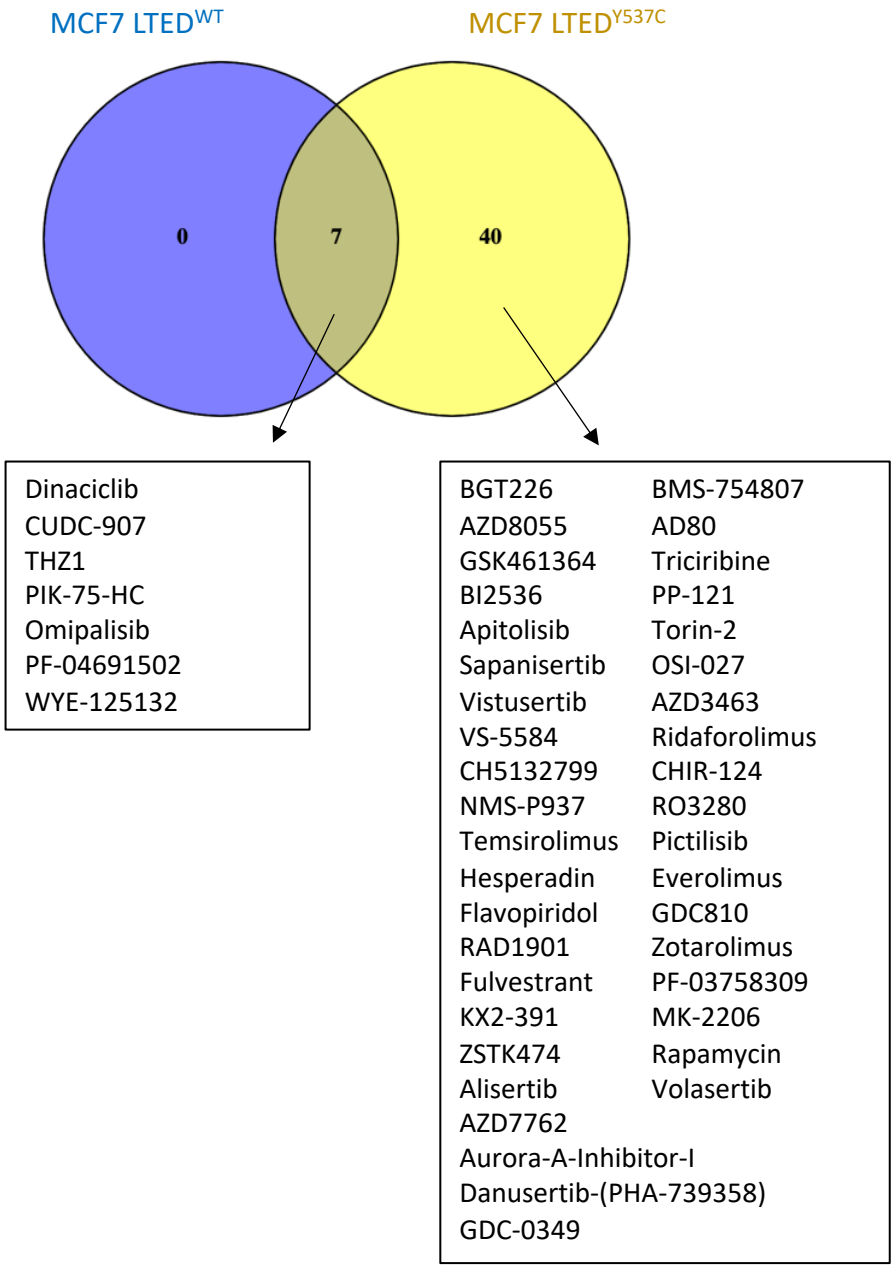

9.3.3 Comparison of SUM44 LTED^{WT} and SUM44 LTED^{Y537S}

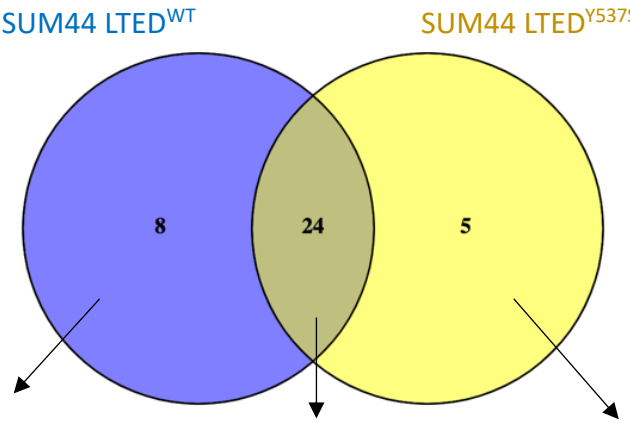

CUDC-101 SNS-032-(BMS-387032) GZD824-Dimesylate CGK-733 Bosutinib Wortmannin PD168393 Pimasertib	CUDC-907 BGT226 Dinaciclib THZ1 PIK-75-HCl Torin-2 Sapanisertib WYE-125132 PF-04691502 AZD8055 Omipalisib Temsirolimus Flavopiridol Zotarolimus Rapamycin Ridaforolimus Linsitinib KX2-391 PF-03758309 Everolimus Aurora-A-Inhibitor-I Triciribine NMS-P937 RO3280	GSK461364 BI2536 AD80 Fulvestrant CHIR-124

9.4 Drugs identified as hits in 3D screens

9.4.1 Comparison of all cell lines (Fig 5.17)

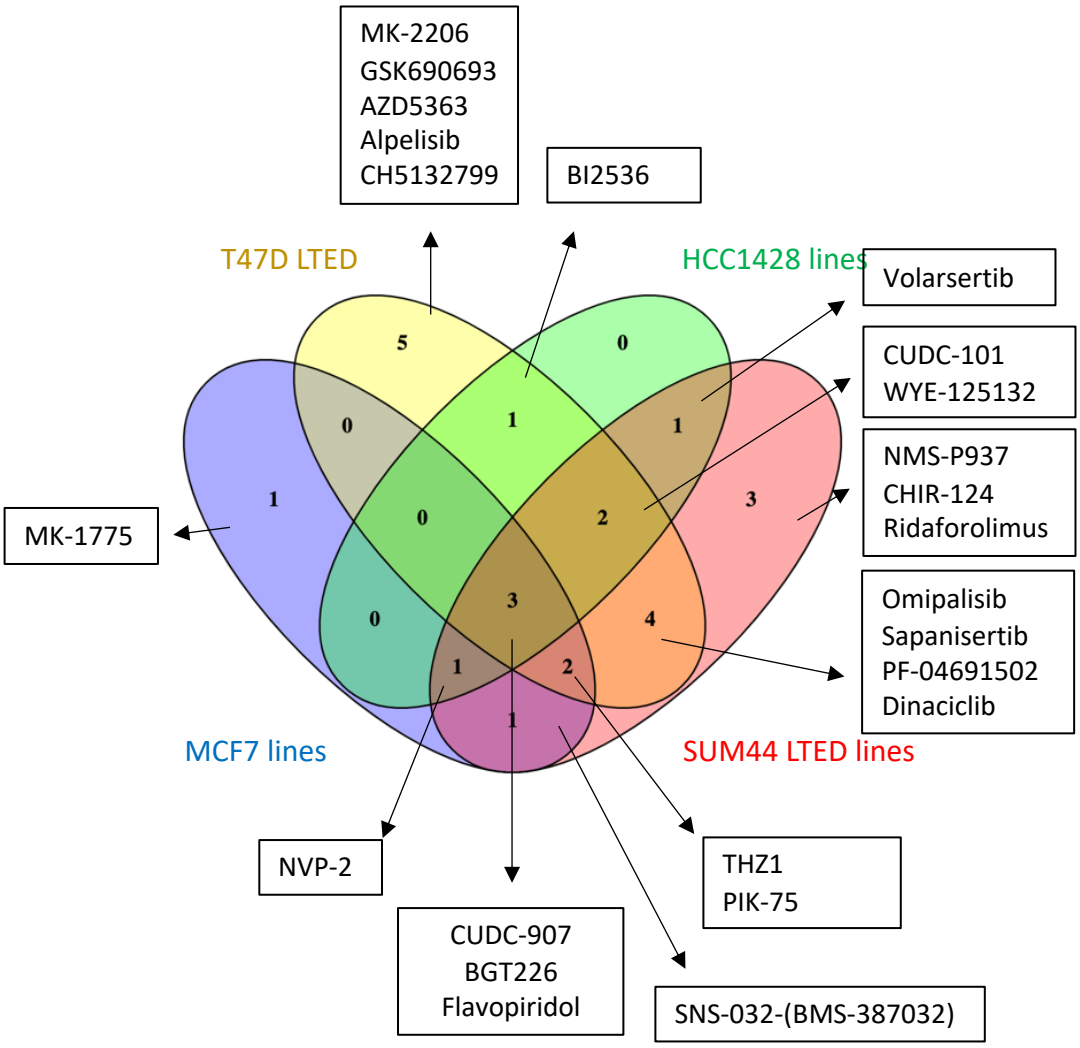

Chapter 10 Appendix 2

10.1 List of siRNAs used in siRNA library and their targets

GeneID	Description
AAK1	AP2 associated kinase 1
AATK	apoptosis associated tyrosine kinase
ABL1	ABL proto-oncogene 1, non-receptor tyrosine kinase
ABL2	ABL proto-oncogene 2, non-receptor tyrosine kinase
ACVR1	activin A receptor type 1
ACVR1C	activin A receptor type 1C
ACVR2A	activin A receptor type 2A
ACVR2B	activin A receptor type 2B
ACVRL1	activin A receptor like type 1
ADCK1	aarF domain containing kinase 1
ADCK2	aarF domain containing kinase 2
ADCK4	coenzyme Q8B
ADCK5	aarF domain containing kinase 5
ADK	adenosine kinase
ADPGK	ADP dependent glucokinase
ADRBK1	G protein-coupled receptor kinase 2
ADRBK2	G protein-coupled receptor kinase 3
AGK	acylglycerol kinase
AK1	adenylate kinase 1
AK2	adenylate kinase 2
AK3	adenylate kinase 3
AK4	adenylate kinase 4
AK5	adenylate kinase 5
AK7	adenylate kinase 7
AKT1	AKT serine/threonine kinase 1
AKT2	AKT serine/threonine kinase 2
AKT3	AKT serine/threonine kinase 3
ALDH18A1	aldehyde dehydrogenase 18 family member A1

ALK	ALK receptor tyrosine kinase
ALPK1	alpha kinase 1
ALPK2	alpha kinase 2
ALPK3	alpha kinase 3
AMHR2	anti-Mullerian hormone receptor type 2
ANKK1	ankyrin repeat and kinase domain containing 1
ARAF	A-Raf proto-oncogene, serine/threonine kinase
ATM	ATM serine/threonine kinase
ATR	ATR serine/threonine kinase
AURKA	aurora kinase A
AURKB	aurora kinase B
AURKC	aurora kinase C
AXL	AXL receptor tyrosine kinase
BCKDK	branched chain ketoacid dehydrogenase kinase
BCR	BCR, RhoGEF and GTPase activating protein
BLK	BLK proto-oncogene, Src family tyrosine kinase
BMP2K	BMP2 inducible kinase
BMPR1A	bone morphogenetic protein receptor type 1A
BMPR1B	bone morphogenetic protein receptor type 1B
BMPR2	bone morphogenetic protein receptor type 2
BMX	BMX non-receptor tyrosine kinase
BRAF	B-Raf proto-oncogene, serine/threonine kinase
BRD2	bromodomain containing 2
BRD3	bromodomain containing 3
BRD4	bromodomain containing 4
BRDT	bromodomain testis associated
BRSK1	BR serine/threonine kinase 1
BRSK2	BR serine/threonine kinase 2
BTK	Bruton tyrosine kinase
BUB1	BUB1 mitotic checkpoint serine/threonine kinase
BUB1B	BUB1 mitotic checkpoint serine/threonine kinase B
CALM1	calmodulin 1

CALM2	calmodulin 1
CALM3	calmodulin 1
CAMK1	calcium/calmodulin dependent protein kinase I
CAMK1D	calcium/calmodulin dependent protein kinase ID
CAMK1G	calcium/calmodulin dependent protein kinase IG
CAMK2A	calcium/calmodulin dependent protein kinase II alpha
CAMK2B	calcium/calmodulin dependent protein kinase II beta
CAMK2D	calcium/calmodulin dependent protein kinase II delta
CAMK2G	calcium/calmodulin dependent protein kinase II gamma
CAMK2N1	calcium/calmodulin dependent protein kinase II inhibitor 1
CAMK4	calcium/calmodulin dependent protein kinase IV
CAMKK1	calcium/calmodulin dependent protein kinase 1
CAMKK2	calcium/calmodulin dependent protein kinase kinase 2
CAMKV	CaM kinase like vesicle associated
CASK	calcium/calmodulin dependent serine protein kinase
CDADC1	cytidine and dCMP deaminase domain containing 1
CDC42BPA	CDC42 binding protein kinase alpha
CDC42BPB	CDC42 binding protein kinase beta
CDC42BPG	CDC42 binding protein kinase gamma
CDC7	cell division cycle 7
CDK1	cyclin dependent kinase 1
CDK10	cyclin dependent kinase 10
CDK11A	cyclin dependent kinase 11A
CDK11B	cyclin dependent kinase 11B
CDK12	cyclin dependent kinase 12
CDK13	cyclin dependent kinase 13
CDK14	cyclin dependent kinase 14
CDK15	cyclin dependent kinase 15
CDK16	cyclin dependent kinase 16
CDK17	cyclin dependent kinase 17
CDK18	cyclin dependent kinase 18
CDK19	cyclin dependent kinase 19

CDK2	cyclin dependent kinase 2
CDK20	cyclin dependent kinase 20
CDK3	cyclin dependent kinase 3
CDK4	cyclin dependent kinase 4
CDK5	cyclin dependent kinase 5
CDK5R1	cyclin dependent kinase 5 regulatory subunit 1
CDK5R2	cyclin dependent kinase 5 regulatory subunit 2
CDK6	cyclin dependent kinase 6
CDK7	cyclin dependent kinase 7
CDK8	cyclin dependent kinase 8
CDK9	cyclin dependent kinase 9
CDKL1	cyclin dependent kinase like 1
CDKL2	cyclin dependent kinase like 2
CDKL3	cyclin dependent kinase like 3
CDKL4	cyclin dependent kinase like 4
CDKL5	cyclin dependent kinase like 5
CDKN1A	cyclin dependent kinase inhibitor 1A
CDKN1B	cyclin dependent kinase inhibitor 1B
CDKN1C	cyclin dependent kinase inhibitor 1C
CDKN2B	cyclin dependent kinase inhibitor 2B
CDKN2C	cyclin dependent kinase inhibitor 2C
CDKN2D	cyclin dependent kinase inhibitor 2D
CERK	ceramide kinase
CHEK1	checkpoint kinase 1
CHEK2	checkpoint kinase 2
CHKA	choline kinase alpha
CHKB	choline kinase beta
CHUK	conserved helix-loop-helix ubiquitous kinase
CIB2	calcium and integrin binding family member 2
CIT	citron rho-interacting serine/threonine kinase
CKB	creatine kinase B
CKM	creatine kinase, M-type

CKMT2	creatine kinase, mitochondrial 2
CKS1B	CDC28 protein kinase regulatory subunit 1B
CKS2	CDC28 protein kinase regulatory subunit 2
CLK1	CDC like kinase 1
CLK2	CDC like kinase 2
CLK3	CDC like kinase 3
CLK4	CDC like kinase 4
CMPK1	cytidine/uridine monophosphate kinase 1
COASY	Coenzyme A synthase
COL4A3BP	collagen type IV alpha 3 binding protein
COMMD3	COMM domain containing 3
CPNE3	copine 3
CRIM1	cysteine rich transmembrane BMP regulator 1
CRKL	CRK like proto-oncogene, adaptor protein
CSF1R	colony stimulating factor 1 receptor
CSK	C-terminal Src kinase
CSNK1A1	casein kinase 1 alpha 1
CSNK1A1L	casein kinase 1 alpha 1 like
CSNK1D	casein kinase 1 delta
CSNK1E	casein kinase 1 epsilon
CSNK1G1	casein kinase 1 gamma 1
CSNK1G2	casein kinase 1 gamma 2
CSNK1G3	casein kinase 1 gamma 3
CSNK2A1	casein kinase 2 alpha 1
CSNK2A2	casein kinase 2 alpha 2
CSNK2B	casein kinase 2 beta
DAPK1	death associated protein kinase 1
DAPK2	death associated protein kinase 2
DAPK3	death associated protein kinase 3
DBF4	DBF4 zinc finger
DCK	deoxycytidine kinase
DCLK1	doublecortin like kinase 1

DCLK2	doublecortin like kinase 2
DCLK3	doublecortin like kinase 3
DDR1	discoidin domain receptor tyrosine kinase 1
DDR2	discoidin domain receptor tyrosine kinase 2
DGKA	diacylglycerol kinase alpha
DGKB	diacylglycerol kinase beta
DGKD	diacylglycerol kinase delta
DGKG	diacylglycerol kinase gamma
DGKH	diacylglycerol kinase eta
DGKI	diacylglycerol kinase iota
DGKK	diacylglycerol kinase kappa
DGKQ	diacylglycerol kinase theta
DGUOK	deoxyguanosine kinase
DLG1	discs large MAGUK scaffold protein 1
DLG2	discs large MAGUK scaffold protein 2
DLG3	discs large MAGUK scaffold protein 3
DLG4	discs large MAGUK scaffold protein 4
DMPK	DM1 protein kinase
DSTYK	dual serine/threonine and tyrosine protein kinase
DTYMK	deoxythymidylate kinase
DUSP21	dual specificity phosphatase 21
DYRK1A	dual specificity tyrosine phosphorylation regulated kinase 1A
DYRK1B	dual specificity tyrosine phosphorylation regulated kinase 1B
DYRK2	dual specificity tyrosine phosphorylation regulated kinase 2
DYRK3	dual specificity tyrosine phosphorylation regulated kinase 3
DYRK4	dual specificity tyrosine phosphorylation regulated kinase 4
EEF2K	eukaryotic elongation factor 2 kinase
EFNA3	ephrin A3
EFNA4	ephrin A4
EFNA5	ephrin A5
EFNB3	ephrin B3
EGFR	epidermal growth factor receptor

EIF2AK1	eukaryotic translation initiation factor 2 alpha kinase 1
EIF2AK2	eukaryotic translation initiation factor 2 alpha kinase 2
EIF2AK3	eukaryotic translation initiation factor 2 alpha kinase 3
EIF2AK4	eukaryotic translation initiation factor 2 alpha kinase 4
EPHA1	EPH receptor A1
EPHA2	EPH receptor A2
EPHA3	EPH receptor A3
EPHA4	EPH receptor A4
EPHA5	EPH receptor A5
EPHA6	EPH receptor A6
EPHA7	EPH receptor A7
EPHA8	EPH receptor A8
EPHB1	EPH receptor B1
EPHB2	EPH receptor B2
EPHB3	EPH receptor B3
EPHB4	EPH receptor B4
EPHB6	EPH receptor B6
ERBB2	erb-b2 receptor tyrosine kinase 2
ERBB3	erb-b2 receptor tyrosine kinase 3
ERBB4	erb-b2 receptor tyrosine kinase 4
ERN1	endoplasmic reticulum to nucleus signalling 1
ERN2	endoplasmic reticulum to nucleus signalling 2
ETNK1	ethanolamine kinase 1
ETNK2	ethanolamine kinase 2
EXOSC10	exosome component 10
FASTK	Fas activated serine/threonine kinase
FER	FER tyrosine kinase
FES	FES proto-oncogene, tyrosine kinase
FGFR1	fibroblast growth factor receptor 1
FGFR2	fibroblast growth factor receptor 2
FGFR3	fibroblast growth factor receptor 3
FGFR4	fibroblast growth factor receptor 4

FGFRL1	fibroblast growth factor receptor like 1
FGR	FGR proto-oncogene, Src family tyrosine kinase
FLT1	fms related tyrosine kinase 1
FLT3	fms related tyrosine kinase 3
FLT4	fms related tyrosine kinase 4
FN3K	fructosamine 3 kinase
FN3KRP	fructosamine 3 kinase related protein
FRK	fyn related Src family tyrosine kinase
FUK	fucokinase
FXN	frataxin
FYN	FYN proto-oncogene, Src family tyrosine kinase
GAK	cyclin G associated kinase
GALK1	galactokinase 1
GALK2	galactokinase 2
GCK	glucokinase
GK	glycerol kinase
GK2	glycerol kinase 2
GNE	glucosamine (UDP-N-acetyl)-2-epimerase/N-acetylmannosamine kinase
GOLGA5	golgin A5
GRK1	G protein-coupled receptor kinase 1
GRK4	G protein-coupled receptor kinase 4
GRK5	G protein-coupled receptor kinase 5
GRK6	G protein-coupled receptor kinase 6
GRK7	G protein-coupled receptor kinase 7
GSG2	histone H3 associated protein kinase
GSK3A	glycogen synthase kinase 3 alpha
GSK3B	glycogen synthase kinase 3 beta
GTF2H1	general transcription factor IIH subunit 1
GUCY2C	guanylate cyclase 2C
GUCY2EP	guanylate cyclase 2E, pseudogene
GUCY2F	guanylate cyclase 2F, retinal

GUK1	guanylate kinase 1
HCK	HCK proto-oncogene, Src family tyrosine kinase
HIPK1	homeodomain interacting protein kinase 1
HIPK2	homeodomain interacting protein kinase 2
HIPK3	homeodomain interacting protein kinase 3
HIPK4	homeodomain interacting protein kinase 4
HK1	hexokinase 1
HK2	hexokinase 2
HK3	hexokinase 3
HSPB8	heat shock protein family B (small) member 8
HUNK	hormonally up-regulated Neu-associated kinase
HUS1	HUS1 checkpoint clamp component
ICK	intestinal cell kinase
IGF1R	insulin like growth factor 1 receptor
IGF2R	insulin like growth factor 2 receptor
IKBKAP	elongator complex protein 1
IKBKB	inhibitor of nuclear factor kappa B kinase subunit beta
IKBKE	inhibitor of nuclear factor kappa B kinase subunit epsilon
IKBKG	inhibitor of nuclear factor kappa B kinase subunit gamma
ILK	integrin linked kinase
INSR	insulin receptor
INSRR	insulin receptor related receptor
IP6K1	inositol hexakisphosphate kinase 1
IP6K2	inositol hexakisphosphate kinase 2
IP6K3	inositol hexakisphosphate kinase 3
IPMK	inositol polyphosphate multikinase
IPPK	inositol-pentakisphosphate 2-kinase
IRAK1	interleukin 1 receptor associated kinase 1
IRAK2	interleukin 1 receptor associated kinase 2
IRAK3	interleukin 1 receptor associated kinase 3
IRAK4	interleukin 1 receptor associated kinase 4
ITK	IL2 inducible T cell kinase

ITPK1	inositol-tetrakisphosphate 1-kinase
ITPKA	inositol-trisphosphate 3-kinase A
ITPKB	inositol-trisphosphate 3-kinase B
ITPKC	inositol-trisphosphate 3-kinase C
JAK1	Janus kinase 1
JAK2	Janus kinase 2
JAK3	Janus kinase 3
KCNH2	potassium voltage-gated channel subfamily H member 2
KCNH8	potassium voltage-gated channel subfamily H member 8
KDR	kinase insert domain receptor
KHK	ketohexokinase
KIT	KIT proto-oncogene receptor tyrosine kinase
KIAA1804	Mitogen-activated protein kinase kinase kinase 21
KSR1	kinase suppressor of ras 1
KSR2	kinase suppressor of ras 2
LATS1	large tumour suppressor kinase 1
LATS2	large tumour suppressor kinase 2
LCK	LCK proto-oncogene, Src family tyrosine kinase
LIMK1	LIM domain kinase 1
LIMK2	LIM domain kinase 2
LMBR1	limb development membrane protein 1
LMTK2	lemur tyrosine kinase 2
LMTK3	lemur tyrosine kinase 3
LRRK1	leucine rich repeat kinase 1
LRRK2	leucine rich repeat kinase 2
LTK	leukocyte receptor tyrosine kinase
LYN	LYN proto-oncogene, Src family tyrosine kinase
MAGI1	membrane associated guanylate kinase, WW and PDZ domain containing 1
MAGI2	membrane associated guanylate kinase, WW and PDZ domain containing 2

MAGI3	membrane associated guanylate kinase, WW and PDZ domain containing 3
MAK	male germ cell associated kinase
MAP2K1	mitogen-activated protein kinase kinase 1
MAP2K2	mitogen-activated protein kinase kinase 2
MAP2K3	mitogen-activated protein kinase kinase 3
MAP2K4	mitogen-activated protein kinase kinase 4
MAP2K5	mitogen-activated protein kinase kinase 5
MAP2K6	mitogen-activated protein kinase kinase 6
MAP2K7	mitogen-activated protein kinase kinase 7
MAP3K1	mitogen-activated protein kinase kinase kinase 1
MAP3K10	mitogen-activated protein kinase kinase kinase 10
MAP3K11	mitogen-activated protein kinase kinase kinase 11
MAP3K12	mitogen-activated protein kinase kinase kinase 12
MAP3K13	mitogen-activated protein kinase kinase kinase 13
MAP3K14	mitogen-activated protein kinase kinase kinase 14
MAP3K15	mitogen-activated protein kinase kinase kinase 15
MAP3K19	mitogen-activated protein kinase kinase kinase 19
MAP3K2	mitogen-activated protein kinase kinase kinase 2
MAP3K3	mitogen-activated protein kinase kinase kinase 3
MAP3K4	mitogen-activated protein kinase kinase kinase 4
MAP3K5	mitogen-activated protein kinase kinase kinase 5
MAP3K6	mitogen-activated protein kinase kinase kinase 6
MAP3K7	mitogen-activated protein kinase kinase kinase 7
MAP3K8	mitogen-activated protein kinase kinase kinase 8
MAP3K9	mitogen-activated protein kinase kinase kinase 9
MAP4K1	mitogen-activated protein kinase kinase kinase kinase 1
MAP4K2	mitogen-activated protein kinase kinase kinase kinase 2
MAP4K3	mitogen-activated protein kinase kinase kinase kinase 3
MAP4K4	mitogen-activated protein kinase kinase kinase kinase 4
MAP4K5	mitogen-activated protein kinase kinase kinase kinase 5
MAPK1	mitogen-activated protein kinase 1

MAPK10	mitogen-activated protein kinase 10
MAPK11	mitogen-activated protein kinase 11
MAPK12	mitogen-activated protein kinase 12
MAPK13	mitogen-activated protein kinase 13
MAPK14	mitogen-activated protein kinase 14
MAPK15	mitogen-activated protein kinase 15
MAPK3	mitogen-activated protein kinase 3
MAPK4	mitogen-activated protein kinase 4
MAPK6	mitogen-activated protein kinase 6
MAPK7	mitogen-activated protein kinase 7
MAPK8	mitogen-activated protein kinase 8
MAPK9	mitogen-activated protein kinase 9
MAPKAPK2	mitogen-activated protein kinase-activated protein kinase 2
MAPKAPK3	mitogen-activated protein kinase-activated protein kinase 3
MAPKAPK5	mitogen-activated protein kinase-activated protein kinase 5
MARK1	microtubule affinity regulating kinase 1
MARK2	microtubule affinity regulating kinase 2
MARK3	microtubule affinity regulating kinase 3
MARK4	microtubule affinity regulating kinase 4
MAST1	microtubule associated serine/threonine kinase 1
MAST2	microtubule associated serine/threonine kinase 2
MAST3	microtubule associated serine/threonine kinase 3
MAST4	microtubule associated serine/threonine kinase family member 4
MASTL	microtubule associated serine/threonine kinase like
MATK	megakaryocyte-associated tyrosine kinase
MELK	maternal embryonic leucine zipper kinase
MERTK	MER proto-oncogene, tyrosine kinase
MET	MET proto-oncogene, receptor tyrosine kinase
MINK1	misshapen like kinase 1
MKNK1	MAP kinase interacting serine/threonine kinase 1
MKNK2	MAP kinase interacting serine/threonine kinase 2
MLKL	mixed lineage kinase domain like pseudokinase

MOK	MOK protein kinase
MOS	MOS proto-oncogene, serine/threonine kinase
MPP1	membrane palmitoylated protein 1
MPP2	membrane palmitoylated protein 2
MPP3	membrane palmitoylated protein 3
MST1R	macrophage stimulating 1 receptor
MST4	Mammalian STE20-like protein kinase 4
MTOR	mechanistic target of rapamycin kinase
MUSK	muscle associated receptor tyrosine kinase
MVK	mevalonate kinase
MYLK	myosin light chain kinase
MYLK2	myosin light chain kinase 2
MYLK3	myosin light chain kinase 3
MYLK4	myosin light chain kinase family member 4
MYO3A	myosin IIIA
MYO3B	myosin IIIB
N4BP2	NEDD4 binding protein 2
NADK	NAD kinase
NAGK	N-acetylglucosamine kinase
NEK1	NIMA related kinase 1
NEK10	NIMA related kinase 10
NEK11	NIMA related kinase 11
NEK2	NIMA related kinase 2
NEK3	NIMA related kinase 3
NEK4	NIMA related kinase 4
NEK5	NIMA related kinase 5
NEK6	NIMA related kinase 6
NEK7	NIMA related kinase 7
NEK8	NIMA related kinase 8
NEK9	NIMA related kinase 9
NIM1K	NIM1 serine/threonine protein kinase
NLK	nemo like kinase

NME1	NME/NM23 nucleoside diphosphate kinase 1
NME2	NME/NM23 nucleoside diphosphate kinase 2
NME3	NME/NM23 nucleoside diphosphate kinase 3
NME4	NME/NM23 nucleoside diphosphate kinase 4
NME5	NME/NM23 family member 5
NME6	NME/NM23 nucleoside diphosphate kinase 6
NME7	NME/NM23 family member 7
NPR2	natriuretic peptide receptor 2
NRBP1	nuclear receptor binding protein 1
NRBP2	nuclear receptor binding protein 2
NRK	Nik related kinase
NTRK1	neurotrophic receptor tyrosine kinase 1
NTRK2	neurotrophic receptor tyrosine kinase 2
NTRK3	neurotrophic receptor tyrosine kinase 3
NUAK1	NUAK family kinase 1
NUAK2	NUAK family kinase 2
NUCKS1	nuclear casein kinase and cyclin dependent kinase substrate 1
NUP62	nucleoporin 62
OXSR1	oxidative stress responsive 1
PACSIN1	protein kinase C and casein kinase substrate in neurons 1
PAK1	p21 (RAC1) activated kinase 1
PAK2	p21 (RAC1) activated kinase 2
PAK3	p21 (RAC1) activated kinase 3
PAK4	p21 (RAC1) activated kinase 4
PAK6	p21 (RAC1) activated kinase 6
PAK7	p21 (RAC1) activated kinase 5
PANK1	pantothenate kinase 1
PANK2	pantothenate kinase 2
PANK3	pantothenate kinase 3
PANK4	pantothenate kinase 4
PAPSS1	3'-phosphoadenosine 5'-phosphosulfate synthase 1
PAPSS2	3'-phosphoadenosine 5'-phosphosulfate synthase 2

PASK	PAS domain containing serine/threonine kinase
PBK	PDZ binding kinase
PCK1	phosphoenolpyruvate carboxykinase 1
PCK2	phosphoenolpyruvate carboxykinase 2, mitochondrial
PDGFRA	platelet derived growth factor receptor alpha
PDGFRB	platelet derived growth factor receptor beta
PDGFRL	platelet derived growth factor receptor like
PDIK1L	PDLIM1 interacting kinase 1 like
PDK1	pyruvate dehydrogenase kinase 1
PDK2	pyruvate dehydrogenase kinase 2
PDK3	pyruvate dehydrogenase kinase 3
PDK4	pyruvate dehydrogenase kinase 4
PDPK1	3-phosphoinositide dependent protein kinase 1
PDXK	pyridoxal kinase
PEAK1	pseudopodium enriched atypical kinase 1
PFKFB1	6-phosphofructo-2-kinase/fructose-2,6-biphosphatase 1
PFKFB2	6-phosphofructo-2-kinase/fructose-2,6-biphosphatase 2
PFKFB3	6-phosphofructo-2-kinase/fructose-2,6-biphosphatase 3
PFKFB4	6-phosphofructo-2-kinase/fructose-2,6-biphosphatase 4
PFKL	phosphofructokinase, liver type
PFKM	phosphofructokinase, muscle
PFKP	phosphofructokinase, platelet
PGK1	phosphoglycerate kinase 1
PGK2	phosphoglycerate kinase 2
PHKA1	phosphorylase kinase regulatory subunit alpha 1
PHKA2	phosphorylase kinase regulatory subunit alpha 2
PHKB	phosphorylase kinase regulatory subunit beta
PHKG1	phosphorylase kinase catalytic subunit gamma 1
PHKG2	phosphorylase kinase catalytic subunit gamma 2
PI4K2A	phosphatidylinositol 4-kinase type 2 alpha
PI4K2B	phosphatidylinositol 4-kinase type 2 beta
PI4KA	phosphatidylinositol 4-kinase alpha

PI4KB	phosphatidylinositol 4-kinase beta
PIK3C2A	phosphatidylinositol-4-phosphate 3-kinase catalytic subunit type 2 alpha
PIK3C2B	phosphatidylinositol-4-phosphate 3-kinase catalytic subunit type 2 beta
PIK3C2G	phosphatidylinositol-4-phosphate 3-kinase catalytic subunit type 2 gamma
PIK3C3	phosphatidylinositol 3-kinase catalytic subunit type 3
PIK3CA	phosphatidylinositol-4,5-bisphosphate 3-kinase catalytic subunit alpha
PIK3CB	phosphatidylinositol-4,5-bisphosphate 3-kinase catalytic subunit beta
PIK3CD	phosphatidylinositol-4,5-bisphosphate 3-kinase catalytic subunit delta
PIK3CG	phosphatidylinositol-4,5-bisphosphate 3-kinase catalytic subunit gamma
PIK3R1	phosphoinositide-3-kinase regulatory subunit 1
PIK3R2	phosphoinositide-3-kinase regulatory subunit 2
PIK3R3	phosphoinositide-3-kinase regulatory subunit 3
PIK3R4	phosphoinositide-3-kinase regulatory subunit 4
PIK3R5	phosphoinositide-3-kinase regulatory subunit 5
PIKFYVE	phosphoinositide kinase, FYVE-type zinc finger containing
PIM1	Pim-1 proto-oncogene, serine/threonine kinase
PIM2	Pim-2 proto-oncogene, serine/threonine kinase
PIM3	Pim-3 proto-oncogene, serine/threonine kinase
PINK1	PTEN induced putative kinase 1
PIP4K2A	phosphatidylinositol-5-phosphate 4-kinase type 2 alpha
PIP4K2B	phosphatidylinositol-5-phosphate 4-kinase type 2 beta
PIP4K2C	phosphatidylinositol-5-phosphate 4-kinase type 2 gamma
PIP5K1A	phosphatidylinositol-4-phosphate 5-kinase type 1 alpha
PIP5K1B	phosphatidylinositol-4-phosphate 5-kinase type 1 beta
PIP5K1C	phosphatidylinositol-4-phosphate 5-kinase type 1 gamma

PIP5KL1	phosphatidylinositol-4-phosphate 5-kinase like 1
PKDCC	protein kinase domain containing, cytoplasmic
PKIA	cAMP-dependent protein kinase inhibitor alpha
PKIB	cAMP-dependent protein kinase inhibitor beta
PKLR	pyruvate kinase L/R
PKM	pyruvate kinase M1/2
PKMYT1	protein kinase, membrane associated tyrosine/threonine 1
PKN1	protein kinase N1
PKN2	protein kinase N2
PKN3	protein kinase N3
PLK1	polo like kinase 1
PLK2	polo like kinase 2
PLK3	polo like kinase 3
PLK4	polo like kinase 4
PMVK	phosphomevalonate kinase
PNCK	pregnancy up-regulated nonubiquitous CaM kinase
PNKP	polynucleotide kinase 3'-phosphatase
POMK	protein-O-mannose kinase
PRKAA1	protein kinase AMP-activated catalytic subunit alpha 1
PRKAA2	protein kinase AMP-activated catalytic subunit alpha 2
PRKAB1	protein kinase AMP-activated non-catalytic subunit beta 1
PRKAB2	protein kinase AMP-activated non-catalytic subunit beta 2
PRKACA	protein kinase cAMP-activated catalytic subunit alpha
PRKACB	protein kinase cAMP-activated catalytic subunit beta
PRKACG	protein kinase cAMP-activated catalytic subunit gamma
PRKAG1	protein kinase AMP-activated non-catalytic subunit gamma 1
PRKAG2	protein kinase AMP-activated non-catalytic subunit gamma 2
PRKAG3	protein kinase AMP-activated non-catalytic subunit gamma 3
PRKAR1A	protein kinase cAMP-dependent type I regulatory subunit alpha
PRKAR1B	protein kinase cAMP-dependent type I regulatory subunit beta
PRKAR2A	protein kinase cAMP-dependent type II regulatory subunit alpha
PRKAR2B	protein kinase cAMP-dependent type II regulatory subunit beta

PRKCA	protein kinase C alpha
PRKCB	protein kinase C beta
PRKCD	protein kinase C delta
PRKCE	protein kinase C epsilon
PRKCG	protein kinase C gamma
PRKCH	protein kinase C eta
PRKCI	protein kinase C iota
PRKCQ	protein kinase C theta
PRKCSH	protein kinase C substrate 80K-H
PRKCZ	protein kinase C zeta
PRKD1	protein kinase D1
PRKD2	protein kinase D2
PRKD3	protein kinase D3
PRKDC	protein kinase, DNA-activated, catalytic subunit
PRKG1	protein kinase cGMP-dependent 1
PRKG2	protein kinase cGMP-dependent 2
PRKX	protein kinase X-linked
PRKY	protein kinase Y-linked (pseudogene)
PRPF4B	pre-mRNA processing factor 4B
PRPS1	phosphoribosyl pyrophosphate synthetase 1
PRPS1L1	phosphoribosyl pyrophosphate synthetase 1-like 1
PRPS2	phosphoribosyl pyrophosphate synthetase 2
PSKH1	protein serine kinase H1
PSKH2	protein serine kinase H2
PSTK	phosphoseryl-tRNA kinase
PTK2	protein tyrosine kinase 2
PTK2B	protein tyrosine kinase 2 beta
PTK6	protein tyrosine kinase 6
PTK7	protein tyrosine kinase 7 (inactive)
PXK	PX domain containing serine/threonine kinase like
RAF1	Raf-1 proto-oncogene, serine/threonine kinase
RBKS	ribokinase

RELA	RELA proto-oncogene, NF-kB subunit
RET	ret proto-oncogene
RFK	riboflavin kinase
RIOK1	RIO kinase 1
RIOK2	RIO kinase 2
RIOK3	RIO kinase 3
RIPK1	receptor interacting serine/threonine kinase 1
RIPK2	receptor interacting serine/threonine kinase 2
RIPK3	receptor interacting serine/threonine kinase 3
RIPK4	receptor interacting serine/threonine kinase 4
RNASEL	ribonuclease L
ROCK1	Rho associated coiled-coil containing protein kinase 1
ROCK2	Rho associated coiled-coil containing protein kinase 2
ROR1	receptor tyrosine kinase like orphan receptor 1
ROR2	receptor tyrosine kinase like orphan receptor 2
ROS1	ROS proto-oncogene 1, receptor tyrosine kinase
RPS6KA1	ribosomal protein S6 kinase A1
RPS6KA2	ribosomal protein S6 kinase A2
RPS6KA3	ribosomal protein S6 kinase A3
RPS6KA4	ribosomal protein S6 kinase A4
RPS6KA5	ribosomal protein S6 kinase A5
RPS6KA6	ribosomal protein S6 kinase A6
RPS6KB1	ribosomal protein S6 kinase B1
RPS6KB2	ribosomal protein S6 kinase B2
RPS6KC1	ribosomal protein S6 kinase C1
RPS6KL1	ribosomal protein S6 kinase like 1
RYK	receptor-like tyrosine kinase
SBK1	SH3 domain binding kinase 1
SCYL1	SCY1 like pseudokinase 1
SCYL3	SCY1 like pseudokinase 3
SGK1	serum/glucocorticoid regulated kinase 1
SGK2	SGK2, serine/threonine kinase 2

SGK223	PEAK1 related, kinase-activating pseudokinase 1
SGK3	serum/glucocorticoid regulated kinase family member 3
SGK494	uncharacterized serine/threonine-protein kinase SgK494
SHPK	sedoheptulokinase
SIK1	salt inducible kinase 1
SIK2	salt inducible kinase 2
SIK3	SIK family kinase 3
SKAP1	src kinase associated phosphoprotein 1
SLK	STE20 like kinase
SMG1	SMG1, nonsense mediated mRNA decay associated PI3K related kinase
SNRK	SNF related kinase
SPEG	SPEG complex locus
SPHK1	sphingosine kinase 1
SPHK2	sphingosine kinase 2
SRC	SRC proto-oncogene, non-receptor tyrosine kinase
SRMS	src-related kinase lacking C-terminal regulatory tyrosine and N-terminal myristylation sites
SRP72	signal recognition particle 72
SRPK1	SRSF protein kinase 1
SRPK2	SRSF protein kinase 2
SRPK3	SRSF protein kinase 3
STK10	serine/threonine kinase 10
STK11	serine/threonine kinase 11
STK16	serine/threonine kinase 16
STK17A	serine/threonine kinase 17a
STK17B	serine/threonine kinase 17b
STK19	serine/threonine kinase 19
STK24	serine/threonine kinase 24
STK25	serine/threonine kinase 25
STK3	serine/threonine kinase 3
STK31	serine/threonine kinase 31

STK32A	serine/threonine kinase 32A
STK32B	serine/threonine kinase 32B
STK32C	serine/threonine kinase 32C
STK33	serine/threonine kinase 33
STK35	serine/threonine kinase 35
STK36	serine/threonine kinase 36
STK38	serine/threonine kinase 38
STK38L	serine/threonine kinase 38 like
STK39	serine/threonine kinase 39
STK4	serine/threonine kinase 4
STK40	serine/threonine kinase 40
STKLD1	serine/threonine kinase like domain containing 1
STRADA	STE20-related kinase adaptor alpha
STRADB	STE20-related kinase adaptor beta
STYK1	serine/threonine/tyrosine kinase 1
SYK	spleen associated tyrosine kinase
TAB1	TGF-beta activated kinase 1 (MAP3K7) binding protein 1
TAF1	TATA-box binding protein associated factor 1
TAF1L	TATA-box binding protein associated factor 1 like
TAOK1	TAO kinase 1
TAOK2	TAO kinase 2
TAOK3	TAO kinase 3
TBCK	TBC1 domain containing kinase
TBK1	TANK binding kinase 1
TEC	tec protein tyrosine kinase
TEK	TEK receptor tyrosine kinase
TESK1	testis associated actin remodelling kinase 1
TESK2	testis associated actin remodelling kinase 2
TEX14	testis expressed 14, intercellular bridge forming factor
TGFBR1	transforming growth factor beta receptor 1
TGFBR2	transforming growth factor beta receptor 2
TGFBR3	transforming growth factor beta receptor 3

THNSL1	threonine synthase like 1
TJP2	tight junction protein 2
TK2	thymidine kinase 2, mitochondrial
TLK1	tousled like kinase 1
TLK2	tousled like kinase 2
TNIK	TRAF2 and NCK interacting kinase
TNK1	tyrosine kinase non receptor 1
TNK2	tyrosine kinase non receptor 2
TNNI3K	TNNI3 interacting kinase
TP53RK	TP53 regulating kinase
TPD52L3	tumour protein D52 like 3
TPK1	thiamin pyrophosphokinase 1
TRIB1	tribbles pseudokinase 1
TRIB2	tribbles pseudokinase 2
TRIB3	tribbles pseudokinase 3
TRIM27	tripartite motif containing 27
TRIO	trio Rho guanine nucleotide exchange factor
TRPM6	transient receptor potential cation channel subfamily M member 6
TRPM7	transient receptor potential cation channel subfamily M member 7
TSKS	testis specific serine kinase substrate
TSSK1B	testis specific serine kinase 1B
TSSK2	testis specific serine kinase 2
TSSK3	testis specific serine kinase 3
TSSK4	testis specific serine kinase 4
TSSK6	testis specific serine kinase 6
TTBK1	tau tubulin kinase 1
TTBK2	tau tubulin kinase 2
TTK	TTK protein kinase
TWF1	twinfilin actin binding protein 1
TWF2	twinfilin actin binding protein 2
TYK2	tyrosine kinase 2
TYRO3	TYRO3 protein tyrosine kinase

UCK1	uridine-cytidine kinase 1
UCK2	uridine-cytidine kinase 2
UCKL1	uridine-cytidine kinase 1 like 1
UHMK1	U2AF homology motif kinase 1
ULK1	unc-51 like autophagy activating kinase 1
ULK2	unc-51 like autophagy activating kinase 2
ULK3	unc-51 like kinase 3
ULK4	unc-51 like kinase 4
VRK1	vaccinia related kinase 1
VRK2	vaccinia related kinase 2
VRK3	vaccinia related kinase 3
WEE1	WEE1 G2 checkpoint kinase
WNK1	WNK lysine deficient protein kinase 1
WNK2	WNK lysine deficient protein kinase 2
WNK3	WNK lysine deficient protein kinase 3
WNK4	WNK lysine deficient protein kinase 4
XRCC6BP1	ATP23 metallopeptidase and ATP synthase assembly factor homolog
XYLB	xylulokinase
YES1	YES proto-oncogene 1, Src family tyrosine kinase
ZAK	Sterile alpha motif and leucine zipper containing kinase AZK
ZAP70	zeta chain of T cell receptor associated protein kinase 70

Chapter 11 Appendix 3

11.1 List of drugs used in 2D drug screen and their targets

Drug name and code	Target
S1003 linifanib	competitive VEGFR/PDGFR inhibitor
S1005 Axitinib	inhibitor of VEGFRs and PDGFb
S1006 Saracatinib	Src inhibitor
S1008 Selumetinib	MEK1 inhibitor and ERK 1/2 inhibitor
S1010 Nintedanib	inhibits VEGFRs, FGFRs, PDGFRs
S1011 Afatinib	inhibits EGFR and HER2
S1012 BMS-536924	IGF-1R inhibitor
S1014 Bosutinib	dual Src/Abl inhibitor
S1017 Cediranib	VEGFR inhibitor
S1018 Dovitinib	multitargeted RTK inhibitor
S1020 PD184352	non competitive MEK1/2 inhibitor
S1021 Dasatinib	multitargeted RTK inhibitor
S1022 Ridaforolimus	mTOR inhibitor
S1023 Erlotinib	EGFR inhibitor
S1025 Gefitinib	EGFR inhibitor
S1026 Imatinib	v-Abl, c-Kit, PDGFR inhibitor
S1028 lapatinib	EGFR and ErbB2 inhibitor
S1032 motesanib diphosphate	competitive inhibitor VEGFR1/2/3
S1033 nilotinib	inhibits Bcr-Abl
S1034 NVP-AEW541	IGF1-R inhibitor
S1035 Pazopanib	inhibits VEGFRs, PDGFR, FGFR
S1036 PD0325901	MEK inhibitor
S1038 Pl-103	PI3K inhibitor
S1039 rapamycin	mTOR inhibitor
S1040 Sorafenib	inhibits Raf-1, B-Raf and VEGFR-2
S1042 sunitib	VEGFR-2 and PDGFRb inhibitor
S1043 Tandutinib MLN518	FLT-3 antagonist
S1044 Temsirolimus	mTor inhibitor

S1046 Vandetanib	VEGFR2 inhibitor
S1048 Tozasertib	inhibits Aurora
S1049 Y-27632	inhibits Rock1
S1055 Enzataurin LY317615	inhibits PKC
S1056 AC480 (BMS-599626)	inihibits HER1/2
S1064 Masitinib AB1010	inhibits Kit and PDGFR
S1065 Pictilisib (GDC-0941)	PI3K inhibitor
S1066 SL-237	MEK1/2 inhibitor
S1068 Crizotinib (PF-02341066)	HGFR inhibitor
S1070 PHA-66575	HGFR inhibitor
S1072 ZSTK474	PI3K inhibitor
S1075 SB216763	GSK3 inhibitor
S1076 SB203580	p38 MAPK inhibitor
S1077 SB202190	p38 MAPK inhibitor
S1078 MK-2206 2HCl	Akt1/2/3 inhibitor
S1080 SU111274	HGFR inhibitor
S1084 Brivanib	inhibits VEGFR2
S1088 NVP-ADW742	inhibits IGF-1R
S1089 Refametinib	MEK 1/2 inhibitor
S1091 Linsitinib (OSI-906)	inhibits IGF-1R
S1092 KU-55933	inhibits ATM
S1093 GSK1904529A	inhibits IGF-1R
S1094 PF-04217903	HGFR inhibitor
S1100 MLN8054	inhibits Aurora A
S1101 Vatalanib (PTK787) 2HC	inhibits VEGFR
S1102 U0126-ETOH	inhibits MEK1/2
S1103 ZM 447439	inhibits Aurora A
S1104 GDC-0879	inhibits B-RAF
S1105 LY24002	PI3K inhibitor
S1106 OSU-03012 (AR-12)	PDK-1 inhibitor
S1107 Danusertib (PHA-739358)	inhibits Aurora
S1109 BI2536	PLK1 inhibitor

S1111 Foretinib (GSK1363089)	inhibits HGFR and VEGFR
S1112 SGX-523	inhibits HGFR
S1113 GSK690693	inhibits Akt
S1114 JNJ-38877605	inhibits HGFR
S1116 Palbociclib	CDK4/6 inhibitor
S1117 Triciribine	DNA synthesis inhibitor
S1118 XL147 analogue	PI3K inhibitor
S1119 Cabozantinib	inhibits VEGFR2
S1120 Everolimus (RAD001)	mTOR inhibitor
S1124 BMS-754807	inhibits IGF-1R
S1133 Alisertib (MLN8237	inhibits Aurora A
S1134 AT9283	inhibits JAK 2/3
S1138 Brivanib	inhibits VEGFR2
S1143 AG-490 (Tyrphostin B42)	inhibits EGFR
S1145 SNS-032 (BMS-387032)	inhibits CDK2
S1147 Barasertib (AZD1152-HQPA)	inhibits Aurora B
S1152 PLX-4720	inhibits B-RAF
S1153 Roscovitine	CDK2 and CDK5 inhibitor
S1154 SNS-314 Mesylate	inhibits Aurora
S1164 Lenvatinib (E7080	inhibits VEGFR
S1167 CP-724714	inhibits HER2
S1169 TGX-221	inhibits p110
S1170 WZ3146	inhibits EGFR
S1171 CYC116	inhibits Aurora A/B
S1173 WZ4002	inhibits EGFR
S1177 PD98059	MEK inhibitor
S1178 Regorafenib (BAY 73-4506)	inhibits VEGFR and others
S1179 WZ8040	mutant EGFR
S1181 ENMD-2076	inhibits Aurora
S1194 CUDC-101	HDAC and RTK inhibitor
S1205 PIK-75	inhibits p110
S1207 Tivozanib (AV-951	inhibits VEGFR

S1219 YM201636	inhibits PIKFYVE
S1220 OSI-930	inhibits Kit (Stem Cell Growth Factor R)
S1226 KU-0063794	inhibits mTOR
S1234 AG-1024 (Tyrphostin)	IGF-1R inhibitor
S1244 Amuvatinib (MP-470)	inhibits c-Kit
S1249 JNJ-7706621	CDK1/2 inhibitor
S1264 PD173074	FGFR1 inhibitor
S1266 WYE-354	mTOR inhibitor
S1267 Vemurafenib	inhibits b-raf
S1274 BX795	PDK inhibitor
S1275 BX912	PDK1 inhibitor
S1342 Genistein	blocks EGF
S1352 TG100-115	PI3K inhibitor
S1360 GSK105961	inhibits PI3K and mTOR
S1361 Glesatinib (MGCD265)	inhibits VEGFR and HGFR
S1362 Rigosertib	inhibits PLK1
S1363 Ki8751	inhibits VEGFR2
S1378 Ruxolitinib (INCB018424	inhibits JAK 1/2
S1392 Pelitinib (EKB-569)	inhibits EGFR
S1451 Aurora A Inhibitor I	inhibits Aurora
S1454 PHA-680632	inhibits Aurora
S1458 VX-745	inhibits p38a (a MAPK)
S1459 Thiazovivin	inhibits Rock
s1460 SP600125	inhibits JNK
s1462 AZD6482	inhibits PI3K
S1470 Orantinib (TSU-68, SU6668)	inhibits PDGFR autophosphorylation
S1474 GSK429286A	inhibits Rock
S1475 Pimasertib (AS-703026	inhibits MEK 1/2
S1485 HMN-214	changes cellular spatial orientation PLK1
S1486 AEE788 (NVP-AEE788)	EGFR/HER2
S1487 PHA-793887	inhibits cdk2,5,7
S1489 PIK-93	inhibits PI3K/PI4K

S1490 Ponatinib (AP24534)	abl, PDGF, src, FGFR
S1494 Ralimetinib (LY2228820)	inhibits p38 MAPK
S1519 CCT129202	pan Aurora inhibitor
S1523 Voxtalisib (SAR245409, XL765)	mTOR and PI3K inhibitor
S1524 AT7519	multi-cdk
S1526 Quizartinib (AC220)	inhibits flt3
S1529 Hesperadin	inhibits Aurora B
S1530 BIX02188	inhibits MEK5
S1531 BIX02189	inhibits MEK5
S1532 AZD7762	inhibits chk1
S1533 R406 (free base)	inhibits syk
S1536 CP-673451	inhibits PDGFRa/b
S1555 AZD8055	inhibits mTOR
S1556 PHT-427	dual AKT and PDPK
S1557	VEGFR
S1558 AT7867	AKT1/2/3 & p70S6
S1561	c-Met, axl, ron
S1568	MEK1/2
S1570	ATM
S1572	CDK7
S1573 Fasudil	Rho kinase
S1574	pan-P38 MAPK
S1577 Tie2 kinase inhibitor	Tie2
S1582 H892HCL	PKA inhibitor
S1590 TWS119	GSK3b
S1802 Acadesine	AMPK
S2013	FAK
S2014	CDK 1/2 inhibitor
S2134	MEK1/2
S2158	Flt3, FGFR
S2161 RAF265	c-RAF, b-RAF
S2162	JAK2

S2163	p70S6K
S2179	JAK2
S2185	EGFR/ERBB2
S2192 AZD8931	pan-ERBB
S2193 GSK461364	PLK1
S2194 R406	Syk inhibitor
S2198	Pim1
S2201	Met/VEGFR2
S2202	EphB4
S2205 Erlotinib analogue	EGFR
S2207	PI3Kdelta
S2214	JAK2
S2216	HER2
S2218 PP2242	mTOR
S2219	JAK1/JAK2
S2220	B-Raf
S2221 Apatinib	VEGFR2
S2226	p110delta
S2227	p110delta
S2231	VEGFR2/3
S2235 Volasertib	PLK1
S2238	mTORC1/2
S2243 Degrasyn (WP1130)	deubiquitinase inhibitor
S2247 Buparlisib BKM120	pan-PI3K
S2266 Asiatic acid	aglycone of asiaticoside, used in wound healing
S2310 Honokiol	Inhibits AKT phosphorylation
S2386	GSK3B
S2391	stimulates SIRT1
S2406	EGFR/mTOR
S2475 Imatinib (STI571)	abl, kit, PDGFR
S2542	AMPK

S2617	MEK1
S2621 AZD5438	CDK1/2/9
S2622 PP121	PDGFR, mTOR
S2624 OSI-027	TORC1/TORC2
S2625	SYK inhibitor
S2626	Chk1
S2634	Bcr-Abl
S2635 CCT128930	AKT2
S2636 A66	p110a
S2638	DNA-PK
S2658	pan-p110, mTOR
S2661 WYE-125132	mTOR
S2670	AKT1
S2671 AS-252424	PI3Kgamma
S2672	FAK
S2673	MEK1/2
S2679	CDK1/2/4/6
S2680 PCI-32765	Btk
S2681 AS-604850	PI3Kgamma
S2682 CAY10505	Pi3Kgamma
S2683 CHIR-124	Chk1
S2686	JAK2
S2688	CDK1/2/4
S2689 WAY-600	mTOR
S2692	JAK2
S2696 GDC-0980	pan-PI3K/mTOR
S2699	Pi3Ka
S2697	activated AMPK
S2700	src inhibitor
S2703	IGF1R
S2718	Aurora A/B
S2719	pan-Aurora kinases

S2720 ZM 336372	c-Raf
S2726	p38a
S2727	pan-ERBB
S2728 AG-1478	EGFR
S2729 SB415286	GSK3a
S2730	PDGFRa/b
S2735 MK-8776	Chk1
S2736	JAK2
S2742 PHA-767491	cdc7/CDK9
S2743 PF502	dual PI3k/mTOR
S2744	pan-Aurora
S2746	pan-Raf
S2747 AMG-458	c-Met
S2749 BGT226	Pi3K/mTOR
S2751 Milciclib	CDK2
S2752	HER2
S2755	EGFR/HER2
S2758 Wortmannin	Pi3K
S2759	dual Pi3K/HDAC
S2761	Met
S2767	VPS34
S2768 Dinaciclib	pan-CDKs
S2769	Flt3
S2770	Aurora A
S2774	c-Met
S2783 AZD2014	dual mTORC1/2
S2784	HER2/EGFR
S2789	JAK3
S2791	pan-PKC
S2796	JAK2/STAT3
S2801	FGFR
S2806	JAK2

S2807	BRAFV600
S2808 GDC-0068	AKT1/2/3
S2811	mTOR
S2814 BYL719	PI3Ka
S2816 Tyrphostib AG	HER2
S2817 Torin2	mTOR
S2820	FAK
S2824 TPCA-1	IKK2
S2842	VEGFR3
S2843 BI-D1870	S6 ribosome for RSK1/2/3/4
S2845 Semaxanib	VEGFR
s2859	Met, VEGFR
S2864 IMD 0354	IKKb
S2867	JAK3
S2870 TG100713	pan-PI3K
S2872 GW5074	c-Raf
S2882 IKK-16	IKK2
S2890	FAK
S2895 Tyrphostin 9	EGFR
s2896 ZM323881	VEGFR2
S2897	VEGFR1
S2899 GNF-2	Bcr-Abl
S2902	JAK1/2
S2904	Chk1
S2911	pan-PKC
S2913 BAY 11-7082	NF-kB
S2922	EGFR
S2924	GSK3A/B
S2928	p38 MAPK
S3012	pan-VEGFR
S3026 Piceatannol	syk
S4001	VEGFR2

S4901	JNK
S4907 SC-514	IKK2
S5001	JAK
S5002	Sphingosine-1-phosphate
S6005 VX-702	p38 MAPK
S7000	ALK
S7007	MEK1/2
S7008 PP2	Lck/fyn
S7016	dual PI3K/mTOR
S7018	PI3Kgamma
S7028	PI3K delta/gamma
S7036	JAK2
S7039	EGFR
S7041	Pim kinase
S7050	ATR
S7051	Btk
S7060 PP1	Lck/Fyn
S7065	Aurora A
S7083	ALK
S7087	PDK1
S7091	FKBP-12
S7093 IPA-3	Pak1
S7094	Pak4
S7102	ATR
S7104	Pim kinase
S7106	ALK
S7114 NU6027	ATR, CDK1/2
S7127 TIC10	Akt and ERK
S7136 CGK733	ATM/ATR
S7145	GSK3
S7153 10058-F4	c-Myc
S7158 abemaciclib	CDK4/6

S7167	FGFR1
S7173	BTK
S7176 SKI II	sphingosine kinase
S7177	sphingosine kinase
S7194	Bcr-Abl
S7195	ROCK1/2
S7198 BIO	GSK3
S7206	mutant EGFR
S7207 Ro 31-8220 Mesylate	pan-PKC
s7208	PKC
S7209	SGK1/2
S7214	p38 MAPK
S7215	p38 MAPK
S7248	PLK1 inhibitor
S7253	GSK-3
S7255	PLK1 inhibitor
S7257	BTK
S7269	Bcr-Abl
S7284	mutant EGFR
S7289	6-phosphofructokinase
S7291	pan-Raf
S7293 ZCL278	Cdc42 GTPase inhibitor
S7297	mutant EGFR
S7317	NUAK kinase
S7319	Rac GTPase inhibitor
S7320 TG003	cdc2
S7330	K-Ras
S7332	K-Ras
S7356	Pi3Ka
S7367	LRRK2
S7368	LRRK2
S7397 Sorafenib	Raf

S7422	CaMKII
S7423	CaMKII
S7435 AR-A014418	GSK3B
S7461 LDC000067	CDK9
S7482	Rac GTPase
S7508	JNK
S8007	ATR
S8050	ATR
NMSP715	MPS1
CCT346	MPS1
S7525	BMK1/ERK5
S8009 AG-18	EGFR
S8057	JAK2/FLT3
CCT245747 CHEK1	Chk1
S7526	Bcr-Abl
S8015	BRAF, c-Raf
S8058	CDK1/4/9
ABT199 BC125	Bcr-Abl
S7528	LRRK2
S8019 AZD5363	pan-AKT
S8078	IKK inhibitor
BAY3497 CCT245737	Chk1
S7565	Lck/src
S8023 TCS359	FLT3
RAD1901	ER
AZD9496	ER
S7566	GSK3B
S8024 Tyrphostin AG 1296	PDGFR
Abemaciclib	CDK4/6
Ribociclib	CDK4/6
S7605	JAK1
S8031	Rac GTPase

ICECT7001	CDK7
Neratinib	EGFR/HER2
S8002	PI3Kbeta
S8032	SYK
AD80	RET
GDC810	ER
S8003 PQ 401	IGF1R
S8036	NF-kB
LDC00667 CDK9I	CDK9
Iressa	EGFR
S8004	S8004
S8040	S8040
MK1775	MK1775
4OHT	ER
S8005	Pim1
S8044	IKK-2 and IKK-1
THZ1	THZ1
Fulvestrant	ER